# Investigation of Integrated Geophysical Methods to Characterize Near Surface Formations for Environmental Engineering

by

A thesis submitted to the School of Graduate Studies

in partial fulfillment of the requirements of the degree of

**Doctor of Philosophy in Civil Engineering**

**Faculty of Engineering and Applied Science**

Memorial University of Newfoundland

**May, 2017**

St. John's

Newfoundland and Labrador

# ABSTRACT

Near surface nondestructive imaging for is aimed at evaluating unconsolidated to moderately consolidated porous or granular sediments. Usual targets of interest are depth to bedrock, depth of water table and mapping of subsurface morphology and evolution of toxic fluid (spills) flows such as oils, concentrated brines and their interactivity. Investigative propositions of interest span vast realm of geo-environmental engineering. This includes such applications as structural health and aseismic monitoring, hydraulic/hydrogeological characterization, geotechnical investigations including critical zones/sites identification in areas of public and industrial infrastructure development, groundwater management and natural resources exploration and exploitation associated activities such as mining and those termed unconventional in oil and gas industry. Conventional field methods include P- and S-wave surveys, and electrical resistivity (resistance) measurements. The presented results are outcomes and findings of two laboratory experimental studies designed, owing to their inherent amenability, on field scale concepts of the said methods, to advantage. In the first of two studies S-wave polarized propagation characteristics are exploited to quantitatively evaluate the combined architectural, rheological and fluid transport properties effect of fractured porous media (sandstone specimen) upon acquired or recorded (ultrasonic) S-wave signature when through transmitted with controlled source pulsing. Various time and frequency based analyses unambiguously delineate fracture geometry, stress effects of fracture stiffness and density, amplitude effects of fracture aperture size against the stationary effects of azimuth variability. Critical findings include the characteristic stop-band artifact in transmitted bandwidth signature of fracture planes and direct correlation of S-wave velocity anisotropy with permeability anisotropy. The second study involved spatio-temporal imaging of an immiscible fluid displacement (oil with brine) through an unconsolidated granular sediment analogue (glass-beads-pack) under controlled constant head flow conditions against gravity, using P- , S-wave and electrical resistance data, acquired as integrated. Dry and saturated granular material characteristics with different saturant (state) effects were evaluated post analyzed integrated offering fresh insights. Peculiar repeatable artifacts in imaged data not only unambiguously discriminated oil from brine, a consistent and significant "attenuation" signature of evolving fluid-fluid interface was discovered in ultrasonic data verifiable form electrical resistance observations. Ultrasonic velocity variation and frequency dependence could be understood employing usual anelastic/ visco-elastic models of wave propagation, typically as Biot theory. Gassman and Biot theory applied to validate the results within a zero frequency and megahertz range appear to offer plausible analytical estimates of P-wave velocities. S-wave velocities are underestimated due to ambiguities surrounding the practiced procedures and methods of quantification of critical parameters, with no consideration to the nature of characteristic S-wave propagation being different compared to P-wave.

# ACKNOWLEDGEMENTS

# Table of Contents

# List of Tables

# List of Figures

# List of Symbols

$a$  Acceleration

A   Area cross-section

$A_o$ , $A_i$ Amplitudes, initial and instant

$\theta_1$ , $\theta_2$  Angles of incidence and refraction

$\omega$   Angular Frequency

$R_o$ Background or sand resistivity

$x, y, z$ or $xyz$  Cartesian coordinates

Q  Charge

$\theta_c$ Critical angle

I   Current

$\rho$  Density

$D$ , $b$  Dissipation and dissipation scaling drag factor in Biot theory

$u$ or $u_{i,j,k}$  Displacement or displacement components

$Z$ Elastic impedance

$W$, T  Energy (work)

$\zeta$ or $\theta$  Fluid content increment in Biot theory

Q Fluid dilation, cross coupling factor in Biot theory

R    Fluid dilation at constant frame volume in Biot theory

$F$  , $F_{i,j,k}$  Force or force components

F  Formation resistivity

$\theta$ , $\Psi$     Helmohlz potentials, compressional and rotational

$S_x$, $\alpha$ , $\beta$     Horizontal fault interfacial slip and associated constants

$U_I$, $U_R$ , $U_T$ Incident, reflected and transmitted ray

$K$, $K_{dry}$ , $K_{fluid}$ , $K_{sat}$ Incompressibility, dry material, saturant, and saturated etc.

$R$ Index of refraction, reflection check

$T$ Index of transmission

$\delta_{ij}$ Kronecker delta

$\lambda$ Lame's constant in elastic wave propagation

A , N   Lame's constants of Biot theory

L    Length

$m$ Mass

$K_{nn}$ , $K_{ss}$ Normal and shear fault stiffness

NDE   Nondestructive evaluation (or NDT)

$\phi_T$ , $\phi_R$ Phase variables

$\nu$    Poisson's ratio

$a$    Pore size

$\emptyset$ or $n$ Porosity in Biot theory

$E_R$ Reflection coefficient

R  Electrical Resistance

ɣ Resistivity

μ or $G\mu_{dry}$, $\mu_{sat}$, $G_{dry}$, $G_{sat}$    Rigidity dry and saturated etc.

$U_i - u_i$     Solid frame (U) and saturant (u) relative displacement expression

$\rho_{12}$        Solid-fluid coupling factor in Biot theory

$C_{ijkl}$   Stiffness components

$\tau$ , $\mathcal{T}$   or   $\tau_{i,j,k}$     Stress (or shear stress) and stress components

$\varepsilon$   or   $\varepsilon_{j,k,l}$     Strain and strain components

$E_T$ Transmission coefficient

$t$     Time

$V$ , $Vp$ , $Vs$   Velocity , P-wave and S-wave

$\dot{u}$ , $\ddot{u}$   Velocity and acceleration

$S_{P,V}$ , $k$ , $\xi$   Vertical fault interfacial slip and associated constants

$\eta$   Viscosity

$\alpha$    Well identified structure factor in Biot theory

V     Voltage

S     Void fraction

$R_w$    Water resistivity

$E$    Young's modulus of elasticity

# Chapter 1: Introduction

## 1.1 Research Context and Background

Near surface geophysics has increasingly advanced, and is used to provide near-surface imaging and evaluation for environmental engineering applications. In many cases, the fundamental understanding of analyses and to interpret survey results is becoming an industrial and commercial practice; and, interpretations are more qualitative than quantitative, though. Often, integrated studies utilizing two or more geophysical methods to provide independent assessment of formations are used; however, the interaction of these methods is also not fully understood or quantified. It is recognized within such community of researchers and practitioners that the fundamental research on these geophysical survey methods is needed to better implement these survey methods and to improve the quality of data and interpretations made.

This research thesis encompasses several laboratory investigations to assist with, fundamentally, designing, executing, and data evaluation of several near-surface geophysical methods that are widely used for two main environmental engineering applications. The first application is the assessment of permeability anisotropy in fractured porous media transmitting polarized S-wave, which can be applied to the optimal orienting of horizontal wells perpendicular to the direction of maximum horizontal permeability for maximization of production or injection flow rate in unconventional developments. The second application is imaging and monitoring immiscible hydrocarbon displacement in unconsolidated porous media, as for example used in remediation practices to remove hydrocarbons in groundwater by driving towards recovery wells by water flooding injection, using integrated seismic transmission and resistivity methods.

Both seismic and resistivity based methods have challenges when applied to near-surface investigations. The research pertains to improve an understanding of specific challenges towards better attaining of their mitigation. The conventional high resolution seismic reflection technique, for instance, is based on inducing a seismic disturbance at or near the ground surface and measuring the arrival times of

compressional or P-waves reflected from subsurface horizons. This method over the years has developed into a reliable tool for subsurface characterizations as part of geotechnical and groundwater studies. The main difficulty however is assuming resolution or control over resolution. The achievable resolution level with a high resolution reflection survey is a function of the frequency of the seismic signal. Recovering a coherent high frequency signal can be difficult and costly. The use of shear or S-waves offers the possibility to substantially increase resolution over a conventional survey under commonly encountered subsurface conditions. In hard uniform rock, the S-wave velocity is usually about half of the P-wave velocity, but the predominant frequency is also about half, implying the S-waves may not effect resolution directly. In a heterogeneous rock or soil environment, however, S-waves can be several times slower than P-waves and have similar frequency content, implying S-waves can substantially increase resolution, towards both the subsurface structural architecture and contained saturants i.e., pore fluids. Field experiments, explained in next sections would show, the resolution obtained using S-waves was double than that obtained using P-waves, with a similar expense of resources. The results indicate that the high resolution S-wave reflection technique can be more effective in conducting subsurface investigations than using conventional technology.

Electrical resistivity relates to the bulk electrical resistance of the ground by measuring spatially varying voltages induced by the flow of electrical current between electrodes implanted at the surface. The methods are particularly sensitive to changes in the chemical content type and content concentration of pore fluids either confined or mobile, and useful for tracking such materials and contaminants, directly. These methods can be used to find structures as faults and buried valleys. Advancements allowing multichannel acquisition capability provides flexibility, offering an increase in rate of DC resistivity fieldwork; as in application of electrical resistivity tomography for investigation of morphologically complex subsurface environments. The resistivity method is the underlying concept of the induced polarization (IP) method in data collection, but the IP method involves analysis of the length of time the earth remains disturbed electrically after the disturbing function has been removed. In an electronic sense, the earth's discharge rate is similar to that of a

capacitor. The rate of decay of the induced voltage is dependent on ion mobility in the charged volume. The ions in clays, for example, are highly mobile. Measurements can be made either in the time domain, with voltage as a function of time, or in the frequency domain, where the phase delays of various frequencies are measured. This method was initially developed for sulphide mineral exploration and has been used in for groundwater exploration. The study thus demonstratively signifies the attainment of resolution for unambiguous description of near subsurface anomalies, especially fractures and immiscible fronts, by integration of data, in acquisition and inferring, not well addressed for it's time.

## 1.2 Research Objectives

As described above, this research is focused on fundamental laboratory investigations of  i) evaluating relative horizontal permeability in fractured porous media for the optimal orientation of horizontal well bores, and ii) monitoring immiscible hydrocarbon fluid displacement in unconsolidated sediments using integrated seismic and resistivity methods. In this context, the specific objectives of this research include:

- Development and validation of laboratory facilities and data analysis methodologies to conduct the investigation.
- Evaluation of S-wave polarization as a means to evaluate permeability anisotropy, in particular, the ability to resolve the ratio of maximum to minimum permeability and their directions with fracture stress variability.
- Evaluation of transmitted P- and S-waves to differentiate between hydrocarbon and brine saturation, including mixed saturation in the immiscible contact zone.
- Evaluation of DC electrical resistivity to differentiate between hydrocarbon saturation, brine saturation, and relative mixed saturation.
- Evaluation by Gassman and Biot theory to determine fluid properties for hydrocarbons and brine.

## 1.3 Thesis Organization

This thesis is organized in 9 chapters, making conclusions the 9th. Chapter 1 introduces the research context and motivation for the research, including a brief summary of some of the challenges and limitations with current practices and data analysis methodologies.

Chapter 2 forms the background literature review, and consists of three distinct parts. Each part provides to understand the application of a specific geophysical method to engineering and environmental problems, focused on near-surface applications. Part 1 focuses on P-wave applications, Part 2 on S-wave application, and Part 3 on Electrical methods.

Chapter 3 includes theory pertinent to both implement experiment design and data analysis and interpretation. It includes fundamental definitions of body waves i.e., P- and S-waves, and the theory of elastic wave propagation through isotropic elastic media including wave based and ray based principles. This is extended to anisotropic media, where specific case of elastic wave propagation in layered fractured anisotropic media is examined, and then to poroelasticity for wave propagation through saturated porous media including scattering phenomenon, particle contact mechanics and theories, and frequency restrictions. Finally, fundamentals of DC resistivity methods are detailed.

Chapter 4 describes the laboratory infrastructure and facilities developed to conduct the research, including the various types of material analogues used to simulate subsurface conditions and formations. Experimental measurement accuracy and repeatability are also discussed.

Chapters 5 through 8 comprise the systematic presentation of experimental results and interpretations from the laboratory investigations. Chapter 5 focuses on the fractured porous media investigation by through transmitted S-waves, while Chapters 6 and 7 are focused of the immiscible displacement study imaged with integrated data.

Chapter 6 also highlights the adequacy and validity of relevant experimental procedures and consequent acquired data where the quantitative validation of the

velocity (for ultrasonic P- and S-wave) results are provided in chapter 7. Only P-wave results of the immiscible displacement experiments are deemed appropriate or sufficient for discussion.  All the results in these three chapters consist of components of specific relevance to application of geophysics for engineering and environmental problems.

Chapter 8 assumes a further validity of the results in conceptual relevance to the Gassman and Biot theories with some sources of ambiguities and uncertainties. Conclusions are summarized in Chapter 9.

A detailed list of symbols is provided in the start of the thesis with sufficient explanation thereof to adhere as much as possible with the conventional symbols of discussed concepts and theory, however where ever required adequate explanation in the list and in the text should alleviate any misrepresentation or confusion.

# Chapter 2: Background Literature

## 2.1 Compressional Waves and Near Surface

### 2.1.1 Historical Development of Reflection and Refraction Techniques

Early or earliest seismological methods were focused on the analysis of waves generated by naturally occurring earthquakes and related seismic events. Mallet (1848, 1851) was a pioneer in using an artificial energy in the form of black powder and a bowl of mercury as a detector. He could record only very low velocities due to sensitivity issues, however. Abbot (1878) later measured P-wave velocities using essentially the same type of detectors and a stronger explosive source. Milne and Gray (1885) were the first to use a seismic receiver spread employing two inline seismographs and explosive and falling weight type energy sources. Otto Hecker (1900) used nine mechanical horizontal seismographs in line to record both P- and the S-waves. Further defining the subsurface conditions by making use of the seismographs was put forward by Milne in 1898 (Shaw et al., 1931). Ludger Mintrop in Germany in 1914 devised a seismograph which could record explosion created seismic waves making seismic exploration a feasible proposition. L.P. Garret in 1905 suggested the use of seismic refraction to find salt domes however at that time suitable instruments had not yet been developed (De Goyler, 1935). Later during the period of 1920 and 1921, Mintrop did some refraction work running lines across known features and discovered the Meisendorf dome, a step forward in establishing the foundations of the technique. Much of this early work was applied to the detection of deeper targets for mineral and oil and gas exploration - additional historical development is outlined in Sherrif and Geldart (1982).

Shallow targets are where the use of the seismic methods for engineering studies may be done such as groundwater exploration, waste site evaluations, industrial mineral and metals exploration and exploration for certain energy materials. Evison (1952) working in New Zealand was first to point out that the region of the earth that had been the least successfully explored by means of elastic energy was the first few

hundred feet below the surface. He observed that the standard seismic techniques developed in the course of the search for oil at greater depths were relatively ineffectual at shallow levels, and concluded that the low resolving power of the techniques of the day were due to the type and the nature of the method, and the energy source used for the most part. For shallow surveying, an energy source capable of generating an impulse of desired frequency and duration was really required. He outlined and identified mainly the problems and frustrations of working in the shallow environment, but still contributed towards ensuring success in future works. The research by Pakiser at al. (1954) at the U. S. Geological Survey pioneered the method using a specially constructed portable shallow reflection seismograph. On the basis of several experiments performed in different areas with significant rigor, the usefulness of high frequencies or high-frequency seismic reflection systems was very clearly demonstrated for mapping both typical shallow horizons (Pakiser & Warrick, 1956). They further expected that the method should help solve a variety of ground water problems involving depth to bedrock, shallow structure (artesian water), and, under certain circumstances, aquifers within unconsolidated materials may be imaged with the help of the shallow reflection seismograph. Similar uses were suggested in engineering geology, for example, finding bedrock depths in permafrost areas, where the high near surface permafrost velocity disqualifies the seismic refraction method, and in addition was suggested finding shallow structures for the natural gas storage near large cities. Mooney (1980) provides sound fundamental knowledge of the application of the shallow seismic methods, including analysis and interpretation for identifying two layered structures, three layered structures and non-horizontal multiple layer structures.

## 2.1.2 Near-Surface Methods

Modern use of shallow seismic reflection methods began with Schepers(1975) who produced some excellent shallow P-wave reflection results. His area of interest and definition for near surface investigations appear to be few meters to a maximum

of 100 m of the earth's crust. His investigations were aimed at solving engineering problems, special focus being upon civil engineering. He had divided the measurements into two categories i.e., for investigation of subsurface cavities and, for hydrological and rock mechanics studies. He experimented with various kinds of sources to determine and examine the frequency band produced. The sources used were different types of hammer or thumper and an electric sparker buried in a water filled bore hole. The acoustic signals generated were received at a distance of 2 m from the source. At that distance of 2 m the recorded frequency band ranged from 50 Hz to 800 Hz width. The dominant frequency recorded was 150 Hz and the duration of the pulses recorded were all about 15 ms. Technically speaking their finding manifested that the two way travel time for the seismic wave within the near surface shall be smaller than the duration of the energy pulse itself for most surveys. An example of survey geometry was illustratively offered where the reflector of interest is assumed to be at 50 m depth and the geophone spread is 25 m. It is suggested that all the reflected energy either P- or S-waves should be recorded within the 50 to 100 ms time window depending upon the velocity distribution.

Hunter et al. (1982) enunciate about the impact of the introduction of multichannel digital engineering seismograph system upon the scope of applications of seismic methods to near surface geologic problems. They attribute it to the advent of much economical computing power, in addition. Special emphasis is drawn upon the instance of use of such system as described by (Hunter, 1980) and (Hunter et al., 1980) in allowing simple applications of reflection seismic technique, be used in a variety of applications where high resolution subsurface structural information is required. They discuss the application of the "optimum window method" in an initial field testing. The essence of the "optimum window" technique is in ensuring a correct selection of source-geophone geometry to observe a shallow reflector using an array of twelve geophones. Special significance lies in application and testing of the technique at several field sites in Canada with differing geologic settings. The tests showed the optimum window technique to be extremely effective in areas of thick unconsolidated overburden with the target as the bedrock surface. Hunter et al. (1984)

in their shallow seismic reflection mapping of the overburden-bedrock interface studies draw due emphasis upon the issue of detectability, suitability of conditions and its impact on attainable resolution. They delineated the unconsolidated overburden bedrock interface and the heterogeneities within the overburden to a depth of 20 m.

Refraction seismics developments for near surface investigations identify generalized reciprocal method (GRM) both a primary and significant contribution (Palmer, 1981). The important aspect is introduction of concept of the refractor velocity analysis function, the generalized time-depth, the optimum XY value and the average velocity. GRM is the generalized technique for processing and interpreting in-line seismic refraction data consisting of forward and reverse travel times. This method is also used for surveying undulating targets. The inline seismic data is used and consists of only forward and reverse travel times. For refractor velocity analysis and time depth calculations, the travel times used are recorded at two geophone positions which are separated by a variable distance or spacing XY. Upward traveling segments of the rays received to each geophone emerge from near the same point on the refractor for an optimum XY spacing, which offers two advantages, making velocity analysis simple and the time-depth showing the most detail. Useful when the overlying strata have velocity gradients, since the depth conversion factor is relatively insensitive to dip angles up to about 20 degrees.

Lankston (1990) provides a classical example of the use of refraction method for shallow or near-surface target investigations. He concludes that in the specific case of a waste site evaluation and in ground water exploration, i.e., cases in which the appropriate study requires high vertical and lateral resolution of near surface targets, the refraction seismic method is one of the most powerful geophysical tools provided appropriate procedure is adopted during field operations. It is argued that refraction seismic method could bear much useful information provided the resolution required is well afforded and appreciated by the interpreter, which at times reflection seismics cannot provide in the near surface, economically and efficiently in comparison. Consequently, the respective method must be selected when it is the -

obvious choice. General criteria for selecting the refraction method and GRM data processing are often met in groundwater exploration and waste site evaluations which are a) the target is shallow b) lateral velocity and dip changes on the target are expected or are themselves the anomaly of interest, and c) there are only a few targets are of interest.

## 2.2 Shear Waves (S-Waves) and Near Surface

Not much research work has been reported specifically where S-waves have been rigorously studied in laboratory for near-surface investigations, in fact, much of the S-wave investigations work reported have been in oil and gas exploration serving specific interests only. This section details literature focused on S-waves and their propagation that are most relevant for the thesis research, including characterization of anisotropy, improved illumination with lateral and vertical resolution, SH and SV polarizations, sensitivity to velocity gradients, attenuation, dependence of resolution upon source type, and appropriate geophone spacing and array geometry.

### 2.2.1 Earlier Developments and Field Trials

The earliest but rather indirect and speculative observation of the S-waves or transverse waves is reported in Horton (1943). A P-wave well velocity measurement survey was done by Shell Oil incorporated in Vernon Parish, Louisiana. Two shots were taken out side of the well at 960 and 1046 feet distances while the seismometer or the geophone was placed inside the well. The examination of the seismograms was reported also to show other well defined events than the primary events. These secondary events were assumed as transverse waves. There potential was quickly realized technically, in enabling to determine the properties of some zones of interest consisting of clays and sands. It was also established that these waves could not be generated either at or close to the shot points, so it was quite evident that they would have emerged or reflected from the interfaces as some kind of converted mode. Horton (1943) was not convinced however if there was ample evidence available that

whether the secondary arrivals treated in the analysis were transverse waves originating from reflection of compressional waves at the base of the weathered layer or they were transverse waves originating at the shot point. The computations based on the premise that they were the former, resulted in obtaining plausible values for the elastic constants and for the variation of these quantities with depth. Indirectly thus the potential of multi-mode acquisition and the potential of transverse waves in probing the near-surface weathering above bedrock was identified but not very well appreciated, perhaps.

Ricker and Lynn (1950) conducted a multi-component acquisition survey where an interpretation revealed the identification of the mode converted S-wave's potential as a tool for improving resolution and delineating subsurface structure. In studying the arrival times a prominent and well isolated disturbance was observed. The arrival time of events occurred in the comparatively quiet region with little noise between the arrival of the primary disturbance i.e., dilatational or P-waves, and the arrival of the ground roll, thus the disturbance was well isolated. Two types of geophones were used or installed, vertical-component and horizontal-component. Such disturbances as strong signals were received by horizontal-component geophones which were installed with their direction of response along the line from the shot point, but were scarcely at all by vertical-component geophones. It was suspected as being a disturbance which had started transmitted as a wave of dilatation or P-wave, but had been detected as a shear wave. The evidence considered was the horizontal in-line motion of the received vibration and the time of arrival of the disturbance.

Since these early studies, research for improving understanding of shear waves had been almost always on two lines, firstly from the point of view of designing an adequate source to generate the shear wave energy of desired characteristics economical and consistent with the nature of problem at hand i.e., band width and geologic issues, and secondly appropriate acquisition of the energy/signal transmitted from the subsurface to map the subsurface where most experiments if not all have been practically exploring or probing the near surface. One of the important

contribution on similar lines is a series of studies described in Cherry and Waters (1968) and Erickson et al. (1968) on the development of a shear wave vibrator and recording system suitably designed specifically to be used for well planned experimental surveys. The system designed would enable to generate P and SH modes with reasonable control over the selected band width.

It is quite interesting to note that not only that the peculiar characteristic behavior of the S-wave propagation was identified but from the perspective of a broader research the use of elastic shear waves in the earth to supplement the information already being gained from compressional waves reflection and refraction methods was considered attractive too. The facts led to believe that it would add new knowledge about the sedimentary section/s by recording shear wave with "suitable travel paths". Cherry and Waters (1968) were somewhat following up on the works of Jolly (1956), however they adopted continuous signal technique in their acquisition. In simple terms however their presentation and/or interpretation of the times series or data was based on cross-correlogram development and examination consistent with the same scheme explained by (Crawford et al., 1960).

Another important feature in the research appeared to be identifying and signifying the need for an appropriate terminology for defining the transverse or S-waves. Cherry and Waters (1968) tend to define it as a disturbance which shall move through an infinite medium that the displacement of the point is parallel to the wave front in distinction to the P-wave where the displacement to the point is perpendicular to the wave front. They confirmed P-wave velocity is always higher than the S-wave velocity and both velocities are controlled by different kind of elastic moduli of the medium. It appears that in their attempted field work they would consider only the SH mode as a legitimate S-wave.

## 2.2.2 S-Waves Used for Near-Surface Characterization

Relatively recently, in developmental context, attention is drawn more towards importance of correct and improved interpretation of S-waves compared to highlighting phenomenological aspects of wave generation and propagation ( Dohr

& Janle, 1980). Dohr & Janle (1980) define the Vp/Vs as velocity ratio and regard it as an extremely important parameter not fairly used for the time. Velocity ratio's sensitivity is said to be ascribed to its being proxy descriptor for the elastic constants. The importance of Vp/Vs is further highlighted referring to some experimental results, done mostly for less than 1 km depths, where it differs from the value for a typical poisson's body value of $\sqrt{3}$. The difference from the typical value of $\sqrt{3}$ in subtleties provided details about the degree of consolidation, porosity and type and/or degree of saturation variation. Further attention was drawn toward where it could be useful in identifying/picking weathering zones too, unlike the sediments for which its value is around 2, as for weathering zones it should be a high value. One important inference drawn from observations/record examinations was that in the case of sediments, S-wave absorption is greater than that of the P-waves and on the analogous grounds it could be deduced that the absorption of SS waves would be greater than the PS waves since for the latter the significant part of travel path is for P-wave mode. A higher sensitivity of the pure SS waves to the velocity gradient than that of PS and P waves was also observed. This manifest was explained on the basis of the path distance travelled by SS, PS and P waves, for SS path would be longer than the P-wave which would be least sensitive and on the other hand PS wave being less sensitive to velocity gradients than the S-waves.

Helbig and Mesdag (1982) provide a detailed account on various developmental aspects of S-wave surveys, and highlighted that S-waves are very useful in imparting desired resolution in aspects of manner the S-waves tend to deform the medium which it propagates through. Stumpel et al. (1984) examined the usefulness of shear waves in determining sediment parameters of such materials as peat. The good penetration of shear waves in partially saturated or gas-containing sandy material was reported as useful for assessing such materials compared with compressional mode suffering high absorption. Either for a natural resource or from construction perspective subsurface evaluation on the basis of differences between P-wave and S-wave absorption is identified i.e., l/Qp and l/Qs. It is also identified that Qp/Qs versus $(Vp/Vs)^2$ may be used for a thorough description of lithological and

13

hydrological properties of sediments. In concluding the usefulness of the shear wave surveys Stumpel et al. (1984) summarize various near surface related problems or situations where reliable solutions could be sought using S-waves. These include lithological boundaries inside an aquifer, clear delineation of the base of an aquifer, location of cracks and voids and fault zones, with assessment of their shear moduli.

The significance of conducting combined P-wave and S-wave surveys for the near surface had prior been highlighted too, by (Imai et al., 1977). Imai et al. (1977) suggested that such practice should provide useful data enabling appropriate understanding of site condition in terms of the dynamic parameters or characteristics used in various engineering studies. Imai et al. (1977) report on a rigorous and thorough survey done almost throughout the Japan where the technique was a sort of modified refraction method especially suited to soil characterization. In employing the technique especially designed geophone would be attached/clamped inside the bore hole ranging from one to two meter in depth, and a weight drop, hammer or a small shot-fire type source could be used suggesting a direct arrival type of acquisition performed. Around 242 of such experiments were done. The final data determined as P-wave and S-wave velocity values for the sites was correlated to various mechanical properties of the soil where a reasonable agreement was reported. However the most reliable empirical relation sought was between the N-value of the standard penetration test or the unconfined compressive strength and the shear wave velocity values.

Prior to the combined S-wave and P-wave tests performed in the Japan as explained above, testing of such methodologies while proceeding with US Geological Survey and the UK National Coal Board cooperative research initiative is also reported in (Hasbrouck & Padget, 1982). The principal method to be tested for investigations was "Shear Wave Seismics". The goal appeared to be devising a seismic method for the exploration of coal in the area, at least initially. In order to find the useful methodology for prospecting firstly, they had to test their equipment for adequate performance and sensitivity, a shear wave search survey, so, for a shallow structure was done. In this tuning up procedure sensitivity of the S-wave

signals to the change in the polarity of source and/or the geophone alignment/geometry was examined. A comparative analysis of the reflected P-wave and S-wave velocity was also performed. Identification of SH refracted and reflected arrivals were made. Issue of attaining reasonable temporal resolution was also addressed by examining S-waves for identifying fine enough discontinuities. The interpretation overall turned out a success for the clay bed surveyed as flat laying beds within and immediately below the clay could be identified, along with the discontinuous horizons further below.

The second shear wave survey was for locating a coal subcrop, with refraction method. Some prior knowledge of the geological and stratigraphic detail of the area helped, especially when the depth of the overburden was available, design an adequate geophone array. The time difference between the refractions through the sandstone above and below the subcrop could be used to determine the depth of the subcrop. The coal bed/seam on the roof and foot side would be bounded by the sandstone layers. The layers or stratum of the sandstone below the seam would terminate and would not extend to the end of the subcorp, thus allowing such an anomalous situation where boundaries i.e., boundary limit effect, could be inferred delineated after adequate data acquisition planning. The third study in this testing and evaluation project was doing a survey for an old abandoned mine. The discussions of results are deducible to confirm that, even for a speculative interpretation, velocity and amplitude change in the signals was reported as interacting with structural anomalies. Frequency response to cavity was termed as "resonating" character of the trace. And the issues of resolution were also found where the transmission of SH was described as not being able to "pass" i.e., see, a feature at times.

In summary, the usage of S-wave surveys for near-surface characterization had developed and been applied to several special situations requiring significant resolution. These include lithology delineation, resolving acoustic transparency or "blindness", delineation of cracks and fissures, faults, fault orientations, preferential alignments of geological units/members, barriers, and acoustic contrasts.

## 2.3 Electrical Methods in Near Surface

Electrical methods normally investigate to depths limited by the geometry of the electrical probe array and are therefore well suited for near-surface investigations (Auken et al., 2006). They have been applied to near-surface geological mapping, waste-site characterization, plume delineation, hydrogeological mapping for the spatial extent of aquifers and their degree of vulnerability, exploration or unconsolidated materials such as gravel, sand, limestone, and clay, geotechnical investigations of building and road construction sites, and location and identification of subsurface utilities, unexploded ordnance, and many others. This section will give a brief summary of their application for near-surface characterization.

### 2.3.1 Early Developments and Practical Issues

Rust (1938) provided developmental details of the early history of electrical methods for prospecting and exploration. In 1830, the first person ever to identify subsurface, or more precisely, exploitable electrical properties for exploration purposes in ore deposits was R.W. Fox. Fox proposed that "electric currents and potentials were associated with certain ore deposits in Cornwall", where he meant occurrence of natural electric potentials. Early electrical probes were highly sensitive to near-field effects, and Ambronn in 1913 reported a two-electrode method in an application of well logging where the drilling fluid in the well served as an unaltering medium in the near vicinity of the electrodes, with one electrode fixed and the other being the tool itself. A modification of the two electrode method was introduced by Schlumberger in 1912 with the development of equipotential line maps and later improved by others (Lundberg & Nathorst, 1919) and patented (Nichols & Williston, 1932). The general idea was that the displacement from the predetermined regular equipotential "characteristic lines" for a constant/in-varying earth would determine the deviated but constant horizons of equivalent potential lines depicting subsurface anomalies, for offering improved interpretation.

16

Wenner of U.S. Bureau of Standards in 1916 introduced the method of "apparent resistivity" measurements, which had shown the promise of exact or numerical computation of the depths of the horizons compared to the potential maps/curves where they would only give a graphical idea when being aberrant from the standard characteristic curves. This work was done using direct current, however equipotential maps using alternating current had also been developed, with the first survey method using an alternating current and telephone receivers as reported by Daft and William (1906). Radio frequencies or RF range had also been proposed for subsurface prospecting and morphological delineation by (Leimbach & Lowy, 1910). In a patent method (Blau, 1933) proposed the electrical transients for the subsurface prospecting. In the transient method a sudden, extremely sharp pulse of current is introduced into the ground by completing the circuit consisting of the ground, electrodes, connecting wires powered by batteries.

Regarding lateral heterogeneities, Gish and Rooney (1925) developed a resistivity method for depth determination in a horizontally bedded earth that is naturally suited to be applied by civil engineers to determine the depth to bedrock. In (Stefanesco et al., 1930) also is reported work on computing the resistivity in a horizontally layered earth. To map lateral discontinuities in the overburden such as faults Hummel (1932) and Tagg (1930) computed resistivity curves for the Wenner configuration across a vertical fault plane, and (Hubbart, 1932) and (Leonardon, 1932) published fault investigations using the Wenner configuration with constant electrode spacing. Hedstrom (1932) developed closed form solutions for situations with one vertical discontinuity plane between two and/or isotropic-media of different resistivities. It was claimed that the description should address situations of nearly vertical rock contacts and dikes, nearly vertical faults, breccias having nearly vertical boundaries.

A mention of laboratory work assumed by the U. S. Geological Survey is made by (Dobrin & Dunlap, 1957) regarding electrical prospecting aimed at making electrical and related measurements on rocks to seek various sorts of data. Measurements included electrical resistivity, dielectric constant, magnetic

susceptibility, remnant magnetization, thermal conductivity, and elastic and plastic behavior. Similar work of E. J. Moore of Pennsylvania State University is also cited on properties of rocks as were also studied effects of pressure, wettability, moisture content and chemical constituents on their electrical properties. A significant initiative was experiments done using synthetic or simulated rock cores or earth materials, at University of Utah, to investigate the changing percentage of lead or the change in the fractional volume of the saturating and conducting fluid. Dobrin and Dunlap (1957) further describe the efforts invested in the development of Induced Polarization Method as Theodore Madden at MIT was reported to investigate the frequency dependence of the impedance of the metallic mineral content in the ore bodies. A prospecting method based on this relation successfully tested in the field was also a significant achievement where U.S. Geological Survey started developing system for logging by induced polarization equipment too. A new electrical prospecting method was also reported to be studied and investigated by Theodore Madden experimenting with a technique on the lines of resistivity prospecting. In that particular method apparent resistivity is recorded with multiple-sender and multiple-receiver apparatus. Semi-quantitative interpretation methods had also been developed for a non-horizontal but layered earth.

## 2.3.2 Modern and Advanced Developments

Rice et al. (1981) while discussing the developments in engineering geophysics signify the contributory advancements in electrical methods, in addition to seismics. They remark electrical resistivity measurements, alongside seismic reflection and refraction as the most commonly used surface method of the time. Especially particular references made about the sensitivity towards assessing fluid saturation effects. Borehole logging requirement, if really required in some applications, is mentioned too for reliability fulfillment. Interesting to note is that regarding implementing reflection and refraction techniques alongside electrical resistivity methods extensive use of shear wave velocity for earth materials is

rendered as more sophisticated measurement, which as required, to calculate their ability to withstand shear forces is also identified.

Attention is also drawn towards usefulness of time lapse electrical monitoring of percolation of the water from such bodies as reservoir or dams into the banks. A successful example is cited where electrical resistivity surveys were done from one to two months continuously. The observation points were fixed which were situated on the significantly large reservoir in the Caucasus in the fissured igneous rocks. The sounding results over time provided sufficient evidence of changing hydorgeological conditions, indicating a gradual filling of pores cracks and fissures with water. Special mention is also made where the percolation of fluids or water, even not chemically hazardous, could change the conditions of internal strength and competence in the embankments and rock slopes due to pore water pressure changes and trigger a land slide or slope failure. In such conditions combination of methods especially electrical resistivity first followed up by seismic S-wave survey is recommended.

Application of seismic and electrical surveys by exploiting the contrast of the physical properties of bedrock and landslide material allow, distinguishing slip surfaces, and investigating the degree of possible rock disturbance/destruction. They also help determine the degree of water saturation, stress, stability of landslide bodies and determination/prediction of the direction and rate of landslide displacements. Ogilvy and Bogoslovsky (1979) offer personal account of investigating on one of the mountain slopes on the Black Sea coast of the Caucasus near the town of Sochi, where flowing landslides began to develop on a slope due to an incorrect agricultural cultivation of the territory, causing loosening and abundant irrigation of the soil layer in particular. Further electrical surveys, for similar circumstances, offer promise to address the problems of slope failure and slides in quarries as in natural slopes, where the development of weak zone, as established within the limits of the linear proportionality of Hooke's law, may also disturb geoelectrical stationarity, as of (Nechaev & Martynov, 1965).

Some interesting but unique examples of the use of electrical resistivity surveys with success in groundwater contamination and pollution assessments have been cited by (Stollar & Roux, 1975). In this regard four small scale surveys have been reported mostly involving industrial installations or activity. The issue of resolution from the point of view of inherent subsurface detectability is also brought to attention. Especially where the underground geologic electrical properties being very close to contained fluids may prove the application of the method unsuccessful, including effects of subsurface infrastructure and human/measurement error too. Such circumstances also emphasize seeking prior subsurface geological knowledge, in planning a subsurface survey. Common aspect of all the surveys was they were conducted to investigate contaminated aquifers overlain by unconsolidated sediments and alluvial deposits.

In one of the site investigated variety of concentrated chemicals from storage tanks or ponds had percolated into the subsurface aquifer and the limits of the contamination were determined to assist in a follow up sample drilling survey and abatement program. Electrical sounding were performed with a 3ft electrode spacing reaching a depth range of 3ft to 50ft, successfully. In another survey around 62 soundings were performed in order to clearly determine the extent of the contamination in the aquifer. Electrode spacing 60ft was maintained for sounding in this survey. This situation was different from the first case as the contamination had reached the aquifer from a surface spill. The extent of contamination was determined accurately as it was confirmed by the subsequent drilling and well sampling surveys. Third of such a survey was done to define the spatial extents of a contaminated plume associated with a solid land fill site of 50 acres. In general this survey was to determine the subsurface geology and bounds of the subsurface aquifer vertically and laterally and further to determine any associated contamination effects from the land fill, for which 17 more sounding tests were performed. Depth to bedrock, extent of the aquifer and various zones of contamination and natural water were also defined successfully along with the extents of the contaminating plumes. The fourth such survey was not conclusive due to some specific reasons as reported being extensive

20

man made features and obstacles, relatively larger depth to the aquifer, insufficient detectability of electrical conductance compared to surroundings, alongside severe geological heterogeneities over the plume to be investigated in the aquifer. All the studies basically had been aimed at contaminated plume characterization with the premise that the contamination does not really tend to diffuse in the porous environment containing the natural water but somewhat remains separate from the main body of water within defined and detectable bounds as it travels from its source to where it is identified at discharge.

# Chapter 3: Theory

## 3.1 Elastic Wave Propagation

This section is a review of fundamentals and principles of elastic deformation propagation in elastic media form ray, continuum and potential theory perspectives as explained. Mathematical descriptions and equations have been described or derived to add clarity, given scope and relevance regarding near surface engineering and environmental applications, as discussed.

### 3.1.1 Body Wave Propagation and Definitions

A seismic source is a mechanical vibration/shock that results in dynamic displacement within a material and radiates elastic waves in all directions. Those waves that propagate away from the source through the volume of a material are called body waves while those that propagate near the surface are called surface waves. Body waves, in isotropic and homogeneous media, propagate as a spherical shell or wave front with the perpendicular to the tangent on the wave front defining the wave or ray direction. Body waves with particle motion parallel to the wave direction are P-waves, and those with particle motion perpendicular the wave direction are S-waves. Surface waves have a more complex particle motion relative to the wave direction and the surface. The particle motions for P- and S-waves and the two most frequently encountered surface waves (Rayleigh and Love Waves) are shown in Figure 3.1.

P-waves can be propagated through both solids and fluids (liquids and gases), while S-wave can only be propagated through solids. Further treatment of P- and S-wave propagation is given in the following sections, specifically within the context of theoretical and empirical models.
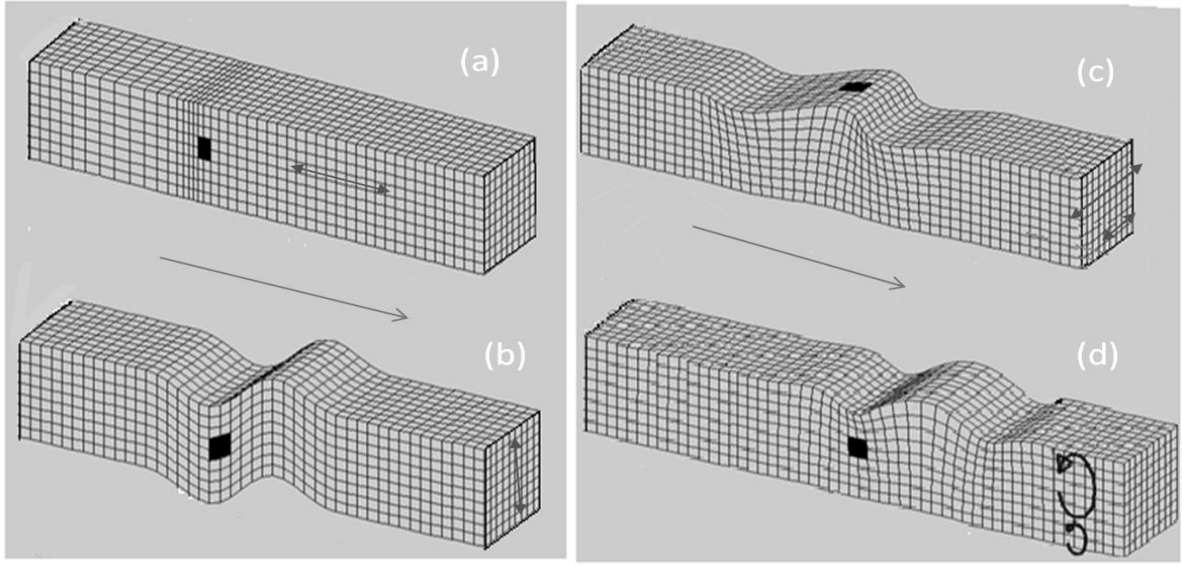
**Figure 3.1. Various common wave propagation modes (a) P-wave, compression or dilatational, (b) S-wave, torsional or transverse (c) Surface , love wave  (d) Surface, Rayleigh wave, modified, (Reynolds,1997).**

### 3.1.2 Elastic Wave Propagation Continuum Approach

In general the continuum theory encompasses the concepts of stressed motion and deformation, law of conservations of mass, linear momentum, conservation of momentum, energy and upon the constitutive relations. According to Newton's law the acceleration or displacement of a point in isotropic elastic continuum is related as follow:

$$F = ma \qquad\qquad 3.1$$

or
$$\frac{\partial \tau}{\partial x} = \frac{\partial^2 u}{\partial t^2}\rho \qquad\qquad 3.2$$

or
$$\rho\frac{\partial^2 u_i}{\partial t^2} = \frac{\partial \tau_{ij}}{\partial x_j} \qquad\qquad 3.3$$

$$2\varepsilon_{kl} = \frac{\partial u_k}{\partial x_l} + \frac{\partial u_l}{\partial x_k} \qquad\qquad 3.4$$

$$\varepsilon_{kl} = \frac{1}{2}\left[\frac{\partial u_k}{\partial x_l} + \frac{\partial u_l}{\partial x_k}\right] \qquad\qquad 3.5$$

In the equations 3.1 through 3.5 the subscripts denote the components of the vectors $\bar{u}$, $\bar{x}$ and $\bar{\tau}$ . The stress tensor $\bar{\tau}$ has two subscripts one subscript defines the orientation of the unit area (Figure 3.2) by its normal vector component and the other subscript denotes the vector components of the force per unit area parallel to the unit area, taking into account the reference axis/directions (i.e., orthogonality). One can derive the wave equation and for this purpose it is necessary to determine and/or take into account the symmetric part of deformation given total distortion (Thomsen, 2002), depicted graphically in Figures 3.2 and 3.3 described below in equations 3.6 and 3.7. The full tensor description of the elastic anisotropic stress-strain for each corresponding stress and strain component can be given as follow;

$$\tau_{ij} = \sum_{k,l=1}^{3} C_{ijkl}\varepsilon_{kl} \qquad\qquad 3.6$$

or $\qquad \tau_{ij} = C_{ijkl}\varepsilon_{kl}$ $\qquad\qquad 3.7$
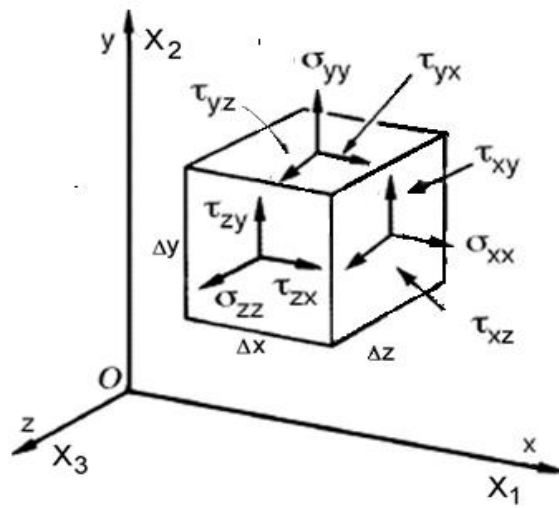
**Figure 3.2. Representation of stresses/components for unit tensor description.**
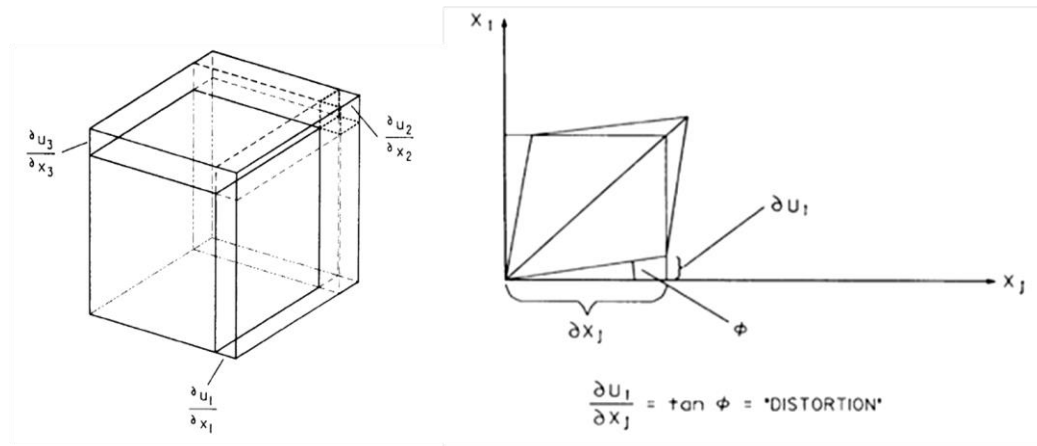


$$\frac{\partial u_1}{\partial x_j} = \tan \phi = \text{'DISTORTION'}$$

**Figure 3.3. Graphical representations of dilatation and distortion (Tatham & McCormack, 1991).**

The term $\varepsilon_{kl}$ according to the theory of elasticity is defined as a strain tensor of infinitesimal displacements, which is a second rank tensor. If it is supposed that the continuum is deformed such a way that a specific point is displaced through a magnitude denoted by vector u(x) as shown in Figure 3.3 then the strain tensor would necessarily have a definition suggesting the way total strain is averaged as depicted in equation 3.5. Incorporating the equations 3.5 and equation 3.6 in 3.3 the wave equation is arrived at:

$$\frac{\partial^2 u_i}{\partial t^2} = \frac{C_{ijkl}}{\rho} \frac{\partial^2 u_k}{\partial x_l \partial x_j} \qquad\qquad 3.8$$

In equation 3.8, $C_{ijkl}$ is the fourth-rank elastic tensor. Since at times it could be rather cumbersome, if not very difficult, to readily contemplate and understand the physical concept presented by the tensor, for one may not easily write down any of such specific case, because of the indices consisting of four numerals or subscripts involved, explained next. However, that problem was eased by Voigt (1910), who pointed out that because of elementary symmetries, the $3 \times 3 \times 3 \times 3$ tensor $C_{ijkl}$ could any stress-strain or stiffness relationship, whether governed by isotropy or anisotropy (although, since it is not a tensor, it introduces awkwardness into any analysis) following the convention in (Helbig and Thomsen, 2005). (Helbig and Thomsen, 2005). Equation 3.8 is a compact or tensorial reprsentation or generalization of the Hooke's law, a form of equation 3.6. The relation, well establieshed, not only allows depiction and examinaion of various kinds of phenonmenon falling within the elastic regime or analogous in concept, but also suffices for the description of the physical meanings of the stress wave propagations under so called cyclical and/or periodic load.

$$
C_{\alpha\beta} = \begin{bmatrix} C_{11} & C_{12} & C_{13} & C_{14} & C_{15} & C_{16} \\ C_{21} & C_{22} & C_{23} & C_{24} & C_{25} & C_{26} \\ C_{31} & C_{32} & C_{33} & C_{34} & C_{35} & C_{36} \\ C_{41} & C_{42} & C_{43} & C_{44} & C_{45} & C_{46} \\ C_{51} & C_{52} & C_{53} & C_{54} & C_{55} & C_{56} \\ C_{61} & C_{62} & C_{63} & C_{64} & C_{65} & C_{66} \end{bmatrix} \qquad C_{\alpha\beta} = \begin{bmatrix} A & H & G & P & Q & R \\ H & B & F & S & T & U \\ G & F & C & S & T & U \\ P & S & C & V & W & X \\ P & S & V & L & K & J \\ Q & T & W & K & M & I \end{bmatrix}
$$

$$
\sigma = \begin{bmatrix} \sigma_{11} & \sigma_{12} & \sigma_{13} \\ \sigma_{21} & \sigma_{22} & \sigma_{23} \\ \sigma_{31} & \sigma_{32} & \sigma_{33} \end{bmatrix} \text{or} \qquad \sigma = \begin{bmatrix} \sigma_{11} & \tau_{12} & \tau_{13} \\ \tau_{21} & \sigma_{22} & \tau_{23} \\ \tau_{31} & \tau_{32} & \sigma_{33} \end{bmatrix}
$$

$$
E = \begin{bmatrix} \varepsilon_{11} & \varepsilon_{12} & \varepsilon_{13} \\ \varepsilon_{21} & \varepsilon_{22} & \varepsilon_{23} \\ \varepsilon_{31} & \varepsilon_{32} & \varepsilon_{33} \end{bmatrix} \qquad \tau = \begin{bmatrix} \tau_{11} & \tau_{12} & \tau_{13} \\ \tau_{21} & \tau_{22} & \tau_{23} \\ \tau_{31} & \tau_{32} & \tau_{33} \end{bmatrix}
$$

$$
\widetilde{\mathsf{T}} = \widetilde{\widetilde{\mathsf{C}}}\widetilde{\mathsf{E}} \qquad\qquad 3.9
$$

The equation 3.9 components, stiffness formulation, correspondence to above tensor representation  be deduced or understood while taking into consideration the vector indices resprestaions of the stress and strain orientations shown for any continuum element in Figure 3.2 (Thomsen, 2002). Equations 3.10 and 3.11, so, are deducibly, expansions of equations 3.7 and 3.9 in concpet. The conceptual role of $C_{ijkl}$ which is the inherent property of a material/medium has special significance from a continuum

$$\mathrm{T}_{11} = C_{1111}\mathcal{E}_{11} + C_{1112}\mathcal{E}_{12} + C_{1113}\mathcal{E}_{13}$$

$$+ \; C_{1121}\mathcal{E}_{21} + C_{1122}\mathcal{E}_{22} + C_{1123}\mathcal{E}_{23}$$

$$+ \; C_{1131}\mathcal{E}_{31} + C_{1132}\mathcal{E}_{32} + C_{1133}\mathcal{E}_{33} \qquad\qquad 3.10$$

$$\mathrm{T}_{12} = C_{1211}\mathcal{E}_{11} + C_{1212}\mathcal{E}_{12} + C_{1213}\mathcal{E}_{13} + \cdots \qquad 3.11$$

perspective in assigning definitions to a medium. The material type and property since would control the manner and speed/velocity with which a wave would be predicted to travel in a medium. Here few definitions would be provided to help arrive at deriving wave equations on the basis of discussion and descriptions so far. Based on the arbitrary description of a body into elements, if all the elements have the same property it is called homogeneous otherwise it is defined as an inhomogeneous body/medium. So if $C_{ijkl}$ of a medium do not assume spatial variation the medium would be defined as homogenous medium however the presence of a spatial variation of this property would mean an inhomogeneous medium.  A truly isotropic medium or body is ideal, however there could mediums or situations which would allow for the condition of an isotropic description. These definitions and assumptions within practically plausible bounds allow us to arrive at such a configuration of the stiffness or elastic tensor where assigning a physical meaning and understanding to elastic wave propagation is much clarified. The condition of isotropy helps reduce the number of elastic constants $C_{ijkl}$ to only two, in effect.   Conventionally the two constants are denoted by λ and μ and collectively described as Lame's constants.  The symbol  μ  signifies a quantity called the modulus of rigidity and in other fields of scientific or engineering studies could be denoted by G which is a measure of capability of the body to resist a shape change.  Shear modulus is defined as pure shear stress divided by shear strain or it is the ratio of the shear stress to shear strain.

From dimensional perspective, depending upon the limiting conditions, it could be determined as $\gamma_{xy} = \frac{\Delta l}{l} = \frac{\Delta u}{\Delta x}, \gamma_{xy} = Tan\phi \ or \ \gamma_{xy} = \phi$, simply. So based on the simple definition the relation obtained is $\mu = \tau/\phi$ , with the physical meanings of a stress required for unit strain and described by units of force per unit area i.e., N/m$^2$. Before arriving at expressing some important relations another important quantity worth mentioning and defining is the bulk modulus. It is the body or material's capacity to resist change in volume tended to be affected by a change in the hydrostatic pressure. Bulk modulus is denoted by *B* or *K* and the relation to determine the bulk modulus is found as $K = V(\frac{dp}{dv})$. The equation shows that the bulk modulus is the change in volume with respect to change in pressure, in the original volume. The units so would have the same dimensions as N/m$^2$ which is also referred to as Pascal in many texts. The mutual relations of the quantities described above and their relation pertaining to elastic tensor formulation enjoy special importance in several forms of wave propagation related analysis and interpretations in science and engineering. The constants are related to the general elastic tensor as follows:

$$C_{1122} = C_{1133} = C_{2233} = \lambda$$

$$C_{1212} = C_{1313} = C_{2323} = \mu$$

$$C_{1111} = C_{2232} = C_{3333} = \lambda + 2\mu \qquad\qquad 3.12$$

Out of the 21 coefficients populating the stress tensor given equations 3.10 - 3.12,

The Hooke's Law becomes;

$$T_{ij} = \lambda \Delta \delta_{ij} + 2\mu \varepsilon_{ij} \qquad\qquad 3.13$$

Where $\delta_{ij}$ is the kronecker delta or unit tensor, and symbol $\Delta$ is equivalent to $\varepsilon_{ii}$ . The above represents a compact form of overall strain response to an external stressing agent both direct strain and torsional/shear strain. As a consequence Lame's paramenters indicated above should also have the uints of stress. The equation is a generalized stress-strain equation with the conditon of cooridinate axis not coinciding with the principal axis of the stress tensor. In order to make tha case of arriving at the wave equatios simpler and avoide redundacy and repitition of symbolic represetations a vecotrial or tensorial representation would be preffered, the equation 3.13 (Wasley, 1973) thus becomes;

$$T_{ij} = \lambda \varepsilon_{ii} \delta_{ij} + 2\mu \varepsilon_{ij} \qquad\qquad 3.14$$

Recalling equations (3.4) and (3.5) the above equations could be rewritten as

$$T_{ij} = \delta_{ij} \frac{\partial u_k}{\partial x_k} + 2\mu \frac{\partial u_k}{\partial x_k} \qquad\qquad 3.15$$

### 3.1.3 Wave Velocity and Empirical Relations

Now rewriting the equation of motion as it was introduced in the beginning, for a per unit volume case, i.e., recalling,

$$F = ma \quad \text{and in corrolory}$$

$$F_i = \rho\ddot{u} \qquad\qquad 3.16$$

$$F_i = \frac{\partial \tau_{ij}}{\partial x_j} \qquad\qquad 3.17$$

Substitution and rearrangment would give the equations

$$\rho\ddot{u} = (\lambda + 2\mu)u_{k,ki} + \mu u_{i,kk} \qquad\qquad 3.18$$

The same equation which is basically the equation of motion, when in the vector notation becomes;

$$\rho\ddot{\mathbf{u}} = (\lambda + 2\mu)u_{k,ki} + \nabla(\nabla.\mathbf{u}) - \mu(\nabla \times \nabla \times \mathbf{u}) \qquad\qquad 3.19$$

From the abvoe equation the equations for the P-wave and S-wave propagation could be derived. Taking the divergence of the above equation while taking into account the identities, operators and indices the rearrangement gives the following form;

$$(\lambda + 2\mu)[\nabla.\nabla(\nabla.\mathbf{u})] = \rho\frac{\partial^2(\nabla.\mathbf{u})}{\partial t^2} \qquad\qquad 3.20$$

31

$$(\lambda + 2\mu)[\nabla.\nabla(\nabla.\mathbf{u})] = \rho\frac{\partial^2(\nabla.\mathbf{u})}{\partial t^2} \qquad 3.20$$

The divergence of the displacement  called dilatation, and it  is a scalar quantity which could be represented as;

$$\vartheta = \nabla.\mathbf{u} \qquad 3.21$$

$$\vartheta = \sum e_{kk} ,= \sum \frac{\partial u_k}{\partial x_k} \qquad 3.22$$

Rearrangement of equations 3.20 given 3.21 and 3.22 the equation obtained is as follow which is the Pwave equation, also called dilatioanal wave as discussed before in basic definitons;

$$\frac{\rho}{(\lambda+2\mu)}\frac{\partial^2\vartheta}{\partial t^2} = \nabla^2\vartheta \qquad 3.23$$

Following rearrangement shows the curl of the equaion of motion as;

$$\frac{\rho}{\mu}\frac{\partial^2(\nabla\times\mathbf{u})}{\partial t^2} = \nabla^2(\nabla \times \mathbf{u}) \qquad 3.24$$

Equaion 3.24 is equation for S-wave or shear wave propagaton. Examination of equations 3.20  to 3.24  in a comparitive setting would clearly reveal that how wave propagation is tied to density and both the mechanical properties of the medium in

scaling displacements in time. A mathematical insight would also show that in P-wave propagation divergence of a gradient in displacement occurs for a size/volume change however in case of a S-wave same occurs for a curl to affect a shape change without any cahange in volume or size. The meanings of equations are tied to the nature of different definitions. Various relations which emanate from the definitions and description of elastic waves, among different elastic constants and properties are provided below;

$$\mu \equiv \frac{1}{2}\left[\frac{E}{1+v}\right] \ , \ \ E = \frac{3\lambda+2\mu}{\lambda+\mu} \ , \ v = \frac{\lambda}{2(\lambda+\mu)} \ , \ K = \lambda + \frac{2}{3}\mu \ , \ K = \frac{E}{3(1-2v)} \ \ 3.25$$

Other relation in addition could be deduced/derived from equation 3.25 considering the definition and dimension of the wave velocities, especially in the rock physics and earth materials context. The equations for compressional wave velocity and shear wave velocities which are usually denoted by $V_p$ and $Vs$ are expressed as follow, (Tatham & McCormack, 1991), (Wasely, 1973).

$$V_p = \left(\frac{\lambda+2\mu}{\rho}\right)^{1/2} \qquad\qquad 3.26$$

$$V_s = \left(\frac{\mu}{\rho}\right)^{1/2} \qquad\qquad 3.27$$

These equations of the velocities owing to the basic assumptions of derivation , for an isotropic solid, indicate a plane wave may propagate with only two distinct velocities, independent of the wave orientation, wave with no roation and wave with

no dilatation. The solution is defined upon that stiffness tensor is symmetric and positive definite or the diagonal of the stress tensor is not zero. This could also be understood by eximinig the strain energy fuction formulation, understanding of which allows not only clear discernment of the work/energy relaion to strain but aslo confirm that the stability condtions are based on the elasticity matrix being positive definite. From the equivalece of stress strain relations, strain energy function could be written as follow;

$$W = \tfrac{1}{2}(C\varepsilon).\varepsilon \qquad\qquad 3.28$$

Where $C$ being the stiffness matrix and $\varepsilon$ being the strain matrix . Equation 3.28 descibes that matrix $C$ is assumed positive definite if and only if $(C\varepsilon).\varepsilon \geq 0$  for all $\varepsilon / \varepsilon \neq 0$.  Following the same, the stability conditons can be examined for the symmetric stiffness tensor itself too.  It could be easily dertemined that for any solution to exist, it should be based on the determinant  of the stiffness tensor;

$$C_{mm} > 0 \qquad\qquad 3.29$$

Thus  a solution only exists  when  the  diagonal elements of the stiffness matrix/tensor are positive,   and gaurantees existance of two solutions (Slawinski, 2010).  In lieu , out of  the discussion to this point, one can express or understand the elastic P-wave and S-wave equations as the propagation of principal stresses and propagation of the shear stresses correspondingly, at significantly different speeds. It should also feel useful that the displacement vecotrs discussed and described above could be examined decompsed into dilational and rotational components, since they exist, for  requirements met. The most usual method is Helmholtz,  due to which it the

components could be written as below after an arbitrary selection of a scalar and vector variable , say θ and ψ respectively. The total  vector displacement decomposed as scalar and vector components could be written as the following equation;

$$u = \nabla\theta + \nabla x\,\psi \qquad\qquad 3.30$$

An addtional condtion that should be imposed is θ and ψ is as below;

$$\nabla.\psi = 0 \qquad\qquad 3.31$$

$$\nabla.u \equiv \vartheta = \nabla^2\theta \qquad\qquad 3.32$$

$$\nabla x\,u \equiv \varphi = \nabla^2\psi \qquad\qquad 3.33$$

The variables pairs $\vartheta$, $\theta$ and $\varphi$, ψ represent a connection between the usual meanings i.e., dilatational and rotational components, and where $\theta,$ ψ are referred to as dilatational poetntial and rotaional potential, components, respectively. The physical meanings of the expression would be that dilatation component is equal to the Laplacian of the scalar potential while the rotational component is equal to the Laplacian of the vector potential . The expressions hold only in a rectangular frame of reference (Grant & West, 1965) and (Slawinski, 2010).

## 3.2 Wave Propagation with Layers, Fractures, and Interfaces

The preceding section dealt with wave propagation in homogeneous media. Rock formations are inherently inhomogeneous with various zones, layers, fractures, joints, and interfaces. This section addresses relevant theory for this.

### 3.2.1 Wave Propagation Normal and Parallel to Layers and Interfaces

Treatment of this subject considering SH particle motion with a preexisting normal stress or memory effects provided, is provided by (Miller & Tran, 1979). Such expressions are formulated or derived as to account for the amplitude and phase of the reflected and refracted waves, and for the partition of energy in the system. The approximate analytical treatment suggests that the net relative displacement across the interface could be understood from as displacement caused by the transmitted energy less the displacement caused by the reflected ray as they would directionally oppose. The relative displacement or slip is described or shown to be inherently controlled by angles of incidence, and refraction and reflection of particular wave number and frequency given velocity characteristics or material properties.

An exact solution, but based only upon Coulomb friction criterion is also described to be useful in the understanding of the wave propagation associated stick-slip type phenomenon. Possible slip zone is assumed to be caused by the horizontal (shear) stress component of the applied or incident (oblique) shearing force. It is characterized by a central maximum and/or a minimum with its bearing upon a certain periodicity associated with the incident and the reflected energy, assumed as an odd function of phase variables with the least wave number of $2\pi$ when the respective phase angles of incidence and reflection are considered minimum. The slip displacement traverses this maxima and minima bound defining a slip zone size with a velocity (i.e., slip velocity) variation, which becomes zero at a certain time, defined as phase variable of partial rate of change of displacement. The end of the slip zone indicates starting of "immediately adjacent" stick zone which could only be realized with the continuity of the shear stress, but occurring in manner possibly similar to that
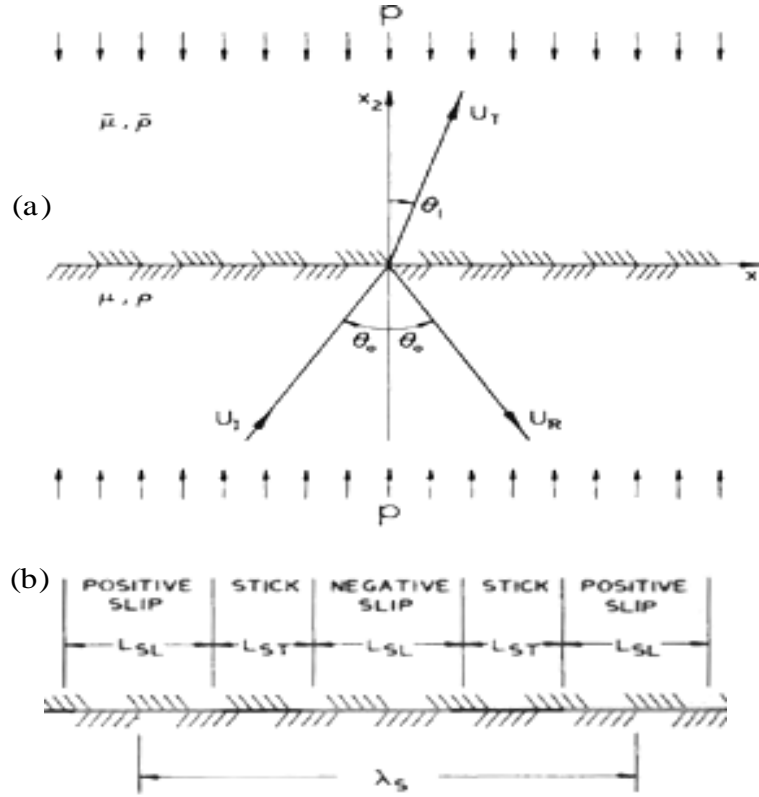
**Figure 3.4. (a) Incident reflected and transmitted waves (rays) across a frictional interface between two semi-infinite comparable unidentical layers under well defined compression. (b) Conceptualized alternate slip (LSL) and stick (LST) length regions due to shearing by duration of single wavelength periodicity (Miller & Tran, 1979).**

for slip zone, crossing a zero, but opposite in sign with time, correspondingly. The stick zone terminates when the frictional stress or energy build up (slip stress) giving rise to finally another slip zone with provision of the continuous stress condition held and thus the process continues, in a periodic sense. Coulomb friction requires that at a given location along the interface two media can remain in perfectly welded contact so long as the local shear stress does not exceed a "slip stress," which is of special significance. Magnitude of slip stress is the product of the local normal stress and the coefficient of friction between surfaces.

When the local shear stress builds up to the slip stress, local relative slipping occurs between the solids. As a result emergence of a pattern of "stick" and "slip" zones formed at the interface during the passage of the incident SH wave is expected, moving with characteristic wave speed. The overall situation is much more

complicated than any simple one dimensional case as sticking or slipping may occur simultaneously possibly at every location along the interface.

The approximate solution is found to provide useful estimates of such additional detail, as the geometry of the alternate stick and slip zones which travel along the interface, developed based on equivalent linearization, for the discussed case. Equivalent linearization in simple terms accommodates, to recall, a) non linearity of displacement and velocity b) hereditary and/or memory effects and c) well defined non-white stimulation in space-time. Given the properties of Snell's law, it is deducible from Figures3.4a and 3.4b that the slipping is accompanied by a reduction in the portion of the energy carried by the transmitted wave, an increase in that portion carried by the reflected wave, and the onset of energy absorption at the interface. The relative slip discussed above across the boundary may be defined as equation of motion for frictional non linearity, considering Snell's law as follow:

$$s_H(x_1,t) \equiv \bar{u}_3(x_1,0,t) - u_3(x_1,0,t) \qquad 3.34$$

$$u_3(x_1, x_2, t) = A_o Sin(kx_1 \sin\theta_\circ + kx_2 \cos\theta_\circ - \omega t) + \\ U_R(kx_1 \sin\theta_\circ - kx_2 \cos\theta_\circ - \omega t - \phi_R) \qquad 3.35$$

$$\bar{u}_3(x_1, x_2, t) = U_T(\bar{k}x_1 \sin\theta_1 + \bar{k}x_2 \cos\theta_1 - \omega t + \phi_T) \qquad 3.36$$

$$U_I(x_1, x_2, t) = A_o Sin(kx_1 \sin\theta_\circ + kx_2 \cos\theta_\circ - \omega t) \qquad 3.37$$

Where $u$ represents displacement, $k$ is the wave number associated with frequency $\omega$ and $\emptyset_T$ and $\emptyset_R$ are the constants with meanings of phase variables. $U_I$ represents incident, and, $U_R$ and $U_T$ are reflected and transmitted rays or energy. An approximate solution leads to the expression of type provided below, ignoring the error terms with a simple arrangement for phenomenological clarity. The linearized form of the
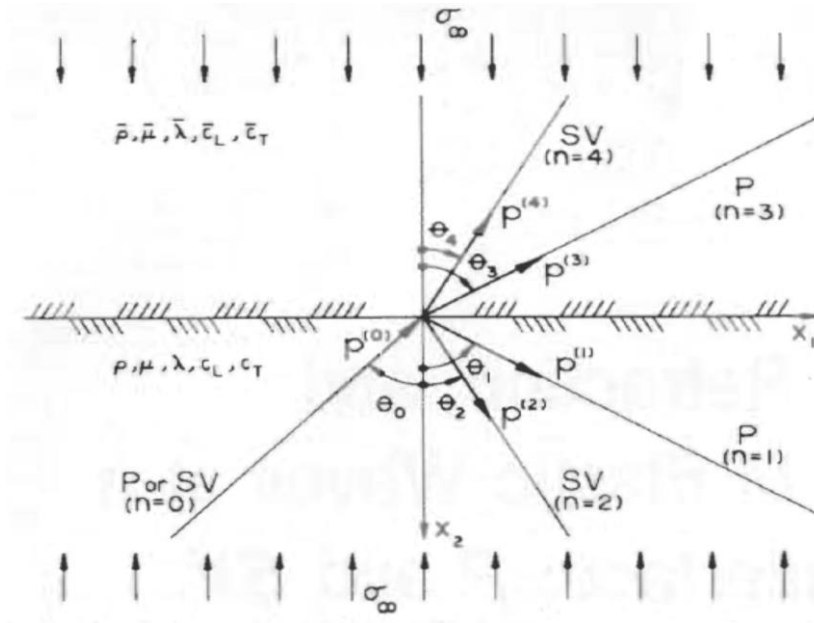
**Figure 3.5. Stress directions, orientation of coordinate directions, angels and unit vectors direction relative to the interface between un-identical elastic layers (Miller & Tran, 1981).**

solution for the slip displacement is provided below with the identification of the controlling factors where S is incident amplitude causing the relative displacement $s$, $k_s$ is the component of wave number of interest associated with the angle $\eta$ in a complex representation sense.

$$s(x_1,t) \equiv \frac{\tau_F - \beta \dfrac{\partial s(x_1,t)}{\partial t}}{\alpha} \qquad 3.38$$

$$\alpha(p,S) = \frac{1}{\pi S} \int_0^{2\pi} \tau_F(p, S\cos\eta)\cos\eta\, d\eta \qquad 3.39$$

$$\beta(p,S) = \frac{-1}{\pi\omega S} \int_0^{2\pi} \tau_F(p, S\cos\eta)\sin\eta\, d\eta \qquad 3.40$$

39

$$s_H(x_1,t) = S\cos\eta \qquad\qquad 3.41$$

$$\eta = k_s x_1 - \omega t + \phi_s \qquad\qquad 3.42$$

$$k_s = k\sin\theta_\circ = \bar{k}\sin\theta_1 \qquad\qquad 3.43$$

The ideas presented to evaluate elastic wave propagation across an interface of identical or unidentical materials considering SH waves is extended to P and SV waves, with coulomb friction type laws holding at the interface similarly, that is demonstrated in (Miller & Tran, 1981). The relative displacement in this case is described as below equations 3.44 through 3.47. Owing to different nature of particle polarization compared to the former case the directional nature of the displacements and the controlling factors are expressed differently however the nature of the control they exercise is similar.

$$s_{P,SV}(x_1,t) \equiv u_1(x_1,0,t) - \bar{u}_1(x_1,0,t) \qquad\qquad 3.44$$

$$s(x_1,t) \equiv \frac{\tau_F - \xi\dfrac{\partial s(x_1,t)}{\partial t}}{k} \qquad\qquad 3.45$$

$$k(\sigma_\infty,S) = \frac{1}{\pi S}\int_0^{2\pi}\tau_F(\sigma_\infty,S\cos\eta)\cos\eta \, d\eta \qquad\qquad 3.46$$

$$\xi(\sigma_\infty,S) = \frac{-1}{\pi\omega S}\int_0^{2\pi}\tau_F(\sigma_\infty,S\cos\eta)\sin\eta \, d\eta \qquad\qquad 3.47$$

An important aspect of the brief discussion of these models , where detail could be sought after in the references there in, is to understand that how different

particle polarizations of an elastic wave propagating "across" an interface are controlled or dominated by friction which is tied to the both  displacement and velocity in a complicated manner restricted by periodicity. The fact can also be further understood by examining Figure 3.5 and comparing with Figure3.4 given geometrical restrictions of associated mathematical descriptions. It could also be deduced from the detailed study of the analyses (not provided here for brevity) that the existence of a viscous bond may show a relatively pronounced frequency dependence and aberrances from usual interpretations with applying of such models. Presence of interfacial friction is propositioned to cause energy absorption and consequent dissipation. For SH  , SV and P oscillations or polarization the incident energy considering all may partition to  reflected, transmitted or refracted part. Amplitude ratios are suggested as a good statistic to quantify or account for dissipation and further to calculate energy ratios. Further that less energy is absorbed at the interface for incident waves of P or $S_V$ (or SV) type than for SH wave of equal shear stress amplitude. Such propositions lead to understand the importance of transient nature of wave propagation and difference in sensitivities of the elastic polarizations towards medium propagated through.

### 3.2.2 Fracture Interface Rheology

An important aspect thus of examining various possibilities of the elastic response phenomenon (predominantly ray theory) against a periodic stimulation is to understand also the control of competing fracture strength factors forming various constitutive relations. To recall , most if not all such descriptions are based upon the ideas offered in (Griffith, 1921) where not only the concept of a material strength is identified in relation to the stress it is subjected to but also signified is the physical or geometrical condition with special mention of the cracks and their direction, in damage progression. Further the idea of structural stability associated with attainment of minimum energy with time is also alluded to. Griffith's idea is useful in understanding time effects especially when stress magnitudes are low and persistive.
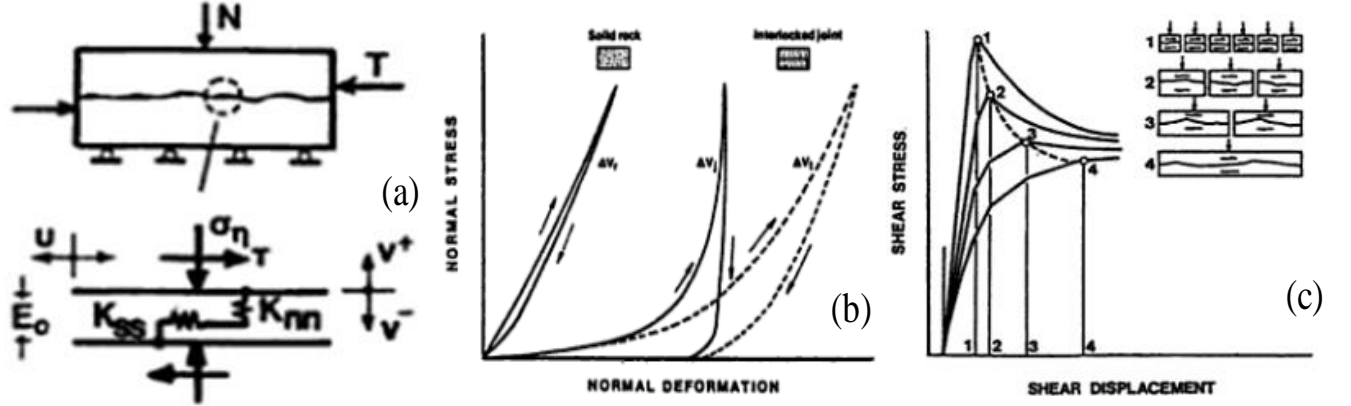
**Figure 3.6. Fundamental components of rock joint behavior, (Bandis, 1990).**

The rheological behavior of an interface which is either rock joint or fracture may be subjected to both a normal and shear stress. Above, Figure 3.6 a shows a schematic of analogue rheological components of a representative rock joint section, and Figure 3.6 b and Figure 3.6 c describe the normal and shear deformational nonlinearities in time against corresponding loading respectively. The behavior could be defined by the following relations, as described by (Bandis, 1990).

$$\begin{pmatrix} d\sigma \\ d\tau \end{pmatrix} = \begin{vmatrix} K_{nn} & 0 \\ 0 & K_{ss} \end{vmatrix} \begin{pmatrix} dv \\ du \end{pmatrix} \qquad\qquad 3.48$$

Where the normal and shear stiffnesses can be represented as below:

$$K_{nn} = (d\sigma / dv)_u \; K_{ss} = (d\tau / du)_v \qquad\qquad 3.49$$

In a rather complete form where asymmetry of stresses is taken into account the relation would follow a tensorial form;

$$\begin{pmatrix} d\sigma \\ d\tau \end{pmatrix} = \begin{vmatrix} K_{nn} & K_{ns} \\ K_{sn} & K_{ss} \end{vmatrix} \begin{pmatrix} dv \\ du \end{pmatrix} \qquad\qquad 3.50$$

For ,

$$K_{ns} = (\partial\sigma / \partial u)_\tau \quad , \quad K_{sn} = (\partial\tau / \partial v)_\sigma \quad , \quad K_{ss} = \frac{K_{nn}}{2(1+v)} \qquad 3.51$$

Poisson's ratio is denoted or symbolized by v. Rock joint or interface mechanical behavior in terms of components could be graphically understood from Figure 3.9. Both displacement dependence and the stress dependence of the strength moduli could be identified, as notion of obvious friction control cannot be overlooked, in addition to few others aspects. The moduli both $\tau$ and K bounded and limited by compression only but not by shear, however; further aperture size not only is effected by compression but also by shear as the reduction of aperture appear nonlinear with normal stress in terms of a size change. The shear stress- displacement curves suggest that fracture behavior subjected to translational shear and constant normal stress may vary from brittle to almost plastic, controlled by surface area of contact, in response. (Sun et al., 1985) provide a suitable detail of the conceptual components associated with the fracture or fault mechanical behavior including interface. Stress-deformation dependence of arrived at relations, the nature of the contacts between the asperities on adjacent joint surfaces, both in compression and shear is considered vital in predicting mechanical behavior.

Adding to the above relations being useful in understanding the nature of a single interface or crack mechanical behavior, (Hegemeir & Nayfeh, 1973) and (Hegemeir & Bache, 1973) provide an asymptotic solution of wave propagation through periodic composite laminates, when normal and parallel to the direction of propagation, respectively. It accommodates perfect joints without friction (no loss) including an effective moduli concept.  A step input is considered and several theoretical cases are examined in terms of outputs, predominantly at the centroid of the units, scaled by the wavelengths as being greater than the units of interest. Very important outcome of their treatment is that the transient pulse based results of continuum theory well approximate those exact ones of the ray theory. That, also means that continuum response understanding based on a mixture theory approach could be followed in different composite analyses. (Ting & Mukonoki, 1979) and (Hu

& Ting, 1983) offer a further examination of the wave propagation response of composite layer medium with perfect interfaces, for the case of normal and layered medium , separately, respectively, on the same lines explained above. Their scheme advocates and accounts for material properties energy loss component in addition to the geometrical effects, describing such cases as viscoelastic analogous. (Hu & Ting, 1983) has particularly identified quantifying parameters for such losses.

## 3.3 Wave Propagation and Poroelasticity

Poroelasticity deals with elastic wave propagation through saturated porous media, and the coupling between the infinitesimal momentary deformation of the rock matrix and the resulting transient flow and pressure fluctuations of the pore fluids. Many poroelastic theories are variations on the widely used Gassman or Biot Theory, which are described in more detail in this section.

### 3.3.1 Gassman Theory

Gassman theory assumes that the rock matrix material and porous frame does not interact with the fluid to alter the chemical and/or material properties of the matrix and frame, asserting that existence of a fluid shall not make the overall system complaint or stiffer compared to the original state. The saturating pore fluid is considered frictionless where all the pores are considered connected allowing for complete communication of fluid through pores, or the fluid within itself is communicative without any insulating or isolating barriers and confinements. The permeability should therefore be considered high for a fluid with a zero viscosity. The overall rock fluid system is considered closed (termed as undrained) meaning that no fluid can enter or leave the system in confirmation with conservative principles. These assumptions warrant to be accounted for while making inferences in situations where they are not strictly met. Various explanations of the assumptions could be understood from such reviews as (Wang, 2000) and (Smith et al., 2003), and other references that provide the original theory (Gassman, 1951 a, b).

Application of Gassman theory involves determining equivalent elastic parameters for the saturated media as functions of the elastic properties of the rock matrix and pore fluid. The bulk moduli of the fluid saturated medium from the known properties of the constituent phases.

$$K_{sat} = K_{solid}\left[\frac{\emptyset K_{dry} - \frac{(1+\emptyset)K_{fluid}K_{dry}}{K_{solid}+K_{fluid}}}{(1-\emptyset)K_{fluid} + \emptyset K_{solid} - \frac{K_{fluid}K_{dry}}{K_{solid}}}\right] \qquad 3.52$$

Another slightly more explicit version of the equation is shown below and (Wang , 2001), where

$$K_{sat} = K_{dry} + \frac{\left(1-\frac{K_{dry}}{K_{solid}}\right)^2}{\frac{\emptyset}{K_{fluid}} + \frac{1-\emptyset}{K_{solid}} - \frac{K_{dry}}{K^2{}_{solid}}} \qquad 3.53$$

$$G_{sat} = G_{dry} \qquad 3.54$$

$K_{sat}$ and $G_{sat}$ are the bulk and shear moduli of the "fully" saturated porous material/rock/sample. In equation 3.52 the magnitude of $K_{dry}$ is affected or scaled by combined fluid solid complex behavior unlike for the similar quantities in equation 3.54, this is because of the inherent difference in the mechanism of the combined fluid solid deformational behavior when subjected to compression and rotation. $K_{fluid}$ represents the effective bulk modulus of the saturating fluid while $K_{solid}$ stands for the bulk modulus of the mineral material as simulated by the ceramic/glass beads in this study. Matrix or frame porosity is denoted by $\phi$ (Lumley, 1994).

The density of the saturated material can be found or calculated by the equation below

$$\rho = (1 - \emptyset)\rho_{solid} + (\emptyset\rho_{fluid}) \qquad 3.55$$

$\rho_{solid}$ represents the grain/bead density or the frame/rock mineral density while $\rho_{fluid}$ denotes the fluid fraction density. The $Vp_{sat}$ and $Vs_{sat}$, compression and shear wave velocities for the saturated material can be found by using the equations (Lumley, 1994)

$$Vp_{sat} = \left[\frac{\{K_{sat} + \left(\frac{4}{3}\right)G_{sat}\}}{\rho_{sat}}\right]^{1/2} \qquad 3.56$$

$$Vs_{sat} = \left[\frac{G_{sat}}{\rho_{sat}}\right]^{1/2} \qquad 3.57$$

Dry rock properties for the reservoir are estimated from laboratory core sample measurements. The cores samples are obtained from the boreholes in the reservoirs. Dry rock porosity and density measurements are performed following standard procedures. P and S waves (100 kHz to 1 MHz) are propagated through the samples and corresponding travel times are used to determine the ultrasonic P and S wave velocities usually denoted as Vp and Vs respectively. Based on the Vp, Vs and density ($\rho$) information from the dry rock core samples the dry bulk modulus (K) and dry shear modulus (G) are determined using following equations usually.

$$K_{dry} = \rho\left[\left\{Vp^2 - \frac{4}{3}(Vs^2)\right\}\right] \qquad 3.58$$

$$G_{dry} = \rho Vs^2 \qquad 3.59$$

In case the pore fluid consists of more than one phase/fraction the bulk modulus of the fluid phase can be estimated/appreciated, for any N number of phases by the equation, which is a form of the Wood's equation;

$$\frac{1}{K_{fluid}} = \sum_{i=1}^{i=n} \frac{C_i}{K_i} \qquad \text{for} \qquad \sum C_i = 1 \qquad\qquad 3.60$$

Where, in equation 3.60, $C_i$ and $K_i$ represent the volumetric concentration and bulk modulus of the *ith* fraction respectively, implying a complete and uniform pore fluid/saturation distribution. In instances where the so called dry parameters could not be determined in laboratory, log determined values could be used in backward Gassman's equation to estimate the dry properties for further analysis; such inputs however may lack accuracy affecting towards results. The input bulk modulus and shear modulus could be determined as average values using the properties of the constituent mineralogical components, using Voigt-Reuss-Hill average (Hill, 1963). These average values are used to calculate the effective macroscopic isotropic representative moduli as follow:

$$M = \frac{1}{2} (M_V + M_R) \quad \text{Where} \quad M_V = \sum_{i=1}^{i=n} C_i M_i \quad \text{and} \quad \frac{1}{M_R} = \sum_{i=1}^{i=n} \frac{C_i}{M_i} \qquad 3.61$$

In equations 3.61 $M_V$ is the Voigt (1928) average and $M_R$ is the Reuss (1929) average where $C_i$ and $M_i$ represent the saturation or the volume fraction of the ith component respectively. (Hashin & Shtrikman, 1963) provide more tightly bound estimates of M than the Voigt-Reuss bound, however if the difference among the magnitudes of individual components moduli is not significant the effective calculated values are similar for both models.

### 3.3.2 Biot Theory

#### 3.3.2.1 Phenomenological Parameters

Biot's theory considers the porous medium in acoustic context being an isotropic disordered homogeneous medium with distinct densities, bulk and shear moduli for the solid and fluid constituent components represented as $\rho_j$ , $K_j$ and $N_j$ respectively for j or i =1,2,3.... may represent fractional components. An important aspect besides other assumptions is specific allowance for fluid solid relative movement or oscillation when considering any responses or deformations to the cyclical or frequent loading or stimulation. The realization of the phenomenon offers insights into understanding the mechanisms of acoustic attenuation and dispersion. It is assumed, in addition to a macroscopic isotropy, that the relative wavelength and grain size is comparable. It means that the grains/pores and inclusions may constitute entities in dimensions larger than the smallest pore or grain but still smaller than the wavelength , in a comparison so the wavelength can cause relative displacements restricted by the virtue of the assuming of a macroscopic bulk and shear moduli. By such definition so conventional vector and tensor representation may hold. Each volume element therefore could be assigned average response displacements or strains for the solid and fluid components. (Plona & Johnson, 1983) offer the phenomenological scheme in manner quite reasonable.

#### 3.3.2.2. Stress Strain and Equations of Motions

Biot follows the theory of infinitesimal strain where the higher order displacement derivatives are neglected and the deformation/s could be viewed as average displacement fields only. Biot formulated the theory by developing the stresses with corresponding strain relationships for each of the constituents i.e., description of dilational and rotational components, both for the fluid and solid system constituents. The formulation is comparable to an elastic formulation owing to assumptions; their meanings however were phenomenological for the nature of the composite system.

In addition to the bulk moduli of the solid and fluid constituents and that of the skeletal frame or drained material as described before, other generalized elastic coefficients were used to relate and describe the stresses to the nature of the strains. The stresses developed in the frame could be described as below

$$\sigma_{xx} = 2N\epsilon_{xx} + A\epsilon + Qe \qquad 3.62$$

$$\sigma_{yy} = 2N\epsilon_{yy} + A\epsilon + Qe \qquad 3.63$$

$$\sigma_{zz} = 2N\epsilon_{zz} + A\epsilon + Qe \qquad 3.64$$

$$\tau_{xy} = N\gamma_{xy}, \quad \tau_{xz} = N\gamma_{xz}, \quad \tau_{yz} = N\gamma_{yz} \qquad 3.65$$

$$\text{where} \quad \epsilon = \epsilon_{xx} + \epsilon_{yy} + \epsilon_{zz} \qquad 3.66$$

In the above equations 3.62 through 3.66 $\sigma_{xx}$, $\sigma_{yy}$, $\sigma_{zz}$ are normal stresses in the x, y and z directions. $\tau_{xy}$, $\tau_{xz}$ and $\tau_{yz}$ represent the shear stresses on the respective planes while $\epsilon$ and e represent dilation in the solid matrix i.e., mould or frame or specimen structure, and in the fluid respectively. A and N has the same meanings as Lame's constants denoted conventionally as $\lambda$ and G respectively. Q is a cross coupling term for the relative volume changes in the solid and fluid constituent components, given conceptual dynamism. The stress $\sigma$ in the fluid is equated to the pressure or the energy per unit weight of the total fluid volume by the virtue of existence or presence. Its magnitude is scaled by the effective porosity only, since any sealed pore space is assumed as continuous solid.

$$-\sigma = np \qquad 3.67$$

$$\sigma = Q\epsilon + Re \qquad\qquad 3.68$$

Porosity, in equations 3.67 and 3.68 is denoted by n while R is a measure of fluid pressure to cause an increase in the fluid volume in pores at constant frame volume. The physical meaning of this is an apparent relevant increase in the fluid volume due to any apparent decrease in porosity caused by change in stress state of the frame. For a zero fluid stress, so, fluid dilation for unit frame dilation would be equivalent to Q/R. It could be deduced that the dilations thus caused would be competitively reversible and compensatory in nature.

Opposed to a Eulerian one, Biot's formulation or description of theory follows mostly a Lagragian, assigning a macroscopic representative spatial sense to the parametric space for the REV. The difference in Eularian and Lagragian description is that in the former the reference frame is not static relevant to REV in space, while in the latter description the reference frame is consider fixed/ static relevant to REV and a varying of parameters, in x, y and z directions for time. It would so invite for determining the total kinetic energy for the considered volume, with energy per unit volume basis as follow:

$$T = \frac{1}{2}\rho_{11}\left\{\left(\frac{\partial u_x}{\partial_t}\right)^2 + \left(\frac{\partial u_y}{\partial_t}\right)^2 + \left(\frac{\partial u_z}{\partial_t}\right)^2\right\}$$

$$+ \frac{1}{2}\rho_{22}\left\{\left(\frac{\partial U_x}{\partial_t}\right)^2 + \left(\frac{\partial U_y}{\partial_t}\right)^2 + \left(\frac{\partial U_z}{\partial_t}\right)^2\right\}$$

$$+ \rho_{12}\left\{\left(\frac{\partial U_x}{\partial_t}\frac{\partial u_x}{\partial_t}\right) + \left(\frac{\partial U_y}{\partial_t}\frac{\partial u_y}{\partial_t}\right) + \left(\frac{\partial U_z}{\partial_t}\frac{\partial u_z}{\partial_t}\right)\right\} \quad 3.69$$

The expression shows that the total energy description at any time depends upon six displacement components only. Due to the assumption that the energy dissipation should occur with solid fluid relative motion meaning $(U_x - u_x) \neq 0$, description for the dissipation factor denoted by D in Biot's theory would be arrived at as follow keeping in view the coordinate system.

$$D = \frac{1}{2} \, b \, \rho \, \{\left(\frac{\partial U_x}{\partial_t} - \frac{\partial u_x}{\partial_t}\right)^2 + \left(\frac{\partial U_y}{\partial_t} - \frac{\partial u_y}{\partial_t}\right)^2 + \left(\frac{\partial U_z}{\partial_t} - \frac{\partial u_z}{\partial_t}\right)^2\} \qquad 3.70$$

$$\text{where} \quad b = \frac{\mu_f n^2}{k}$$

$\mu_f$ stands for fluid viscosity, k stands for permeability and n denotes porosity.

$$\rho_{11} + \rho_{12} = (1 - n)\rho_s \quad , \qquad \rho_{12} + \rho_{22} = n\rho_f \qquad 3.71$$

Presented formulations given the structure of expression could be understood further form (Corapcioglu & Tuncay, 1996). Considering above equations and over all representative system density $\rho$ could also be determined where a simple addition should allow that owing to assumptions.

$$(\rho_{11} + \rho_{22} + 2\rho_{12}) = (1 - n)\rho_s + n\rho_f \quad , \qquad \rho = (1 - n)\rho_s + n\rho_f \qquad 3.72$$

The symbol $\rho_{12}$ is mostly termed as a mass coupling factor based on the phenomenological understanding of an existence of a poroelastic-coupling. The coupling could be a solid-to-fluid coupling or fluid-to-solid one. The former has the meaning of change in fluid pressure or mass with the change in the stress state of porous frame, the latter however is similar affectively on the solid due to changes in the fluid mass or pressure. The effects considered are virtual in nature. Factors $\rho_{11}$, $\rho_{12}$ , $\rho_{22}$ are termed as "mass coefficients" . Following Lagragian approach the equations of motion where the relative forces both on fluid and solid phases are taken into consideration could be described as follow.

$$F^s{}_x = \frac{\partial^2}{\partial t^2}(\rho_{11}u_x + \rho_{12}U_x) + b(u_x - U_x) \qquad 3.73$$

$$F^f_x = \frac{\partial^2}{\partial t^2}(\rho_{12}u_x + \rho_{22}U_x) + b(U_x - u_x) \qquad 3.74$$

Similar equations with stresses and corresponding displacements could be written too in y and z directions. In this regard stress gradient could be taken as a force agency related to a measure of displacements, to rewrite the equations.

$$\text{div } \sigma_s = \frac{\partial^2}{\partial t^2}(\rho_{11}u_x + \rho_{12}U_x) + \pi(u_x - U_x) \qquad 3.75$$

$$\text{grad } \sigma_f = \frac{\partial^2}{\partial t^2}(\rho_{12}u_x + \rho_{22}U_x) + \pi(U_x - u_x) \qquad 3.76$$

The usual more compact form of the equations, so, appears as follow

$$\frac{\partial^2}{\partial t^2}(\rho_{11}\epsilon + \rho_{12}e) = \nabla^2(P\epsilon + Qe) - b\frac{\partial}{\partial t}(\epsilon - e) \qquad 3.77$$

$$\frac{\partial^2}{\partial t^2}(\rho_{22}e + \rho_{12}\epsilon) = \nabla^2(Q\epsilon + Re) + b\frac{\partial}{\partial t}(\epsilon - e) \qquad 3.78$$

One of the very important aspects, in considering Biot theory as an inferring aid in ultrasonic and/or seismic investigations, is fluid solid relative displacement effect in a vector sense i.e., (U- u), scaled or affected by a possible drag type factor identified as b or $\pi$. Implicit within this factor is combined complicated behavior of viscosity, permeability and tortuousity. It is assumed that the flow caused within the dimension defined by (U±u) is Poiseuille type, for ( a predominance of) viscous effects which could be understood as well identified in (Corapcioglu & Tuncay, 1996) and (Wilmanski, 2005).

### 3.3.2.3. Dynamics and Fluid Solid Coupling Effects

An implicit expression of above equations could be given as below. The significance of the expression in this form is that it provides a better insight into seemingly elusive contribution of apparent mass coefficient and density when understanding non-dissipating and dissipating mechanisms.

$$\tau_{ij} = \rho \frac{\partial^2 u_i}{\partial t^2} + \rho_f \frac{\partial^2 w_i}{\partial t^2} \quad , \quad \frac{\partial^2 u_i}{\partial t^2} + \sum \frac{\partial w_i}{\partial i} = -\sigma_f \qquad 3.79$$

$$\text{where} \quad w_i = n(U_i - u_i) \quad , \quad \sum \frac{\partial w_i}{\partial i} = \text{div } \mathbf{w}$$

Considering a uniform porosity one can arrive at the very important viscodynamic variable referred to in the Biot theory, and defined as an "increment fluid content". (Wang, 2000) defined it as an "increment fluid content" within the context development of its understanding given theoretical considerations. The apparent physical meanings of which are a volume of fluid flowing in or out of the representative volume under consideration consisting of a system of pore/s and or grain/s. The symbols used for this variable had been $\theta$ and $\zeta$ in literature.

$$\zeta = \sum \frac{\partial w_i}{\partial i} = \text{div } \mathbf{w} = \theta \qquad 3.80$$

The above expressions lead to understanding/s of a phenomenological significance that, at any instant the overall system resilience so shall depend upon the three invariants of the strain components and $\zeta$ too, in addition. The strain energy denoted as $\mathbf{W}$ should be a function of six strain components and $\zeta$.

$$\mathbf{W} = W(I_1, I_2, I_3, \zeta) \quad \text{or} \quad \mathbf{W} = W(e_x, e_y, e_z, \gamma_x, \gamma_y, \gamma_z, \zeta) \qquad 3.81$$

Owing to assumptions **W** has the meaning of an isothermal free energy. The terms on the right hand side are therefore affected by physical chemistry of the macroscopic fluid solid system. It shall also include interfacial and surface energy effects too in thermodynamic context, given dissipation. Original references such as (Biot, 1961), and (Stoll, 1989) provide a significant detailed of the formulation approach leading to usual stress strain relations. In addition, associated with formulations fundamentals, (Bourbie et al., 1987) and (Stoll & Bryan, 1970) also extend the discussion to attenuation related aspects and attenuation quantification considering porous and saturated sediments. Another approach in examining the above so called equations of motions for a microscopic view of Poiseuille type flow is the case where b is replaced by a corrective factor. The corrective factor is equivalent to the product of drag factor and a complex function represented as bF(ω). The equations then would take the following form;

$$\frac{\partial^2}{\partial t^2}(\rho_{11}\epsilon + \rho_{12}e) = \nabla^2(P\epsilon + Qe) - bF(\omega)\frac{\partial}{\partial t}(\epsilon - e) \qquad 3.82$$

$$\frac{\partial^2}{\partial t^2}(\rho_{22}e + \rho_{12}\epsilon) = \nabla^2(Q\epsilon + Re) + bF(\omega)\frac{\partial}{\partial t}(\epsilon - e) \qquad 3.83$$

The complex correction factor bF(ω) is also assigned the meaning of a frequency dependent complex permeability causing a scaling of the flow regime in relation to change in frequency, where all the implicit parameters of porosity, viscosity and permeability are assumed frequency dependent. The introduction of the complex factor in the equations of motion is considered inadequate because of phenomenological difference in representations in Cartesian space and Complex space as indicated by (Wilmanski, 2005), so mostly the Fourier transform of the equations are taken for the application or consideration of such factor, and to assume a relevant complex solution. Rewriting the above equations 3.82    and 3.83 considering density relations could lead to further insight regarding inertial versus viscous flow effect frequency dependence of the flow in general, as ahead;

$$(1 - n)\frac{\partial^2 \epsilon}{\partial t^2}\rho_s = \rho_{12}(\epsilon - e) - bF(\omega)\frac{\partial}{\partial t}(\epsilon - e) + \nabla^2(P\epsilon + Qe) \qquad 3.84$$

For, either $\omega=0$ where $F(\omega)=1$ or $b = 0$, $\rho_{12}$ does not vanish. This means that even for a very low viscosity fluid, comparable to an ideal one, or a very low frequency, the inertial effect of the factor $\rho_{12}$ due to a relative solid fluid solid acceleration, as a mass coupling or force would exist. It could be so deduced that combined effect of b and $F(\omega)$ controls the wave attenuation, and for a system of uniform and constant porosity and permeability viscosity is an important parameter.

For lower frequency this assumption holds however beyond a certain frequency range a (near static fluid) boundary layer is formed next to the solid phase surface. The nature of flow in the boundary layer compared to that well beyond it is not identical. The boundary layer since then tends to assume a greater magnitude of friction along the solid phase surface only because of higher or increased inertial effects. In force terms one can say that the frictional force becomes in magnitude less enough to become out of phase with the external cyclical force. It allows deducing the idea of a structure of the confined flow or fluid where one can assume that owing to nature of application of force the solid and fluid phases become less consonant and "laminar" with frequent cyclical motions i.e., structure vanishes. The relative solid fluid motion/s thus considered a primary aspect of embodying the description of wave motion, at the scales discussed, of the saturated porous medium. The total energy, may be assumed to be kinetic by the virtue of such motions. If either of $U_x$ or $u_x$ approaches in close proximity dimensionally or magnitude wise mutually then the dissipation factor shall vanish, and owing to assumptions the total kinetic energy would depend only upon solid and fluid mass fractions. The above statement could be summarized by the components the expression below as equation 3.85. It constrains the physical properties within meanings of dimensions of frequency effects and vice versa.

$$\frac{a2}{2}\,\omega(c) = \frac{\eta}{\rho_f} \qquad\qquad 3.85$$

It constrains the physical properties within meanings of dimensions of frequency effects and vice versa. Small letter "a" symbolizes viscous skin or boundary depth and $\omega(c)$ a critical frequency, which indicates a conceptual flow type regime crossover. A concise but comprehensive detail of the phenomenon could be sought from Bourbie et al. (1987), and from references there in.

3.3.2.4. Application of Biot Theory

The application of Biot Theory is normally to determine the resultant wave velocities and related parameters. The equations below show roots of the rearranged Biot equations which are usual choice of doing analytical comparisons of experimental results, explained in detail by (Plona & Johnson, 1983).

$$V_{p\infty}(fast, slow) = [\frac{\Delta \pm \{\Delta^2 4(\rho_{11}\rho_{22} - \rho_{12}{}^2)(PR - Q^2)\}^{1/2}}{2(\rho_{11}\rho_{22} - \rho_{12}{}^2)}]^{1/2} \qquad\qquad 3.86$$

$$Vs_\infty = [\frac{\mu_{fr}}{\rho - n\rho_{fl}\alpha^{-1}}]^{1/2} \qquad\qquad 3.87$$

Where $\qquad \rho_{12} = -(\alpha - 1)n\rho_f \qquad\qquad 3.88$

$$\alpha = (\frac{1}{2})\{n^{-1} + 1\} \qquad\qquad 3.89$$

In equation (3.86) "±" sign correspond to the determination of the "fast" i.e., " +" or "slow" i.e., "-" wave velocities where

$$\Delta = P\rho_{22} + R\rho_{11} - 2Q\rho_{12} \qquad\qquad 3.90$$

$$P = \frac{(1-\phi)(1-\phi-\frac{K_{fr}}{K_o})K_o + \phi K_o \frac{K_{fr}}{K_{fl}}}{1-\phi-\frac{K_{fr}}{K_o}+\phi\frac{K_o}{K_{fl}}} + \frac{4}{3}\mu_{fr} \qquad\qquad 3.91$$

$$Q = \frac{\{(1-\phi-\frac{Kfr}{K_o})\phi K_o\}}{\{(1-\phi-\frac{K_{fr}}{K_o}+\phi\frac{K_o}{K_{fl}})\}} \qquad\qquad 3.92$$

$$R = \frac{\phi^2 K_o}{1-\phi-\frac{K_{fr}}{K_o}+\phi\frac{K_o}{K_{fl}}} \qquad\qquad 3.93$$

This functional form explained through equations 3.86 through 3.93 appears to have a less ambiguity in terms of preserving the physical meanings without violating theoretical restrictions. Further this form has least or no parameters assuming or offering a close similarity of understanding or a conceptual origin leading to confusions. The fact has been found and related by (Corapcioglu & Tuncay, 1996) as different authors may assign different physical meanings to same phenomenon, suggesting caution hence.

### 3.3.3. Granular Contacts in Porous Media

#### 3.3.3.1. Principles of Contact Mechanics

Given Biot's phenomenological descriptions of wave propagation, for any detailed analyses beyond velocity predictions involving granular sediments, understanding the role of the nature of intergranular contacts in terms of possibilities

of their compliances and directional dependence is indispensible. The description based on Hertz theory mostly suffices for understanding the magnitude and orientation of the principal axes of the contact surface. Contact surface is assumed as an ellipse, and a sense of a normal distribution of component of the traction across the contact area, given the nature of contact or approach of two bodies, as shown (Mindlin, 1949). It is demonstrated that information allows for the determination of a normal and tangential compliance as normal and tangential forces are considered in the formulations both for circular and elliptical contact area. The components of tangential compliance are found to be greater than the normal compliance but not more than twice. One of the most important aspects discussed is occurrence of deformation at a constant contact area without providing for a relative slip, and further allowance for a torsional compliance component is also propositioned. The concept of an influence of a relative slip as a tangential traction, assumed though to hold within or not exceeding product of normal component of traction and force of friction is speculated. The consequence on overall deformation behavior and Poisson's ratio conjectured where it may approach a zero value.(Duffy & Mindlin, 1957) also apply Hertz theory in examining the case of two elastic spheres in terms to extending the theory to elastic description of granular materials.

They include both normal and the tangential external forces upon the situation considered and assume a nonlinearity of stress-strain showing dependencies of elastic behavior on entire stress loading history. The array or the arrangement evaluated is a face centered cubic, where in their formulation for the nature of arrangement external forces and contact forces are incremental in nature, and in integration of strains is imposed.
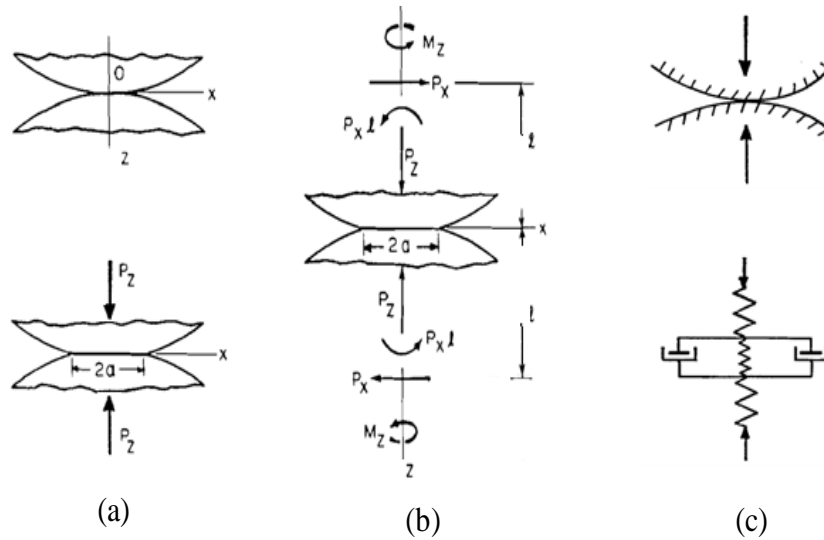
**Figure 3.7. (a) Nature of granular contact unstressed free and under normal force, (b) Intergranular contact under pressure (Mindlin, 1949) (c) Granular contact in presence of saturant represented with a rheological model (Biot, 1961).**

Digby (1981) has further, based on Hertz theory, addressed the case of random granular particles. Fundamental to Digby (1981) approach is examining the contact problem considering adhesion and its consequence upon strength moduli. Nature and impact of the external force is considered significant. One very important aspect, deducible, given the possibilities of the nature of contacts in terms of the mechanics they may give rise to, is occurrence of such complicated phenomenon as forward or backward scattering associated mode conversion and interference, when under cyclical elastic load, offering insights into overall strength properties. Theses aspects could, given Biot theory, be understood from Figures 3.7 and 3.8.

3.3.3.2. Implication of Contact Stiffness in Biot Theory

Biot's wave propagation directly abides consolidation theory of Terzaghi, where phenomenological assumptions are (1) statistical isotropy, (2) infinitesimal strain reversibility, (3) a linearity of stress strain, (4) saturant incompressibility and (5) the flow is Darcian through porous soil (i.e., Poiseuille and/or Navier-Stokes regime). An additional requirement, in the sense of an assumption, as unavoidable
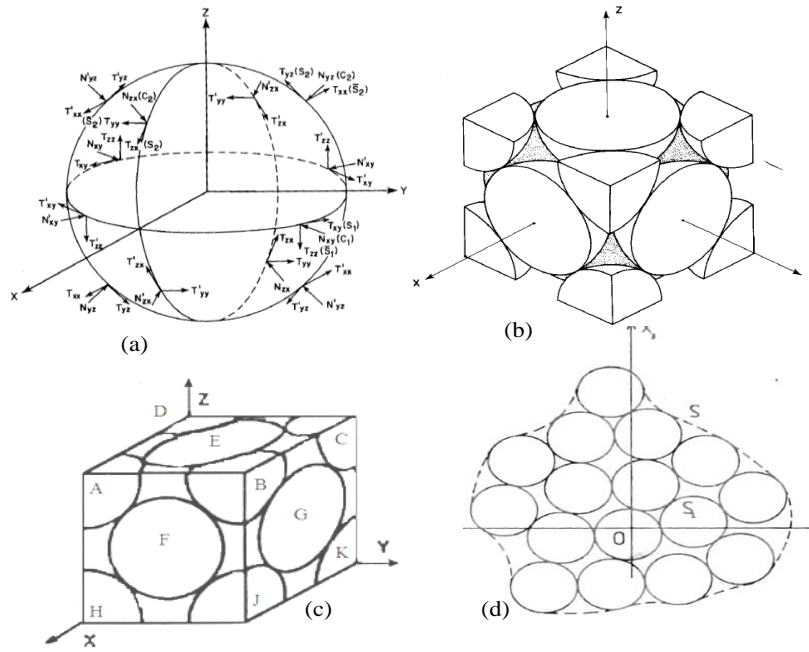
**Figure 3.8. (a) Direction of various contact forces acting upon a typical spherical grain (Stoll, 1989) , (b) Arrangement of spheres in a face- centered cube (Mindlin, 1949) (c) Element of volume of face-centered cubic array of spheres(d) A random set of spheres within a large number bounded by a surface under stress (Digby, 1981).**

consequence of Terzaghi's work regarding assumptions (2) and (3) is existence of adhesive properties of the constituting particulate matter or their surface e.g., soil or sand grains. It is assumed that there should exist such surface properties to hold or support tension and hold such a pattern or arrangement (symmetry) to assume minimum potential energy (Biot, 1941). In further refinement and development of the theory, Biot realized the phenomenological importance of the frictional effect or control coexisting with viscous or lubrication effects of saturation in wave propagation also, hence the notion of viscoelasticity and/or thermo-viscoelasticity was introduced (Biot, 1961).

## 3.4 Direct Current Resistivity Methods

This section has two objectives, firstly to enable the reader understand the functioning of electrical resistance measurement apparatus and the nature of data acquired, and secondly to lessen possibility of any instance of ambiguity in following the integration of interpretation of analyzed data.

### 3.4.1 Ohmic Resistance and Resistivity

Almost all the applications and methods using the DC resistivity method are based on Ohm's law. The law states that electrical charge caused to flow at a constant time rate across a constant value resistor is directly proportional to the magnitude of the potential difference across the resistor by which it is stressed. The equation as in 3.94 for the Ohm's law can be developed or expressed as follows;

$$V = RI \quad , \quad V \propto I , R = \frac{V}{I} \qquad\qquad 3.94$$

Where $V = V_1 - V_2$ which represents the potential difference with units of volts symbolized as V and $I = Q/t$ with units of coulombs charge per unit time, referred to as amperes and denoted by A. The unit to describe the magnitude of the quantity R called the electrical resistance which is the property of the material or the body upon which any voltage is applied, is termed ohm and denoted by the symbol $\Omega$.

Consider now a material specimen of definite dimensions defined by a length L and a cross sectional area A, as shown in Figure3.9. The resistance R of the material is directly proportional to the length and inversely proportional to the cross sectional area, A, of the object, this is shown mathematically as follows;

$$R \propto L , \quad R \propto \frac{1}{A}, \quad R = \gamma(\frac{L}{A}) \qquad\qquad 3.95$$
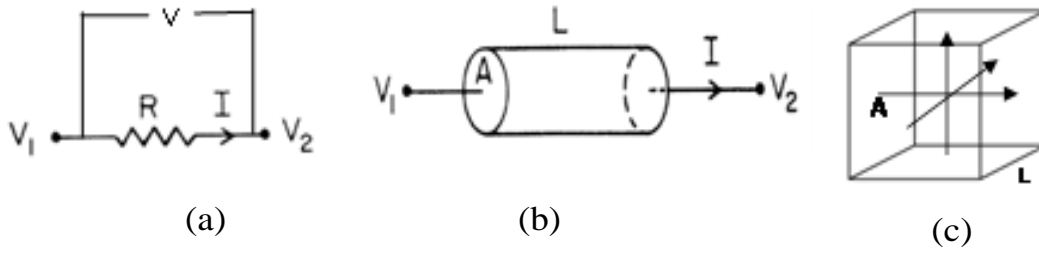
**Figure 3.9. Graphical representations of ohm's law, (a) resistive circuit, (b) resistance of a material element and (c) directional/preferential resistivity (Mooney, 1980),(Reynolds, 1997).**

Considering the above proportionalities and equation 3.95, the quantity ɣ (also denoted by ρ) which occupies for the constant of proportionality is defined as resistivity with having a magnitude equivalent to R for a unit cube, measured between opposite faces. The units by dimensions would be ohm-meter denoted by Ωm. It is also called the specific electrical resistance of the material (Mooney, 1980) and (Reynolds, 1997).

### 3.4.2 Current Density and Potential Gradient

Electrical resistivity when envisaged and examined at much smaller scale requires consideration of a current density description instead of a total current flowing through a finite volume. A potential gradient, thus, instead of a potential drop across a specific dimension or specimen is supposed. Usual symbols for current density and potential gradient representation are **E** and **J.** Lets a small parallelepiped of a small volume with equivalent dimensions as $\Delta x$, $\Delta y$, $\Delta z$ is assumed fixed by a point P, and further that the direction of the current density of any vector **J** at P is along Z axis. If the current field is defined and continuous, given the geometric and spatial considerations the resistance across the parallelopiped is defined as follow in equations 3.96.

$$R = \frac{E\,\Delta z}{J\,\Delta x\,\Delta y} \quad \text{or} \quad R\frac{\Delta x\,\Delta y}{\Delta z} = \frac{E}{J} \quad \text{or} \quad ɣ = \rho = \frac{E}{J} \qquad 3.96$$

For Δx.Δy forming the area under influence of the flux in direction Z and as long as at the point P, $\Delta v = \Delta x \Delta y \Delta z$ is defined, the corresponding resistivity value is determinable since it has the meaning of density. In case of an isotropic medium as stated above, in such a case the **E** and **J** would be in same direction or vice is also true. The directional form of ohm's law could be given as (Mooney, 1980) and (Reynolds, 1997).

$$J = \sigma E \qquad \text{where} \qquad \sigma \equiv \frac{1}{\gamma} \qquad \text{so} \qquad E = \gamma J \quad \text{or} \qquad -\nabla V = \gamma J \qquad\qquad 3.97$$

The above equation is true for the condition of isotropy only.

### 3.4.3 Resistivity Anisotropy

There might be  instance that resistivity measurement/s taken in one direction could be different from those taken in another direction even for similar lengths or dimensions involved, as an example shown in the Figure 3.10 (c). In such cases when the material exhibits variations in the electrical properties with direction it is referred to as assuming an anisotropy. The degree/amount of anisotropy is defined by anisotropy coefficient which is the ratio of the maximum to the minimum anisotropy. The value of which usually lies between a range of 1 - 2, without reference to any units being a ratio. In case anisotropic situation the equation, analogous to that of a mechanical stress-strain relation ratio (Mooney, 1980: Reynolds, 1997),  takes a tensor form, below.

$$J = \sigma E \; J_i = \sigma_{ik} E_k \qquad\qquad 3.98$$

In this form of the equation 3.98 the conductivity $\sigma_{ik}$ appears not as a scalar but as second rank tensor. The significance of the magnitude of the any of the elements of this tensor would depend upon the so called symmetry of conductivity in the three space or frame of reference. Taking into account the stability conditions discussed
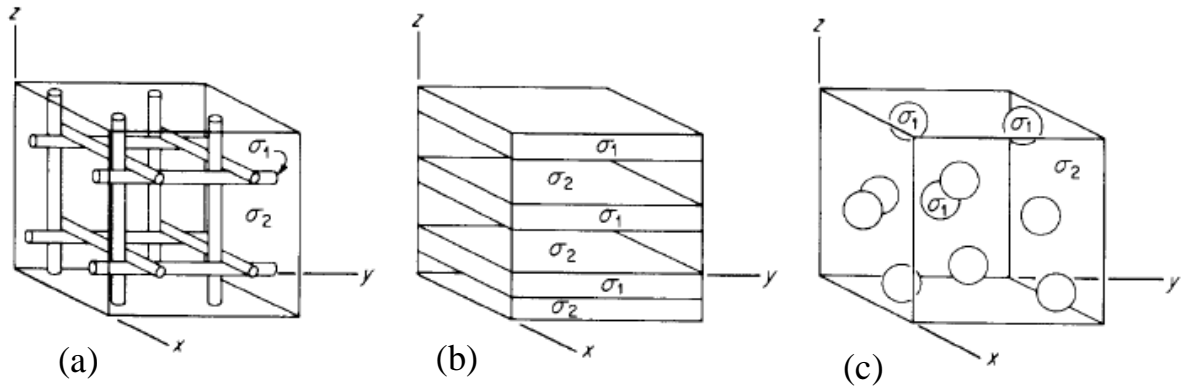
**Figure 3.10. Typical extreme cases/models of two component conductivity materials (a) rods (b) layers and (c) spheres (Grant & West, 1965).**

previously, in this case too for the equation to be valid the following condition as of inequality or equation 3.99 should hold

$$\sigma_{mm} > 0 \qquad\qquad 3.99$$

In case so if $\sigma_{mm} = \sigma$ where all the other elements vanish, the situation reduces to that of the isotropic case. The usefulness of Ohm's law in providing an empirical relation for understanding the response behavior of the materials when stressed with an electric potential lies in it being a linear law. There are however some preconditions, in accepting and applying linear approximations. The current densities used in usual surveys are quite low i.e. not exceeding 1 A/m$^2$, so linearity can be assumed. There are cases however where the current densities are quite high and earth materials might not obey the ohm's law, especially in near vicinity to the current electrodes. Unexpected effects as a consequence of nonlinearly at time could be observed, to be further accounted and accommodated for (Mooney, 1980), (Grant & West, 1965).

### 3.4.4 Implications of Resistivity Anisotropy

In terms of the anisotropy of the conductance and/or electrical resistivity in earth materials, the much common pronounced effects in terms of range and diversity could be one of three limiting cases shown in Figure 3.10. The exaggerated examples are typically true representatives for it is quite evident that most of the earth material

current is established through the interstitial aqueous electrolytic solution rather than the conventional electronic drift or transport through the rock or earth material itself. This translates to the fact that the ground water which permeates through the rock formations has a greater conductivity due to the dissolved salts. In the latter case due to occurrence of semi-metallic minerals in rock formations they would allow significant electrical current conductivity or conductance. The electrical conductivity of semi-metallic minerals is several orders of magnitude greater than that of the electrolytes/electrolytic solutions, as the current could lead the path of least resistance from offered. Complex cases could be modeled or viewed as one of or a combination of the extreme or simplest cases represented in the Figure as in 3.10 a where one of the conductivity component is geometrically distributed like cylinder rods lying in equal numbers along three coordinates the second case, Figure 3.10  b, is termed as platy structure where there is a vertical consistent successive pattern in the variability of  two conductivity/resistivity plates assumed. The third case depicted in 3.10 c is the one where one component of conductivity is taken as that of randomly occurring spheres in the rock or earth material matrix.  Of special significance is the platy model or structure since it depicts a clearly strong anisotropy of a conducting medium and provides an example of real earth situations. Complete mathematical derivations and formulations are provided in Grant and West (1965) to be sought for further details of such models, not attempted on purpose.  Despite that it could be readily deduced that existence of an electrically anisotropic character in a two component material may account for directionally restricting the continuity of conductivities. Variability in the interconnectedness or continuity of the interstitial water, for instance, especially in the case of platy or layered structure can significantly affect conductivities. Similar real life cases are significantly complicated to be mathematically examined readily for the degree of variation of electrical resistivity. They since could assume any combination from among the models explained. For plausibility of interpretation a control or situation specific background simple model/s could be kept in view to help account for variability of resistivity in a qualitative sense. Possible sources of errors or discrepancies could also be identified and dealt with, especially with complementing aproiri information from other sources.

### 3.4.5. DC Resistivity Conduction Method

Application of the DC resistivity method involves conduction of the electric current using electrodes. Two pieces of equipment are essential, one for the generation and induction of the current, a source, and other for the measurement of the potential difference. Each of the pieces of equipment is connected to a pair of electrodes. With the use of the current electrodes a stationary current field is setup within the subsurface. A potential drop with depth gives rise to an electric potential field too. This field could be distorted by the variations in the subsurface anomalous conductivity. The detection of these anomalies in the electric field is the objective by employing the potential probes. The assumption in this procedure is that current flowing in the potential electrodes or potential measuring circuit is significantly small to cause any interactive alteration in the measured filed. The type and choice of configuration depends upon the nature of the problem confronted. Two types of surveys are planned in field applications and practices, to address horizontal problems and to address the vertical problems, accordingly. The former case addresses the issues of determining the depths of rather flat laying uniform beds as in undisturbed sedimentary rocks by changing the electrode spacing about a fixed location and observing the change in potentials while the in the latter the vertical beds are surveyed by focusing on identification of anomalies corresponding to mineral prospects in the near surface (Grant and West, 1965).

As an end note, the literature review embodied P-wave, S-wave and electrical resistivity based methods; and, the aspects and issues brought forth as presented for topics of discussion aimed only at offering a conceptual clarity of fundamental principles behind the refinement and perfection of such, as methods of day. Further the objectives of study sought for, and for bearing of understanding of apparatus design upon plausibility of inferring, were kept in view, for principally following same principles intended not to violate standard practices. Available standard methods, if sought for interest, include ASTM standards, D7128-05(2010), D5777-00(2011), G57- 06(2012), D6431- 99-(2010) among others explained with them.

# Chapter 4: Experimental Apparatus and Materials

## 4.1 Fractured Porous Media Characterization using S-Waves

This work involved the use of a fractured porous media specimen fabricated from stacking multiple slabs of a sandstone material. The specimen was held encapsulated by using a sealant coating, before loading it cyclically to change/vary the normal stress acting across the surfaces of the slabs. In this configuration, the contact surface or interface between the adjacent slabs functioned as fractures in the synthetic fractured porous media specimen. During the cyclical fracture loading, air was flowed through the specimen in directions parallel to and perpendicular to the fractures, and S-waves were propagated along the length of the specimen in the direction of the fractures with various polarizations with respect to the fracture plane. The following section describes the equipment and materials used to conduct these combined fractured porous media, permeability and S-wave polarization experiments.

### 4.1.1 Instrumented Axial Loading Frame and Permeability Measurement

A uniaxial loading frame was used to apply the cyclical normal loads to the fractured specimen. The loading frame and the specimen holder are shown in Figure 4.1a,b and c along with a AlazarTech 2-channel PCI-2 ATS460 card based DAQ system or module capable of storing digitized data as *.txt or *.dat compatible files in an external storage medium.

Permeability and S-wave measurements were made separately with the specimen subjected to the same load steps by applying cyclical loading at controlled predetermined constant rate, exploiting the capability of the loading frame. See Section 5.2 for further details on the specimen testing procedures. The S-wave transducers used were standard contact category Panametrics-V153 (videoscan) model rated and 0.5" nominal size with a frequency range of 100 to
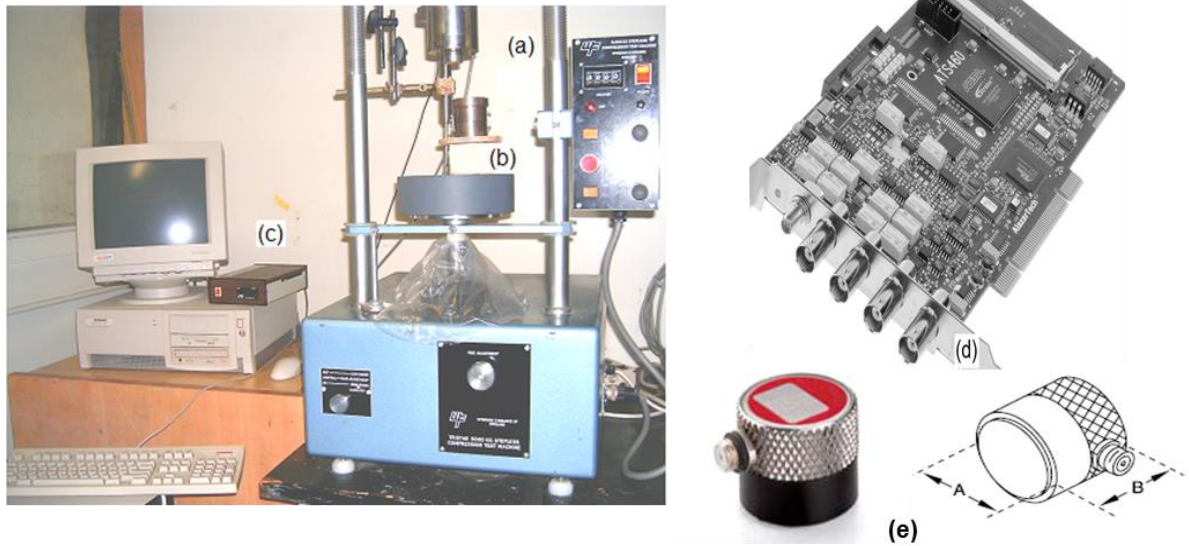
**Figure 4.1. (a) Programmable loading frame with (b) upper and lower adjustable/tractable specimen loading platens and (c) PC-based data acquisition module. (d) Associated DAQ card with BNC connectors. (e) Ultrasonic S-wave sensor specified by letters A and B i.e., contact face diameter and depth for any nominal size**
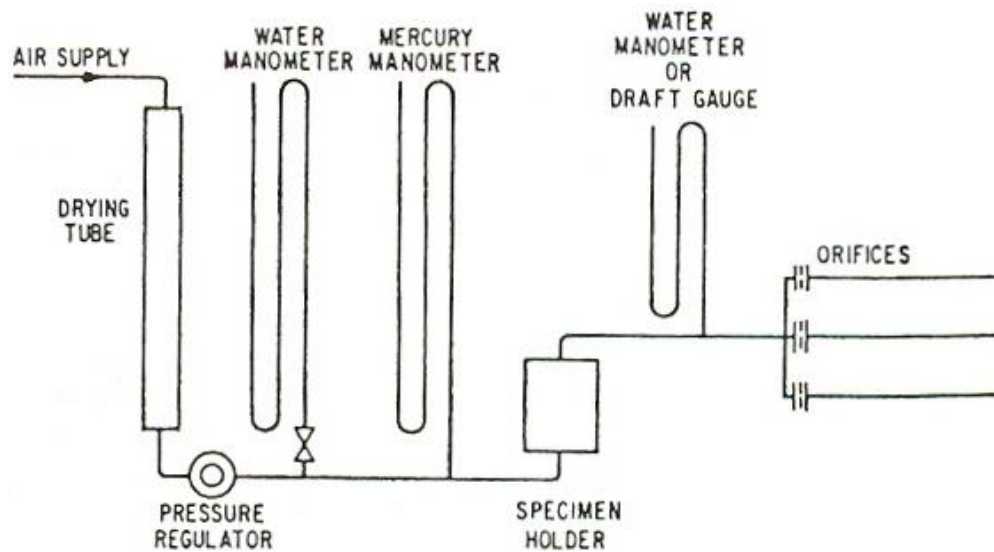


**Figure 4.2. Typical flow circuit schematic of (ASTM, D4525) air permeability measurement method.**

1000 kHz and were sampled (in through transmission propagation) at 4 MHz using a PC-based digital oscilloscope, shown in Figure 4.1c. The permeability measurements were made using a flow apparatus conforming to ASTM standard test method, used for estimating permeability of rocks by flowing air (i.e., ASTM-D4525) as depicted in Figure 4.2. At each load step or "fracture stress condition/state", for both normal and parallel to fracture/ crack orientations, several permeability tests were run by varying the air pressure differential across the specimen sample and the corresponding air permeability values were recorded. After performing adequate number of tests and calculating the air permeability, the equivalent liquid permeability values were determined. Permeability of air or gases at low pressure is relatively higher than that of liquids, due to the phenomenon of "slip flow" or the Klinkenberg effect, which has to be taken into account to estimate the equivalent corresponding liquid or *in situ* gas permeabilities. The significance of the effect with suggested corrections is detailed in Jones et al. (1972) where several other references are provided. These experiments were conducted while the candidate was a graduate student in the Subsurface Imaging Group (SIG) at Dalhousie University, Canada. Flow data, reduced to an equivalent liquid permeability values, included in thesis was generously provided by postdoctoral researcher Dr. Ali Mukati of the same SIG.

### 4.1.2 Fractured Porous Media Specimen

The fractured porous media specimen was fabricated by stacking six 1 cm thick slabs of a clean quartz sandstone (Figure 4.3a). The length of the specimen was 10.8 cm with an overall thickness of 6.5 cm, giving an approximately 1 mm aperture to each of the five fracture interfaces for any asperities or protruding micro structures. The sandstone is from the upper member of the Horton Bluff Formation, found in the Minas and Cumberland Basin of Nova Scotia, Canada, and is characterized by a thick, quartz rich sandstone, which at some outcrop locations is pure enough to be used to manufacture glass and, so, is labeled as glass sandstone. This basin hosts over pressured natural gas at a depth of approximately 2500 m in the province of New Brunswick (Canada), approximately 100 km to the northeast of the sampling location
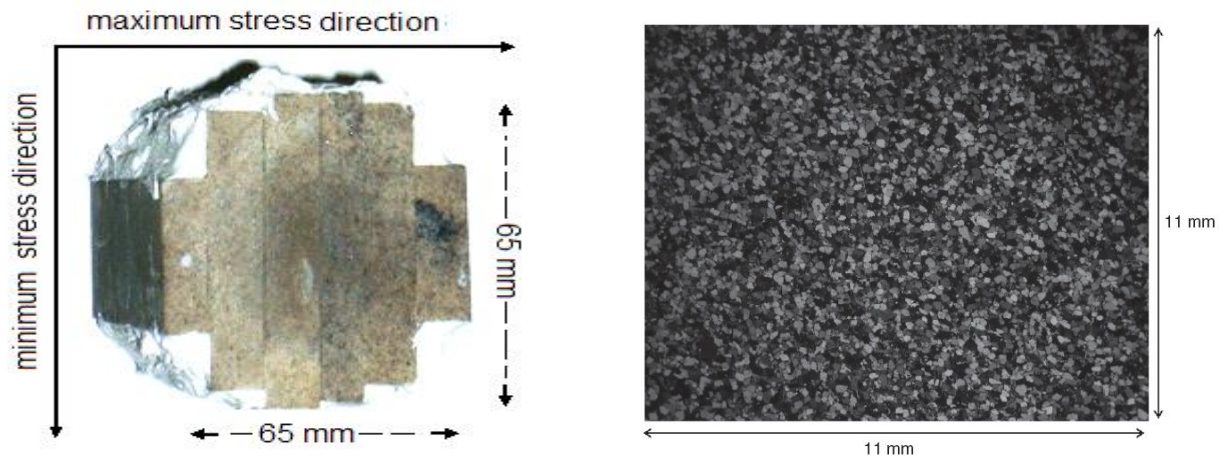
**Figure 4.3. (a) Faulted reservoir rock or bedrock sandstone analogue depicting directions of load variability (b) Thin section of quartz sandstone under cross-polarized light (XPL) (Frempong et al., 2007).**

(Ryan, 1998). The formation is dominated by 90% or more quartzarenites ranging from quartz pebble conglomerates to fine-grained quartz sandstone. Minor kaolinite, lithic fragments, traces of pyrites, and some ubiquitous plant detritus are the only components of the rock other than quartz. The microstructures of the quartz sandstone specimens were examined in thin section with particular attention given to grain size distributions and the nature of the grain scale distribution of any quenched melt quartz. They contained fine grained, rounded shapes of quartz averaging about 160 μm in grain size (Figure 4.3b) with consistent traces of pyrite and minor kaolinite.

## 4.2 Porous Media Flow and Fluid Displacement

In this work, a uniform porous media was mounted in a vertically oriented flow cell and fully saturated with a liquid hydrocarbon. This hydrocarbon was displaced by flowing brine until no hydrocarbons were detected at the downstream discharge of the cell, with this procedure being repeated at several different brine flow rates. During the experiments, a series of 8 pairs of electrical resistivity probes measured the DC electrical resistivity along the length of the flow cell (Figure 4.4), and pairs of P-wave and S-wave transducers measured the transmission of P and S waves across the diameter of the cell perpendicular to the flow direction.

(a)



(b)
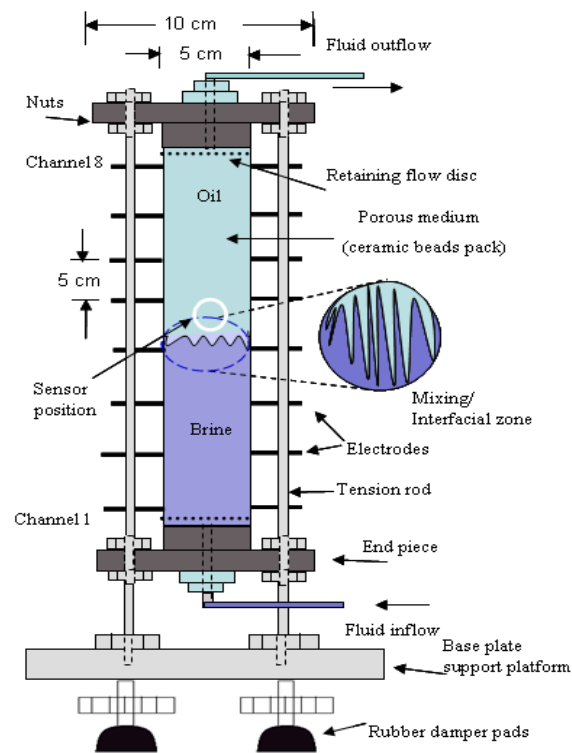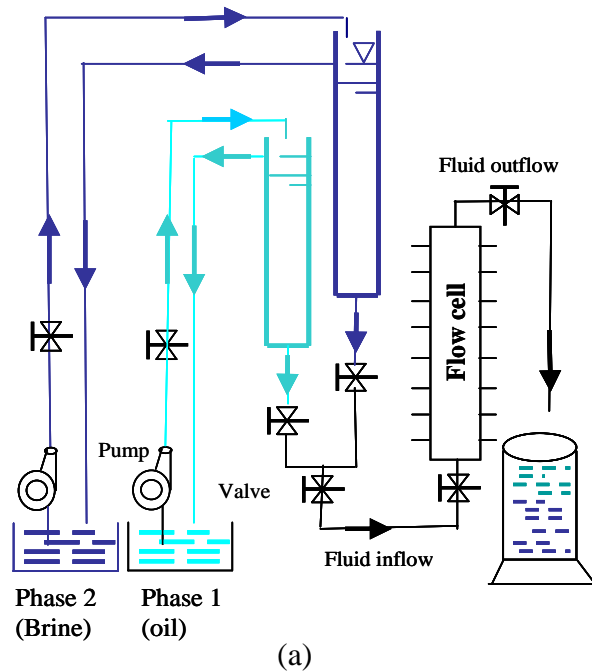
**Figure 4.4. (a) Flow control system feeding the flow cell and (b) flow cell system details.**

This section describes the equipment and materials used to conduct these porous media fluid displacement experiments with integrated geophysical measurements. The flow cell is shown schematically and in photographs in Figures 4.5 and 4.6. It consists of a transparent PVC tube with end-plugs held together using tension rods mounted within top and bottom holders. The loose porous media material is retained and confined between the end-plugs, while any tightening of nuts holding the tension rods compacts the porous media grains. The end-plug design accommodates flow-discs and circular seal rings around the shafts. These provisions ensure retaining of the solid granular material packed inside the cell and allows for uniformly distributed flow through the porous medium along the cell without any leakages. The flow-cell apparatus would allow attaching or connecting two ultrasonic source-receiver pairs (i.e., P- and S- wave) oriented diametrically at the midspan of the cell attached on smooth flattened pads. To facilitate Darcy fluid flow in the flow-cell, under constant head conditions with a specified initial flow rate, a flow-control system was developed separately. Both of the two systems in relevance to their functions are shown in the schematics of Figure 4.4 and 4.5 with photographs of the actual laboratory setup in Figure 4.6. The flow control system was externally powered by 1.5 hp centrifugal pump. The flow takes place against the gravity with maintenance of constant fluid head means that that the inlet pressure energy with respect to position is maintained at the expense or allowance of variation of flow velocity given the nature of fluid parameters for conservation of total energy (i.e., P.E and K.E).

The integrated (geophysical) data acquisition system is shown schematically in Figure 4.7 and includes ultrasonic pulse transmission and electrical resistivity components. The ultrasonic transmission system, as shown in Figure 4.8 is based on a Physical Acoustics PCI-2 analog to digital (A/D) conversion card installed in an IBM compatible standard computer system meeting operational, memory and storage requirements. A manually operated external push button triggering system for generating an RF pulse of standard duration was used. Further a controlled stable gain
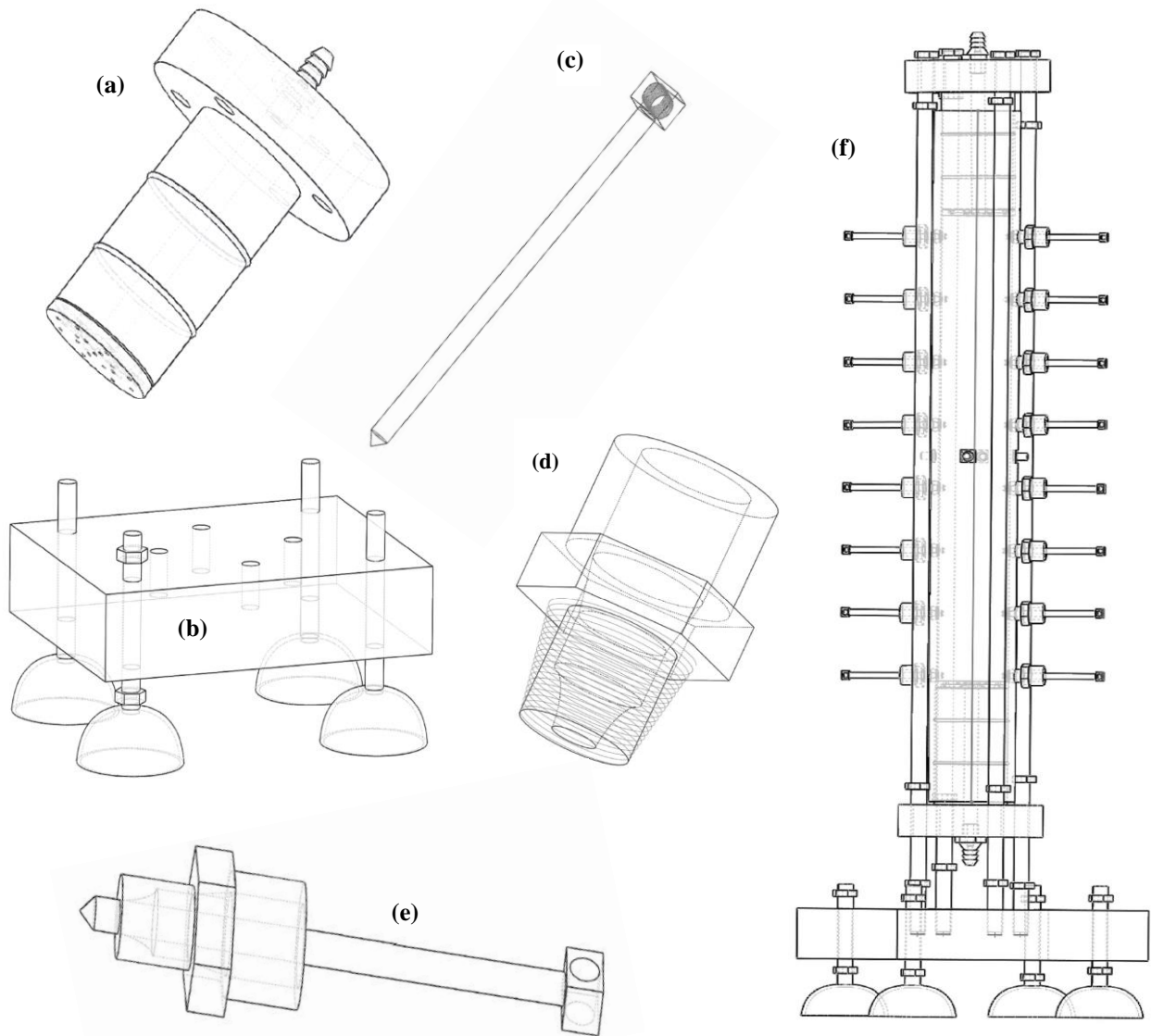
**Figure 4.5. Component drawings of the porous media flow cell for (a) top and bottom end plugs, (b) leveling base, (c) copper electrical resistivity probe. (d) probe holder, (e) assembled resistivity probe, and (f) assembled flow cell.**

addition with ensuring a synchronized causal digitization was facilitated by a 5077PR Panametrics pulsar unit used to stimulate the source transducers. The received signals were adequately and consistently amplified using Physical Acoustics standard 2/4/6 preamplifiers before digitization by PCI-2 18-bit A/D card. A manual double pole switching system was devised to enable two channels system to handle a four channel operation for synchronized simultaneous triggering and acquisition. P- and S-wave data were acquired sequentially at a reasonable sampling rate, for Panametrics 1MHz sensors/transducers used, with consistent time stamps, and without compromising --

**Figure 4.6. Laboratory arrangement of immiscible fluid displacement through porous analogue in flow cell (a) Flow cell system with feeding fluids (b) Flow cell system ready for test with ultrasonic sensor position marked midspan (c) relative position of sensors (d) relative position of components (e) retainer discs (f) plug-in end-piece and (g) base plate with adjustable damper pads.**

resolution. All transducers used were contact coupling type with a nominal contact circular cross-section of half inch diameter. Successful and efficient adaptability of such ultrasonic DAQ system components for other relevant NDE studies in past is referred to elsewhere too in this document to fully comprehend it's high speed and reliable acquisition capabilities. A compatible version of Physical Acoustics AEwin (Acoustic Emission For Windows) software was used for optimal sampling rate selection and save data in *.csv files for detail post processing to examine and evaluate features of interest. Wave forms and corresponding FFT could be either examined real-time or in a replaying, too.

For electrical resistance measurements, eight copper electrode pairs opposite each other are attached with special self-sealing screw on fittings equi-spaced along the length of the flow-cell. Ultrasonic ( P- and S-wave) and electrical resistance measurements or acquisition could simultaneously be achieved using all, the four ultrasonic and eight electrical resistivity (resistance) channels (see Figure 4.5).The corresponding electrical resistance (DC) data acquisition system is shown in Figure 4.9, consisting of a 12-bit ColeParmer eight channel data acquisition card interfaced with an eight channel programmable Velleman relay switchboard. The switchboard serves input connection or interface as several electrodes are traversed in sequence discretely while the DAQ does the A/D conversion  continuously registering the measurements of each channel separately as an output file *.xls type, as all eight channels are recorded at the output USB (2) port to the computer system. ResistanceLab software with GUI control interface was developed in LabView environment in association with the supplied or vender drivers softwares. The software provided the flexibility of assigning adequate sampling rates for DAQ card and also for the switch board for an automated switching.

The reliable and reasonable functioning of the system with accurate preliminary results was reported in (Hassan et al., 2007) after the concept had been introduced through (Hassan et al., 2006).

(a)
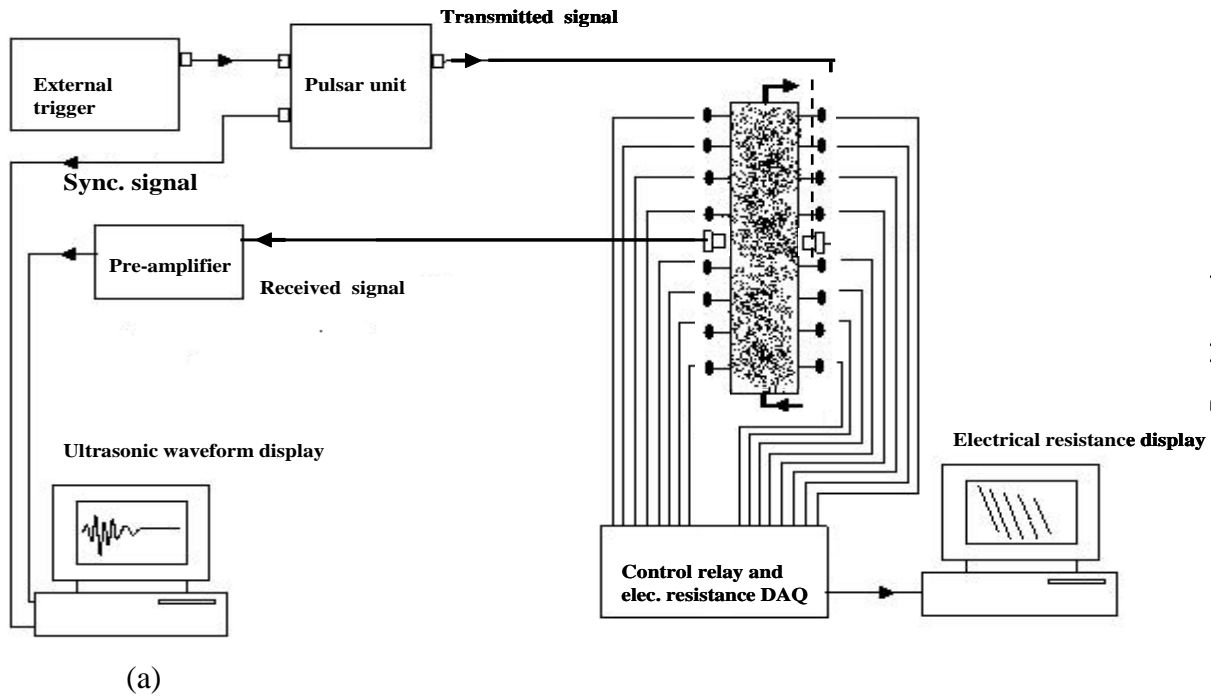
**Figure 4.7. Schematic of various components of integrated data acquisition, (a) ultrasonic (b) electrical resistance (resistivity).**
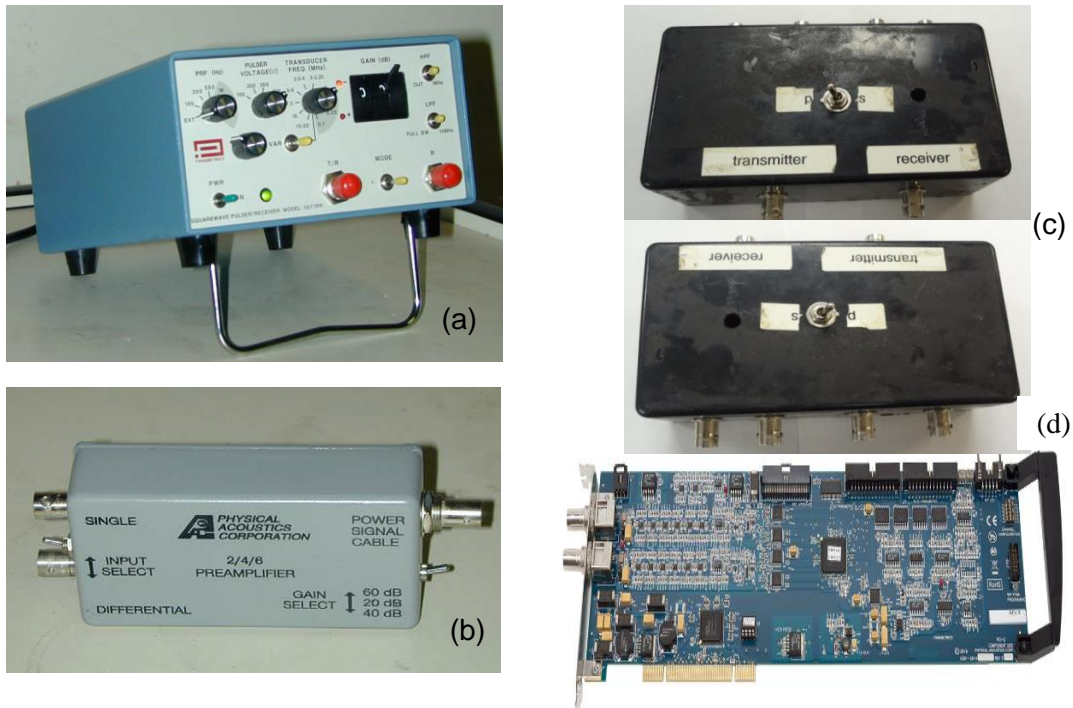


**Figure 4.8. (a) Panametrics pulsar unit with the capability to transmit single or repeated pulses when internally or externally triggered (b) Four-to-two channel switch box for sequential simultaneous P- and S-wave ultrasonic acquisition (c) Pre-amplifier (d) PCI-2 A/D card.**
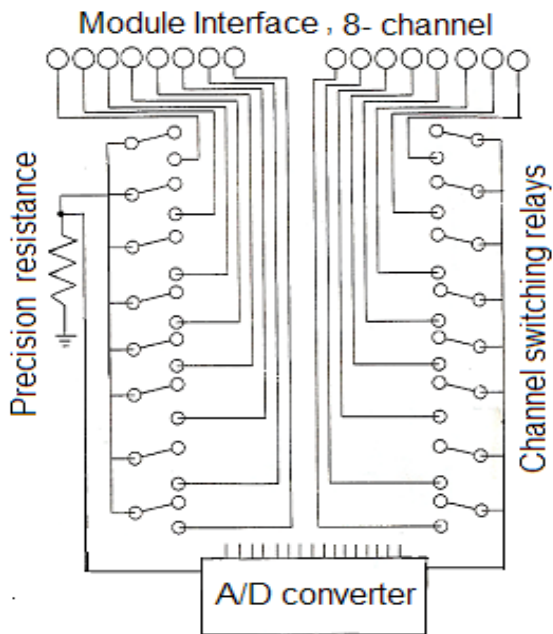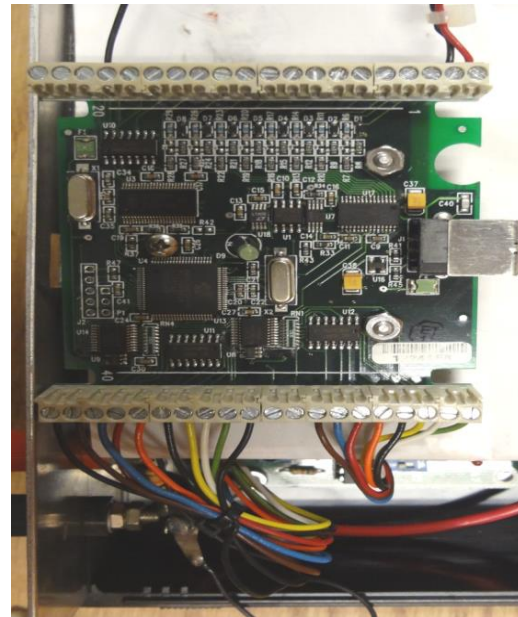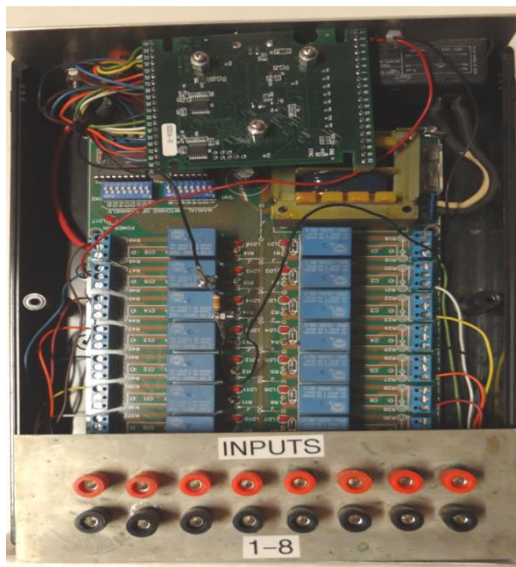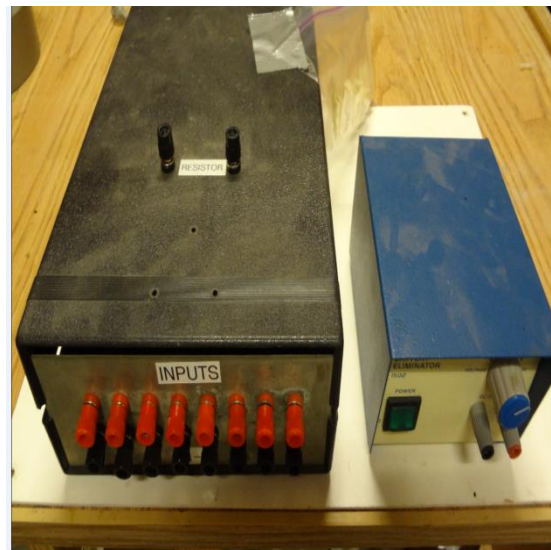
**Figure 4.9. Components of electrical resistance DAQ. (a) Circuit schematic (b) Digitizer (c) Programmable switch board interfaced with digitizer and I/O (d) Electric DAQ module with power supply.**

### 4.2.2 Porous Media Analogue and Immiscible Fluids

The porous media consists of spherical 0.5 mm diameter soda-lime beads manufactured by BioSpec product for medical uses. However, when placed and compacted in the flow-cell, the beads approximate a clean uniform sandstone as shown in Figure 4.10 which compares the material texture to several other porous media, with the corresponding material properties as summarized in Table 4.1.

The immiscible liquids used for the liquid displacement experiments consisted of the commercial produce Taltine TriArt (Turpentine grade oil) as the initially saturated hydrocarbon, and a brine with 3.5% (w/v concentration) NaCl content as the displacing liquid. These liquids were chosen based on safety for handling, sufficient density and viscosity difference to affect a reasonable response to ultrasonic pulse and DC resistivity, and to have good approximation of subsurface transport or flows of oils and other industrial chemicals spills and their interfaces including brines and sea water.

## 4.3 Data Analysis and Interpretation

### 4.3.1 Detectability and Repeatability

Detectability means and implies that the magnitude of change in response to the elastic wave disturbance is sufficient to account for any ascertaining of the nature of underlying or corresponding change of state. In an otherwise sense the variabilities of the change of state should be substantial enough to be detectable by the available capacity or resources. Repeatability means that different vintages of sets of data are similar. In a practical sense would mean that both the acquisition design and the coverage be same in a geometrical sense at different times.
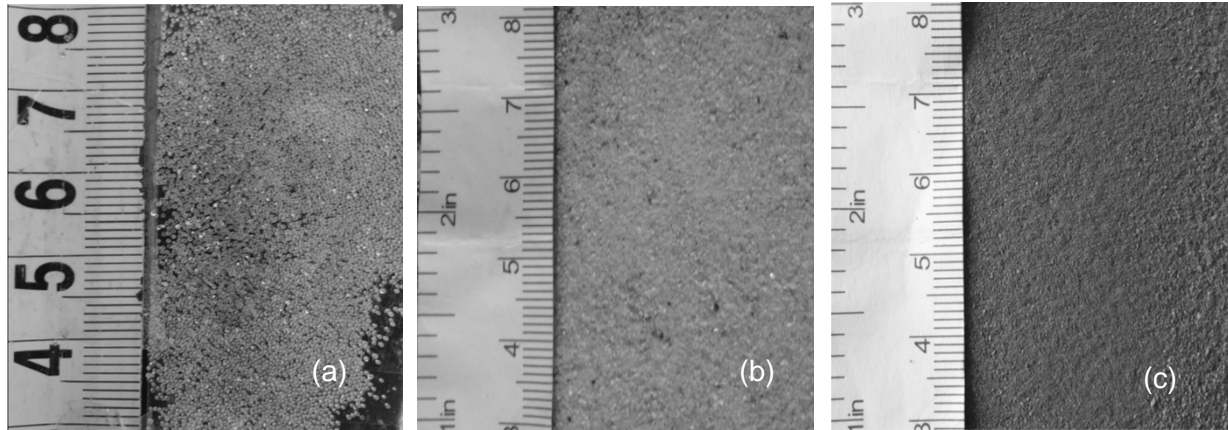
**Figure 4.10. (a) BioSpec soda lime (glass) spherical grains/beads compared with (b) clean sand and (c) a laboratory type soil sample.**

Table 4 .1. **Properties of constituents of laboratory unconsolidated core analogue**

| No. | Property | Value | Units |
|---|---|---|---|
| 1. | Bead/grain dia. | 0.5 | mm |
| 2. | Bead/grain material density ($\rho_s$) | 2.5-2.6 | Sp.gr. approx. |
| 3. | Grain bulk modulus (guessed and from literature) | 4 and 40 | GPa |
| 4. | Porosity of granular pack (Ø) | 26 | v/v % |
| 5. | Structure factor of porous granular pack (α) | 2.4 | dim. less |
| 6. | Adjusted /measured frame bulk modulus ($K_b$) | 4.0 | GPa |
| 7. | Measured frame shear modulus (N) | 2.44 | GPa |
| 8. | Mineral oil /displaced fluiddensity ( $\rho_f$ oil) | 0.761 | Sp.gr |
| 9. | Mineral oil bulk modulus ($K_f$ oil) | 1 | GPa |
| 10. | Mineral oil viscosity | 10 | cP |
| 11. | Brine/displacing fluiddensity ($\rho_f$ brine) | 1.028 | Sp. gr |
| 12. | Brine salinity | 3.5 | w/v % |
| 13. | Brine viscosity | 1.3 | cP |
| 14. | Brine bulk modulus ($K_f$ brine) | 2.45 | GPa |
| 15. | Fluid mixed-zone bulk density estimate ($\rho_f$ mixt.) | 0.891 | Sp.gr |

Detectability and repeatability may be naturally desired or suited at field scale for efficiency but for time lapse type analyses involving fluid effects and associated subtleties of overall energy regime change it is essential, for consistent interpretability to infer (Johnston, 2013).

In the fracture porous media study using S-waves both detectability and repeatability were assumed and issues resolved by observing the consistent similarity of variations in ultrasonic response to effects of azimuth variation and stress variation, independently and separately. By this procedure, several repeat tests for each combination of azimuth for the source and receiving transducer and/or azimuth were naturally performed. For the case of the immiscible fluid displacement experiments, several preliminary and post experimental measurements were carried out to confirm the reliability and the adequacy of measurements to evaluate detectability and repeatability. This includes calibration of instruments using standard methods or materials as water test, granite, concrete, aluminum and standard resistances of known ohmic value e.t.c to confirm detectability. Further measurements were also reproduced with CompuScope high speed PCI-2 A/D card supported by GaGeScope oscilloscope software both for dry and wet saturated analogue to confirm repeatability. Certain features of interests were also reproduced and checked in anatomical context by using Tektronix digital and analog oscilloscopes too, before examination and explanation in detail.

### 4.3.2 Time Lapse Approach

Various analyses developed are graphically constructed, and explained and interpreted with respect to specific scenarios of interest of geology and engineering (e.g., geo-environmental and geotechnical). These scenarios are then discussed in evaluation with pertinent references, in the next chapters of this thesis. Mathematical models, empirical and analytical relations used in all analyses along with definitions of quantities and parameters are either explained or could be readily understood from specific analysis discussions, in relevance. Quantitative measures or values of different parameters of experimental constituents are provided (such as are given in

Table 4.1) using conventional symbols and units. Special attention, while examining data for inferring, is naturally bound to an identification of primary "features of interest" or "attributes".

These are extracted by data sub setting and/or binning allowing avoiding the redundant data representation with focusing only upon essential, definitive and defining aspects, well fitting with a time lapse time approach. Coincidently cogent and reliable inferring is maintained given difference in types of data by keeping a spatiotemporal consistency assisted by drawing realistic correspondence. It is observed or ensured by extracting, conforming and corroborating features and information by strict time stamp reconciliation, and restricting of those instances of interest as being spatially fixed/defined within their data subset (time), for all different data sets, but not the vice.

# Chapter 5: Fractured Porous Media Evaluation using S-waves

This chapter presents the results of the first component of the overall experimental investigation, the ability of polarized S-wave transmission to characterize porous fractured media and implications with inferring subsurface permeability anisotropy. The formation analogue for this investigation is a permeable formation that has a single dominant fracture set characterized by consistent fracture spacing and orientation, such as a fractured coal seam and many types of bedrock aquifers. The fracture properties targeted for this investigation include identifying i) dominant fracture set spacing and orientation, ii) fracture specific stiffness and implications for pore and fracture fluid changes, and iii) permeability anisotropy focused on the directions of maximum and minimum permeability.

## 5.1 Permeability and Wave Propagation in Fractured Media

Flow is a porous formation can be described using Darcy's Law in the form (Pickup et al.,1994) in Equation 5.1:

$$v = -K\frac{1}{\mu}\nabla P, \qquad\qquad K = \begin{bmatrix} K_{xx} & K_{xy} & K_{xz} \\ K_{yx} & K_{yy} & K_{yz} \\ K_{zx} & K_{zy} & K_{zz} \end{bmatrix} \qquad\qquad 5.1$$

Where $v$ represents velocity, $\mu$ is dynamic viscosity, K is the tensor permeability, and $\nabla P$ is the pressure gradient. In a homogeneous and isotropic medium, K reduces to a single scalar value and flow is in the direction of the maximum pressure gradient. However, for the anisotropic media, as considered in these experiments which are characterized by a single dominant fracture set, the maximum and minimum permeability orientations ($K_{max}$ and $K_{min}$) are often aligned parallel and perpendicular, respectively, to the dominant fracture set orientation (e.g., Siegfried, 2011; Mazotti et al., 2009; Flores et al., 2011; Flores, 2014).
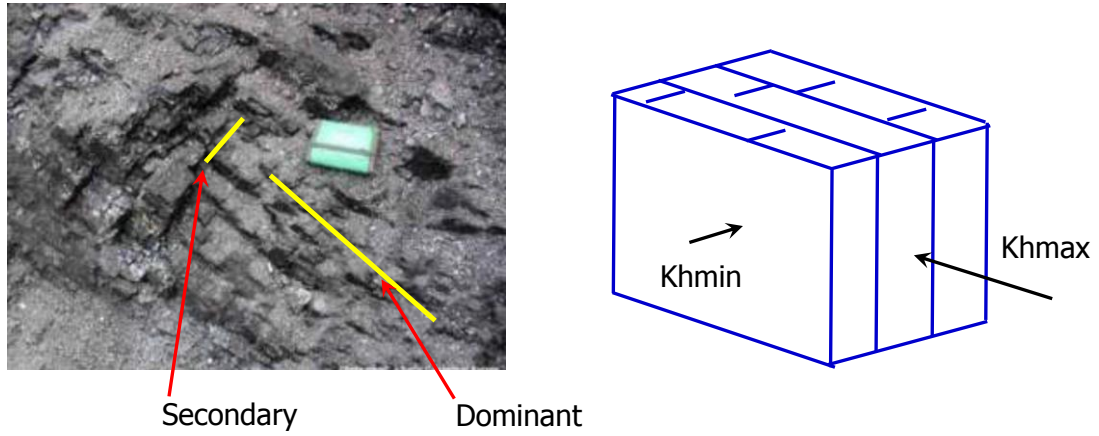
**Figure 5.1. Identification of dominant and secondary joints or cleats in a typical coal formation (left) and the corresponding orientation of the maximum and minimum horizontal permeabilities (right) with Khmax oriented parallel to the dominant joint set.**

In these formations, subsurface flow is maximum when the pressure gradient is aligned with the direction of maximum permeability. Further, when the dominant fracture set is oriented vertically, the $K_{max}$ and $K_{min}$ directions define the directions and maximum and minimum horizontal permeability and flow.

The existence of elastic anisotropy in rock and earth materials introduces and defines a directional dependence of the wave propagation velocity. The elastic property anisotropic variation in a continuum of interest is geometrically understood as controlled by the elastic symmetry of the material. From a wave propagation modelling perspective, a tensor representation is incorporated. Wave equation based on laws of motion with usual symbols is presented incorporating a conventional symmetric stiffness tensor formulation, is given in Equation 5.2:

$$\frac{\partial^2 u_i}{\partial t^2} = \frac{c_{ijkl}}{\rho} \frac{\partial^2 u_i}{\partial x_l \, \partial x_j} \quad , C_{\alpha\beta} = \begin{bmatrix} C_{11} & C_{12} & C_{13} & C_{14} & C_{15} & C_{16} \\ C_{21} & C_{22} & C_{23} & C_{24} & C_{25} & C_{26} \\ C_{31} & C_{32} & C_{33} & C_{34} & C_{35} & C_{36} \\ C_{41} & C_{42} & C_{43} & C_{44} & C_{45} & C_{46} \\ C_{51} & C_{52} & C_{53} & C_{54} & C_{55} & C_{56} \\ C_{61} & C_{62} & C_{63} & C_{64} & C_{65} & C_{66} \end{bmatrix} \qquad 5.2$$

By Voigt (1910), because of elementary symmetries, the fourth-rank elastic tensor $C_{ijkl}$ can be mapped into a $6 \times 6$ matrix $C_{\alpha\beta}$, which may be used to describe any anisotropic propagation mechanism by populating quantities corresponding to particular symmetry (Helbig & Thomsen, 2005).Further treatment of this general anisotropy is given in Winterstein & Stefani (1987), Crampin (1989), Winterstein (1990), Huntington (1958) and Fedorov (1968).

In anisotropic solids, shear wave splitting is a significant diagnostic tool for identifying and evaluating the anisotropic character due to cracks and fractures. Shear wave splitting or birefringence is a manifest of particle motion associated polarization. In an anisotropic region, a selective shear wave splitting into two or more components or modes with the fixed polarization directions and velocities takes place. These split shear waves have different velocities and will thus explicitly separate in time, so  upon emerging in an isotropic zone, or while being recorded, the waveform of the original incident pulse cannot be reconstructed, and a characteristic signature is recorded on the shear wave train. This signature carries information about the physical and structural properties in the ray path direction, as described in Crampin (1978, 1981, 1985a,b), Crampinet al. (1985), and Crampin & Booth (1985). Shear waves are hence sensitive to fractures and fracture network or micro fractures and the fluid content within, shear waves manifest an appreciable degree of sensitivity to the variations in the stress field in rocks (Wehner et al., 2000). Shear waves anisotropy can then be used as tool not only to predict the permeability tensor but also the degree of variation in permeability in time, in relevance to variation of processes of geological nature.

These split shear waves have different particle motion polarizations for different directions of propagation, and will only have SV and SH polarizations as specified for propagation in specific "symmetry" directions through the anisotropy (Crampin, 1978). For S-wave polarization and S-wave splitting, only SV and SH polarization describe the particle motion with respect to seismic line over a flat reflector/s as depicted in Figure 5.2 i.e., definition with respect to an arbitrary line direction in isotropic medium.
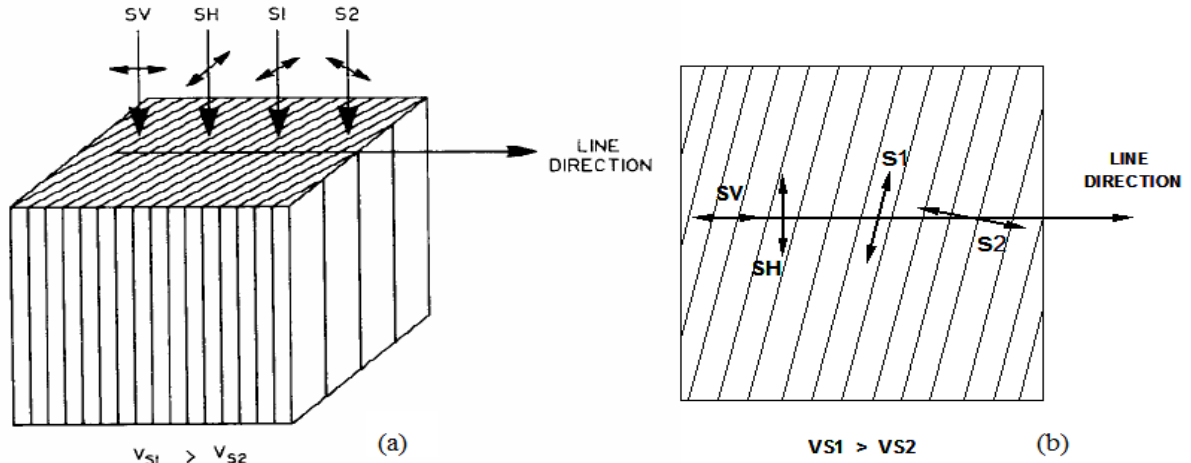
**Figure 5.2. Polarization/directions of S-wave in case of propagation in vertical fractures, in (a) isometric and (b)in top view, oriented at some arbitrary direction to the seismic line direction, modified, (Tatham & McCormack, 1991).**
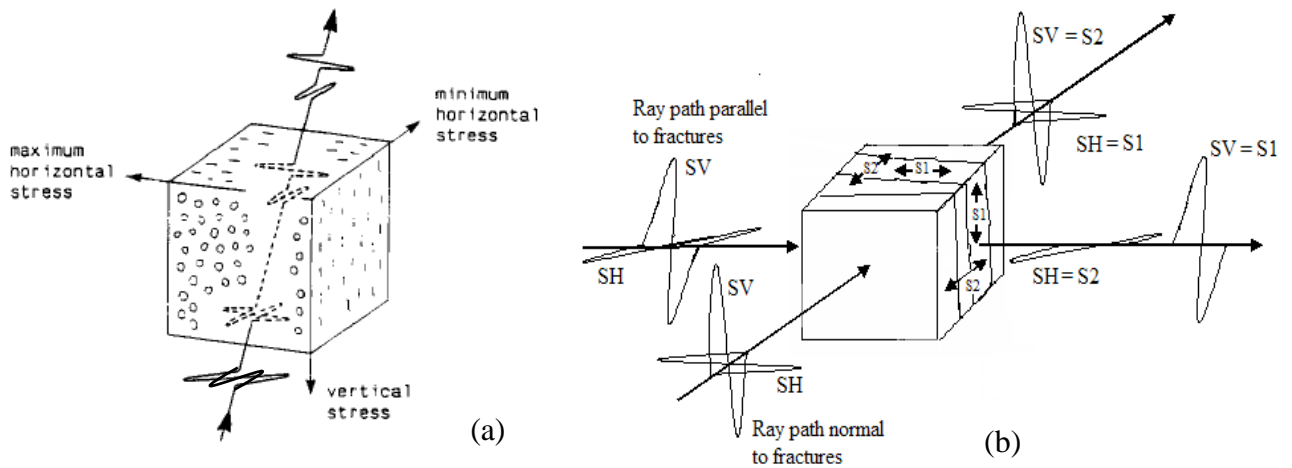


**Figure 5.3. Phenomenon of splitting of an emergent S-wave in S1 and S2 components (a) S-wave splitting and polarization direction when it enters with an arbitrary polarization in an anisotropic medium (b) S-wave splitting and its possible polarizations in response to propagation through a cracked solid with a specific crack orientation, modified (Tatham & McCormack, 1991).**

However in case of cracks or planes (or the anisotropy source) oriented in some arbitrary direction to the seismic line direction, the shear wave polarizations while propagation are defined with respect to the crack orientation. In such a case they are usually referred to as split S1 and S2 waves with S1 representing polarization parallel to major crack/fracture orientation and S2 being polarization perpendicular to S1, as shown in Figure 5.3. The response of S-wave in terms of particle polarization while propagating through an anisotropic material in general, and a series of flat reflectors or planes aligned parallel or normal to seismic line direction could be understood from Figure 5.3. It can be inferred by observing Figures 5.2 and 5.3 components that in case of vertical parallel cracks aligned normally to the seismic line direction SV=S2 and SH=S1. In general terms, S1 and S2 are the polarizations of the emergent shear wave denoting the split fast and slow shear wave components determined by the anisotropy of the formation. Owing to the fact that S1 has the highest velocity while S2 has the lowest velocity they sometimes are also denoted as $S_{fast}$ and $S_{slow}$ respectively. Experimental studies (Crampin 1978, 1981, 1985a) show that the polarization of the faster split shear wave is a stable phenomenon, and the S1 direction shown can be used to identify the orientation of the crack geometry.

## 5.2 Experimental Specimen and Testing Procedures

The fractured porous media specimen was fabricated by stacking slabs of a clean quartz sandstone ranging in thickness from 8 to 12 mm (Figure 5.4a). Prior to specimen assembly, the slabs were saturated with distilled water under vacuum conditions for 24 hours and then oven dried for 24 hours at a temperature of 50ºC to ensure the pores were completely clean and dry. The length of the specimen was 108 mm with an overall thickness of 65 mm, giving an approximately 0.5 mm aperture to each of the five fracture interfaces and any asperities or protruding micro structures. Properties of the sandstone are given in Frempong et al. (2007) and in Section 4.1.2.The specimen was encapsulated in a silicon based flexible material that both sealed the specimen for flow and held the stacked slabs together. Flow ports were installed through the flexible coating to allow for flow across the 65 mm thickness of
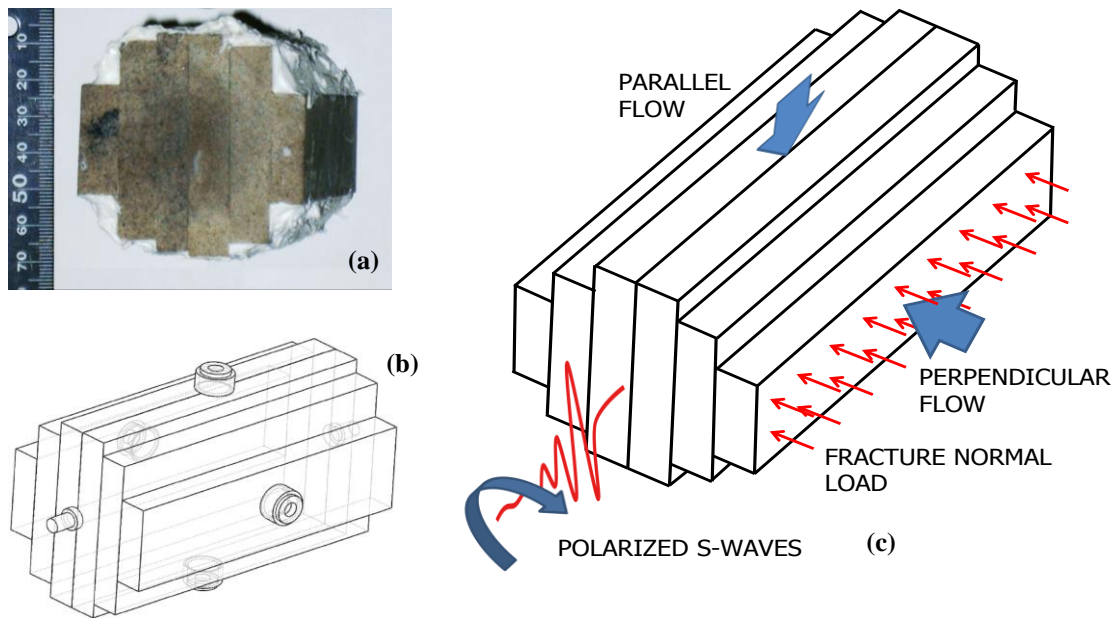
**Figure 5.4. (a) Cross-section of the fractured sample specimen showing sealant application for restricting airflow. (b) Schematic of the specimen showing the location of flow ports for flow parallel and perpendicular to the fractures, and the S-wave transducers for transmitting along the specimen length. (c) Sketch showing the directions of i) parallel and perpendicular flow, ii) the transmission of S-waves and their polarization, and iii) the normal loads applied to the fractures.**

the specimen in directions parallel to and perpendicular to the fracture set orientation (Figure 5.4b).

The specimen was loaded cyclically in a uniaxial compression frame (see Section 4.1.1) which applied normal load to the 5 fracture interfaces in the specimen (Figure 5.4c). This cyclical loading was conducted in 2 stages. In the first stage, the fracture loads were applied in 10 steps from 0 kg to a maximum of 1350 kg (see Table 5.1), unloaded at the same load steps to 0 kg, and then this was repeated for a second loading cycle. Throughout these cycles, closure displacement of the fractures was measured and, at each load step, air was alternately flowed in the directions parallel to and perpendicular to the fracture set to measure air permeability (see Section 4.1.2). The air permeabilities are not considered to be equivalent to the permeability for a single phase liquid due to the phenomenon of gas slip or the Klinkenberg Effect (Tanikawa & Shimamoto, 2006) and needed to be corrected. This was done using standard correction procedures and validated using an empirical method developed by Jones (1972).Table 5.1 gives the equivalent liquid

permeabilities (or Klinkebergpermeabilities) determined for the upward loading portion of the first loading cycle, with $K_{max}$ and $K_{min}$ denoting flows parallel to and perpendicular to the fracture set orientation, respectively.

For the second loading stage, the flexible coating was removed from the ends of the specimen so that the S-wave transducers could be attached using ultrasonic S-wave couplant – this facilitated the transmission of S-waves along the 108 mm length of the specimen. As well, only the first 9 loading steps in Table 5.1 were used (in part because the results from the first loading stage indicated only minimally different results at the two top fracture loads of 840 kg and 1350 kg) and only a single upward loading cycle was conducted. At each loading step, the transmitting S-wave transducer was oriented parallel to the fracture set (orientation T0) and the receiving S-wave transducer was rotated from parallel to the fractures to 180° in increments of 30° in progression (R0, R30, R60, R90, R120, R150 and R180). Then the transmitting S-wave transducer was rotated 30° (T30) and the full 180° angular or azimuthal displacement sweep of the receiving transducer was repeated. This was continued by resetting the transmitting transducer in 30° increments up to 180°. By this procedure, achieved was a full azimuthal (and multimode type) coverage while manipulating and setting both the transmitting and receiving transducer through 180° as all possible combinations in between at each loading step. The acquisition and the data reduction procedure for adequate analyses without compromising resolution could be understood from Table 5.2.

Analysis of the recorded S-waveforms was done by several means. First of all, the time domain waveforms were evaluated to identify the travel times of the S-waves by the first breaks and to measure the greatest signal amplitude. From these, the group S-wave velocity was calculated as the specimen length divided by the travel time, and the peak amplitude were determined as the absolute value of the greatest signal amplitude. Secondly, the S-waves were windowed and the amplitude Fast Fourier Transform (FFT) frequency spectra were calculated. Finally, spectral ratios of the S-wave FFTs were determined by dividing the FFT spectra for a non-attenuating specimen of the same approximate dimensions as the fractured porous specimen by

**Table 5. 1 An example of quantifying permeability anisotropy**

| Load | | Permeability(mD) ( Klinkenberg) | | Anisotropy |
| --- | --- | --- | --- | --- |
| Step | Kg | $K_{max}$(mD | $K_{min}$ (mD) | |
| 1 | 0 | 2.469131 | 0.327563 | 7.537882 |
| 2 | 20 | 2.080805 | 0.327563 | 6.352381 |
| 3 | 50 | 1.805764 | 0.327563 | 5.512723 |
| 4 | 100 | 1.565607 | 0.327563 | 4.77956 |
| 5 | 200 | 1.5 | 0.327563 | 4.579272 |
| 6 | 310 | 1.397107 | 0.327563 | 4.265156 |
| 7 | 410 | 1.326527 | 0.327563 | 4.049686 |
| 8 | 620 | 1.245543 | 0.327563 | 3.802453 |
| 9 | 840 | 1.134442 | 0.327563 | 3.463279 |
| 10 | 1350 | 1.073756 | 0.327563 | 3.278014 |

**Table 5. 2 Various source-receiver relative acquisition azimuths w.r.t fracture plane trajectory orientation**

| Source/Receiver Relative Azimuth (S_R) | R_0° | 30° | 60° | 90° | 120° | 150° | 180° |
| --- | --- | --- | --- | --- | --- | --- | --- |
| S_0° | S0_R0 | S0_R30 | S0_R60 | S0_R90 | S0_R120 | S0_R150 | S0_R180 |
| 30° | S30_R0 | S30_R30 | S30_R60 | S30_R90 | S30_R120 | S30_R150 | S30_R180 |
| 60° | S60_R0 | S60_R30 | S60_R60 | S60_R90 | S60_R120 | S60_R150 | S60_R180 |
| 90° | S90_R0 | S90_R30 | S90_R60 | S90_R90 | S90_R120 | S90_R150 | S90_R180 |
| 120° | S120_R0 | S120_R30 | S120_R60 | S120_R90 | S120_R120 | S120_R150 | S120_R180 |
| 150° | S150_R0 | S150_R30 | S150_R60 | S150_R90 | S150_R120 | S150_R150 | S150_R180 |
| 180° | S180_R0 | S180_R30 | S180_R60 | S180_R90 | S180_R120 | S180_R150 | S180_R180 |

the S-wave FFT. This was done following procedures outlined in Butt (2001), with the slope of the natural logarithm of the spectral ratios being proportional to the magnitude of S-wave attenuation.

## 5.3 Experimental Results

### 5.3.1 S-wave Polarization and Fracture Orientation

Amplitude polarization and magnitude sensitivity to both fracture orientation and stress variability is shown in Figure 5.5. The plots in 5.5 a and b show the S-waves or ultrasonic section recorded for the first load step (e.g., Load step 1 stress path). Figure 5.5 c details the overall loading scheme of the specimen in terms of stress path comparable curves for Load steps 1- 9. This corresponds to the transmittng and receiving transducers being oriented alligned together at the same angle relative to the fracture set, and rotated in range from $0^o$ through $180^o$ in $30^o$ increments. The plots show different amplitude (gain) scales to highlight the features of the waveforms, for otherwise same data. These results highlight two important observations. The first is that the amplitude of waveforms changes polarity over the $0^{\circ}$-$180^{\circ}$ sweep or angular displacement coverage, confirming that the recorded waveforms are in fact polarized S-waves. A small P-wave arrival amplitude is also noted on some signal traces as indicated, however, this is not unexpected since the S-wave transducers do generate and record some P-waves as has been observed in other experimental studies.

The second observation from Figure 5.5 a is that peak amplitude is maximum when the waves are parallel to the fracture orientation while minimum when oriented perpendicular. This is seen in more complete detail in Figure 5.6 a, given detail of Figure 5.5c, showing absolute peak amplitude of the S-waves (sections) over the $180^o$ rotation for each of the 9 load steps, and the S-wave group velocities for waves oriented parallel to and perpendicular to the fractures, denoted as VS1 and VS2, respectively in Figure 5.6 b. These data show that for all 9 fracture loads and stresses, the peak amplitude of the waves oriented parallel to the fractures is consistently higher than those for the waves oriented perpendicular, and that the group velocity parallel to the fractures is higher than the perpendicular group velocity**.**
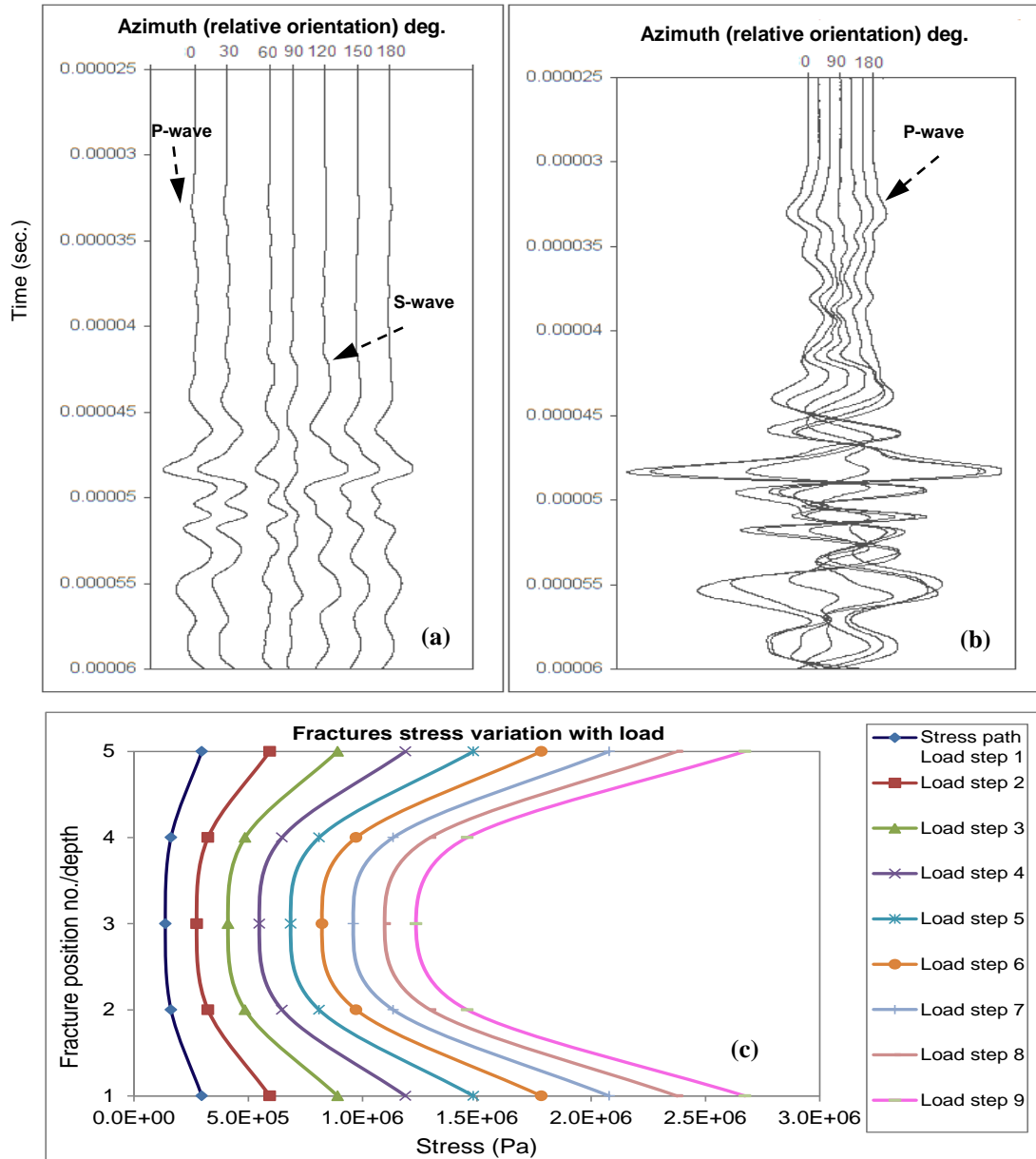
**Figure 5.5.(a) and (b) S-wave waveforms recorded as a function of aligned transmitting and receiving transducers rotated with respect to the fracture plane orientation from angles of 0° through 180° with 30° increments, at Load step 1 (Hassan et al., 2013). (c) Direct stress variability upon fracture planes of fractured medium analogue with load (step 1-9), as fracture 3 is middle or half depth.**

It is noticeable in Figure 5.6 a that at higher fracture loads and corresponding stress as shown in Figure 5.5 c, the ratio of both peak amplitudes and phase amplitudes for the waves oriented parallel to and perpendicular to the fractures is observed reduced or flattened and the group velocities are higher, suggesting that the amplitude of the perpendicular transmitted wave increases relative to the parallel wave at higher fracture load – this is discussed further in Section 5.3.3.

91
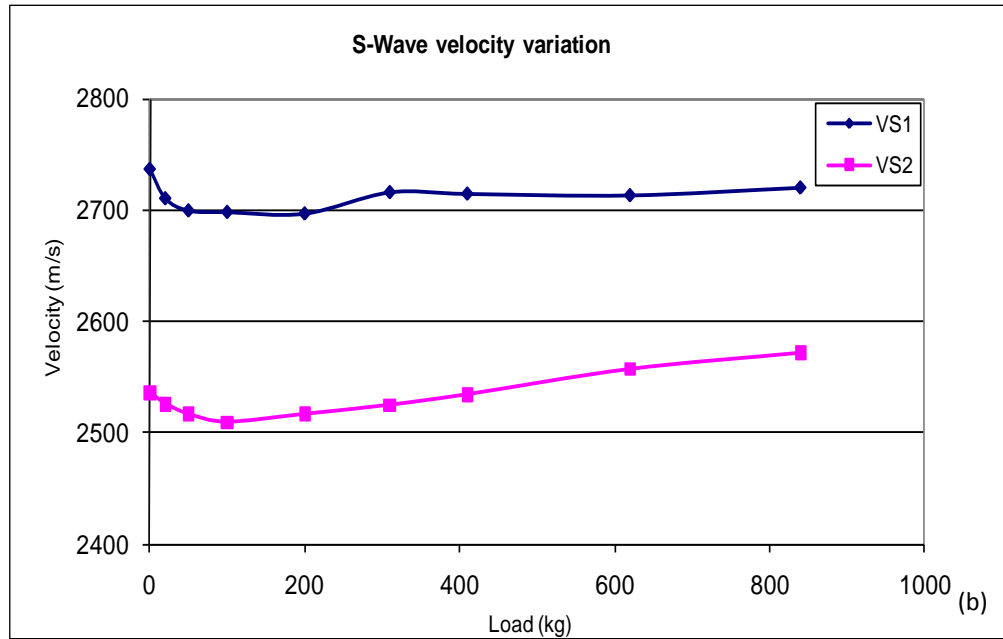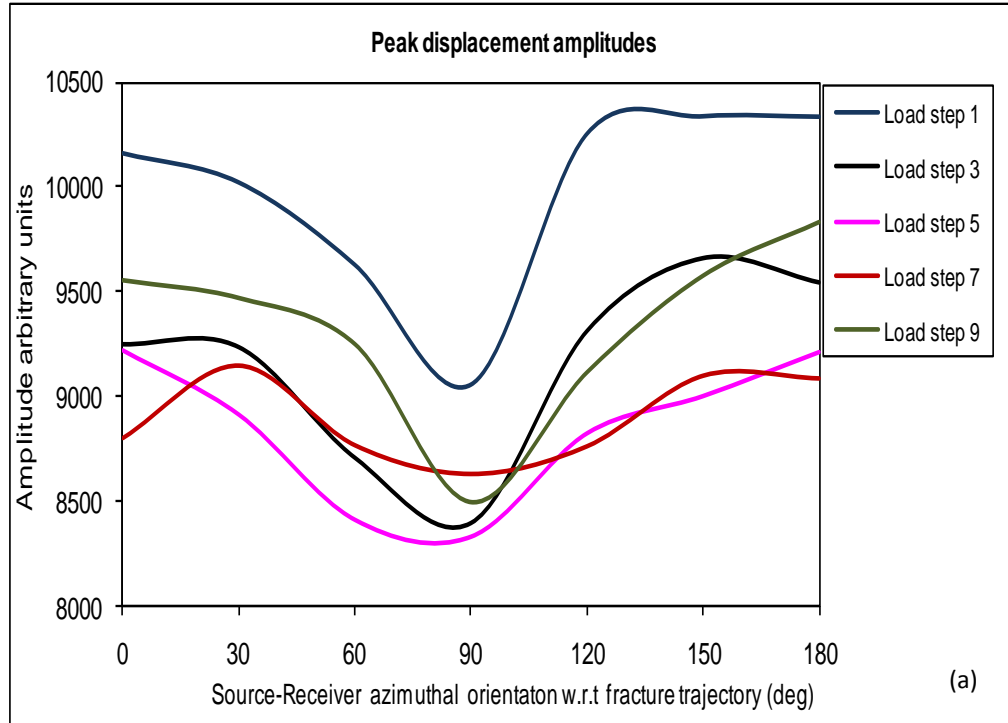
**Figure 5.6. (a)  Absolute peak amplitude variation with load/stress. Top curve for Load step 1 is obtained from ultrasonic section shown in Fig. 5.5 a , other such wave form sections  corresponding to rest of the curves are not shown for same characteristic attributes (b) Velocity variation with load, VS1 corresponds to 0° and 180° amplitudes from above as more stable than VS2 corresponding to 90° amplitudes, velocity behavior facilitates anisotropy quantification (Hassan et al., 2013).**
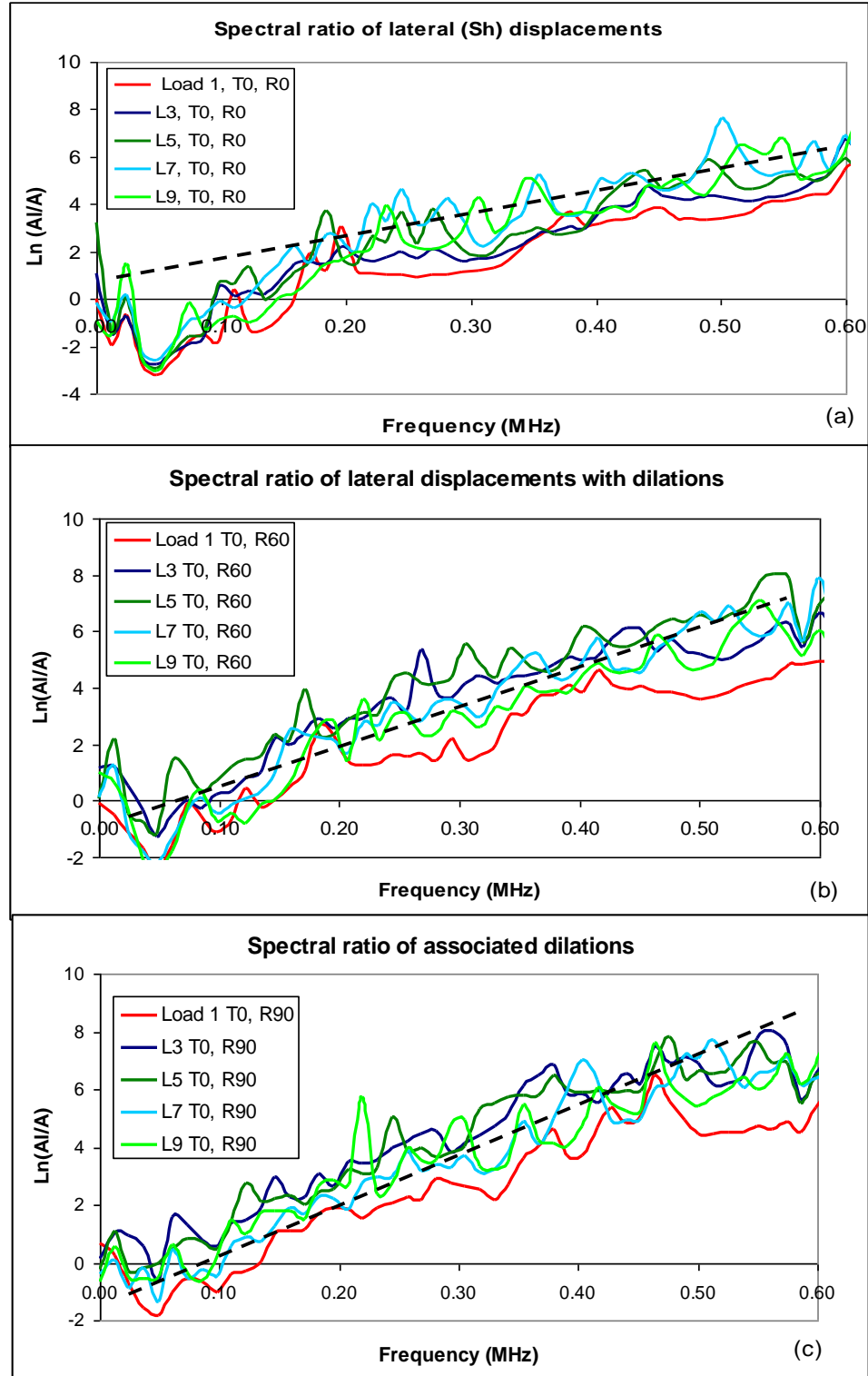
**Figure 5.7. Relative attenuation characteristics of transmitted S-wave displacement amplitudes with stress/load state variation when source polarization is parallel to fracture trajectory and receiver azimuthally rotated (a) receiver parallel to fracture set 0° (b) receiver at 60° (c) receiver at 90°. (Hassan et al., 2015 c)**

Figure 5.7 plots the spectral ratios for the waveforms transmitted parallel to the fracture for all 9 load steps, and recorded at receiving transducer orientations that are parallel (0°), intermediate (60°) and perpendicular (90°) to the fractures. Given that the slope of these spectral ratios is proportional to the level of waveform attenuation, these results show that the S-waves amplitudes at all frequencies are higher parallel to the fractures and lowest perpendicular, consistent with group velocities and peak amplitudes results shown in Figure 5.6.

Overall, these results show that S-wave group velocities and amplitudes will be highest when the waveforms are polarized parallel to the dominant fracture set, results which are consistent with the past studies discussed in Section 5.1.

## 5.3.2 Fracture Spacing and Stiffness

It is a known phenomenon that regularly spaced features such as fractures, bedding planes, free surfaces for buried receivers, e.t.c., can result in the selective enhancement or reduction of specific frequencies in the signal when the wavelengths are at a specific length scale compared to the spacing of the features. These are attributed to the superposition of the primary and reflected waves from the features and resulting constructive or destructive interference at the characteristic wavelengths. The reduction of specific frequencies or frequency bands in the received waveforms are often call receiver notches (Cieslewicz & Lawton, 1998) or transmission notches (Nolte et al., 2000; Angel et al., 2009) when they are observed in received waveform frequency spectra. At the outset of this investigation, one objective was to determine if such phenomena could be observed for fractured porous media, and hence the design of the fractured porous media specimen with regularly spaced fracture interfaces.

Figure 5.8 plots the frequency spectra for the S-wave transducer, the received S-waveform transmitted through the non-attenuating aluminum (T-63 type) reference specimen and the received S-waveform transmitted through the fractured porous media specimen at load step 1 with both the transmitting and receiving transducers oriented parallel with the fractures.
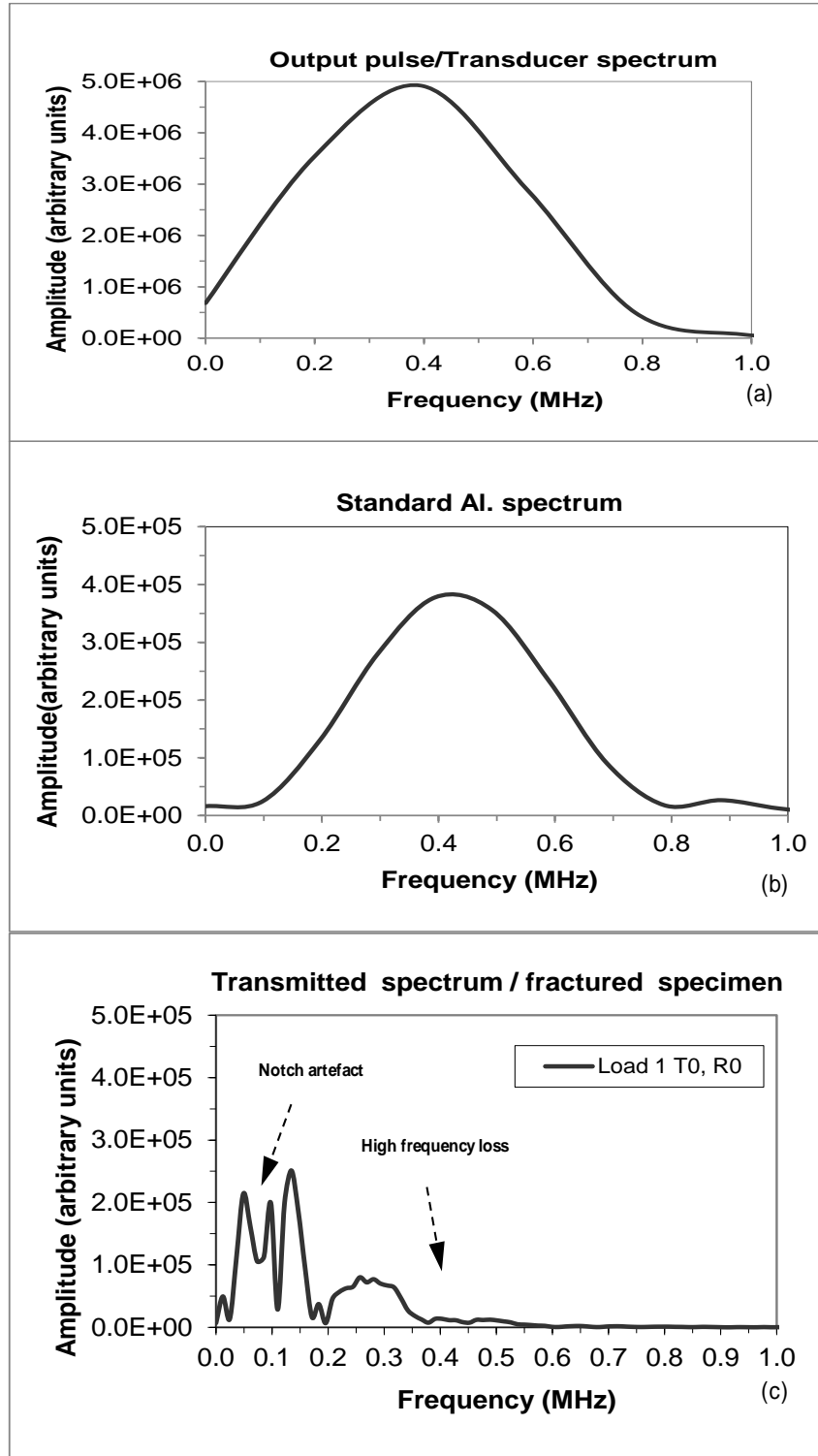
**Figure 5.8. (a) Spectral characteristics of the source pulse.(b) S-wave transmitted response spectrum of a similar intact aluminum (core). (c) Typical transmitted bandwidth when a single wave form is examined (Hassan et al., 2014 b).**

This clearly shows that i) the S-wave transmitted through the fractured porous media specimen is attenuated, as indicated by the loss of higher frequencies and the shift of frequencies to lower values relative to the non-attenuated aluminum waveform, and ii) that there are several transmission notches present in the fractured porous media specimen spectra. Figure 5.9 carries this analysis further and plots the corresponding transmitted spectra over the full fracture load range for the transmitting transducer oriented parallel to the fracture and the receiving transducer orientated at 0°, 60° and 90° relative to the fracture. These results show that the transmission notches (stop band or gap band) are present in all the waveform spectra, however, there are several notches or bands that occur at consistent frequencies or frequency bands for most of the waveforms. The consistent notches are highlighted in panel (b) and labeled as *~1.5d* and *~3d*. Given that the S-wave group velocity perpendicular to the fractures is in the range of 2500 m/s to 2600 m/s (see Figure 5.6) the frequency bands identified correspond to wavelengths that are approximately 1.5 and 3.0 times the average fracture spacing of d = 1 cm, hence the label terminology used. Basic ray tracing based assessment would reveal that this is the fracture spacing where 180° out of phase primary and reflected waves destructively interfere, however, more rigorous wave propagation modelling (which is beyond the scope of the current laboratory study) can be done to confirm this relationship. Fracture specific stiffness is related to the amount or degree of aperture closure that occurs for each incremental increase in fracture normal load, and is given as the fracture normal load required per unit amount of fracture closure. Generally, the aperture of a fracture will decrease with normal load and will become asymptotic to a maximum fracture closure (Greenwood and Williamson, 1966) – at this point, specific stiffness is tending to infinity and the fracture will not close any further. The pressure and composition of pore fluids present in the pores and fractures in saturated formations can change fracture stiffness by counteracting fracture normal loads or changing fluid stiffness. Therefore the ability to identify changes in fracture stiffness may indicate changes in either pore fluid pressure or composition in fractured porous formations and has potential as a tool to monitor fluid changes in the subsurface.
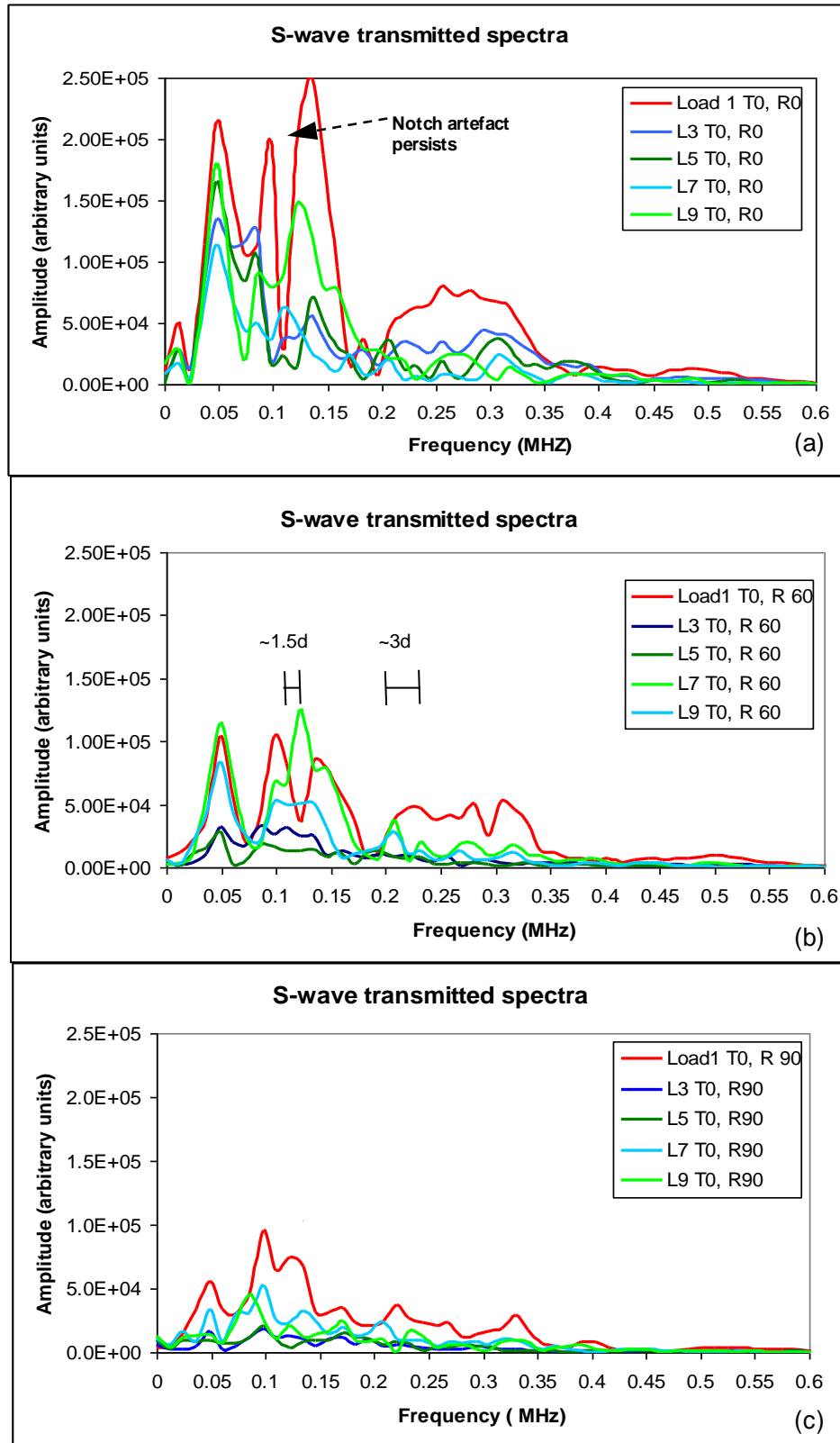
**Figure 5.9. S-wave spectra over the full range of fracture loads with source polarization parallel to fracture and the receiver oriented (a) parallel to fracture set at 0° (b) at 60° (c) at 90°.**
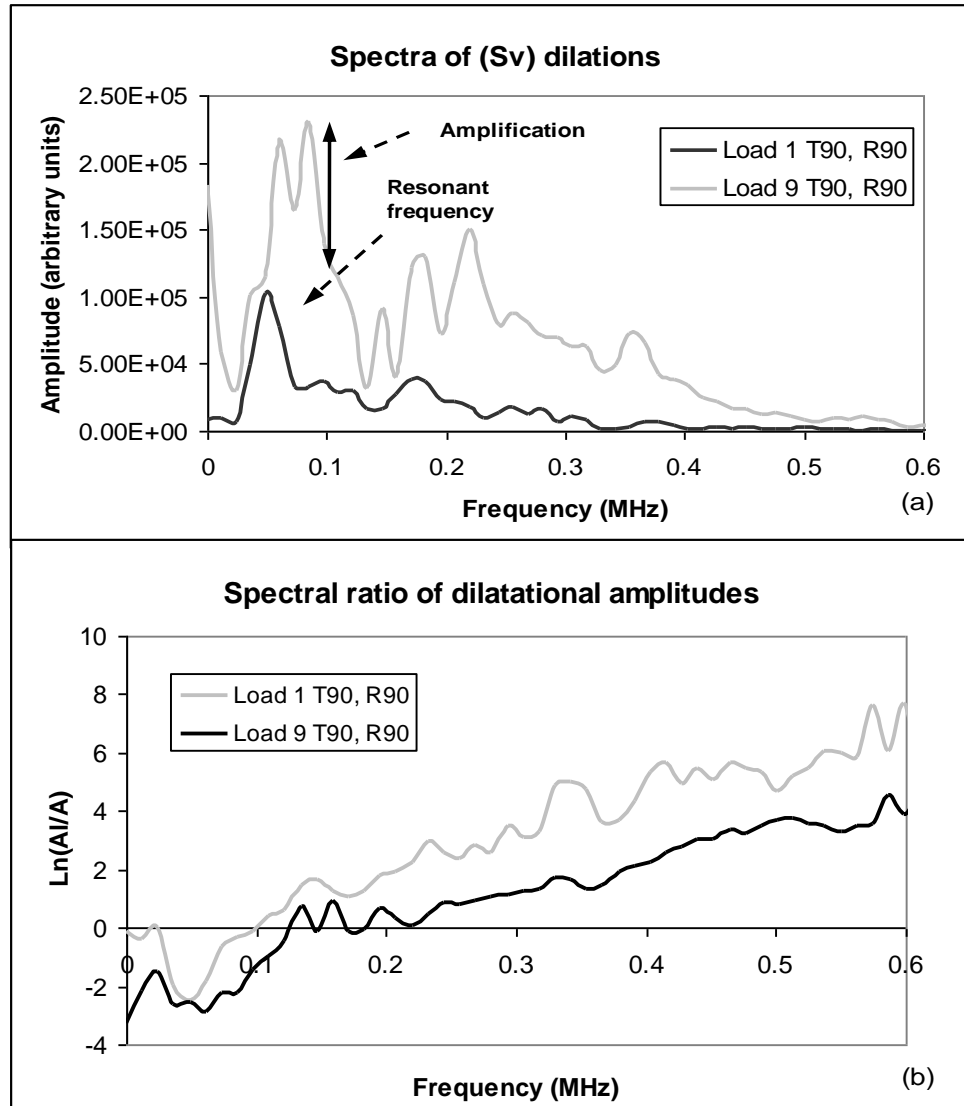
**Figure 5.10. Dilatation spectra compared for normal stress (scale) and (direction) (Hassan et al., 2015 c).**

Figure 5.10 plots the frequency spectra and spectral ratios for waveforms with transmitting and receiving waveforms oriented perpendicular to the factures at the 1st and 9th loading step. These results show that with increasing fracture load and stiffness, the amplitude of the transmitted waves oriented perpendicular to the fractures is increased. This is consistent with the reduction of the ratio of peak amplitude for parallel to perpendicular polarized waves shown in Figure 5.6b, as discussed earlier. Overall, these experimental results indicate i) that notches in the receiving transducer frequency spectra have a characteristic relationship with the

dominant fracture set spacing, and ii) increasing fracture load and stiffness results in an increase in the peak amplitude of perpendicular polarized wave form relative to the parallel polarized waveform peak amplitude.

### 5.3.3 Permeability Anisotropy

Figure 5.11a plots the permeability estimated for flow oriented parallel to and perpendicular to the fractures for the incremented loading and decremented loading portions of both loading cycles during flow. Note that in this figure, M stands for matrix flow and denotes flow oriented perpendicular to the fractures, while F stands for fracture flow and denotes flow oriented parallel to the fractures. Further, the matrix flow is labelled as $K_{max}$ while the fracture flow is labelled as $K_{min}$, following the conventions in Ayan, et al. (1994). From this data, several patterns are evident. The first is that the matrix permeability is constant at approximately 0.3 mD for all portions of both loading-unloading cycles. Changes in fracture load or stiffness have no effect on the matrix flow indicating that the fractures have a negligible role in the flow perpendicular to the fractures. Secondly, the fracture flow is highest for the 1$^{st}$ loading step and then decreases rapidly over the first few loading steps, becoming asymptotic to a permeability of approximately 1.1 mD at the highest load steps. This permeability pattern is nearly identical for unloading portion of loading cycle 1 and for both loading and unloading portions of loading cycle 2 (with initial permeability in the 2.3 to 2.7 mD range) indicating that the closure and opening of the fracture is predominantly elastic. The permeability pattern for the uploading portion of 1$^{st}$ loading cycle is different, initially starting with a permeability of 6.4 mD but also becoming asymptotic to 1.1 mD at high fracture load, indicating that closure of the fracture on this initial upward loading cycle is partially permanent. Overall, this indicates that the fracture permeability becomes asymptotic to a minimum value at effective full fracture closure, but this permeability is greater than the matrix permeability.
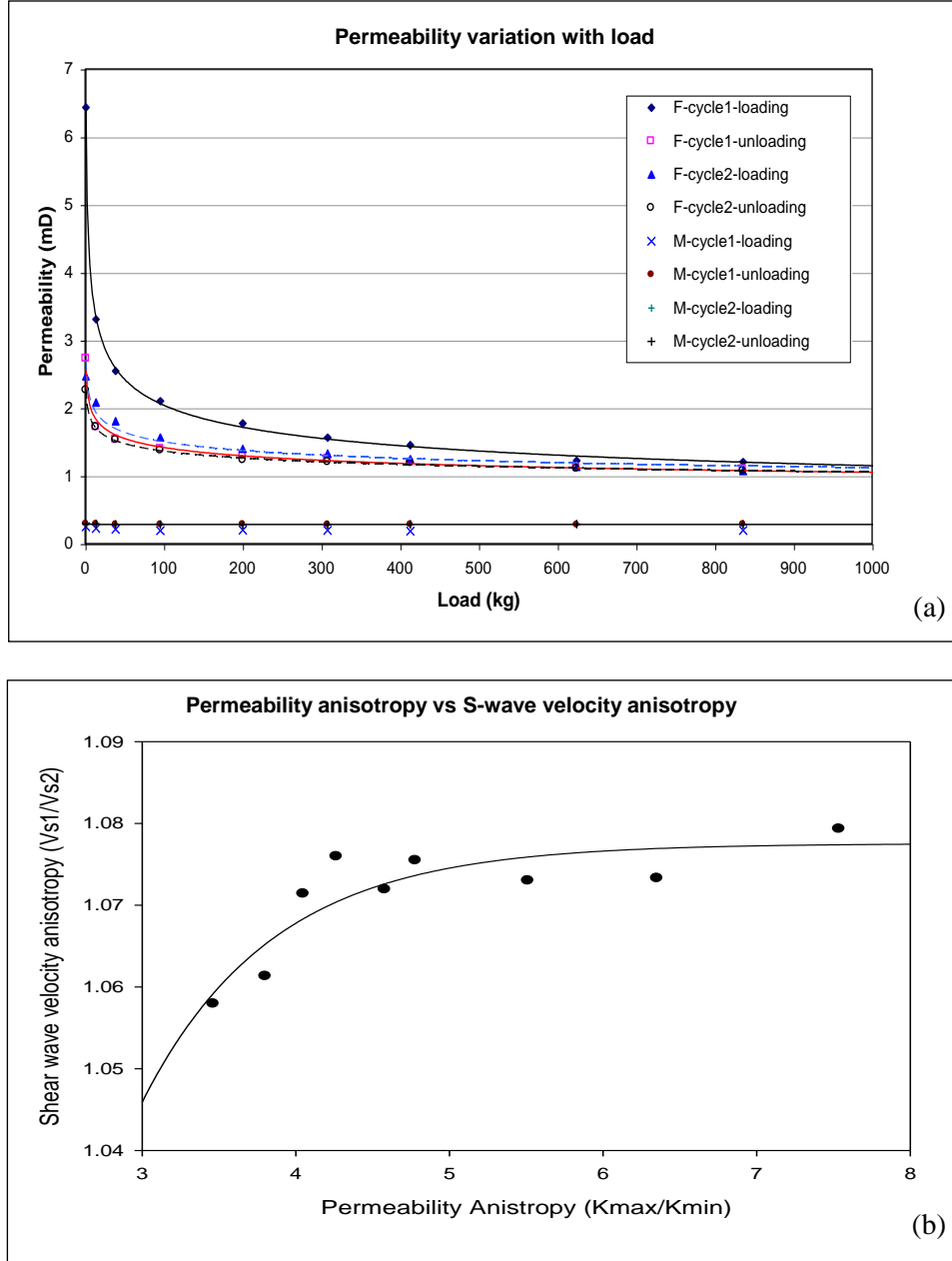
**Figure 5.11. (a) Permeability variation with fracture load, and (b) permeability anisotropy and S-wave velocity anisotropy correlated (Hassan et al., 2013).**

permeability ($K_{min}$) data given for the upload loading portion of the $1^{st}$ loading cycle in Figure 5.11a and tabulated in Table 5.1. these results show that when the permeability anisotropy and velocity anisotropy are changing with fracture stiffness (up to about a fracture load of 100kg from Figures 5.11a and 5.6b) the velocity anisotropy is approximately constant and therefore there is no relationship between permeability and velocity anisotropy. For fracture loads greater than this, however, there is an approximately linear relationship between permeability and velocity anisotropy. This indicates that with appropriate calibration (which is beyond the scope of the current investigation) the anisotropy of the maximum and minimum permeabilities oriented parallel to and perpendicular to the dominant fracture set can be estimated.

## 5.4 Summary

At the outset of this investigation, it was presumed that the direction of the maximum permeability would be oriented parallel to the fracture set orientation and it was expected that the S-wave measurements might provide information about the fracture set geometry and characteristics. These expectations were based, in part, on the review of published literature and theory. From the experiments and data analysis, it was shown that for a fractured porous media that is dominated by a single fracture set:

S-waves that are polarized parallel to the fracture set orientation will have the greatest group velocity, peak amplitude and phase amplitudes compared to S-waves polarized at other orientations.

Transmission notches occur in the transmitted S-waveforms spectra at frequencies corresponding to wavelengths that are 1.5 and 3 times the fracture set spacing.

Increases in fracture stiffness cause increases in both the time domain and frequency domain transmitted wave amplitudes for waves polarized perpendicular to the fracture set orientation relative to waveforms oriented parallel to the fractures.

The maximum permeability direction is oriented parallel to the fracture set orientation and for stiffer fractures there is an approximate linear relationship between the VS1/VS2 velocity anisotropy and the corresponding $K_{max}/K_{min}$ permeability anisotropy.

Based on these results, it can be envisaged that a carefully planned and executed S-wave transmission survey can determine features of a fractured porous formation related to the orientation and spacing of the dominant fracture set, the direction of maximum permeability parallel to the dominant fracture set, and some indication of the permeability anisotropy.

# Chapter 6: Immiscible Fluids Experiments – Porous Media Model

This Chapter focuses on the porous media model used for fluid displacement experiments, including characterization of the porous media material and baseline ultrasonic transmission measurements of the unsaturated dry model, and validation of the model geometry materials and experimental measurements.

## 6.1 Characterization of the Dry Granular Porous Media

### 6.1.1 Dynamic Behaviour of Intergranular Contacts and Friction

In characterization of granular media most important aspects are the notions of existence and control of static friction in bonds and contacts and dilatancy proposed by Coulomb and Reynolds in years 1773 and 1885 respectively (Jager et al., 1996). For idealized granular packs as usual analogues for granular media or typical sand pile models, effect/control of nature of contacts in terms of tractions/displacements in the presence of inter granular friction based adhesion or saturation when acoustically simulated i.e., P- or S-wave, several possibilities of the elastic wave propagation/polarization aspects including strength properties and/or moduli may arise. An understanding of such possibilities is provided in rigorous analytical wave propagation descriptions developed for several possible media/interfaces by Walton (1975, 1977), Miller and Tran (1979, 1981) and (Digby, 1981) following Hertz and Mindlin theory, well discussed in previous sections. Significantly important aspect of a wavelength dependent time restricted /causal morphology of successive grain scale interfacial stick-slip occurrences is also identified. The elusive length scale dependent attribute of intergranular friction in acoustically stimulated granular medium is also examined and explained by (Luding, 2005) and (Goldenberg & Goldhirsch, 2005). Their experimental and numerical investigations suggest a possible micro to macro scale crossover as an isotropic

behavior to an anisotropic behavior, due to a shift from wave like to diffusive mechanism of information transmission/wave propagation, which possibly affects a strength behavior alteration. Manifestation of such alteration is enhanced elasticity by material reorganization or force chains formation. Aimed at understanding micro or grain scale behavior against periodic stimulation (Radjai & Roux, 1995) and (Radjai et al., 1995) in their numerical and experimental investigations/ examinations of 2D macro models of granular material have identified a rotational deformation/displacement field invisible beyond a crossover asymptotic dimension controlled by length scale i.e., number or elements or particles, coupled with global or translational steady state. They imply that an apparent mass associated rotational inertia with friction contributes at grain scale affecting the strength behavior. Their dynamic experimental evaluation of the morphology of rotation processes e.g., rolling vs. translational sliding combined effects, of plastic cylindrical elements as macro proxy of grains reveal a fragmented structure marked by stages or possibilities of "rotation" and "frustration" episodes as characteristic stick-slip model where frustrations may account for a friction controlled material reorganization. Assuming hyperstatic contact conditions (Radjai et al., 1996) in their simulation with four different samples/numbers and distributions of circular disks/ particles evaluated the force distribution pattern. The confined samples under zero gravity were vertically stressed with load of several tens of Newton. They identified power law decay against an exponential decay in the forces lower and higher than those of their respective averages. This conforms to the plausibility of reorganization leading to force chain formation, implying that a sub-network with stiffer contacts bears more stress than that with compliant ones, controlled by a friction mobilization effect. In an experimental evaluation of force chains formation concept as percolation comparable phenomenon in compressed granular media (Hidalgo et al., 2002) have also found deformation acoustic distributed amplitude response following a power law, similar in sense.

104

## 6.1.2 Baseline Ultrasonic Measurements

The theoretical overview in the preceding section is evaluated through ultrasonic measurements for porous media in the dry condition with no liquid saturation. The ultrasonic transducer configuration is shown in Figure 6.1 a, using 1MHz ultrasonic source-receiver sensor pairs where velocity estimates from measurements are shown in Figure 6.1b, explained further ahead. The configuration is previously alluded to in a well elaborated previous section, being principally the same, for offering sufficient control and propriety, also used in the immiscible displacement experiments in a dynamic context. The 20 ms traces in panels of Figures 6.2 and 6.3 a-d marked as P1-P4 and S1-S4 atop represent P- and S-wave measurements, respectively. Panels P1-P3 and S1-S3 represent dry measurements while panels P4 and S4 of same are measurements of brine saturated medium offering overall quasi-static characteristics. Measurements of saturated medium are consistent with spectral results described in complete detail in next sections in dynamic context. Several panels in Figures 6.4 a-f describe P- and S-wave intrinsic input and output pulse (spectral) characteristics including and juxtaposed with standard spectra of Al sample of consistent geometry in Figures 6.4 e and 6.4 f. Figures 6.5 a and b represent magnitude compared to those of S-wave in dry medium. S-wave response to saturation effects, however, in temporal pattern and magnitude of displacement amplitudes, and velocity is significant compared to those of P-wave in proportion. This clearly implies an altered granular material elasticity controlled by propagation characteristics and saturation effects combined. Apart from deduction of consequent changes in rigidity and compressibility manifested in velocity estimates presented in Figure 6.1, the causative mechanisms could be inferred by comparative examination of "temporal variations character" of time domain signals/traces of P and S panels of Figures 6.2 and 6.3. In mechanistic sense the elastic energy transmission in saturated medium occurs in a short single/distinct wave like pulse for both ultrasonic P- and S-waves i.e., P4 and S4, in dry medium however character of transmission signature
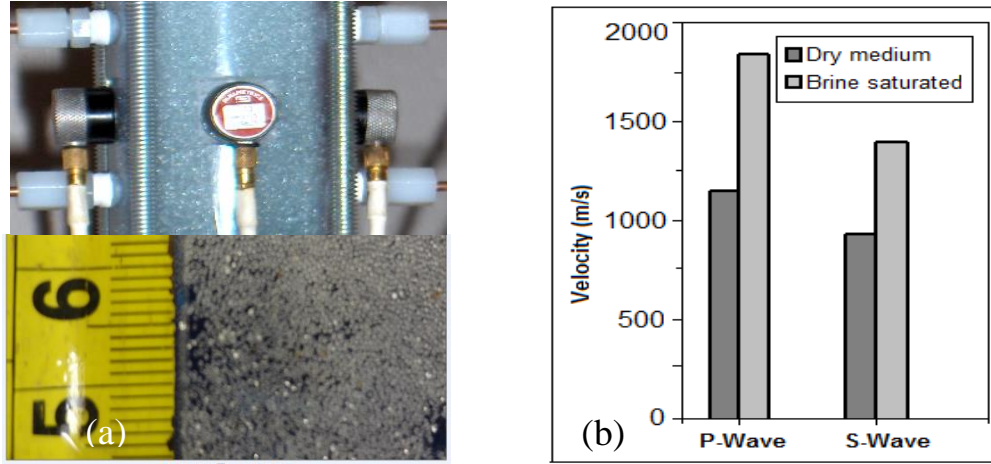
**Figure 6.1. (a) Measurement configuration of granular pack. (b) Velocity estimates dry and saturated granular pack (Hassan et al., 2015d).**

appears to be series or sequence of well separated or delayed instances in time, each representing a discrete state. Further two groups, a "faster" or less time separated low amplitude followed by a "slower" one with greater time separation high amplitude steep instances/occurrences could be observed for each of P1-P3 traces, with trend being opposite in S1-S3 traces. A very interesting observation is that "faster" instances/amplitude events contain repeated sub-occurrences as magnitude fluctuations with a little to a without "zero-crossing" in all of P1-P3 and S1-S3 traces. It could be both deduced and posited that a material fragmentation is observed and/or caused due to a granular reorganization affecting elastic properties during ultrasonic energy transmission. The reorganization is possible consequence of high frequency content of transmitted band in case of P-wave transmission and comparatively low frequency one in case of S-wave transmission where localized stick-slip events may occur as hardening events in P-wave transmission as opposed to energy decay events in S-wave transmission owing to polarization aspects/effects related stick-slip phase issues.
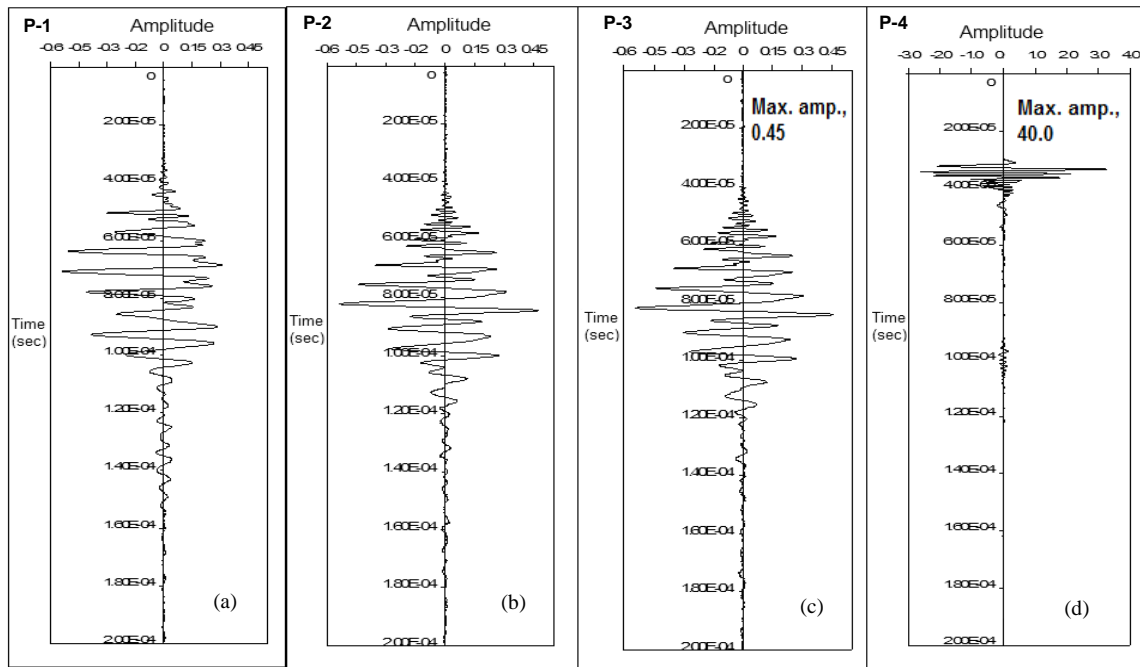
**Figure 6.2. (a), (b) and (c) P-wave ultrasonic measurements (wave forms) of dry granular sediment analogue of 25 ms duration (d) Measurement for brine saturated analogue (Hassan et al., 2015 d).**
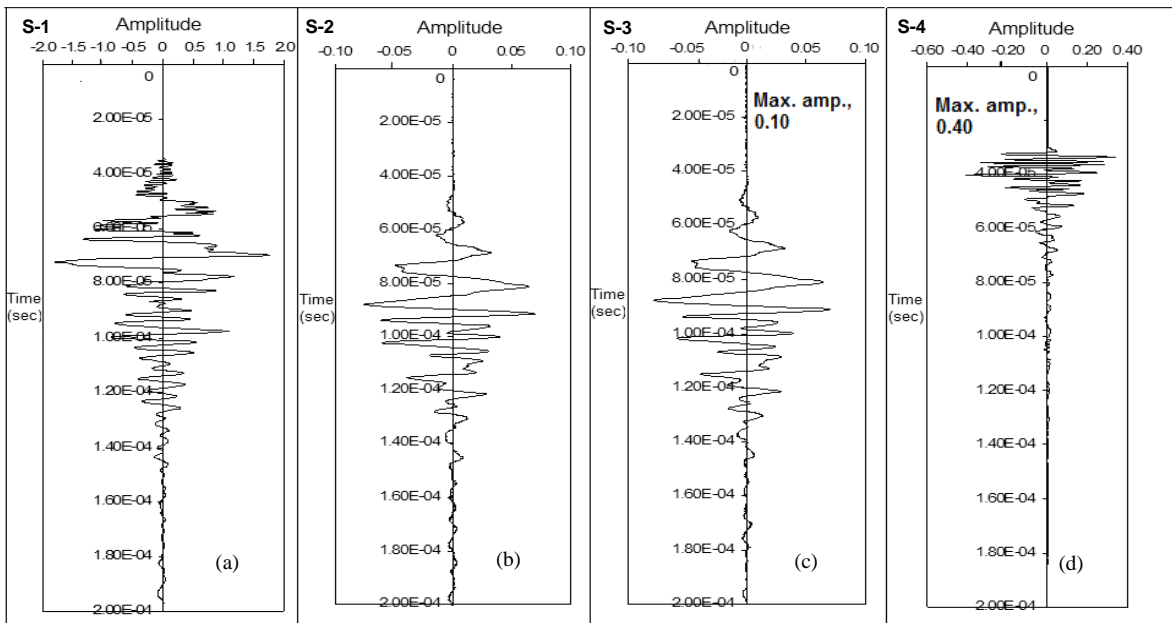


**Figure 6.3. (a), (b) and (c) S-wave ultrasonic measurements (wave forms) of dry granular sediment analogue of 25 ms duration (d) Measurement for brine saturated analogue (Hassan et al., 2015 d).**
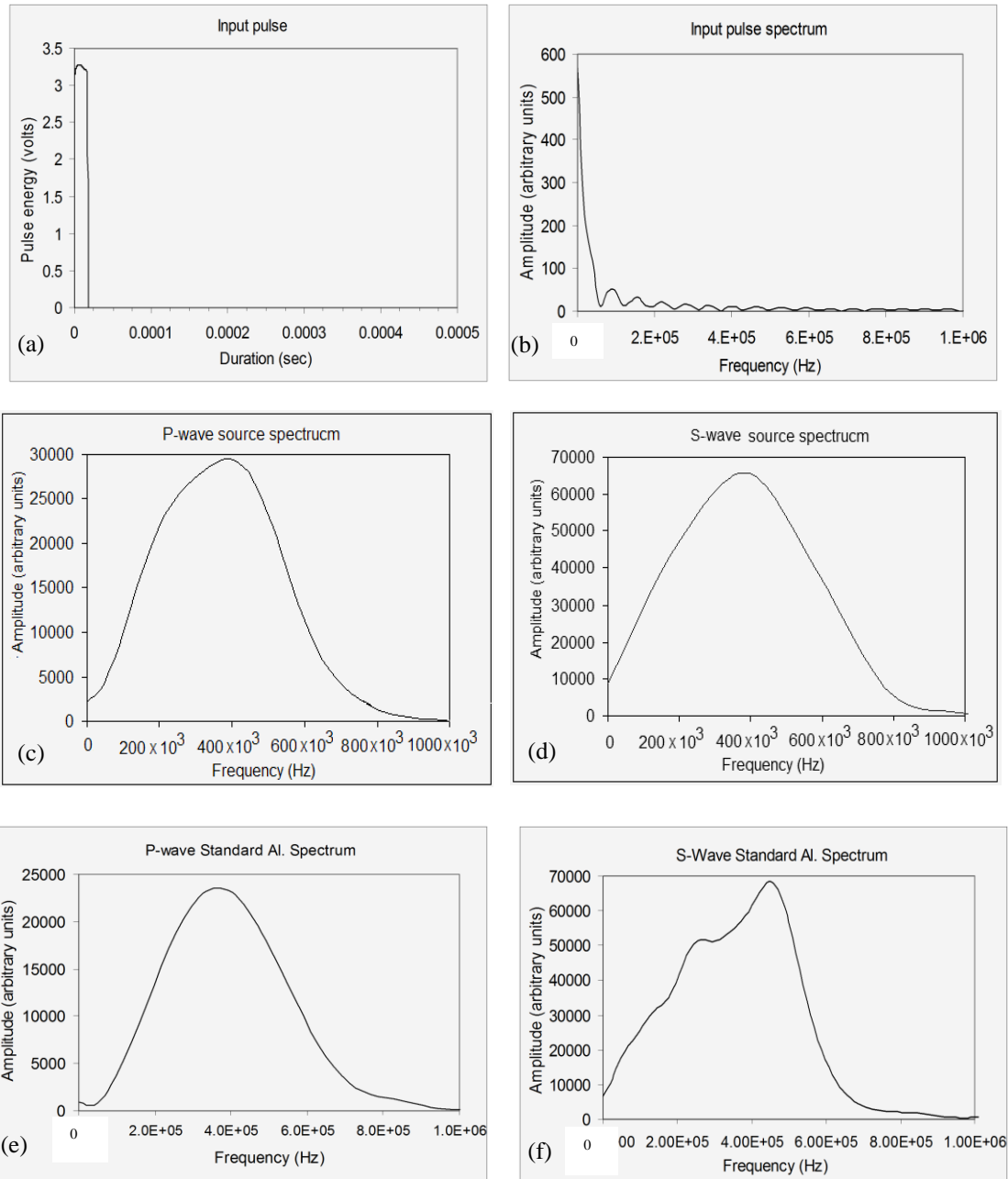
**Figure 6.4. Ultrasonic measurement input characteristics. (a) Input pulse (b) Input pulse spectral distribution (c) P-wave transmitted source spectrum. (d) S-wave transmitted source spectrum (e) and (f) P- and S-wave standard (Aluminum) spectra.**

108
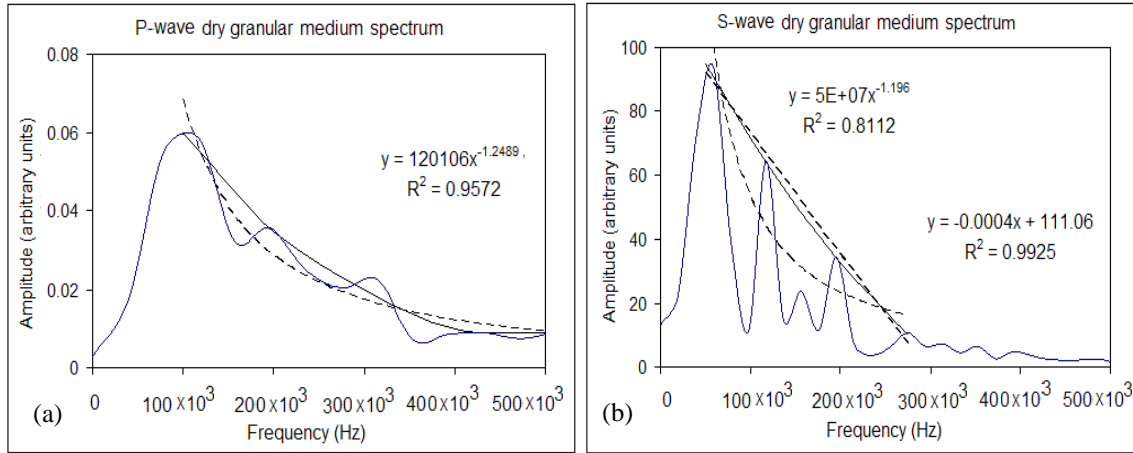
**Figure 6.5. (a) P-wave dry medium (resonance) spectrum, with power law type decay. (b) S-wave dry medium (much pronounced resonance) spectrum, with power law type decay (Hassan et al., 2015 d).**

The fragmentation reorganization could be unambiguously confirmed from resonance type P- and S-wave spectral effects, more pronounced in case of S-wave propagation, as shown in Figures 6.5a and 6.5b respectively. Amplitudes clearly decay from lower to higher frequencies as a power law, specific to the case. Seemingly quiescent periodic seismic and aseismic macro events are capable of altering the unconsolidated near surface dry material strength properties at micro scale to cause unexpected accelerated or "louder" macroscopic events.

Micro behavior examination, under ultrasonic stimulation shows that intergranular friction controlled acoustic emission and/or stick-slip type events may constitute or embody a macro material reorganization, where their morphological nature against P- and S-wave stimulation is different in a purely characteristic sense. High frequency occurrences and/or transmission appear capable of irreversibly altering grain scale surface and/or friction properties as an enhanced elasticity effect. It may cause/generate unexpected response contrary to convention especially in case of S-wave transmission under saturated conditions. With peculiar nonlinearities dry unconsolidated granular material behavior is significantly different from quasi-linear effective medium type that of saturated one, requiring caution and an understanding of length scales for any acoustic stimulation based geotechnical and geo-environmental inferring.

Principal objective in explanation, seemingly, is renewing the import of enhanced characterization of the unconsolidated granular material in dry (air filled) state, when stimulated by ultrasonic P- and S-wave pulse transmission in a comparative sense, given above elucidation. However, and none-the-less, additional pertinent objective, to the case at hand, is render more insightfulness to previously explained results, and to address certain peculiarities of subsequent results. These results are aimed at a spatio-temporal description of near subsurface hazardous fluid flow process morphology, in principle, where an integration of interpretation and data fusion is assumed. Results are presented in graphical form, supported by pertinent theory and citations, for rendering sufficient plausibility and/or understanding of discussion given the objectives. Most of the explanation pertains to results of (Hassan et al., 2015 d).

## 6.2 Adequacy and Validation of Experimental Measurements

### 6.2.1 Ultrasonic Measurements

For any discontinuity and associated anomaly to be resolvable, its sensitivity to probing bandwidth is important. Given the grain or bead size of 0.5 mm, the transducer diameter "d" being 13 mm with maximum propagation length of about 5 cm, the adequacy criterion for attaining resolution suggested by(Malhotra & Carino, 2004), i.e., d = 4 $\lambda$, is met, considering the packed system as an aggregate. Adequate resolution for the length scales covering a bead size, few beads and comparable the propagation length, given physical properties suffices for plausible interpretation.

The ultrasonic measurements were conducted using the transducer arrangement shown in Figure 6.1. With a wall thickness of 5 mm the dimensions of inner core space housing the porous media analogue would be 5.09 cm x 45 cm cross-section offering a volume of around 225.5 cm$^3$. To facilitate a realistically reliable coupling and pulse communication for ultrasonic measurements two pairs of indentation pads or seats at midspan, with pairs mutually orthogonal and diametrically mirroring, were machined. Each seat with 2 cm x 2 cm surface (area) and of 1mm depth each, would accommodate or allow attachment/connecting of an

ultrasonic source or receiver transducer/sensor, facilitating a perfect through transmission configuration both for P-waves and S-waves source-receiver pairs in same horizontal plane at a right angle, mutually. Gel and permanent glue couplants, both types were tested to determine and understand the bearing of nature of coupling on the morphology of acquired signals in terms of consistency, adequacy and quality. Permanent glue type adhesive was chosen and used as couplant for a firm contact helping uninterrupted continuous acquisition for several hours in any given experiment or run. Three sets of reliable readings (data sets) with establishing desired control, assumed reasonable, were examined.

## 6.2.2 Electrical Resistivity Measurements

For controlled continuous but discrete electrical resistance measurements separate electrode probe pairs were used at each horizon or length scale of interest. Probes were around 8 cm equal lengths, and each was high conductivity 3 mm round section copper conductor. One end of probe was conically pointed to around $45^o$ taper and inserted 5 mm inside of the flow cell tube to form a single conductive point contact directly with medium inside the tube. The electrical contact could be appropriately maintained and confirmed by passing or guiding the probes through special fittings provided on tube exterior. These fittings allowed fulfill two purposes, firstly a precise and consistent adjustment and alignment of probes, and secondly tightly holding/securing them in place preventing fluid leakage and associated issues of short circuiting when any fluid may be flowed through the tube during its functioning or positioning to interface with other equipment. Figures are shown in sufficient detail in pervious chapters. Probe pairs in terms of separation were spanned along the length of the tube considering the nature of sampling rates and category or nature of flows or rates involved,  as in terms of defining parameters control.

## 6.2.2 Flow Measurements

The invaded or the displaced fluid phase of the immiscible displacement process was introduced first into the unconsolidated core analogue soda lime beads pack for attaining complete saturation. It was ensured or confirmed that the saturation was one hundred percent and spatially uniform as air was vacuumed out if needed i.e, full saturation condition. For creating or choosing the initial flow rates of the displacing or invading fluid phase to replacing or displacing the invaded, to start with, nature of similar subsurface flows was kept in view. An adequate understanding of the nature of such subsurface flows for different subsurface processes can be sought and inferred from (Newman et al., 1956), (Curtis, 1967), (England et al., 1987),(Woessner & Sullivan, 1984) and (Becker et al., 2004). The flow rates of choice, with the overall geometrical restrictions of the apparatus functioning were, 0.044 ml/s, 0.11 ml/s and 0.64 ml/s corresponding to values of about 4 L/d, 10 L/d and 55 L/d defining or identifying a slow, intermediate and a fast flow rate experiment correspondingly. Categorically stated, the chosen flow rate variation range was to or would fall within the limit of seepage type, observed at reservoir scale or flows measured/observed in near surface aquifer characterization. An external flow-control system, powered by a 1.5 hp centrifugal pump, with control valves provided at the top and bottom end pieces, would allow a regulated selective flow of fluid through the flow cell against gravity at predetermined constant head controlled initial flow rate, while ultrasonic and electrical resistance data were simultaneously acquired.

An end piece inserted each at the bottom and top end of the flow cell tube, held the granular or bead material forming unconsolidated sediment inside the tube. A round bored hole, 1cm, in the centre of each end-piece covered with flow-disc at its inserted end is provided. Flow-disc surface is engraved with specially designed radiating porous grooves covered by a mesh. Flow-disc as for its design, acts as a retainer disallowing escape of granular material with fluid flow ensuring only a steady and uniformly distributed inflow or outflow of fluids. Two continuous circular sealing rings about 3.75 cm apart provided at the middle of the 9 cm long end-piece

shaft or insert would press against the outer surface of end-piece insert and interior of the tube to allow a unidirectional flow only and keep the end-piece appropriately oriented in place. End-pieces were kept aligned  and connected by steel tension rods to allow stressing and compaction of the granular bead material for achieving sufficiently stiff grain to grain contact while keeping the flow-cell tube mechanically isolated and relaxed. Tension rods were anchored to an aluminum base-plate with dimensions of 19.5 cm x 15.5 cm x 4 cm with adjustable threaded rubber damper-pad mounted bolts, screwed at each corner to allow perfect leveling, stability and mechanical isolation of the flow-cell system.

As alluded before noticeable aspects are that any measurement by the ultrasonic sensor attached flow cell midspan during functioning of the apparatuses is the same affecting the electrical resistance probes at position 4 and 5 , while fluid intake is always at bottom and discharge at the top. Reduced reliable cross-section of data, without compromising continuity and mutual relevance in time and space, of significant events unambiguously representable by vivid attributes and features of interest is presented, arbitrarily but equally organized to offer a 2-D spatio-temporal effect.

## 6.3 Aspects of the Immiscible Fluid Interface

Drops of a liquid when exposed to atmosphere tend to acquire a particular shape, which should be controlled by the physical properties of a given liquid. Water drops for example show to be uninfluenced by gravity effects at times as they do not collapse and flow on a surface. They appear to contract themselves to attain a minimum surface area, as close possibly as to a sphere. The reason for this physical behavior is that surface molecules are not as much affected by intermolecular cohesion as those towards the inner part of the volume of the water.
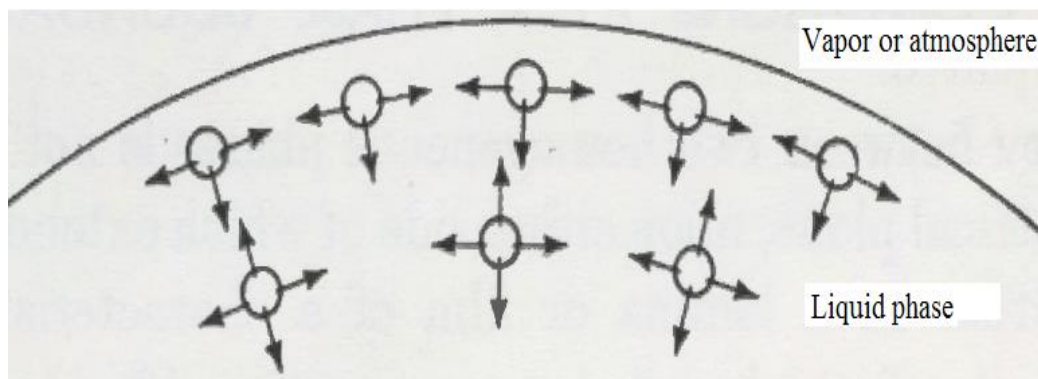
**Figure 6.6. Surface tension phenomenon depicted with possibilities of intermolecular forces and their orientation modified, (Davies & Rideal, 1963).**

The restriction of attaining the minimum energy of equilibrium results not only in formation of minimum surface area but causes surface molecules hold tightly together, spontaneously, as if in tension. This phenomenon is called surface tension. Surface tension is defined usually as forming of an interface by liquid surface exposed to atmosphere (atmospheric conditions) only, shown in Figure 6.6 . When both phases are liquids however, understanding of an interface happens to be different by definition. When water, for example, is placed in direct contact with oil, the interface formed has a contractile tendency. Contractility implies acquiring a minimum area with a definite molecular arrangement and orientation given their (chemical) properties and type. Orientation of dipolar molecules specifically occurs at an interface when, as a specific example, the hydroxyl group, say, of an alcohol molecules would immerse in water to form and interfacial layer. The interfacial layer between two fluids is at times termed as a monolayer. Free surface of a liquid fluid, given broader context of the discussion, could in behavior be deduced as layer with tensile stress. Physical existence of elastic stress is difficult to realize, despite that the dimensional restrictions of mathematical formulation does support it.
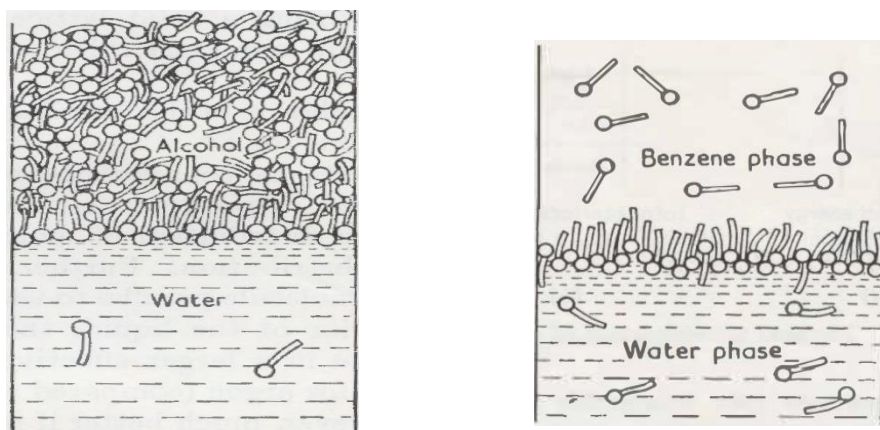
**Figure 6.7. Depiction of interfacial monolayer formation with molecular orientation and possibilities of motion for electrochemical equilibration for two phase water based bulk immiscible systems, modified, (Davies & Rideal, 1963).**

Persistence of existence without variability of deformation is argued to occur by equilibration due to concurrent mutual exchange of low and high energy molecules from free energy (i.e., Helmohltz free energy) surface and bulk volume of fluid with the meanings of providing for a chemical potential balance. Such propositions and possibilities are depicted in Figure 6.7. Further such equilibration to occur could be understood considering the kinetic molecular theory. Fluid bulk phase could be considered at rest while molecules in an agitated state of motion assume several possibilities of effecting entropy given when interfacial molecules have a different liquid (on either of) one side of the monolayer. Total surface energy is considered greater than the free surface energy on grounds and definition that it is excess of the potential energy possessed by the number of molecules within the bulk phase when compared to same number of molecules forming a surface. Arguments point to a unit basis of dimensionalities of Helmohltz free energy definition.

Adding to the above, monolayer is also propositioned to have strength properties, both of compressive and shear strength, indirectly confirming to assume elasticity. Compressive and shear strength properties have usual meanings, however shear strength is understood as capability of withstanding of torsional effort by concentric circular layers. Two very important consequences of these properties are that monolayers, including immiscible interfaces have significant wave damping capacities. It is clearly understood that both molecular concentration (density effect) and the surface aspect (fluid structure) of the viscosity should affect the wave, and

115
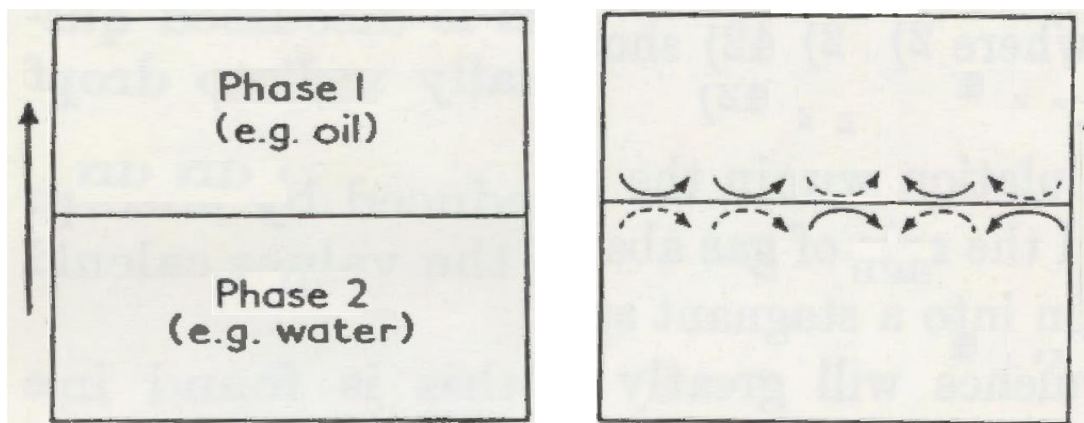
**Figure 6.8. A stable and unstable immiscible bulk oil-waver interface is shown. Eddy type features or mechanisms are shown to equilibrate energy through momentum exchange modified (Davies & Rideal, 1963).**



(a)  (b)  (c)
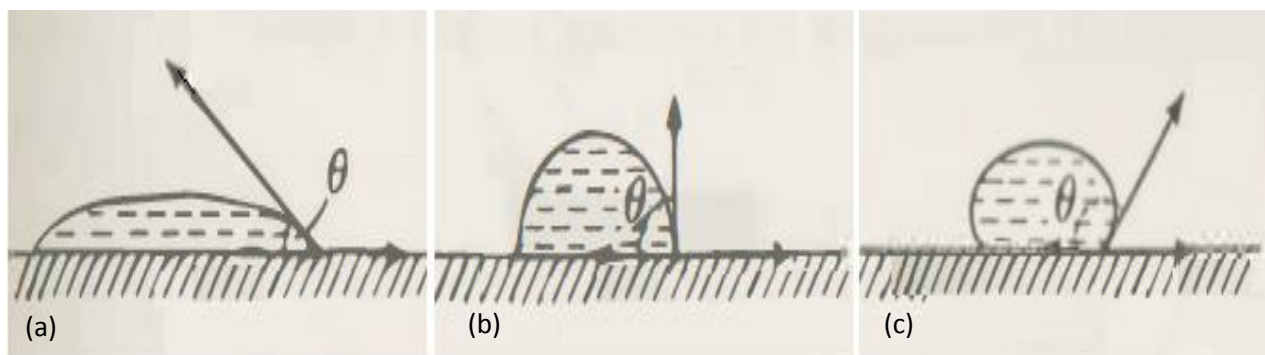
**Figure 6.9. Contact angle (θ) as a measure wetting by spreading of a fluid on solid surface (a) Low contact angle showing preferential wetting comparable to hydrophilic in an aqueous case. (b) A higher contact angle showing less spreading (c) Very high contact angle depicts fluid phobia as in hydrophobia modified (Davies & Rideal, 1963).**

should cause any wave damping. Findings however suggest that it is difficult to ascertain which parameter may control or is responsible for maximum damping. Viscosity appears to affect a drag type effect too in monolayers, and further a direction alongside frequency dependence of any stimulated wave damping is deducible, as manner of direct measurement methods imply. On each side of the interfacial immiscible monolayer occur different liquids. The molecules of those liquids would have tendency to suffer a mutual attraction, for both like and unlike molecules. Cohesion defines the attraction force between like molecules while adhesion is the one between unlike molecules. If the attraction between unlike molecules surpasses that of like (same) ones, miscibility is initiated, as surface the

116

energy is naturally minimized further. A work of adhesion is defined as the force per unit area required to overcome the cohesion ,where work of cohesion with similar conceptual meanings and dimensions for a single liquid is twice as much as its surface tension, as two propositions are slightly different. In energy terms thus complete miscibility occurs when work of cohesion approaches minimum. A conceptual mechanism of exchange of work for miscibility is shown if Figure 6.8 where a stable and moving or agitated mixing oil-water "immiscible" interface is shown side by side. Such energy exchange is characterized by speculated to occur by local or eddy flows within global flow involving momentum exchange. For specific and clear appreciation of wettability and affinity of different phases of an immiscible process or system, contact angle is the primary parameter. A simple pictorial definition or concept of contact angle is shown in Figure 6.9. The variability in contact angle is an indirect measure of degree of variability between cohesion and adhesion. Changes of cohesion and adhesion since determine degree of miscibility or immiscibility, and consequently effects of mobility given material property variation restriction of the energy variation, for conservative principles. Wettability has a greater significance in case of a three phase system where solid phase is also involved, and several parameters and their interaction in a complicated manner affects the consistency of the solution or mixed phase. Most of discussion in this section follows concepts explained (Davies & Rideal, 1963), alongside several pictures for relevant illustration.

# Chapter 7. Immiscible Fluid Experiments – Time Domain Ultrasonic Waveform Analysis

## 7.1 Experiments Overview

Three fluid displacement experiments were conducted following the experimental procedures previously outlined in Chapter 4. These were done at different flow rates to evaluate the evolution of the immiscible interface and the development of the "mixed zone" due to the potential for viscous fingering as the less viscous brine displaced the more viscous oil. This was done, in part, to evaluate the potential to differentiate between the single phase oil and brine, and the mixed interface zone occurrence between them using both the ultrasonic and resistivity measurements. Tests 1, 2, and 3 were done at constant discharge flow rates of 0.044 ml/s (lowest flow rate), 0.64 ml/s (highest flow rate) and 0.11 ml/s (intermediate flow rate), respectively. For all tests, the displacement of the oil by the brine was observed visually in the transparent flow cell (since the fluids were dyed with different colours – see Chapter 4) and samples were collected at the discharge line. Each test was run until there was no evidence, either visually or from sampling, that the displacement of the oil was not complete. Results and analyses presented in this chapter focus on analysis of ultrasonic velocity and amplitude, evaluation of porous media matrix strength associated properties, fluid substitution based evaluation following formulation of Biot theory given Gassman restrictions. Chapter 8 is focused on spectral analyses of corresponding ultrasonic waveforms and the similar electrical resistivity measurements to identify the pore fluid characteristics.

## 7.2 Recorded Ultrasonic Waveforms and Amplitude Interference

Figures 7.1 and 7.2 show the P-waves recorded during each of the three immiscible fluid-displacement experiments. These ultrasonograms show the recorded waveforms at specific times during the overall experiments; Figure 7.1 shows the experiment with lowest flow rate and Figure 7.2 shows the experiments with the intermediate and highest flow rate, respectively.
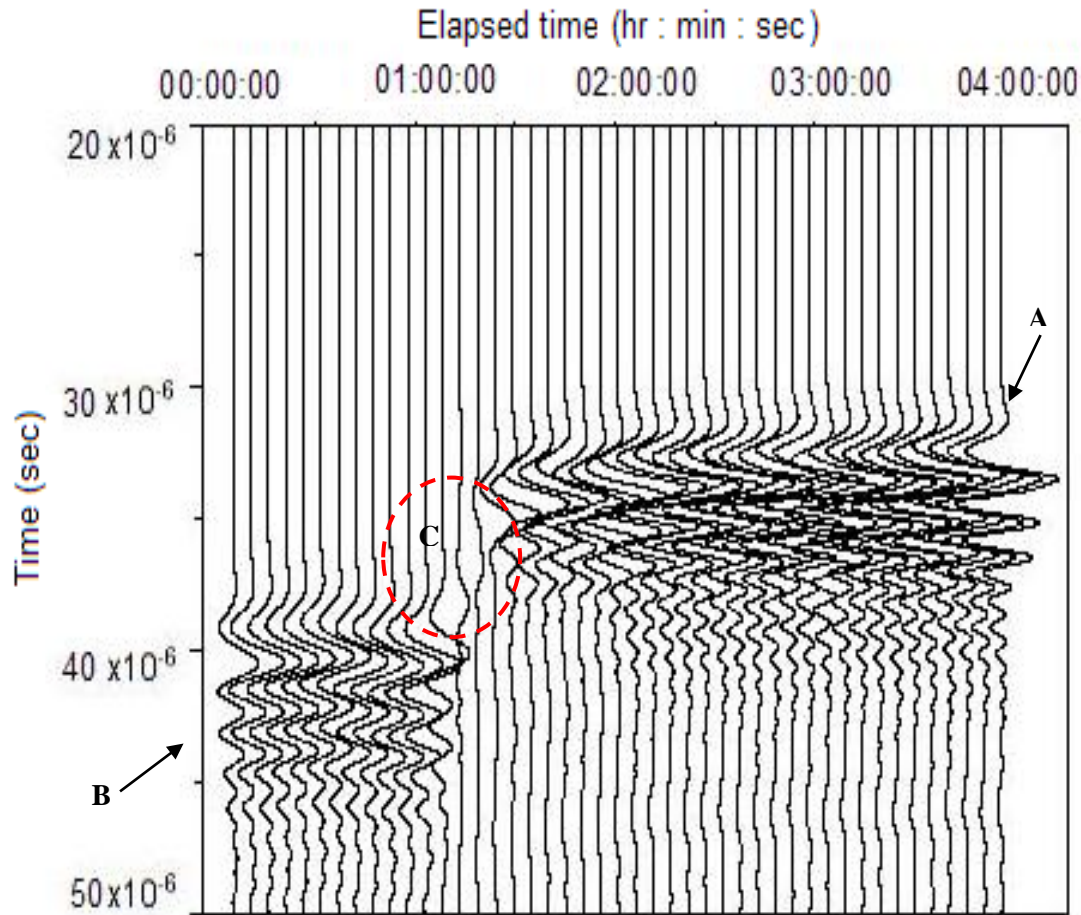
**Figure 7.1. P-wave ultrasonograms of the immiscible displacement Test 1, with a slow initial invading flow rate of 0.044 ml/s. Conspicuous features are marked A for illuminated region, B for less illuminated region and C the interfacial region (Hassan et al., 2014 a).**

All three experiments show similar waveform patterns and these have been labelled and discussed in the detail of Figure 7.1, recognizing that the same analysis is applicable for the other two experiments. In this figure, there are 3 distinct patterns labelled as A, B and C. Region A has the highest amplitudes and corresponds to the test time when the porous media between the sensors was saturated with brine. Region B has the next highest amplitudes and corresponds to the time when the region between the sensors was saturated with oil. Region C is circled in the figure and can be categorized as a dim spot, with low amplitudes that show indications of alternating polarity, and corresponds to the time that the mixed interfacial zone between the oil and brine passed between the sensors. The clarity of the dim spot in Region C is greatest in the experiment with the lowest flow rate and least discernable
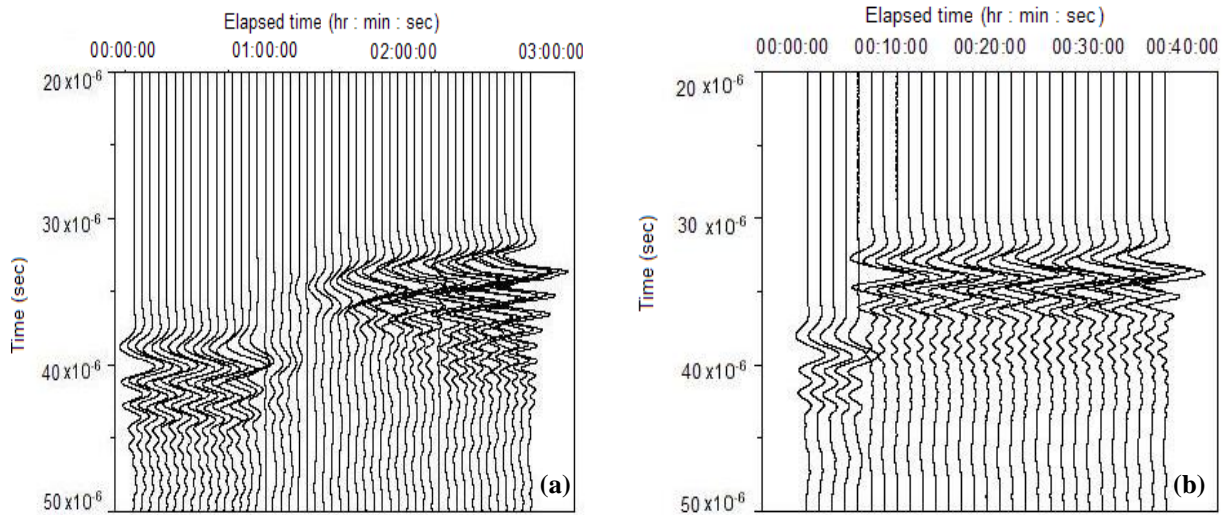
**Figure 7.2. P-wave ultrasonograms of (a) the immiscible displacement Test 3 at an intermediate initial invading flow rate of 0.11 ml/s, and (b) for Test 2 at a faster initial invading flow rate of 0.64 ml/s (Hassan et al., 2014 a).**

in the experiment with the highest flow rate. This suggests, as apparently observed, that the mixed or interfacial zone between the oil and brine phases is the sharpest with the highest flow rate, and gets progressively more diffuse at lower flow rates.

Figures 7.3 and 7.4 show the recorded S-wave ultrasonograms corresponding to the P-wave records in Figures 7.1 and 7.2, respectively. The observed S-wave patterns are labeled and discussed in Figure 7.3 for the lowest flow rate experiment, again recognizing that the analysis is applicable to the other two experiments. The waveform patterns shown for the S-waves are similar to those shown for the P-waves, with the oil saturated Region B and the brine saturated Region A clearly observed, with the brine saturated waveforms having higher amplitudes than the oil saturated waveforms. However, the S-waveforms i) generally have a longer signal length as compared to the P-waveforms, and ii) the transition Region C, corresponding to the progression of the mixed interfacial zone in the region between the sensors, is present but less discernable than for the P-waves. Both of these factors are consistent with greater dispersion of the S-waves and corresponding greater complexity in the waveform interference patterns when transmitted through the mixed phases.
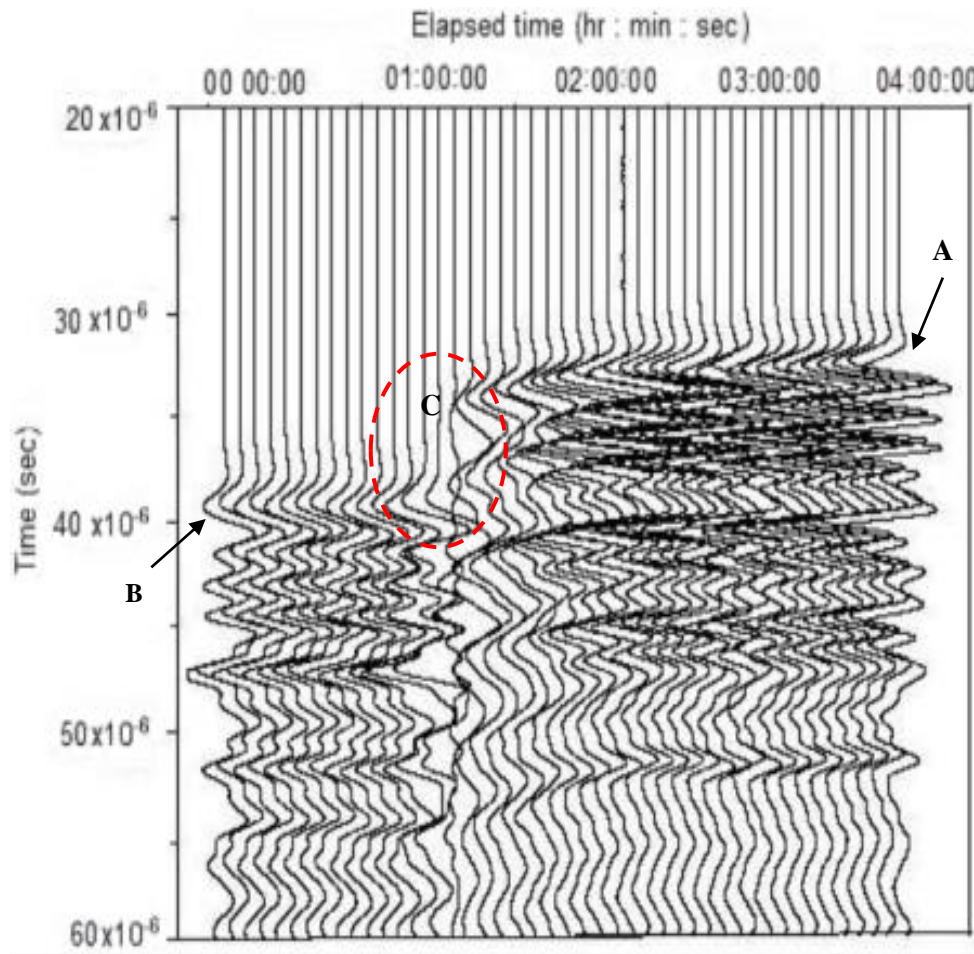
**Figure 7.3. S-wave ultrasonogram of the immiscible displacement Test 1, with a slow initial invading flow rate of 0.044 ml/s. Features of interest are similarly identified A for illuminated region, B for less illuminated region and C the interfacial region (Hassan et al., 2014 c).**

From these P-wave and S-wave ultrasonograms, four observations can summarized. First of all, both the amplitude and velocity of waves transmitted through single phase brine will be higher relative to waves transmitted through single phase oil. This observation is analyzed quantitatively in more detail in the next section. Secondly, the transmission of both P-waves and S-waves through a mixed interfacial zone of oil and brine will appear as a dim spot. This is shown more clearly in Figure 7.5 which shows all 6 wave ultrasonograms side by side, with the dim spots highlighted. These dim spot may due to i) the interference of reflected waves at the various interfaces between the two immiscible liquids, ii) diffraction and scattering effects at these interfaces, or iii) a combination of both phenomena as discussed by
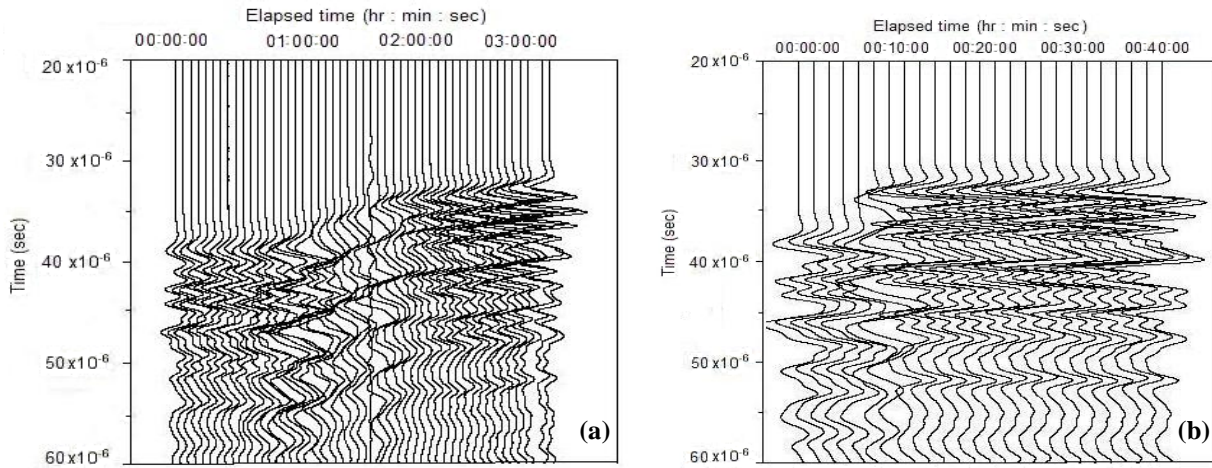
**Figure 7.4. S-wave ultrasonograms of (a) the immiscible displacement Test 3 at an intermediate initial invading flow rate of 0.11 ml/s, and (b) for Test 2 at a faster initial invading flow rate of 0.64 ml/s (Hassan et al., 2014 c).**

Sears (1958) and Widess (1973). Thirdly, S-waves appear to show more scattering when transmitted through the mixed phase zone with more instances of phase inversion and amplitude variation shown in the traces. This indicate that S-waves may be more sensitive to identifying the presence of the mixed phase interfacial zone. Finally, the dimensions of the dim spot can be correlated to the geometrical extent of the mixed zone and the degree to which the initial piston displacement of the oil by the brine will be dispersed by the viscous fingering of the low viscosity brine through the higher viscosity oil.

All of these observations have implications for the planning of field seismic surveys and the waveform analysis for the identification of single phase oil and brine in the subsurface and, in particular, the nature and extent of the mixed zone between the two phases. Specifically, this has potential to enable seismic surveys over an oil contaminated aquifer to monitor the determine the spatial distribution of water, oil and regions of mixed phases in the subsurface.
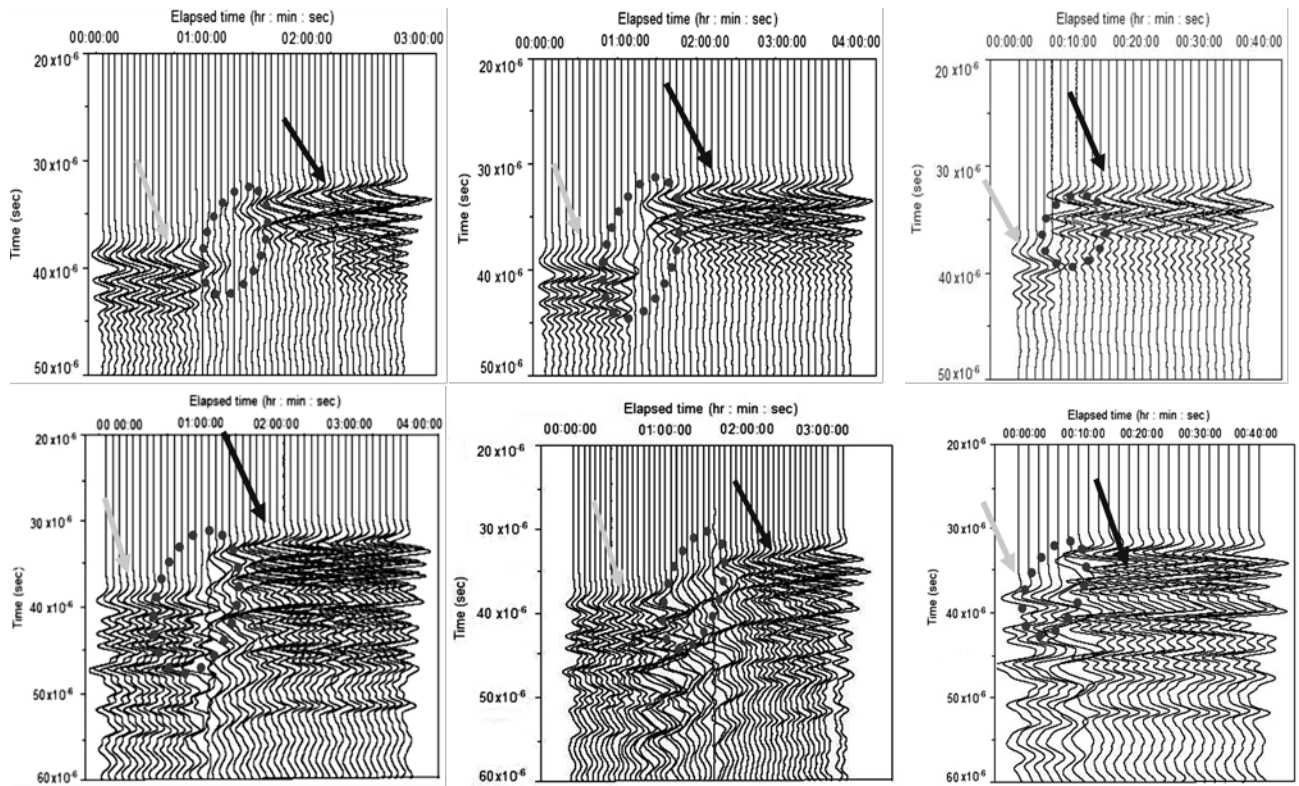
**Figure 7.5. P-wave (top) and S-wave (bottom) ultrasonograms of three immiscible displacement tests juxtaposed with conspicuous features of interest marked, as other features related to diffraction and interference effects also become contrastingly visible. Left Test 1 (.044 ml/s), middle Test 3 (0.11 ml/s) and right Test 2 (0.64 ml/s).**

## 7.3 Velocity and Amplitude Analysis

From the ultrsonograms in Figures 7.1 to 7.5, representing the three immiscible displacement experiments, corresponding velocities and integrated amplitudes are determined. Velocities are determined from the first arrivals of the P- or S-waveforms, and the integrated amplitudes are calculated as the sum of the rectified waveform amplitudes and are analogous to the area under the waveform. Velocity results for all three experiments are presented on single graphs in Figures 7.6 and 7.7, and corresponding integrated amplitude results are given in Figures 7.8 and 7.9, to facilitate easier comparison. Application of these results to interpret the dynamic immiscible fluid-displacement process is consistent with the sediment- acoustic related works of (Stoll, 1977), (Plona & Johnson, 1980), (Johnson, 1980), (Salin & Schon, 1981), (Costley & Bedford, 1988), (Plona, 1980) ,(Shwartz & Plona, 1984), (Chotiros, 1995), (Chotiros, 2002), (Hamilton & Bachman, 1982) and (Gueven et al., 2013), in terms of understating of parametric definitions, restrictions and their control upon outcomes of analysis devised, at scale of interest.

123
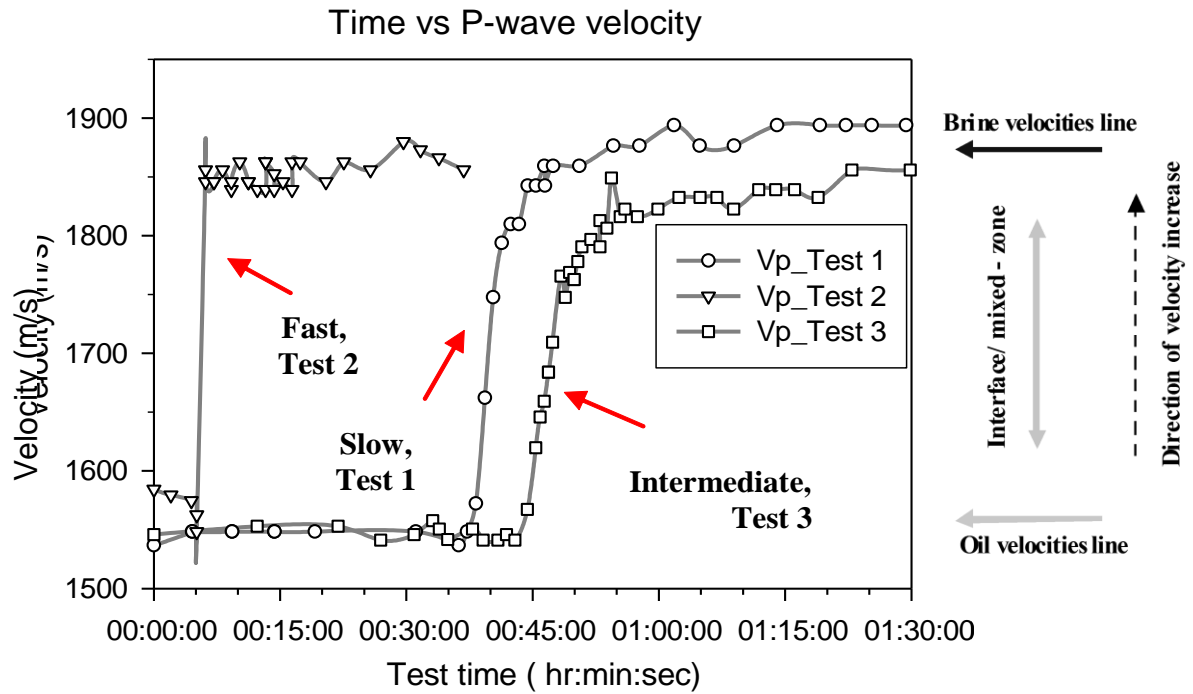
**Figure 7.6. P-wave velocity variation for all tests corresponding to occurrence of different possible phases (Hassan et al., 2014 a).**
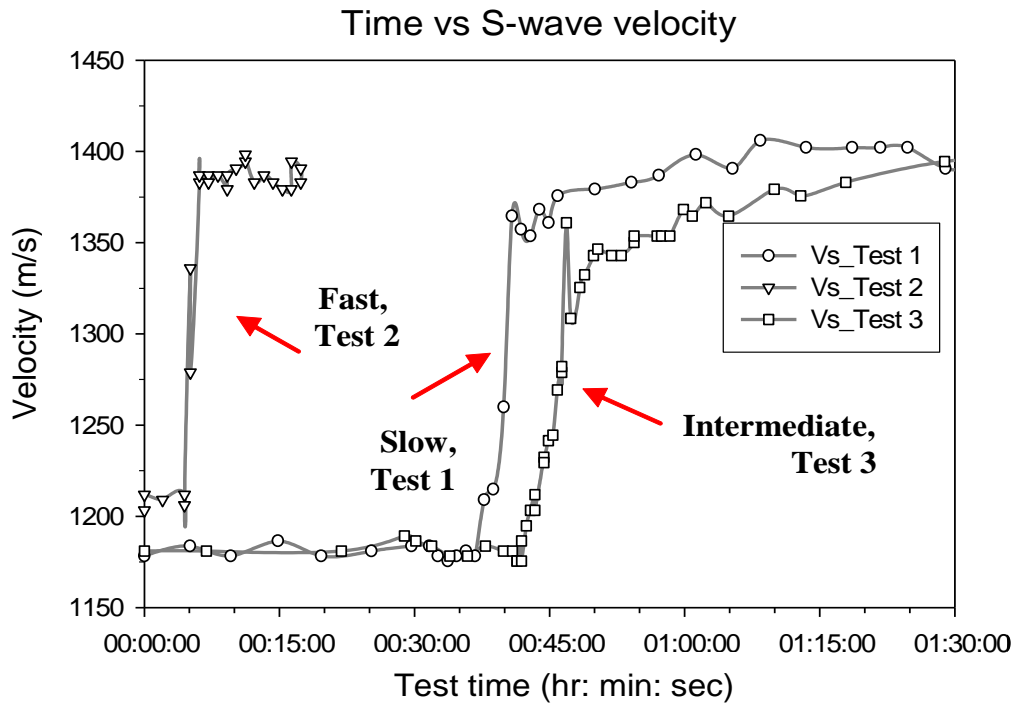


**Figure 7.7.S-wave velocity variation for all tests corresponding to same occurrences as depicted in Figure 7.6 (Hassan et al., 2014 c).**

A marked difference in velocities for oil phase and brine phase could be readily pointed out both for P- and S-wave velocities in Figures 7.6 and 7.7, respectively. Both wave velocities are at a consistent stable value for the duration of oil saturation, and then begin to increase during the period of mixed phase saturation, and then stabilize at a higher value during the final brine saturation phase. The slope of the velocity curves, alongside the spread of individual readings on them confirm initial speculation of a possible degree of miscibility and its flow rate dependence. Similarly, the integrated amplitudes presented in Figures 7.8 and 7.9 show a similar pattern, with times of single phase oil and brine saturation having approximately constant amplitude. However, the period of mixed phase saturation is marked by consistently reduced P-wave amplitudes and S-waves amplitudes, that fluctuate between amplitudes both higher and lower than the single phase amplitudes. This is seen at the test times of 50 min, 1 hour and 5 min after the onset of the flow of the invading fraction/brine in all three tests, respectively. This correlates with the time of the dim spots in Section 7.2, and confirms the greater sensitivity of the S-wave amplitudes to transmission through the mixed phase.

These observations suggest a very distinct localized oil-brine contact interface involving complex of both fluid-fluid and fluid-solid surface interactions of three phases including those of oil, brine and granular surface. In reminiscence, two important points could be invoked. Firstly, not only that interfacial monolayer assuming even for a very miniscule one, tends to assume minimum energy an interfacial tension, it has resilience. Secondly it could be understood that due to preferentiality of spreading on solid surface between invading and invaded fluid and capillary type effects formation of viscous boundary layers over solid surface would occur with possibility of causing such phenomenon as variable local interfacial slip against drag type effects (stokes drag). The nature of complexity is exaggerated by the fact that fluids forming the interface would be in significantly confined geometry where parametric effects might also be different than those in their unconfined form.
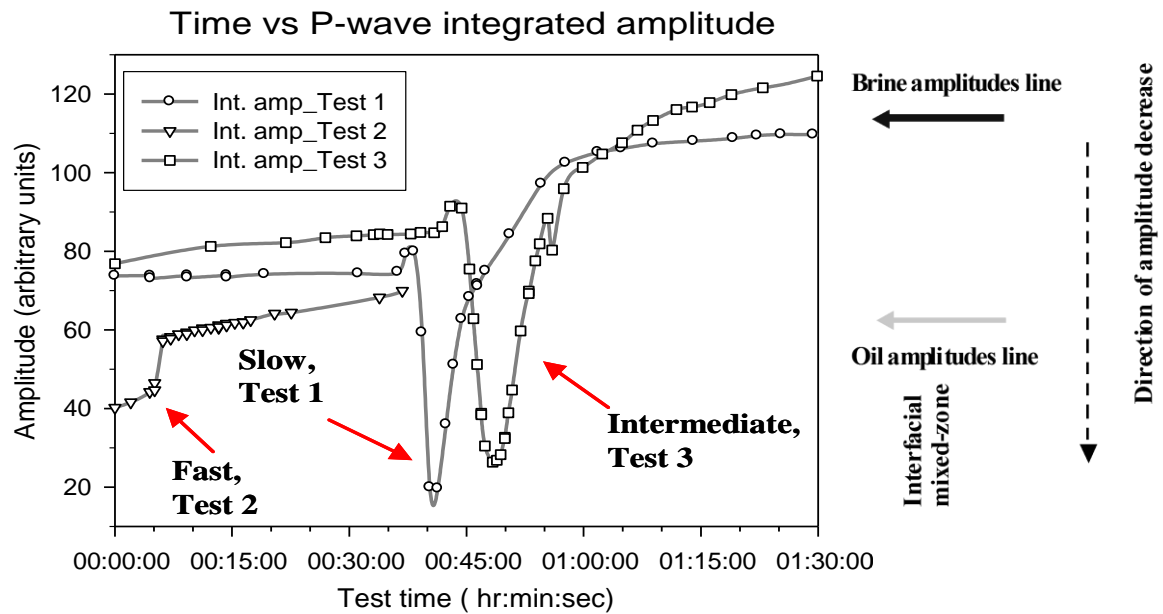
**Figure 7.8. P-wave integrated amplitudes variation for all tests corresponding to occurrence of different possible phases and identified features of interest (Hassan et al., 2014 a).**
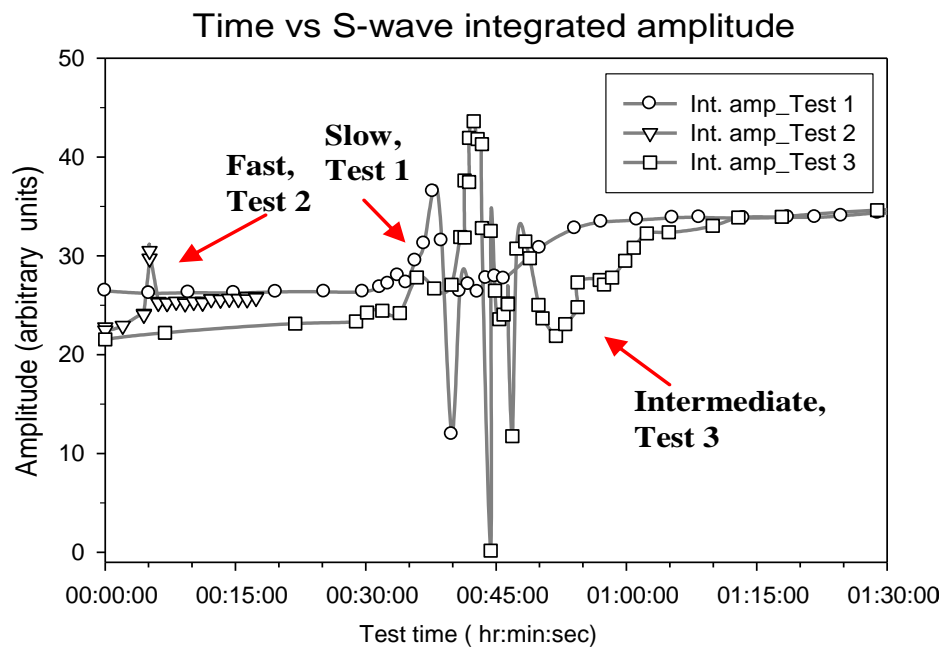


**Figure 7.9. S-wave integrated amplitudes variation for all tests corresponding to same occurrences as in Figure 7.8. A higher sensitivity is indicated (Hassan et al., 2014 c).**

126
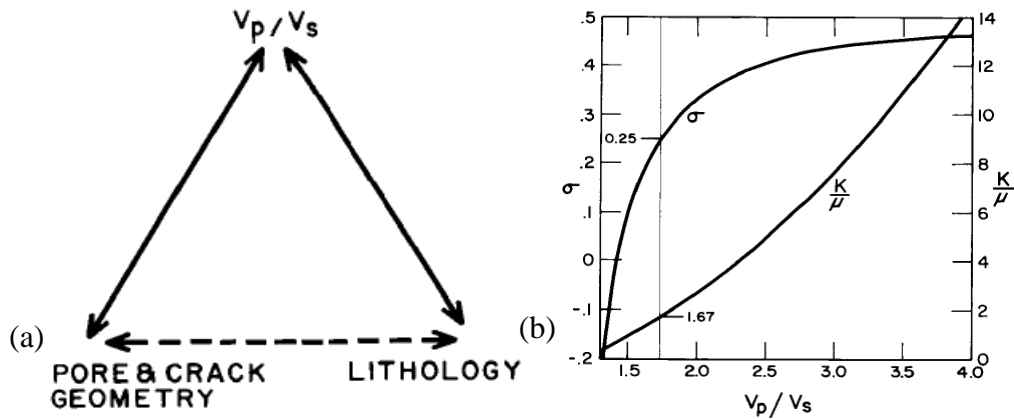
**Figure 7.10.** A conceptual linkage of Vp/Vs to subsurface description aspects **(a)** translated to correlation of strength properties or moduli and **(b)** Poisson's ratio (Tatham, 1982).

Detail of such implications purely in a narrow and phenomenological sense or understanding could be found in (Heinbuch & Fischer, 1989),(Vinogradova, 1996),(Travis et al., 1997), (Vinogradova, 1999), (Markov, 2007), (Brenner, 2011). Where such aspects as geometrical conditions as narrow confinement and implications of shapes including simple spherical surfaces or spheres are discussed. A detailed discussion is avoided for sake of brevity. Continuing the discussion, regarding importance of understanding interfacial tension and wettability, application of macro scale immiscible displacement as water flooding is well known. Water flooding is performed to displace oil, primarily residual. Wettability alone turns out to be a crucial factor. Displacing a wetting fluid by non-wetting fluid turns out to be inefficient compared with situation of displacement of non-wetting fluid with wetting one. To overcome inefficiency, primarily in oil-wet media, reducing the interfacial tension or increasing viscosity of the displacing fluid is usually the method of choice. Reducing interfacial tension in water flooding sense means reducing fluid-solid contact angle, as, for example if it is less than 90º for any fluid, the fluid would be significantly solid surface wetting.
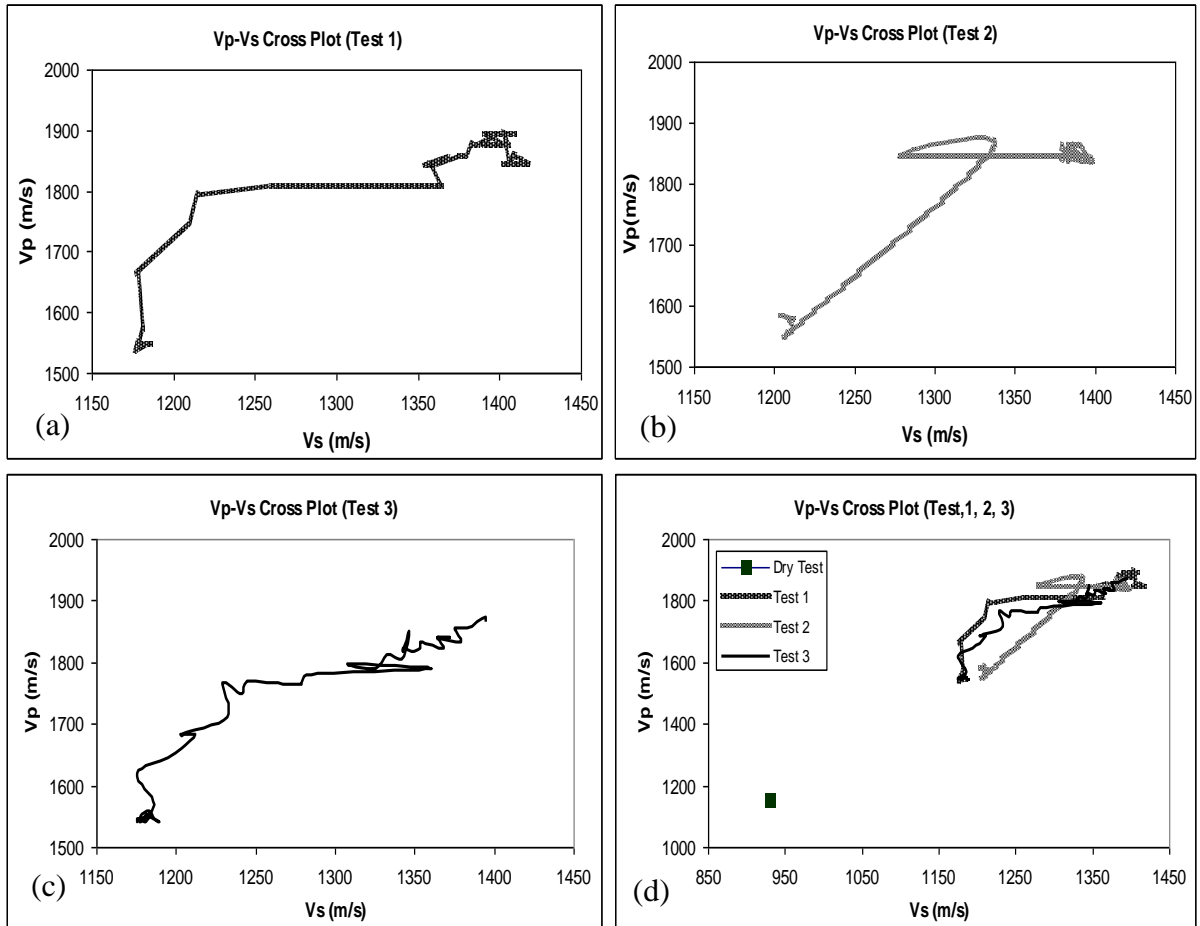
**Figure 7.11. (a)-(c) Vp-Vs cross plots of all three immiscible displacement tests for observing mutual sensitivities and anomalies. (d) Dry measurements presented with saturated measurements in similar context.**

(Mungan, 1964) and(Mungan, 1966) has correlated and emphasized to regulate wettability to control efficiency of immiscible displacements where interfacial tension was found sole factor to cause low recovery.(Rimmer et al., 1996) have in their experimental modelling arrived at similar conclusions from a geo-environmental remediation perspective (i.e., NAPLs and LNAPLs) that wetting-nonwetting issues in floods and displacements affect the efficiency of the process significantly affecting the interfacial region. (Bolster et al., 2011) in their stochastic models speculate and investigate contribution of the gravity difference effects (density) based buoyancy effects upon the immiscible interface or front stability. They propose that immiscible interfacial spreading by deformation or evolution and -

stability could both be affected by gravity difference and heterogeneity depending upon length scale.

In summary, the results presented in this section are consistent with the observation in Section 7.2 that both P-wave and S-wave velocities and amplitudes are lower in single phase oil than in single phase brine saturation, and that amplitude dim spots with either low amplitudes for P-waves or winding fluctuating type amplitudes for S-eaves can occur. Further analysis of the dim spot amplitudes with the results from similar investigations suggests that the mixed phase zone consists of multiple discrete interfaces between the immiscible oil and brine phases. From a field seismic survey perspective, this indicates that S-waves would show greater sensitivity to identifying these mixed phase zones in the subsurface.

## 7.4 Vp/Vs and Poisson's Ratio

The time domain wave velocities can be further processed by evaluating the Vp/Vs ratios and corresponding Poisson's Ratios. This will provide additional properties of the porous media matrix and potential dynamic fluid interactions, as shown graphically in Figure 7.10. This evaluation can be started by determining Vp and Vs cross-plots to remove time dependent sensitivities, as shown in Figure 7.11. From these cross-plots, two important aspects can be noted. Firstly that the overall character of variability is not equally linear, and secondly in each of the graphs of all tests a more flat P-wave velocity character as an invariability span with respect to a variable S-wave could be noted. That is to say that the subtle higher sensitivity of S-waves in comparison to P-wave is better exaggerated in cross-plot compared to that, compressed, in time constrained plots. Which also means that where, at instances the strength moduli or properties appear to change, those could possibly either only be due to rigidity change or a significant contribution that of, for a near constant bulk modulus, as could be figured out in graphs shown in Figures 7.11 (a) to (c). A measurements meaningfulness of the overall responses by comparison of dry measurement point to saturated measurements curves in Figure 7.11(d) is also
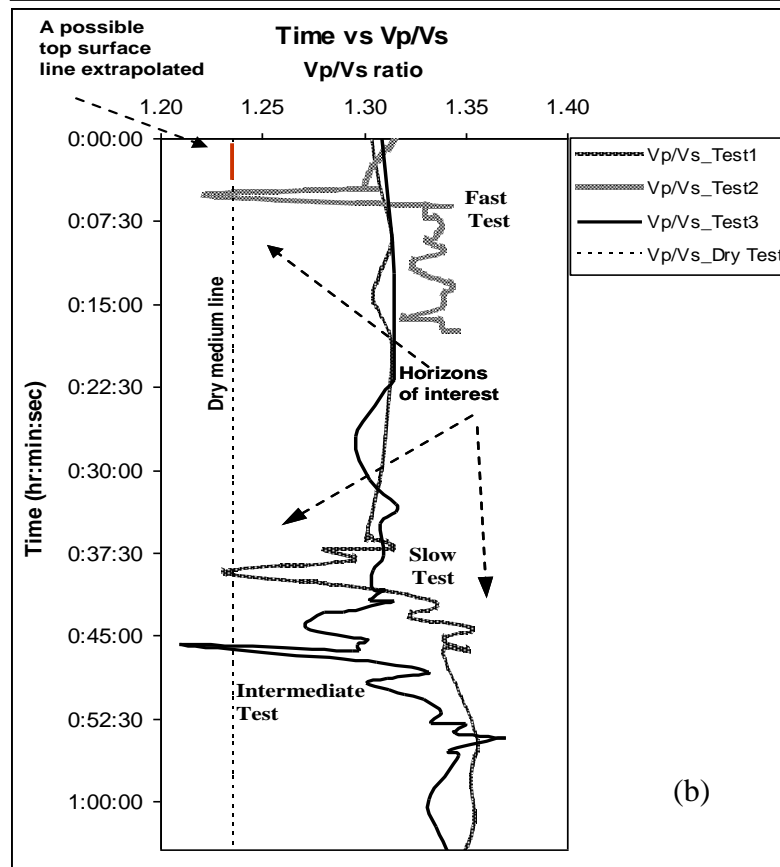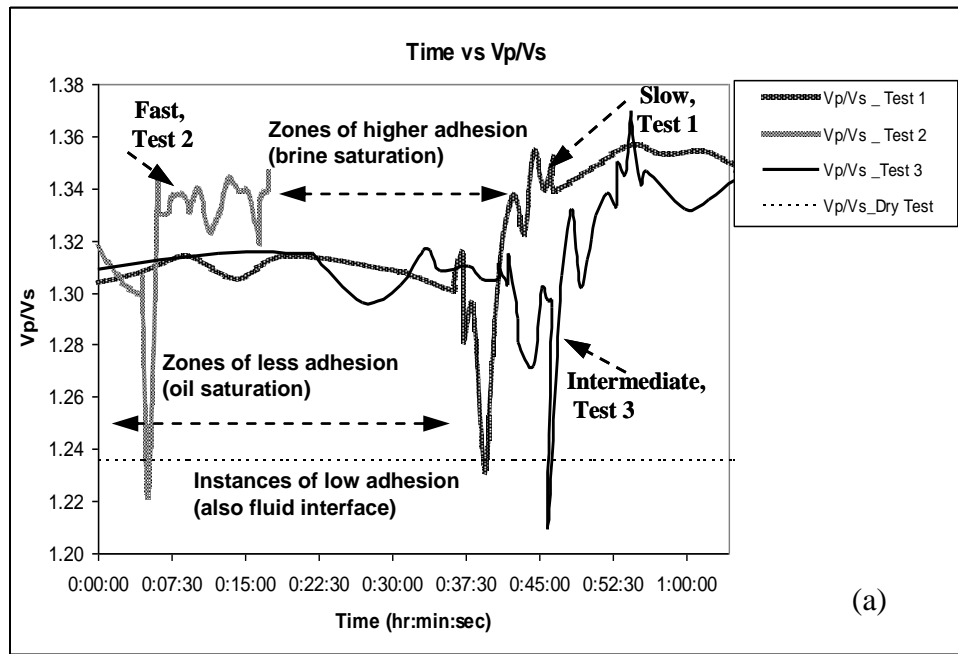
**Figure 7.12. (a) Anomalies in Vp/Vs ratios variations confirm and correspond to findings of velocity and amplitude analyses, with further insight of strength aspects. (b) A pseudo depth section presentation of the Vp/Vs ratios to exemplify a vertical spatial evolution sense of fluids displacement (Hassan et al., 2015 b).**
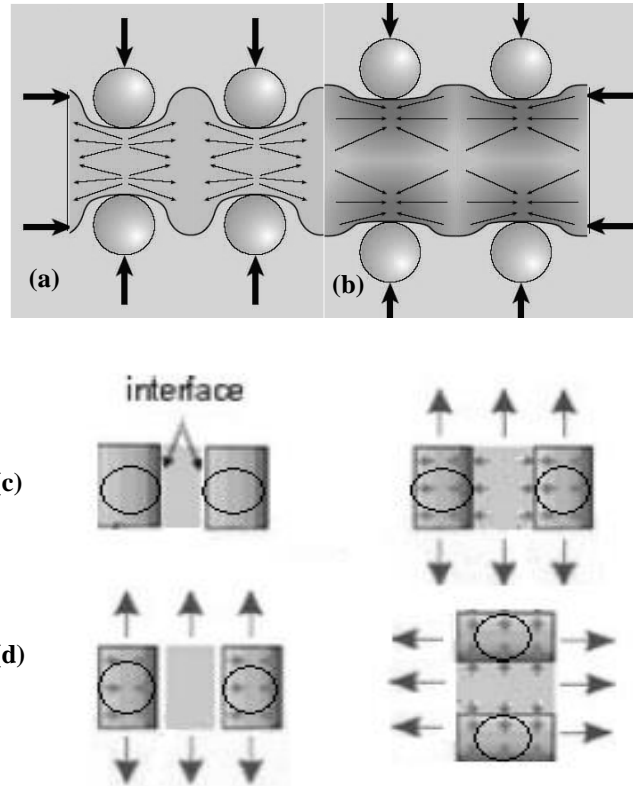
**Figure 7.13. (a) A positive Poisson's ratio stressed or stimulated granular material behavior when saturated, overall lateral deformation is positive. (b) Mechanical behavior under stimulation if same material was a negative Poisson's ratio one, as overall lateral deformation tends to be negative. (c) and (d) Interparticle interfacial behavior of stressed and nonstressed positive Poisson's ratio granular material element. (e) and (f) Interpretable interfacial behavior of a stressed negative Poisson's ratio material,modified, (Liu, 2007).**

in further analyses and discussion also by illustration of Figure 7.13. For dry medium Vp/Vs is significantly low as expected for an unconsolidated to moderately consolidated medium, recallable from initial analyses (i.e., $< \sqrt{2}$).

Interestingly anomaly identified in cross-plots is exaggerated in different yet insightfully peculiar manner as identifiable clearly in Figure 7.13 (a) and (b). It is evident that anomaly, low dip in Vp/Vs, corresponds to or signifies the existence or the formation of the interface when reconciled with the measurement time stamps, on elapsed time axes. In a deformational characteristics context it is deducible that composite Vp/Vs value corresponding the existence of interface development and evolution is primarily controlled by Vs. This implies a significant change in the

This implies a significant change in the overall rigidity or shear modulus in the sense of a stiffening effect or altered (rheology) elasticity where, apparently, two propositions could be speculated. On one hand formation of or the evolution of volume of the interface while immiscible displacement may cause an abrupt change in the state of the fluid phase of the saturated medium from oil to brine (density change), introducing a pore pressure gradient type effect, by the virtue of an existence (potential). Such a change may in theoretical sense tend to alter or increase total continuous area of contact surfaces including granular matrix, naturally effecting Vs, disproportionate compared to Vp. On the other hand, certain micro viscous effects may, simultaneously, also tend to occur during the process of the interfacial development and evolution as the brine phase replaces the oil phase. This may include complicated granular surface lubrication effects with brine in addition or in combination with displaced and residual oil phase, comparable to thin film formations, including fluid-fluid and fluid-solid interfaces (viscosity change). Complexity of unequal but disproportionately affecting variation of density and viscosity effects, additionally, combined with fluid mobility (a well defined net vertical flow) may also induce buoyancy type effects.

The analyses exercise, so, could further be elaborated by examining the Poissso's ratios. The poison's ratios determined from, velocity values are, a negative value for almost all the experiments involving fully saturated states, given propositions. Since further to recall, Poisson's ratio for the dry granular analogue is also negative, and consequently appear to have a significant control over the saturated material deformational characteristics, in a stimulated repose sense. For its composite nature (Greaves, 2013) has provided an interesting historical account of the development of a Poisson's ratio to be understood as a legitimate material strength related parameter and/or metric. It is somehow meant to be related to resistance against fracturing. Several hypotheses are described starting from molecular theory to modern concept of shape to volume correspondence and comparison, providing more detail of which appears beyond scope. Earlier a very comprehensive and concise review of the possibility of existence of situations of negative Poisson's ratio in granular materials was provided by (Bathurst &Rothenburg, 1988).

In their 2D numerical computer experiments the ratio of normal to tangential stress upon granular surface contacts was found to be a critical aspect for both disks and spherical grains/shapes. Stress-strain formulations based on microstructural parameters such as interparticle stiffness, contact density and average interparticle distance are also explained. The theory assumes a conceptual expression of Poisson's ratio which is a function only of the ratio of tangential (shear) to normal (direct) contact stiffness. The theoretical results were significantly consistent to postulate a possible existence of negative Poisson's ratio in granular materials. It was however speculated that such materials could only be designed and chances of their naturally occurring or observed were considered slim. The appearance of negative Poisson's ratio supported by plausible velocity and amplitude analyses offers and interesting proposition to further look into the possibilities of deformational analyses alongside Vp/Vs , thus.

The negative Poisson's ratio for granular materials suggests that the ratio of the internal tangential to the normal stress exceeds unity apparently. In an engineering sense it translates to the fact that susceptibility of lateral deformations becomes significantly greater than that of normal considering the definition of lateral strain for unit normal strain as of (Liu, 2007). Liu (2007) offers a detailed review of plausible conceptual definitions along with the types of negative Poisson's materials. Before further elucidation the conventions of Poisson's ratios should be clarified further at to what actually physically it means, since some times the same quantity is even represented by opposite signs, implying different meanings but only apparently. This is even essential in the case at hand where the material is granular and saturated.

A modified picture from Liu (2007) shown in Figure 7.13 could help clarify any ambiguity about the physical meanings associated with the deformation of a saturated negative Poisson's ratio granular material when cyclically stimulated. There apparently could be an elasticity enhancement of solid fraction due to an affected reduction of solid volume (cohesion type effect) at constant elemental volume. However further the tendency of attaining constant volume, causing an excess pore pressure or increase could also be speculated for an overall all global low structural rigidity.
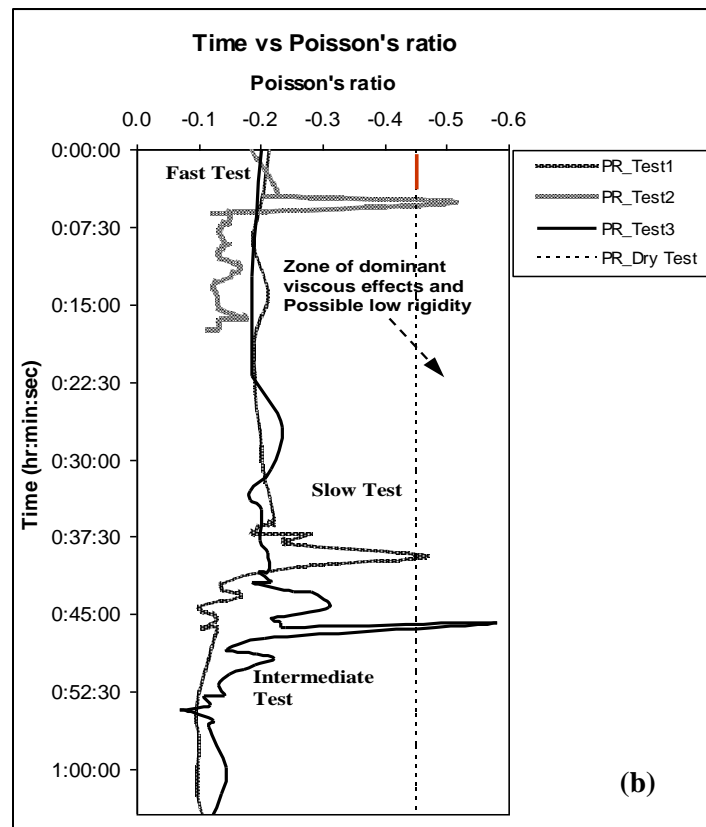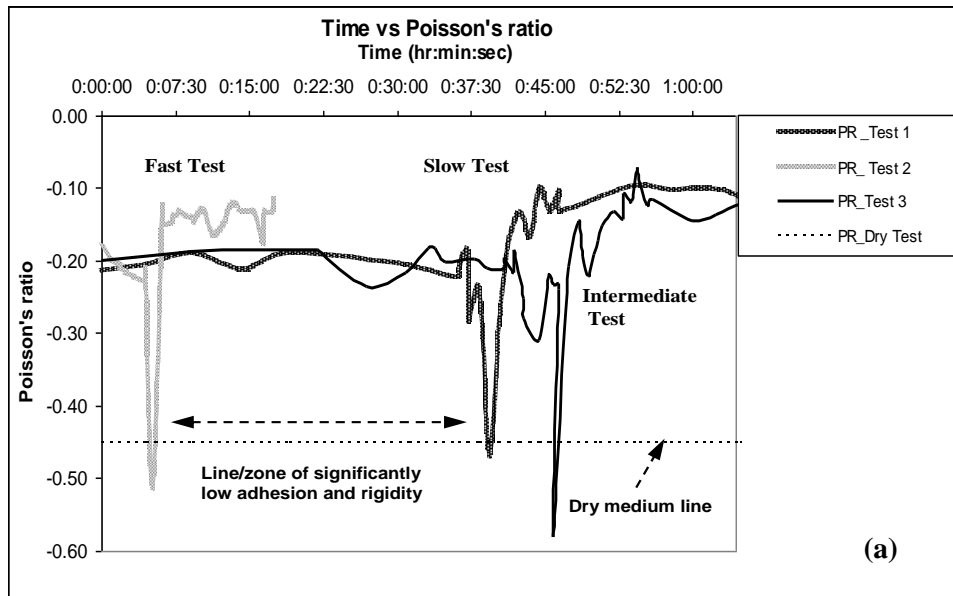
**Figure 7.14. Comparable to Figure 7.12. in concept (a) anomalies in Poisson's ratios correspond to that of Vp/Vs. (b) Pseudo depth section presentation of the Poisson's ratios to exemplify a vertical spatial evolution sense of fluids displacement and related strength effects (Hassan et al., 2015 b).**

This may effect Vp and Vs differently given their definitions in presence of other complicated controls. It could thus be understood that clearly visible anomalies as significantly low Poisson's ratio, similar to those of Vp/Vs ratios, not only

134

substantiate the identification of an occurrence of an interface phenomenon but also point to situation where the control of normal stiffness is apparently significantly less. A complex of factors specially related to unequal density and viscosity as explained above most probably affects liquefaction type effects in deformational context, as other propositions given the nature of process under consideration and deformational regime seem irrelevant. In this context the graphs of Figure 7.14 are comparable to those of 7.12 and clearly depict identical anomalies. They could also be presented in form comparable to a Poisson's ratio pseudo depth section of a vertically developing or pluming contaminant or toxicant where possible zones or horizons of toxic contamination could be fixed with confidence. Associated impacts upon strength properties due to effects of parametric variability of sediment could, further, also be ascertained. One useful and significant observation is that, with a consistent comparison to similar graphs for Vp/Vs ratios that for the interfacial zone the Poisson's ratio is even lower in value than that of the dry granular material unconsolidated analogue. If analogue is considered compared to a sand pile model then the possibility of liquefaction type effects inferred occurring at the interfacial zone appears quite plausible.

## 7.5 Analytical Fluid Substitution Validation

The analysis in this section is a culmination of the results in this chapter to quantify the interaction of pore fluids, phase interactions, and matrix deformation effects on elastic wave propagation. This is done specifically to evaluate the ability of using seismic methods to identify phase of water, oil and regions of their immiscible mixture in the subsurface. This relies heavily on Biot and Gasmann theory that has been previously introduced in Section 3.3. However, additional background is provided in this section, followed by detailed analysis of the three immiscible displacement experiments conducted. Assumptions regarding material properties are discussed and justified as required.

### 7.5.1 Background

In applying static fluid substitution type analyses, (Rasolofosaon & Zinszner, 2009) has pointed out that the a important aspect in any experimental investigation liable to be tested by Biot theory should be assuming an appropriateness in terms of the procedures adopted or conducted. Any extra ordinary discrepancies are due to experimental error and lack of understanding of the parameters of interest. In their analyses, 78 standard cores saturated with variety of petroleum related fluids were ultrasonically investigated. Grain material bulk and rigidity moduli from measurements and estimated from rock physical and/or petrophysical properties, along with analytical results (application of theory), were found to have reasonable correlation. It is implied that the strong viscous effects which can affect dispersion and attenuation should also be accounted for adequately too.

In a relevant context, this rather ambiguous issue has been addressed by (Jones, 1969) in examining the application of Biot theory to describe a subsurface feature, considering an assumed semi-infinite continuum. It is concluded explicitly that the application of the theory within meanings of a low frequency limit assumes much significance and any affective viscous effects causing dispersion and/ or assuming frequency dependence do not qualify to enhance direct strength and/or depth description of the subject of interest. In a physical sense the reason is that with phases dispersed the earlier recorded dispersed phase would still provide the same information as that of a purely non-dispersive front. It could be thus deduced that dispersed phases does carry the time rated information, if not descriptive of the static strength characteristic. While examining Biot theory, the viscous effects are brought to attention within the context of dissipation. The formulation arrived at is comparable to a superposition of dissipation effects constrained within an error function definition (neglecting higher order terms) describing a change in the "acceleration" and a functional form with the meanings of velocity, to clarify the point.

To elaborate upon it further, Biot theory, described as a progression of various equations in simplified functional forms, could be recalled to understand the
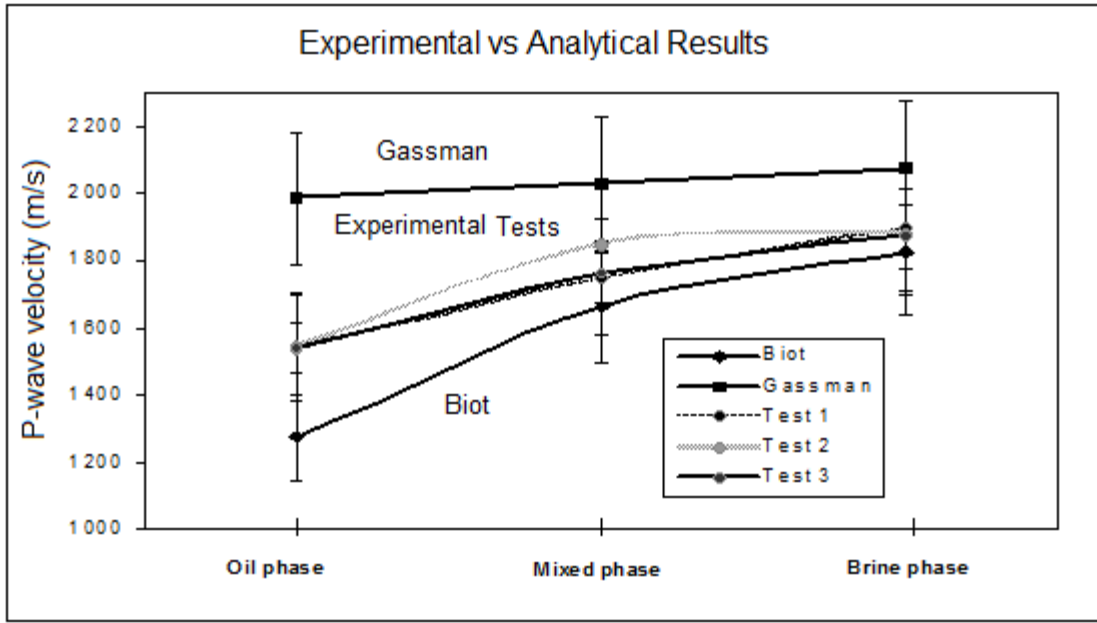
**Figure 7.15. Experimental P-wave values of the immiscible displacement experiments compared with the analytical results generated by usual models of wave propagation based on Gassman and Biot theories.**

parametric sensitivity before the application of the equations to test the basis of experimental findings. The ones relevant to this context are:

$$\rho_{12} = -(\alpha - 1)\phi\rho_f \qquad\qquad 7.1$$

$$b = \frac{\eta\phi^2}{k} \qquad\qquad 7.2$$

$$\tilde{\rho}_{12}(\omega) = \rho_{12} - \frac{ibF(\omega)}{\omega} \qquad\qquad 7.3$$

$$\tilde{\rho}_{12}(\omega) = -\{\tilde{\alpha}(\omega) - 1\}\rho_f \qquad\qquad 7.4$$

$$\tilde{\alpha}(\omega) = \alpha + \frac{ibF(\omega)}{\omega\rho_f} \qquad\qquad 7.5$$

A certain hierarchy of the parametric control could be discussed to assume a phenomenological grasp of the notion of frequency dependence or in other way limits of frequency cross over within understanding or definitions of low and high

frequency. The fluid-solid coupling factor $\rho_{12}$, an apparent mass, by nature embodies the meanings of an inertial drag imparted from the fluid to solid, with the tendency to attain unison in displacement against cyclicality or periodicity of a forcing agent. With an increase of frequency, the relevant displacement and acceleration would contribute only to the displacement amplitude attenuation. Viscous drag is related to virtue of the saturant to withstand shear deformation under cyclicality of mechanical stimulation. The important factor to understand is the "b" that embodies the viscous effects of Biot theory. It is related to or dependent upon viscosity and permeability. Interrelation of both $\rho_{12}$ and b could along with defining parameters be understood from equations 7.1 and 7.3. Given sign conventions they are not competing entities and to introduce the notion of frequency dependence they appear as the composite expression as given in Figure 7.15 and shown in a simplified form in equation 7.4, and still another useful form in equation 7.5. The appearance of affective "b" always in combination with the effective unit mass, as an imaginary component, as alluded to and understandable from examining above equations, reveals that structure facture $\alpha$ is in fact a very critical parameter with given the rest unaltered or constant. Though the physical properties of the constituents, fluid and solid, do participate but what scales their influence is the magnitude of the structural factor, referred to as tortuousity. Further still the appearance of these factors only effect the acceleration terms but not velocity terms, where the $F(\omega)$ is the function to introduce or define the frequency shift when the depth of viscous skin equals the pore size, beyond which the regime is considered high frequency. Factor $F(\omega)$ is afforded to be an estimate based on the physical and geometrical restrictions associated with investigative evaluations. An important or interesting point is that appreciating the control of, and adequately determining the, structure factor alone in the functional form of Biot equations is sufficient for high frequency analyses, and any discrepancies could be examined by varying that factor if possible. Comparative spectral examination, as explained offers a useful method to ascertain various conceptualized scenarios of geo-environmental interest, however testing velocity data against Biot theory, should indirectly verify the speculated inferring. In such analyses, Berryman (2009) has pointed out that fluid

effects upon seismic (or acoustic) signatures in unconsolidated sediments are not only controlled by fluid bulk moduli but are influenced by viscosity effects too. In an indirect sense it is deducible that the effects of viscosity upon rigidity of a stiff porous frame are different from that of a granular frame, which could be further examined or elaborated upon.

### 7.5.2 Results and Implications

The graphical illustration of Figure 7.15 depicts or tends to advocate the adequacy of the inferred outcomes of the three experiments of the dynamic immiscible displacement study. All three experiments are represented by quasi static state descriptors given as Oil phase, Mixed phase and Brine phase. Oil phase point is a single minimum possible velocity chosen to identify existence of 100% oil saturation. Brine phase point or points, in a similar sense correspond to a maximum velocity point perceived to represent 100% brine saturation. These two points are not averages of various readings but two extreme readings to provide a sense of minima and maxima. Contrary to the maxima and minima points chosen, the mixed phase points are calculated by applying a fractional weighted averaging method to account for a variability of saturation or fluid fraction. Thus for a certain spread of values of the dynamic process precise representative static values are generated. The drained bulk and rigidity moduli (dry frame moduli) are estimated from the ultrasonically determined velocity measurements.

In order to understand the response of the form of conventionally adjusted models of fluid substitution type analyses chosen i.e., Gassman and Biot, the adjusted and unadjusted values of these dynamic moduli were used for input. Adjustment of the frame bulk modulus is suggested at various instances regarding such analyses as emphasized by Mavko et al. (2009) and Rasolofosaon & Zinszner (2009) to account for or create real porous rock effects. Both the adjusted or unadjusted moduli along with the information of the other petrophysical (porosity, density etc.) properties are used in a fluid substitution type analysis, after creating composite bulk moduli and densities of the saturated porous media. Gassman equations and Biot equations in

simplified functional form as previously discussed in Section 3.3, with estimates of adequate corresponding inputs are used to estimate P-wave velocity values of the saturated medium. Analyses are performed for all three saturants using the drained strength information or moduli. After several analyses and trails with adjusted and unadjusted frame bulk moduli and any other associated parameters, certain important facts especially given anomalous behavior of granular porous media were understood. Provided further with an understanding that the analyses were not to test the limitations of the theory to examine a "data fit", the analyses were rather done to examine the adequacy of the experimental outcomes in a predictive sense. In holding with an empirical nature or sense of inputs, the restriction of constancy of rigidity with complete disregard of saturation effects i.e., conventional $\mu_{sat} = \mu_{dry}$ of frame, was maintained, with the fact in hind sight that a zero frequency solution is sought from ultrasonic measurements. Further a guessing or estimating solid grain and frame bulk modulus in a suitable range, as is brought to attention with illustration and citation of several references through a fluid substitution exercise by Smith et al. (2003) was another restriction to be held, such as a ratio of $K_{dry}/\mu_{dry}$ (for dry or drained frame) should not be less than unity, among others if possible. These restrictions lead to observation of certain computational issues. All the experimental and analytical points resulting from this analysis are plotted in Figure 7.15 with error bars corresponding to 1 standard deviation.

In case of the Gassman model it either would require, for an input, an adjusted frame bulk modulus or a statistically consistent guessed grain bulk modulus to offer a stable zero frequency fluid substation solution. In the former case the solutions obtained as single points would be reasonable adequate in terms of proximity to the experimentally determined velocity values but overall sensitivity of the values would be compromised as they in composite analyses would not allow to infer an occurrence of transition from one to the other fluid phase in dynamic sense. This is to say that the velocity would only change disproportionately with corresponding change of parameters. In the latter case, however, the nature of sensitivities as alluded to would be very well preserved but the overall values would be visibly overestimated, if not

significantly as visible in Figure 7.15. This means that by connecting or plotting different points in temporal succession of experimental imaging of different fluid fractions the nature of the immiscible displacement process could easily be understood from velocity values. Such stability issues when using Gassman equation could be attributed to its very empirical nature where it is mostly used to evaluate or analyze solid porous rock cores with strength properties falling within a certain amenable range or ranges. The magnitudes, since, could be significantly different from those of granular unconsolidated media, not falling or covered within the guiding correlation schemes. In addition it is at times difficult to evaluate or comprehend the consistency of units of inputs in a dimensional sense from one cited analysis type to another due to a black box nature of the models as signified by Smith et al. (2003) too. In the existing analysis the conjectured value of the solid grain or bead bulk modulus appeared to be one order of magnitude ($1x10^{1}$) lower than the corresponding values identified for similar materials, especially compared to quartz.

While the application of the Biot theory it was observed that statistical or computational sensitivity was much higher. The implemented model was understood as equally sensitive to adjusted or unadjusted strength parameters, given the case at hand especially. This could be attributed to or speculated for the more phenomenological and flexible nature of the Biot model in terms of mutual scaling of parameters, as compared to the more empirical and restricted Gassman's ones, apparently both considered identical though. Several computational trials showed that Biot model, at least in functional form, with input parameters understood and identified, on the lines explained by Plona and Johnson (1983) and Berryman (1980) offered the most stable solution, even with contributory influence of some parameters as dissipation constant and, especially, structure constant surrounded by certain conceptual ambiguities given their quantification method. It is clearly observable that that the two solutions naturally provide an upper and lower bound for the experimental measurements.

Before extending the discussion towards closure certain points regarding the granular material or beads used in the experiments should well be brought to notice,

for direct implications upon either estimation of certain input parameters or generated solutions. The soda lime bead material which is used in the study is found not to be a typical glass type material as quartz in terms of strength and gravity properties. The solid material bulk moduli had to be guessed or conjectured from reported results in accordance with the measured dry porous frame bulk compressive and shear moduli. Density also could not be measured by comparing with water gravity or other comparable methods. The exact volume determination of a fixed weight of beads either in dry confined state or by water immersion turned out to dissimilar in each trial. This was attributed to strange flowage properties observed while handling the beads in different ranges of volumetric confinements, as most of times they would increase in volume against any small exerted pressure overtime contrary to maintaining either same volume or attaining any settlement associated decrease. This appeared to be due to some sort of surface interaction with air or water which could also be significantly temperature dependent, further discussion of which appears beyond scope of analysis. Apart from that in few photographic analyses it was observed that not all beads were exactly spherical as reported and it could be speculated on this ground that they could have a non-uniform size. This would cause both the analytical estimation of the structure factor and its translation to the dissipation factor characteristics incorrigibly quite aberrant compared to what would occur in the physical experimentation.

In addition the ambiguities surrounding the quantification of tortuousity itself, also translatable to meanings of structure factor, which is directly related to porosity could be understood form (Wyllie & Gregory, 1955). Some basic calculations for tortuosity estimation to enable an understanding of the physical characteristics it shall embody in association with porous media flows is shown in (Lorenz, 1961).(Clennell, 1997) has not only highlighted the misconceptions surrounding the definition of tortuosity, very detailed account of various definitions among different realms are also described following an analogous mannerism. While explaining various understandings of tortuosity it has been explicitly stated that the meaning of the parameter is conceptually same or comparable to the one identified in Biot theory as

structure factor. A very important aspect brought to attention is that characteristically such parameters appear to possess an adjustable impedance type balancing tuning nature. Further at times or at instances very nature of the parameter could be exploited to fit the data to the theory. In this study however the structural factor is not guessed or indirectly determined but calculated by using the relation conceived by (Berryman, 1980) also found adequate by (Johnson, 1981), as by definition it takes into account the grain or bead diameter or size.

The S-wave results are not plotted for inability of the models to provide stable solution marked by significant underestimation. This might be affected by speculated significantly strong bearing of viscosity on strength moduli for the un-cemented and un-sintered unconsolidated material evaluated. As implied and inferred before it could introduce a viscous resilience type rheological effect, affecting overall enhanced rigidity, not accommodated by the form of the models used as a convention. This aspect in another way is a significant finding where S-wave propagation is found to show predominant sensitivity to fluid saturant and associated effects in granular unconsolidated sediments. An interesting confirmatory observation is that the measured S-wave dry velocities and ones predicted from Gassman and Biot theory are almost identical. They are much lower compared to the case of experimental saturated measurements however they are higher when compared with the analytically predicted saturated velocities consistent with convention. This appears to not only indirectly substantiate inferring but also point to the aspect of viscous effects upon strength properties not appropriately accommodated or translated into the existing wave propagation models in a proportionate contributory sense, especially without compromising the conceptual restriction of an unaltered rigidity. The analyses have to be modeled around a constant rigidity fundamentally.

# Chapter 8: Immiscible Fluid Experiments – Integration of Ultrasonic Attenuation and Electrical Resistivity

## 8.1 Ultrasonic Wave Spectral and Attenuation Analysis

Chapter 6 focused on the adequacy validaty the experimental apparatus and the nature of the procedures with recorded data while Chapter 7 focused on the time domain analysis of the ultrasonic P and S- waveforms recorded during the three immiscible displacement experiments. The analysis in this section is focused on spectral and attenuation analysis of these same waveforms, focused somewhat on fluid properties that can be estimated from these data. All the experimental details as described in Chapter 6 and 7 are the same as in this chapter.

### 8.1.1 Background Theory

Since geophysically stimulated response of subsurface fluids can help locate them reliably, subsurface fluid saturation description with elapsed time, either in time or space, seems a technically viable monitoring idea, usually termed as 4D. Time-lapse or 4D monitoring methods emerged from reservoir engineering where elapsing time is the fourth dimension, now a well-established concept. Aspects of time-lapse acoustic monitoring methods in relevant context could be understood from such sources as (Lumley, 2001) and (Johnston, 2013). In seismic applications, examination of variations in an apparent character of attenuation related extracted attributes provides a way of monitoring changes in the subsurface fluids in comparing time separated survey results, while isolating them from the background. Since the fluid saturations detection either confined or mobile, by ultrasonic pulse transmission i.e., P- and S-wave, has already been established, reasonable detectability allows us to observe and examine time-lapse type changes in an immiscible fluid displacement experimental setting. Plausible inferring based on static type analyses i.e., velocity and amplitude, further instills confidence to exploit higher sensitivity of spectral and
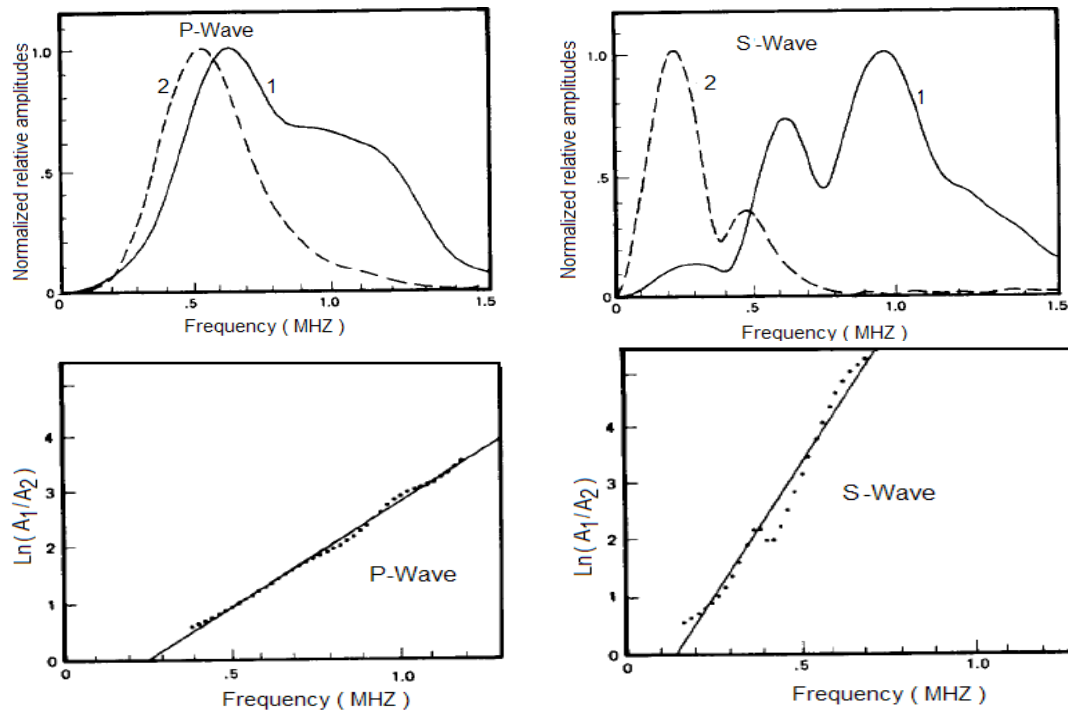
**Figure 8.1. P- and S-wave attenuation examination method illustrated, Spergen limestone example from Toksoz et al. (1979).**

attenuation characteristics to subsurface fluids for a dynamic analyses based examination; better described and in fitting with a time-lapse type workflow devised based upon concept shown in Figure 8.1 and elaborated further upon , ahead. This would demonstrate potential application of such method for monitoring of fluid flow processes over an extended time when densities and viscosities of invading aqueous and invaded non-aqueous fluid have reasonable contrasts. In the experimental test explained since specific gravity of oil used was 0.761 with a viscosity of 10 cp. The specific gravity of brine with 3.5% salinity was 1.02 and viscosity assumed comparable to that of seawater 1.30 cp. The specific gravity of ceramic/glass beads material was about 2.6 with 0.5 mm size giving 26% porosity. Interpretation of results, on previous lines would, assume a near surface process characterization perspective given engineering and environmental considerations.

145

Attenuation characteristics examination or extracting corresponding attributes from acoustic data exacts understanding underlying attenuation causing mechanisms. Attenuation is broadly understood as loss of amplitude of propagating wave. It includes effects of geometrical spreading in space, the effect of the continuum filling the space and the type and size of heterogeneities and/or elements of dislocations contained in the continuum, relative to the propagating wavelengths, given the conservative principles. As identified in (Jones, 1986), attenuation is an anelastic process of seismic energy conversion to heat, affecting a decrease in amplitude, with frequency and phase content of propagating wavelet altered. (Berryman, 1988) has also examined such phenomenon for seismic scale with description of possible mechanisms, beneath, in detail. Considering principle of superposition ingrained in wave propagation, the concept of damping of a sinusoidal locus of oscillating continuum particle makes understanding of attenuation and attenuation mechanisms easier since it provides understanding of logarithmic decrement of the oscillation i.e., ratio of logarithmic value of two successive amplitude peaks.

In mechanistic sense, the above cited attenuation related effects by definition fall within anelastic and/or viscoelastic regimes as acoustic perturbations are cyclical loading analogous, with corresponding time redistricted stress-strain states. For less frequent perturbations, stress remains proportional to strain with full strain recovery, characterized with a relaxed modulus sense. If the loading is more frequent for time then strain may not be fully recovered for each instance of stress, defining an unrelaxed modulus. This signifies deduction of complex and absolute dynamic moduli and corresponding compliances due to the restrictions of periodicity. The real part of a complex compliance is referred to as storage compliance and the imaginary part as loss compliance with their significance in determining energy dissipated in unit cycle, per unit volume basis. The ratio of the energy dissipated to the maximum stored energy is defined as specific damping capacity denoted by $2\pi.\tan\emptyset$ where $\emptyset$ stands for friction energy loss per unit cycle. Brevity in elucidation of concept thus far is intentional, more details in theory if needed are available in (Nowick & Berry, 1972) and Bourbié et al. (1987) with more relevant references there in. When examining wave attenuation in saturated porous media for non-destructive or non-

intrusive evaluations, infinitely small recoverable deformations are essentially assumed but defined as viscoelastic. Despite different definitions a time dependence is assumed opposed to an instantaneous equilibration. When macroscopic response of such media to wave propagation is examined, parameters and mechanisms identified in Biot theory, for representative equivalent volume tensor approach, assume significance. These parameters and/or corresponding aspects form phenomenological descriptions to facilitate qualitative interpretations, further provide models for quantitative verifications and estimates. The important aspects are saturation/fluid density, fluid-solid and solid-fluid inertial coupling, nature of relative fluid-solid displacements, grain boundary friction, variations of effective and/or pore pressure at constant volume and vice-versa, variations of apparent permeability, saturation viscosity and viscous relaxation, and global and local flow regimes. Detailed definitions and derivations of these parameters with specific reference to limits of frequency dependence can be found in (Biot & Willis, 1957), where sufficient details also provided in previous chapters and relevant instances.

Quantification of attenuation by ultrasonic pulse transmission method in dry and saturated rocks has been described in (Toksoz et al., 1979). The derived analytical description used as a relative measure is described in detail which is essentially time and space independent spectral matching, and further allows a computation of ratios within adequate restrictions of bandwidth of interest. Thus the name spectral ratio method, where bandwidth restricted variable amplitude spectra could be characteristically examined with ratios computed either in relative sense or against a standard well defined and understood benchmark. An example, in recollection, of spectral ratio results of Spergen limestone for attenuation examination characteristics is shown in Figure 8.1. Points worth noticing are, that, just the logarithmic values of standard ratios against frequency are sufficient to quantify attenuation and if the spectral curves are well behaved area under their curves offer a very good sense of damping and dissipation effects provided ratios are kept consistent, as illustrated by the analytical expression indices. Once the well behaved curves are successfully acquired or constructed against the standard spectra;
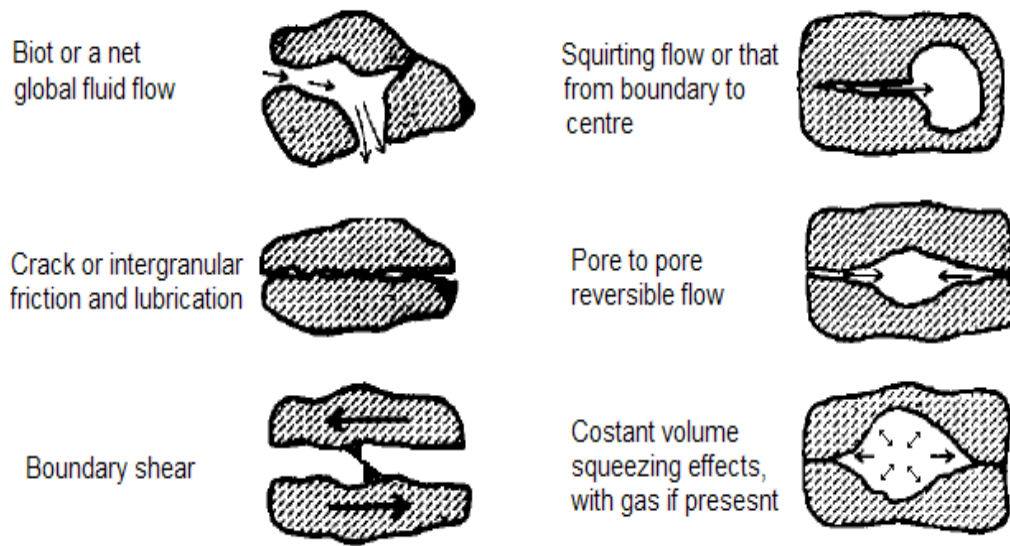
**Figure 8.2. Possible mechanisms causing wave attenuation (Johnston et al., 1979).**

identifying mechanisms contributing to overall attenuation, in relation to parametric controls, in correspondence to frequency becomes plausible. In this regard well identified study of (Johnston et al., 1979) may provide useful information for understanding wave attenuation, who hypothesized studied and discussed possible mechanisms of attenuation in dry and saturated media, in addition to dry. Geometrical and structural effects, other than thermodynamic or thermochemical, are also hinted to effect energy loss, as discussed before. Figure 8.2 illustrates and summarizes more accepted and standard of such mechanisms. Given micro and macro scale implications Nowick & Berry (1972) signify assigning rheological models (to reconstruct such mechanisms) to relaxation and/or dissipative acoustic loss mechanisms description i.e., Zener model, and imply including standard models i.e., Voigt and Maxwell, and/or their combinations for dynamic analyses and anelastic and/or viscoelastic spectra generation and examination. They since can mirror acoustically stimulated response characteristics of such continua/system components, identified above.

Ultrasonic S-waves excitation or stimulation has since, generated such spectra which differ in nature compared to those obtained for the case of P-waves, reported in (Hassan et al., 2015 a). The S-wave spectral results characterizing various instances

148

of fluid-displacement process in this context are marked with nonlinearity. Anatomy in appearance is of a resonant type when, considering amplitude and frequency shifts, and transmitted against received bandwidths in comparison to those for P-waves. The P-wave spectra were since demonstrable and explainable with usual and rather basic models and/or understandings of elastic wave attenuation mechanisms for description of fluid-displacement process against consideration of an elapsed time. Some theoretical considerations central to lucidity of the presentation and comprehensibility of exposition of results are discussed. In terms of theoretical delimitations, all the spherical beads constituting the pack or granular analogue are assumed to be equally spherical with maximum elastic contact with each other following mechanics of regular arrays and discrete particles. Such assumptions allow complying with the conditions of the Hertz theory confined within exact regimes for overall oscillatory or dynamic behavior analyses of granular media as previously discussed too.

Walton (1975) has mathematically illustrated such an ideal but useful model. Hassan et al. (2014 a) offering specific references has signified the plausibility of the assumptions in terms of matched comparisons of some prior results of this study with previously published predictions based on the similar theory. Apart of other models addressing aspects of wave propagation discussed previously, the model of Walton (1975) addresses or describes a problem of a marine or ocean sediment. It is since a saturated one with a cubic packing of spherical particles addressing the aspects of a single modulus affected by vertical compression with and without influence of gravity. Descriptions of both P- and S-waves are formulated. It additionally may, also, offer further notions of distinct salience regarding ensuing description of analyses, especially. This includes possibility of change in the nature of the area of the intergranular contacts during the transmission of the elastic wave. An existence of a viscosity associated incompressible and rotational saturant boundary layer on the grains or beads too, additionally, adding to the effective diameter besides a non-rotational but viscous part, as of detailed contextual elucidation by Walton (1977), is identified. In this regard, given the context, (Buckingham, 2000) and (Buckingham, 2004) while theoretically examining wave propagation through

saturated unconsolidated granular medium (i.e., marine sediments), has specifically referred taking into account of a frequency dependence too. The salience of appreciating a frequency dependence is implied when effects of inter granular friction and shearing may cause considerable effect. In describing effective attenuation, frictional heat based attenuation related to intrinsic thermodynamics of wave phenomenon, due consideration to amplitude loss caused by scattering from anomalies is brought to attention. The anomalies may arise or evolve due to an existence of physical inhomogeneities and fragmentation during wave propagation.

In Buckingham (2000), especially, such aspects in addition to inter granular friction are more acutely elaborated upon as micro events of stick-slip type relaxation against dynamically accumulated strain in presence of a saturant. Association of such micro events to a frequency dependent viscous strain hardening type effect is also explicitly identified. Implications of such an association are also discussed with respect to flow regime transitions as whether or not conforming to a typical Navier-Stokes regime. In order to render the understanding of the relatively involved concepts simpler, regarding properties of the medium types in question or discussed (Hamilton, 1971) and (Hamilton & Bachman, 1982)could be referred to, at this juncture. Contrary to the Hookean elastic model, which could suffice for strength description of some earth materials, saturated sediments do not follow that linear model, as implied before. For they fall into an anelastic viscoelastic regime. For empirically relating physical elastic properties to the measured dynamic response viscoelastic models have to be conceptualized to arrive at such desired solutions. In this regard Kelvin, Voigt, Maxwell, Linear solid or Zener models are examples of few simpler models as cited before. Suitable combinations of these models could simulate materials with "viscoelastic properties" with time rate dependences and restrictions of periodicity. Such models are thus capable of describing material behavior both in terms of strength related moduli and attenuation characteristics. Buckingham (2007) has also drawn attention towards inquiring descriptive capabilities and appropriateness of wave propagation models by comparing grain shearing and a proposed viscous-grain-shearing model. While making a special mention of viscous

effects with associated time dependencies, a conceptual modification of such models is suggested and/or demonstrated by incorporation of suitable elements. Saturated granular media stimulated at high frequencies may give rise to complicated wave phenomenon, however, where certain attenuation or amplitude loss mechanisms are better understood and accounted for considering aspects of ray based approach. S-waves are involved, the complexity evolves even further due to forward and/or backward scattering, mode conversions and ensuing interference.

Interference effects hold importance in inferring received or reconstructed signals especially where there could be much pronounced scale dependence in effect, affecting resonance conditions. (Einspruch et al., 1960) considering the scattering of S-wave by a spherical discontinuity has provided relevant accounts of such conditions or phenomena (i.e., scattering and interference) in a generic sense but with sufficient specificity. Particular cases when a scatterer is a cavity, a rigid sphere, a fluid-filled cavity, and an elastic material having acoustic properties different from those of the surrounding medium are sufficiently thoroughly analyzed. (McBride & Kraft, 1972) in their numerical experiments also investigated the occurrence of the scattering phenomenon while evaluating solid elastic materials with solid inclusions. Their study is comparable to that of by Einspruch et al. (1960), as their analytical formulations for numerical experiments conceptually were similar. In their work however focus is reported on the case of the scattering of a transverse wave from a spherical elastic inhomogeneity or scatterer explicitly. Their findings clearly suggest occurrence of resonance in observable spectra with further deducible insight that scale dependence of S-wave regarding resonance is of different kind than that of P-wave. In (Brill et al., 1980) is explained the resonance phenomenon with assigning of its possible significance to nondestructive evaluations in geological and non-geological engineering materials with focus on S-wave propagation and transmission. Occurrence of resonance due to an S-wave incidence and/or transmission caused by idealized spherical fluid filled cavities (i.e., water), is examined and discussed, in a theoretical context. Scattering and interfering amplitudes are shown to exhibit as resonance fixed, and scaled by frequency and scatterer and/or anomaly size.

theoretical context. Scattering and interfering amplitudes are shown to exhibit as resonance fixed, and scaled by frequency and scatterer and/or anomaly size.

Where it is made evident that S-wave transmission, through granular media, associated resonance spectra is well observable as a phenomenon, its extended prospects had been duly and rather readily appreciated, too. (Gaunaurd & Uberall, 1979) primarily foresaw its usefulness at laboratory scale involving nondestructive testing or evaluation of materials and/or compositions and medical diagnostics. While as viewed by McMechan (1982) more promise rests in seismological and planetary and interplanetary related surface and subsurface studies. It, therefore, is well envisioned that application to inferring and characterizations involving geoenvironmental studies is not excluded.

### 8.1.2 P-wave Analysis

Better grasp of the exposition of results provided ahead demands clear understanding of working design principle of immiscible fluid displacement experiment. In recollection, the positioning of the sensor midspan flow-cell tube was chosen to allow reliable single point measurement, by ensuring a provision of sufficient time for the flow through saturated sediment (analogue) against gravity to fully develop and stabilize before measured or "imaged" at sensor position. All wave forms or traces were acquired at the same position/horizon for each of three immiscible displacement experiments performed. Two successive measurements/traces could be arbitrarily spaced in time i.e., 1 to 3 sec., in range, based upon visual assessment of flow velocity, with each measurement conforming Nyquist criterion. Statistical benchmarks to several analyses are discussed before in chapter seven to serve for all subsequent analyses. Among those shall include graphical depictions of characteristics of the acquisition system, time and frequency domain characteristics of the input pulse and a sampled spectrum of the same pulse with source and receiver attached face-to-face to acquire unattenuated spectrum corresponding to the transmitted bandwidth. With method of acquisition unaltered same through transmitted pulse technique was used upon a standard aluminum sample for keeping
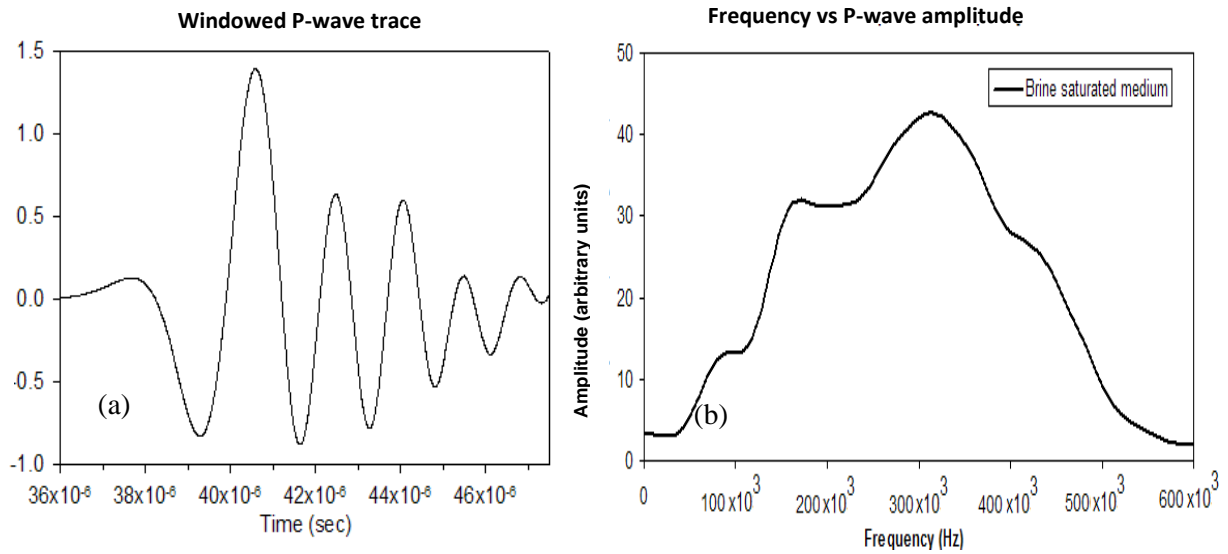
**Figure 8.3. (a) Time irrespective maximum energy P-wave windowed waveform. (b) P-wave spectrum of brine saturated medium (Hassan et al., 2014 d).**

geometrical similitude and sampling restrictions conformation in view, and to create a spectral function to assist in adequate comparative analyses of attenuation characteristics with consistent quantification, hence. Such a P-wave and S-wave spectrum for a detailed dry granular or porous medium was also created to assist with detailed analyses.

To start the analyses assuming all the benchmark characteristics are well understood, Figure 8.3 a shows an example of windowing of P-wave traces, in order to localize a time-irrespective maximum energy impression for a better frequency spectral expression in FFT analyses of data. Figure 8.3 b shows such a FFT spectrum for brine saturated condition, isolated amongst the several spectra generated corresponding to same features of interest in discipline with elapsed time, as explained previously in time domain. Location of peak frequency and amplitude alongside transmitted bandwidth can be readily clarified, which would be further discussed in terms of possible shifts and variabilities in response to parametric changes. Figure 8.4 shows input and output responses juxtaposed, for dry matrix. Each of the panels of Figure 8.5 comprises such multiple spectra organized to depict their temporal sequence in a self-explanatory sense, as they are uniformly labeled
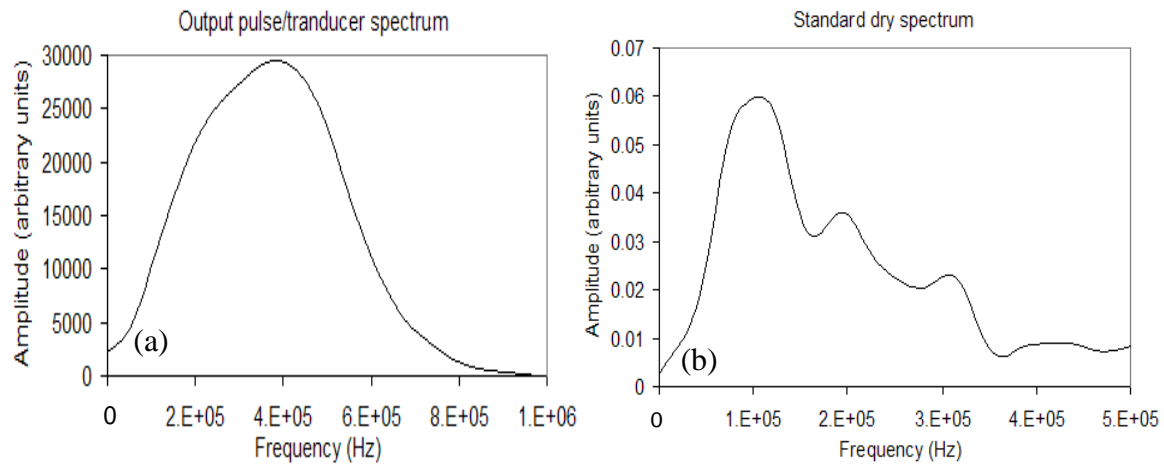
**Figure 8.4. Standard P-wave ultrasonic spectra (a) Transmitted bandwidth (b) Dry medium response spectrum (Hassan et al., 2014 d).**

sequentially with time elapsing, and to further facilitate comparison among spectra of different tests are broadly categorized , earlier, intermediate and later curves to be assigned to oil phase, mixed-zone/phase and brine phase. Considering flow-cell orientation, sensor position/s and direction of flow, an earliest curve corresponds to event of pure oil phase flow i.e., deep red, and a latest curve corresponds to event of pure brine phase flow i.e., dark blue, while intermediate curves, with other colors correspond to different stages of mixing and interface evolution in time, with interface curves marked by green color, when "imaged". To facilitate analysis and interpretation scale, labeling and color coding in all panels of Figure 8.5 is kept fairly consistent. In reconciling the interpretation with time-lapse work flow it is assumed that three experiments may represent three different locations involving same medium where evolution of same process is simultaneously monitored over time, or same location monitored at three different times, with sufficient invariable detectability and repeatability confirmed.

A slow flow rate experiment was conducted only at time 1 which was followed by a faster flow rate one at time 2. The intermediate flow rate, falling within that of other two, experiment was conducted at time 3 lastly. This strategy allowed for selecting reasonable range of flow rates in terms of a spatio-temporal spread to allow for various similar features of interest imaged even for different flow regimes. At the same time flow rates were moderate enough to be well synchronized with in the

sampling restrictions of acquisition system with definite equable preservation of resolution. They were also found to be comparable to be predominant subsurface flow regimes as likewise identified on respective panels of Figure 8.5 in terms of units given consistent dimensions. A sense of spectral bounds of interpretation could be made from examination and comparison of standard spectra as shown in Figures 8.4 a and b, explained also in chapter seven, with those of Figure 8.5 a, b and c. From Figure 8.4 a and b a significant loss in transmitted amplitude and bandwidth is visible. There is no fluid effect and there are no associated factors to alter any adhesion. Such energy could be attributed to grain boundary type relaxation in the absence of any cementation. This could be assumed as one possible dominant mechanism causing significant attenuation in the case at hand, in further analysis. However it has been observed quite clearly that fluid saturation effects are quite predominant, adding interest to the attenuation analyses.

An isolated examination of each panel in Figure 8.5, so, clearly suggests a strong fluid response possibly density dependence of amplitudes against a constant background density. The amplitudes corresponding to brine flow marked as events h and i, since, are much higher than those of oil flow marked as initial ones a, b and possibly c. Significantly low amplitudes for intermediate curves in green color interestingly appear out of pattern and marked as e-f, f-g and g-h respectively in all three tests. They are since temporally bound by those for oil and brine, this leads to identification of mixing zone or interface occurrence, which is very consistent with time domain findings. Such a significant localized loss expression bound between spectra of pure fluid fractions is quite clearly due to the monolayer type interfaces where dominant energy loss mechanism should be a complex of immiscible fluid-fluid interfacial slip. In addition back ground grain boundary relaxations type mechanism plays a part, and possibly much enhanced due to lubrication type effects as fluid-solid interfaces adding further to losses caused due to fluid-fluid slip effects. Despite amplitude loss, especially given that velocity values were appreciable, such a bandwidth loss might also hint a liquefaction type effect, as if effect of
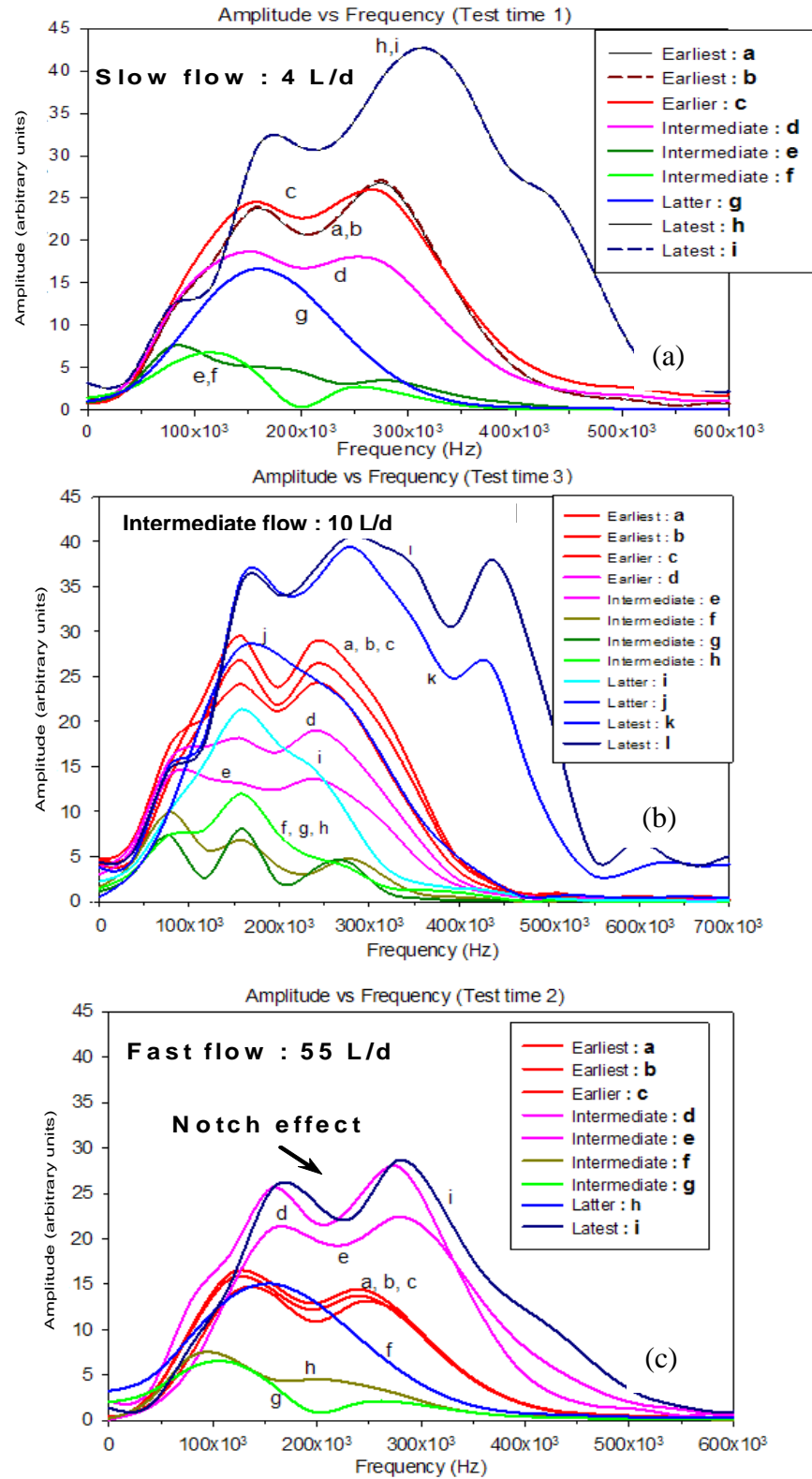
**Figure 8.5.Time-irrespective spectra of immiscible displacement experiments (a) Test 1 (b) Test 3 and (c) Test 2. Explained spectral curves are identified in sequence to understand aspects of attenuation, other features of interest are marked too (Hassan et al., 2014 d).**

of structural strength is compromised due to a variation or lack of apparent effective pressure or confinement effects of direct type in nature. Other curves lying between these three distinct curves identifying the pure fractions oil and brine and a possible interface clearly indicate an initial onset of mixing of brine in oil and evolution of a mixed interface followed by brine flowing only, when examined in a temporal sequence. Besides amplitude effects frequency shift related effects could also be identified. The peak amplitude frequencies corresponding to interface zone, oil and brine are consistently around 100, 300 and 400 kHz in all panels, respectively. This suggests a viscosity controlled effect too, where a viscous type relaxation contribution is accompanied by a selective frequency dependence manifested as frequency shift. As the effect is assumed viscosity associated it appears less magnitude for brine flow and more for that of oil flow in comparison with frequency shift, but maximum for interfacial or mixed-zone. Viscous effects could be understood manifested as two types of mechanisms, a more localized interfacial slip type loss in addition to a global viscous relaxation related to a fluid structure in pore space confinement.

A generalized examination of any one panel from Figure 8.5 panels reveals pretty much similar effect of background granular medium, and fluid density and viscosity control. Mobility or flow rate variation and packing related effects could be understood by mutual comparisons of all panels. In such a comparison much lower overall amplitudes in case of test number two in Figure panel 8.5 c reveal a very clear unambiguous flow rate effect upon amplitudes loss. As they are significantly low in comparison to those of other two tests, it is evident that flow rate effect also appears to be one of dominant amplitude loss mechanism. Packing effect however is quite negligible compared to flow rate effects as is also deducible from comparing panels of Figures 8.5 a and b where corresponding flow rates are not as much different in magnitude as that associated with Figure 8.5 results. With other parametric control of amplitudes pattern or loss preserved it is unambiguous that overall amplitudes reduce with increasing initial invading flow rate, identifiable by successive sequential mutual comparison of Figure 8.5 a, c and b.

A particular "notch" type effect or stop band artifact also appears interesting as prominently marked in Figure panel 8.5 c. This type of the artifact could be speculated to occur by certain interference and/or tuning type effects. The distribution of such notch type artifacts on the frequency axis suggests that they might be a result of diffraction effects of a possible brine plume formation in oil. Such plumes, possibly fewer in number, could be vigorously formed as viscous fingers with definite stable structure as in case of high flow rate test represented by Figure 8.5 c, with an overall greater amplitude loss, and the intermediate spectral curves of evolving mixing zone i.e., pink curves, being much closer to that of pure brine flow curve. For cases corresponding to Figures 8.5 a and 8.5 b however, following same line of reasoning it could be arrived at that there could be greater number of smaller plumes or diffuse type mixing without vigorous fingering facilitated by a lower flow or mobility related amplitude loss, suggesting little to no fingering. Amenability of miscibility and/or efficiency of immiscible displacement appear also to depend upon a certain flow rate or regime. It could be deduced that a moderate to slower flow rate of an invading fluid would cause better and stable displacement as a higher flow rate may cause an early break through by invading fluid, while passing through the invaded, with defined preserved structure. Jones (1962) has theoretically investigated the effects of fluid through porous media upon the elastic wave velocities. The flow velocity is considered to assume a preexisting velocity field with a particular direction in relevance to the elastic wave velocity field. The elastic velocities are described by the parameters of the Biot theory, with an overall Euler formulation consideration and regarded as an impressed field upon the preexisting flow field. Given the restrictions of the direction of wave propagation the assumptions provide for a simple superposition of coincident velocity components. Velocity components are defined comprising those of solid and the fluid components explicitly and are small enough that their products and powers are neglected to accommodate for infintesimality. In terms of velocities little fluid flow effect comparable to that of saturation state existence was found, however, both in case of P- and S-waves. In (Jacobsen et al., 2003) however the aspect of, specified or categorized as, acoustic signature of fluid flow in a complex (micro structured) porous medium

resulting in clear saturant impression, is numerically investigated. They have used T-matrix approach contained in many-body problems framework. The results are presented in graphical form as including spectra, against a standard case of an intact or uncracked saturated medium, a quartz matrix, where the saturant is water. Each case, including or given the standard one, is mutually presented compared to or tested against Brown-Korringa model, effective medium fluid substitution type analytical results. The effect of crack orientation and spatial distribution in relation to the standard case is compared. Frequency dependence of both P- and S-wave velocity and strength moduli is expressed in correspondence to imposed restrictions of matrix material definitions. Impressions of orientation and spatial sensitivities of the saturated cracks or pores offer insights of fluid effects including flow but only in an induced interactivity context as of intention to study the combined effects of microstructure and fluid upon the overall wave characteristics with the assumption that fluid would be caused to flow as inter-cavity, communicating from one to the other at the scales of interest. A theoretically satisfying stochastic component assumption for theoretical macro-description, to accommodate various cavity sizes and shapes, within meanings of randomness, is suggested.

### 8.1.3 S-wave Analysis

Diffraction caused interference and/or resonance artifacts were understood as observed in case of S-wave time domain data to be much more pronounced and involved and alluded in previous analyses in Chapter 7. Such peculiarities are further examined in frequency domain, as naturally ensuing from above P-wave spectral analyses, on accounts of strong sensitivity to background medium structural strength characteristics under saturated conditions or saturant state. S-wave spectral analyses extended results are, thus, also explained within the context of a controlled immiscible fluid displacement monitoring study. Some deeper and fresh insights are intended to be invoked with inferring supported by additional theory where ever required especially owing to the nature of the S-wave propagation characteristics. As
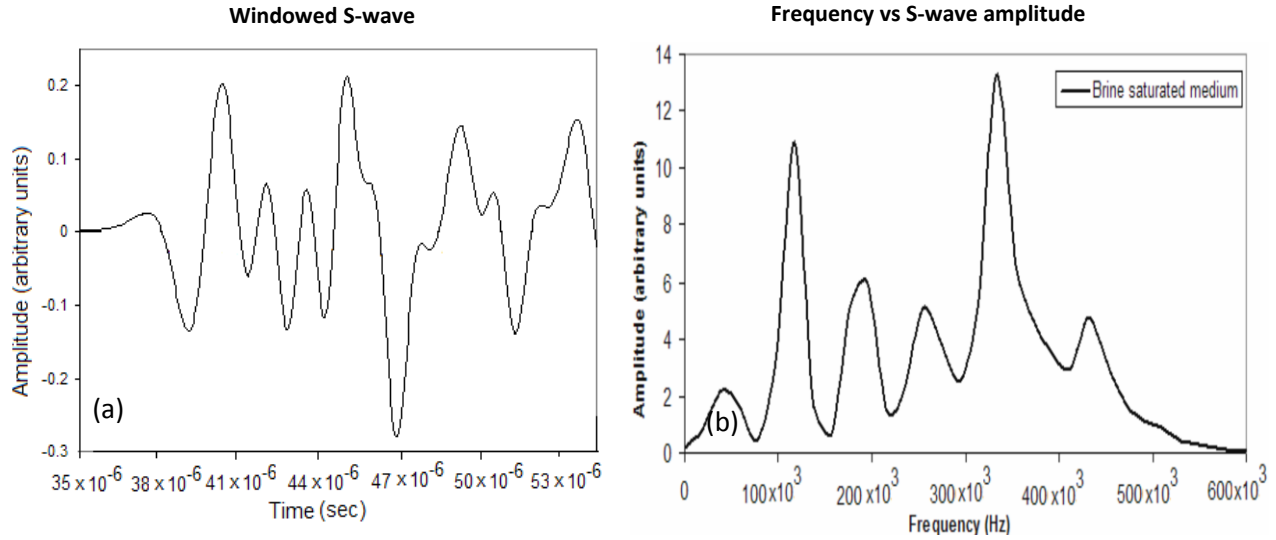
**Figure 8.6. (a) Time irrespective windowed S-wave waveform (b) S-wave spectrum for the saturated medium, spectral peculiarities w.r.t to Figure 8.3 b could be identified (Hassan et al., 2015 a).**

S-wave data were acquired integrated with P-wave data, all the geometrical and parametrical controls related to function of apparatus while experiments and are same. By concept spectral peaks observed are more of a resonant and nonlinear type, in comparison with those of P-waves. A pattern of frequency dependence of viscosity and density associated amplitude, is also phenomenologically different from those of P-waves but does enable isolate different fluid phases, distinctly. Interface and/or the mixed-zone (in onset) appears to assume highest amplitudes but at lower frequencies only, an observation apparently contrary to dim spot appearance in time domain, further explained. Brine and oil associated amplitudes could be categorically isolated .S-waves stimulated spectra, hence, may offer a method of with enhanced parametric quantification or calibration of fluid-release with possibility of attaining a chemical species specific responses central to effective hazard response. The significance of inferred results in this section is naturally assumed twofold. Firstly, an adequate description of analyses and results of the obtained or represented S-wave spectra within configuration restrictions of the experiments on scientific grounds, in reconciliation with important aspects of theory explained above. Secondly, imparting
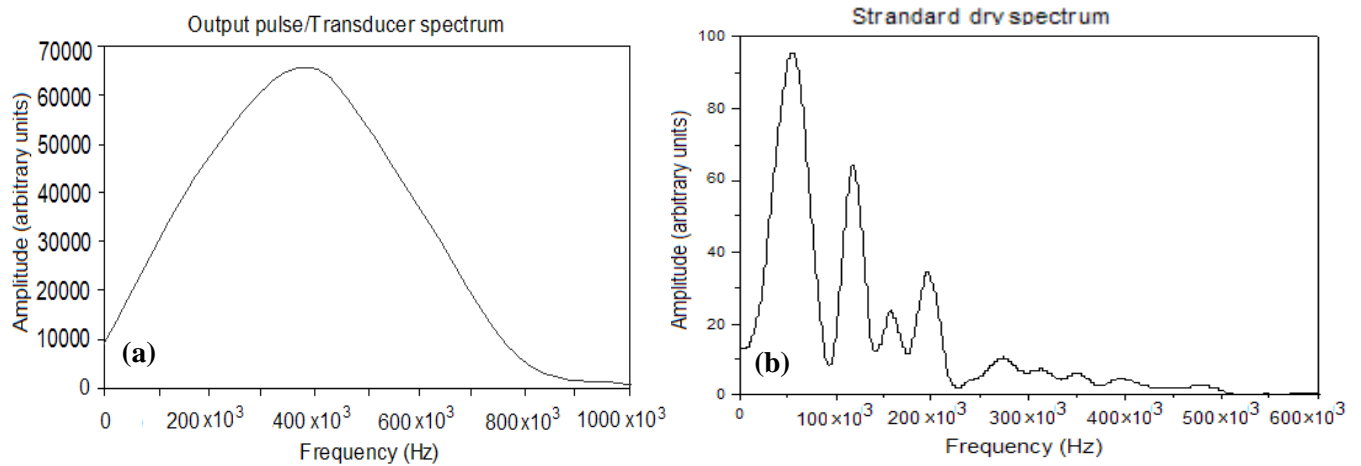
**Figure 8.7. Standard S-wave ultrasonic spectra (a) Transmitted bandwidth (b) Dry medium response spectrum (Hassan et al., 2015 a).**

of an associative conceptual emphasis of the inferences towards geo-environmental applications, in broader context. The results are presented as a series of graphical illustrations appropriately labeled, following usual sense to observe a quantitative meaningfulness, as each readily examinable self-contained alone while allowing clear mutual comparative analyses too. Figures 8.6 a and b serve the purpose of understanding the nature of S-wave spectral results with respect to frequency domain representation of a single trace analyzed, to commence with. Figure 8.6 a windowed S-wave trace, causal and time irrespective, where windowing is done following same procedure as that for P-wave shown in Figure 8.3 a. Understanding or description of Figure 8.6 b, given details of Figure 8.7 alluded to further, is significantly useful in developing further discussions and explanation. It very clearly depicts the theoretically speculated rather peculiar resonant nature of S-wave spectrum as alluded to in above discussion, and importantly as it is for brine saturated granular medium, acquired or measured experimentally. In addition it also shows the nature of controls in terms of frequency and scale dependence, comparatively different from the same coincident P-wave spectrum shown in Figure 8.3 b.

Comparing these two Figures, 8.6 b and 8.3 b also reveals that the response of P-wave to saturated granular media is more of a linear type however there are marked nonlineariaties in the response of S-waves, relative to bandwidth of interest. As of

161

analyses the transmitted bandwidth of ultrasonic S-wave source is shown juxtaposed with dry granular medium spectral characteristics in Figures 8.7 a and b. This is to allow an easy proportionate comparison of several spectra when acquired under same acquisition restrictions.

Comparison of Figure 8.7 b with Figure 8.4 b, in recollection as explained in dry medium characteristics, also holds importance in understanding possibilities of nature of dry medium control against saturant control upon the ultrasonic signature, in proportionate sense. The results presented in this section are also described in Hassan et al. (2015 a) to some detail. All the S-wave spectra, are frequency domain representatives of the features of interest described in the time domain ultrasonogrms, and are coincident with and organized in the same pattern as those of P-wave's events. The spectra are shown in Figure 8.9 constituting or populating three panel figures associated with Test 1, Test 3 and Test 2 respectively, shown in an order , corresponding to same as those of described for P-wave, for different increasing  flow rates. Before inferring the spectra presented in Figure 8.9, it is found advisable to discuss the significant patterned occurrence of the composite spectral curves, by isolating spectra of such traces or measurements which are typical representatives of immiscible displacement process components or constituents to enable a plausible holistic inferring. Figures 8.8 a, b, c and d represent such typical curves where trace numbering almost exactly identifies elapsed time in minutes. Figure 8.8 a shows a very localized single peak for the oil flow which is both frequency and amplitude shifted with respect to the dry granular medium shown in Figure 8.7 b. The spectrum shown in Figure 8.8 b is very interesting and important because it shows only and amplitude shift as resonant frequency is unchanged. Given the sequence of events and temporal restrictions of acquisition it should represent the interfacial monolayer before the evolution of the interface which apparently is significantly different if not contrary to observed in case of P-wave spectra for similar feature. Before this apparent contradiction is further argued, Figure 8.8 c and 8.8 d are examined where Figure 8.8 c shows a significant amplitude shift as a reduction without frequency shift, so an onset of an interfacial evolution can be deduced. Figure 8.8 d also offers
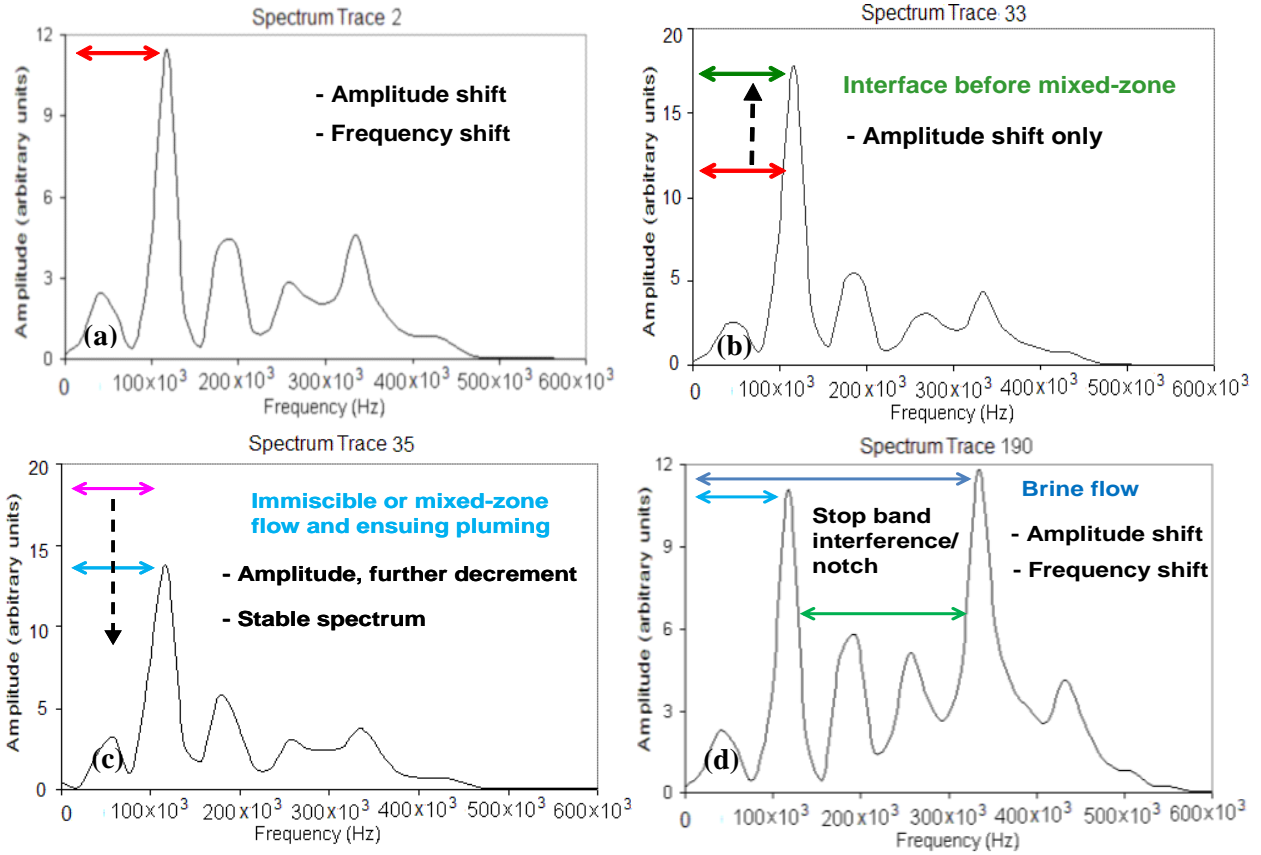
**Figure 8.8. S-wave parametric response during immiscible displacement. (a) Initial oil spectrum. (b) Spectrum of the monolayer interfacial zone with dominant viscosity effects. (c) Spectrum of viscosity dominant evolving mixed phase front. (d) Spectrum of instance of dominant brine flow (Hassan et al., 2015 a).**

interesting results, for keeping the sequencing in view, as it bears two resonant peaks. Given succession of the invading and invaded fluids it could be deduced that the high frequency resonant peak corresponds to density effects and indicates occurrence of brine flow, while the lower resonant peak persist showing viscosity sensitivity and possibly also towards background matrix effects.

The reason for the spectral signature of, or one corresponding to, the interfacial monolayer (type structure envisaged) appears not to resemble, rather paradoxically opposite in apparent nature, as of respective P- and S-wave spectral instances, could be that in frequency domain it is resolved differently owing possibly to the characteristically incomparable nature of P-and S-wave polarized propagation and parametric sensitivities. The interfacial spatio-temporal monolayer anatomy including immediate interfacial zone collectively may only appear as a single attribute in the time domain dimension sense as a

163
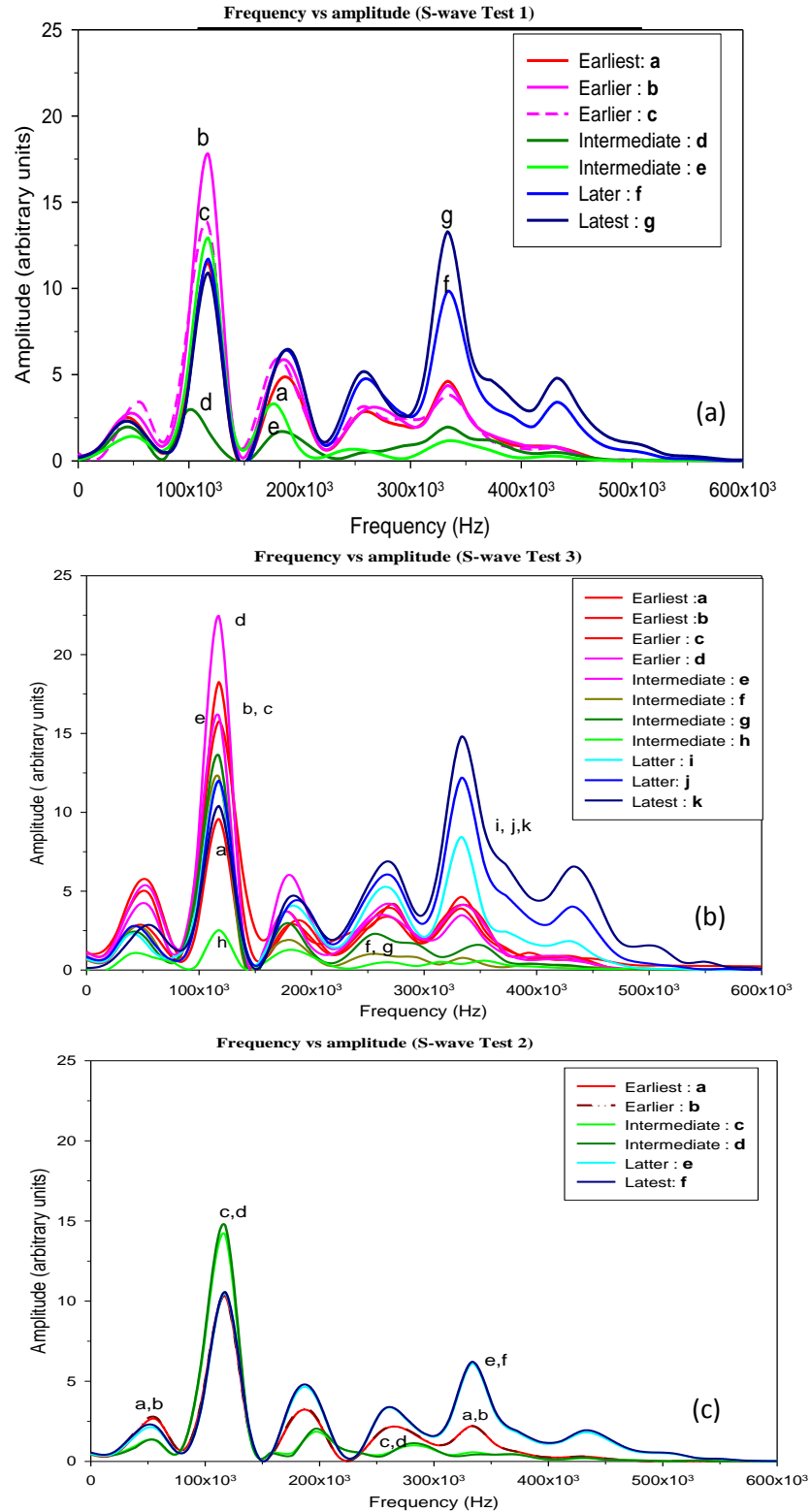
**Figure 8.9. Time-irrespective spectra of immiscible displacement experiments (a) Test 1 (b) Test 3 and (c) Test 2. Explained spectral curves are identified in sequence to understand aspects of attenuation, other features of interest are marked too (Hassan et al., 2015a).**

dim spot, when encoded by P- and S-wave. Further any specific micro-structural anomaly as such may be captured or encoded to P- and S-wave time domain signature differently, and may not be well resolved or visible being time compressed in time domain ultrasonograms or traces. However the subtleties invisible in the time domain were much were much visible in frequency domain showing higher sensitivity of S-waves. While examining the composite spectra in panels of Figure 8.9 a, b and c, directly, enable identification of two resonance peaks at frequencies of about 100 kHz and 350 kHz marked by a significant apparent amplitude and frequency shifts as discussed above. A collective yet closer examination following the labeling order and identifiers further, clearly isolate each fluid phase distinctly, in a spatio-temporal sense. Highest amplitudes associate with occurrence of earlier to intermediate events clearly i.e., flow of interfacial or mixed-zone, compared to those of oil flow and brine flow marked as earliest and latest events. Magnitudes of brine and oil associated amplitudes are lower and comparable but distinctively appear at different frequencies.

Brine effected amplitudes unambiguously and isolatably assume higher frequencies while oil associated amplitudes somehow tend to overlap those of mixed phase. Two resonant peaks are thus defined with the intermediate bandwidth being significantly attenuated in comparison. Considering the geometrical restrictions of imaging for any given test, it could be deduced that at lower frequencies viscosity or viscous effects control amplitudes, while at higher frequencies they appear density and inertial effects sensitive. This phenomenon clearly indicates a frequency sensitivity or dependence of viscosity. At the primary resonance frequency the apparent viscous strain hardening is pronounced affecting increased displacement communication response. However, when further increase in frequency causes the "viscous resilience" break down and inertial effects dominate, density effects so appear to manifest as a much higher frequency peak only. The interface appears to evolve during the course of fluid-displacement as plumes due to vicious fingering, where the spectral signature of loss amplitude loss is much pronounced in S-wave compared to that of P-wave. The complexity of the occurrence of the phenomenon

with associated reasons in an immiscible displacement could be understood from (Homsy, 1987) explanation of same appears out of scope as important relevant factors are already elucidated. This structure of pluming flow is assumed to have caused significant intermediate bandwidth loss due to diffraction and/or multimode scattering affected destructive interference and tuning effects. Such effects, given especially their precursors, could be understood in detail in detail from (Yamakawa, 1962), (Berryman, 1985), and (Gurevich et al., 1993), in addition to specific references discussed. This implies that ray theory holds in determining arrival time and velocity but when analyzing the amplitudes and energy variations consideration of diffraction effect and its consequences become inevitably important.

Contributory loss effects additionally, those of flow rate and background inter-granular shearing are also identifiable and deducible. The eventual flow of pure brine during the displacement is marked by high frequency amplitudes only. While occurring after the displacement of pure oil followed by the mixed phase, this shows clear higher density sensitivity of frequency instead of viscosity. Sequential temporal S-wave spectra clearly not only help isolate different fluid phases but also provide peculiar stable resonant signatures significantly intimate to density and viscosity where this aspect is not as clearly resolved in consistent instances of P-wave spectra.

Flow rate effect upon amplitudes is easily deducible, given the morphological sense of the fluid flow process during displacement. Amplitudes since for Test 2 i.e., 55 L/d test, in a mutual comparison of panels of Figure 8.9 appear much lower than those of rest of the two tests. This observation is also in line with that of P-wave spectra. It could be assumed that high amplitude viscous strain hardening response is flow rate dependent too. It appeared to occur due to complex viscous and interfacial affects combined, over the background, captured with typical S-wave polarization. It could be inferred that S-waves can indirectly capture significant amount of saturation related information due to their higher sensitivity to any subtle changes affecting the structural strength properties and rigidities, so they are not blinded to fluids though they see through it, depending upon the type of the saturated medium or sediment. A speculatively interesting aspect of this analysis is that density and viscosity information as combined may form particular and diagnostic or characteristic

parametric identifier in enabling robust and reliable identification of subsurface toxic or contaminant fluid percolations/flows and assessment of fate. The information could also help introduce geotechnical control in addition to a geohydrological. Such studies could provide a sufficient knowledge base to calibrate methods and simulators by generating consistently appreciable and reliable inventory of outcomes.

## 8.2 Electrical Resistance Measurements

### 8.2.1 Background Theory

The electrical resistivity data are also organized in a manner consistent with that of P- and S-wave ultrasonograms, thus electrograms. In this regard detailed account of interpreting resistivity data as part of field procedures where heterogeneities of subsurface resistivity magnitudes are encountered is provided by(Griffiths & King, 1980). According to (Grant & West, 1965) the apparent variations in electrical resistance in sediments and strata is presumed comparable to an interstitial type where resistance is electrolytic controlled type. Similar reason is offered by Griffiths and King (1980) implying that presence of water with dissolved electrolytes allows direct detection and resolves such bodies and boundaries which are non-conductive in disseminated form with dry interstices or fissures between fragments. Such factors are naturally embodied or realized into an immiscible displacement scheme involving oil and brine phases, given resolvable above the background. In this regard for soda-lime direct current resistivity values vary between extremes of $1x10^5$ and $1x10^{10}$ with units of ohm-cm for a corresponding temperature range of $0^o$ C to $350^o$ C , so in principle an insulator. To rule out any possibility of current leakages or dilution into the background medium measurements were made to confirm that magnitudes of resistance of packed beads values were of same orders of magnitude compared to those cited in (Kingrey et al., 1975) discussed above. An importance aspect regarding near surface surveys could enable appreciating relative electrical resistance resolvability since geological boundaries are delineable only if the resistivity varies in sizable magnitudes, by a factor of 2, at instances by factor of 5 to 10 considering the background. An interesting and specific example is that of that of permafrost where

delineating or isolating permafrost from frozen ground requires resistivity of permafrost be ten times higher, otherwise edges are more difficult to resolve for they tend to show as irresolvable transition zone type instead of a definite delineable sharp boundary (Hoekstra et al., 1975). These examples also imply that usage of an integrated acquisition be tried to attain better resolution as of (King et al., 1988). Given the usefulness of transparent apparatus component, development of such transparent core analogues or apparatus arrangements in concept, capable of assisting in visual examination in reservoir studies is reported before, for better tuning and calibration. Usage of such apparatus for examining fluid phases or fluid flow processes for laboratory experiments with a consideration field scale could be understood further some examples briefly described. An earlier experimental apparatus typically for a physical visualization based examination of immiscible displacement type processes aimed at an improved understanding the porous media flows was designed by (Meurs, 1957).Viscosity ratio was one important parameter considered in terms of possibilities of affecting fluid displacements, where it was referred to as wettability controlled relative permeability or stratification. The viscous fingers were found apparently to have a tendency of following a flow path, along a single isolated well defined fluid streams lines, comparable.

In their rather static experiments (Chen & Wada, 1986) used a laser fluorescence technique to study porous media flows. Sequential photographs of a sample, laser illuminated form top and exposed at a right angle, by a camera, of consistent cross sections examinable as in elapsed time were used for a visual examination. They were motivated to improve an understanding of interactions of solid grain structure with entrapped oil blobs in water; an immiscible mixture consistency, for an occurrence of the viscous fingering phenomena caused due to interfacial forces and wettability. Use of visuals or images was demonstrated as a useful means of studying two-phase flow in porous media. A selective cross-section of the modified photographs is shown in Figure 8.10 where more illuminated regions are oil, grayer regions are water and darker regions represent quartz grains, delineable.

The quartz grains used were not more than 100 μm size and the sample was
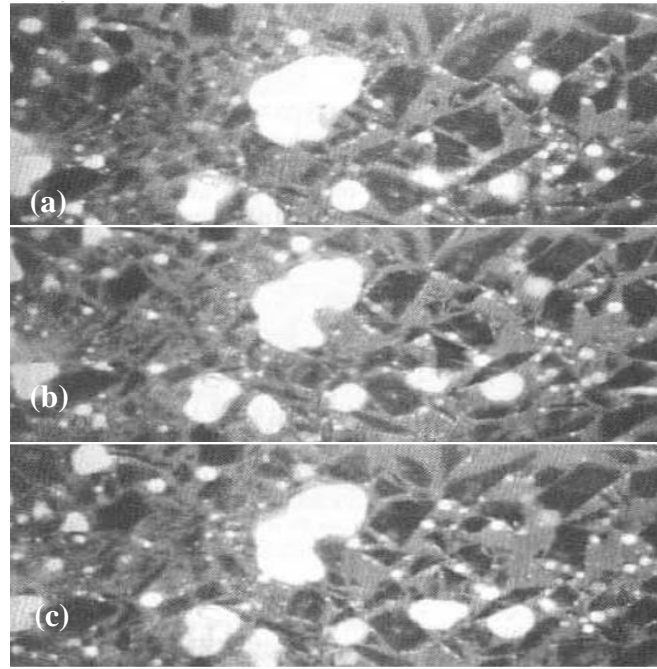
**Figure 8.10. Laser assisted sequential (a), (b) ad (c) static photographic images depicting cross-sectional distribution of phases in a multiphase flow, illuminated oil trapped in grayer water in a matrix of quartz appearing dark (Chen & Wada ,1986).**
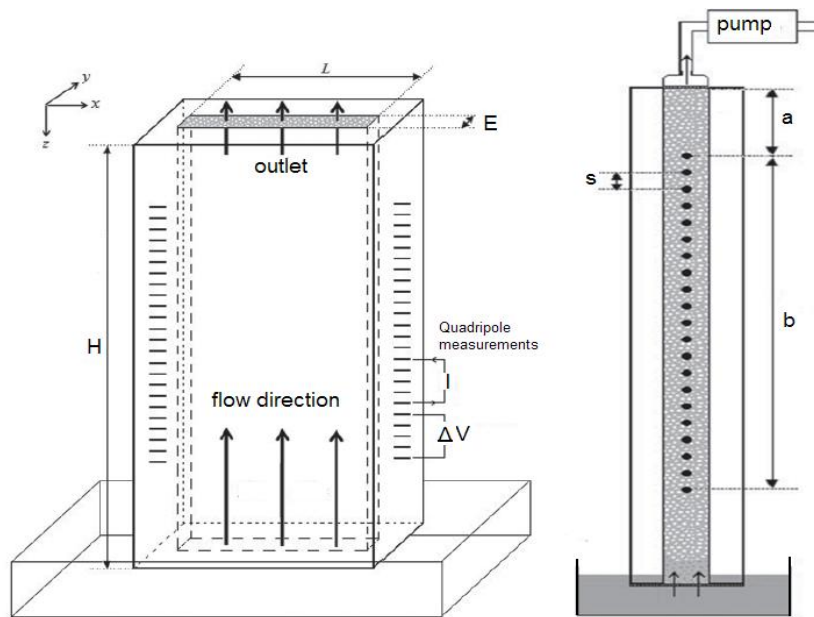


**Figure 8.11. Front (left) and side (right) view of configuration and apparatus used by Lekmine et al. (2009) in their tracer solute ER profile determination in porous media flow experiment. Dimensions in centimeters are L=27.5, H=8.5, E=1.**

For overall size secured only a micro meter stand, as its larger dimension would not exceed more than ten grains of quartz chosen to be used in experimental observations.

Lekmine et al. (2009) used a similar apparatus used in this investigative study (see Section 4.2). They studied a flow and evolution of dyed brine through porous medium, as a proxy of contaminant solute, using a transparent 0.2 mm glass bead pack as shown in Figure 8.11.The fluid flow process could both be video analyzed and resistivity imaged. Experiments also demonstrated that a well defined measurement protocol enable understand an acceptable compromise between spatial and temporal resolutions for developing improvement and calibrations. The dynamic monitoring offered a reliable estimation of position and size of the mixing front. An important aspect emphasized for design protocol was repeatability achievement while accommodating density and flow rate variability. Other pioneering citable works include Apparao et al. (1969), where resolution of anomalies, contingent or morphological architecture, with Wenner configuration was investigated in depth sounding sense. Contemporary references with cited ones are detailed in section 3.2.

## 8.2.2 Electrical Resistance Results and Integrated Evaluation

Recollection of the certain features already studied tends to provide as sense of what is expected in the following analyses. The basis of the physical design of reflection and refraction seismic and resistivity surveys. It should be clear that the electrode array was symmetrically installed with probes successively equidistant spanning the length of flow-cell tube, as it was designed following standard methods (well known ASTM) for filed-scale seismic and DC resistivity surveys allowing a reliable data acquisition and subsequent conventional interpretation. It also helped realize resolution issues in data analysis and interpretation of the results in geological sense while using ultrasonic frequencies, keeping in view the theory of elastic wave propagation. Immiscible fluid-displacement process is characterized with integrated data approach where ultrasonic through transmission results are already discussed. These are evaluated by examining simultaneously acquired DC resistance measurements. P- and S-wave ultrasonograms are reproduced in this section also, discussed already, shown --
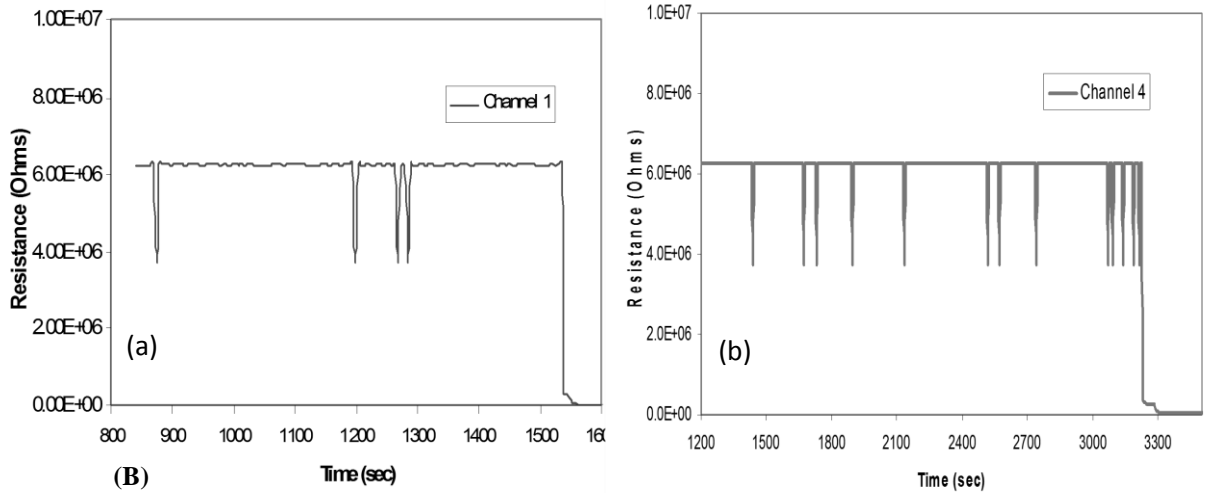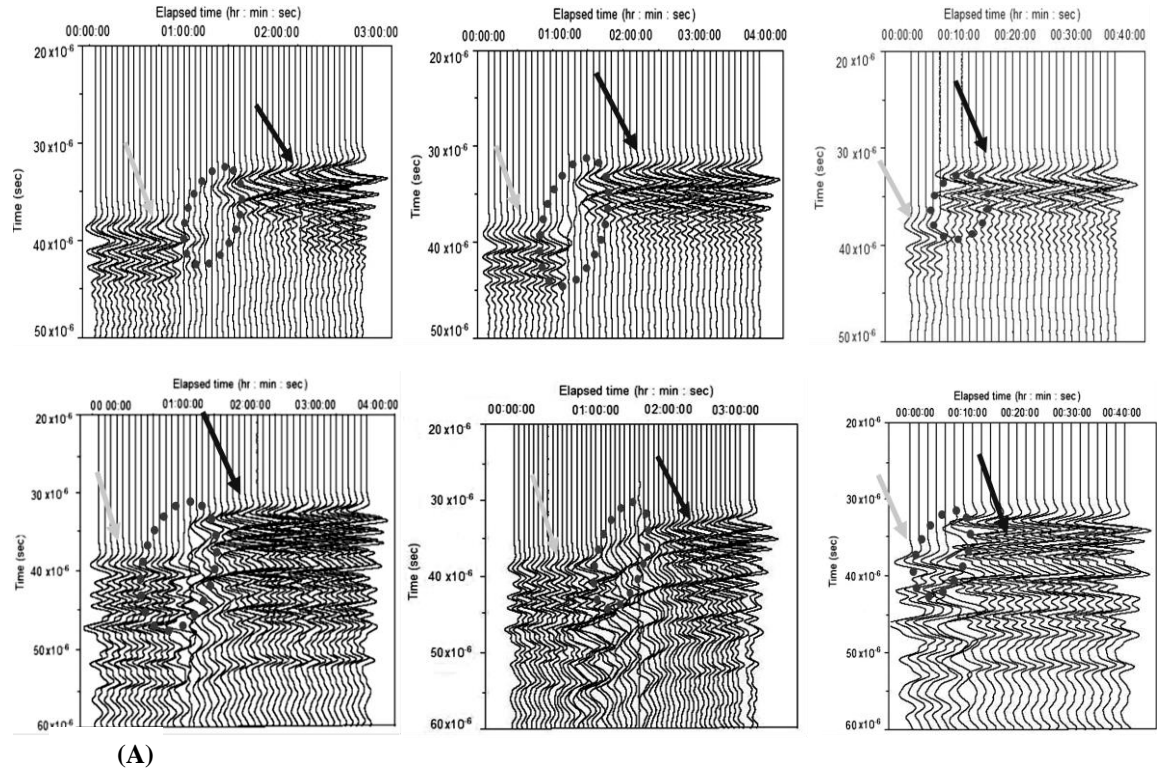
**Figure 8.12-(A) Previously examined ultrasonograms with features of interest clearly marked in elaspsed time. Top P- and bottom S-wave ones, (L-R) Test 1, Test 3 and Test 2, respectively. (B) An example of monitoring Ohmic resistance variation against elapsed time during the immiscible displacement tests modified (Hassan et al., 2007) , (a) electrogram 1 and (b) electrogram 4.**

171

in Figure 8.12-A, where the primary features of interest marked which are dim spot, circled, for interface or interfacial region, illuminated region indicated dark arrow brine flow region and less illuminated region of oil flow identified by a lighter colored gray arrow. This is to facilitate a coherent development of next analyses with sufficient useful information to assume brevity and avoid redundancy of explanation. In order to understand each figure appropriately an example of electrogram signal is provided in panels a and b Figures 8.12-B. In these figures ohmic resistance variation is shown at horizon of channel 1 and horizon of channel 4 for certain experimental trials before the conversion of the resistance values to logarithmic scale. Logarithmic scale is employed to better resolve the apparently disproportionate distribution or variability of the electrical resistance values or the legitimate signal compressed within a large range and /or spread of maximum and minimum resistance magnitudes. The final logarithmically converted results are presented as composite curves for channels one to eight (Channel position 1-8) in single graphs for all data corresponding to individual immiscible displacement tests identified and presented in sequence as Test 1, Test 3 and Test 2 respectively as usual.

Each of electrograms presented in Figures 8.13, 8.14 and 8.15 consist of a top panel-a and bottom panel-b. All panels-a depict a switching of a channel from a maximum to a minimum resistance while panels-b show a measure of variability of electrical resistance at each channel horizon or in physical sense an electrolytic concentration signature. In each figure significant apparent electrical resistance change, from a maximum to a minimum, for all tests is clearly identifiable suggesting that variations between these maxima and minima are also appropriately captured. Labeling details of Figure 8.14 clarify the nature of variations from a maximum to minimum resistance for all figures in a broader sense. Instance of occurrence of these variations in principle should correspond to same features of interests depicted in Figure 8.12 considering elapsed times of all relevant tests.

The corresponding elapsed times of occurrence precisely are about 50 min, 1hr and 5 mins. respectively, after the onset of the flow of the invading fraction or brine solution. If the electrograms "figures" are now examined considering the
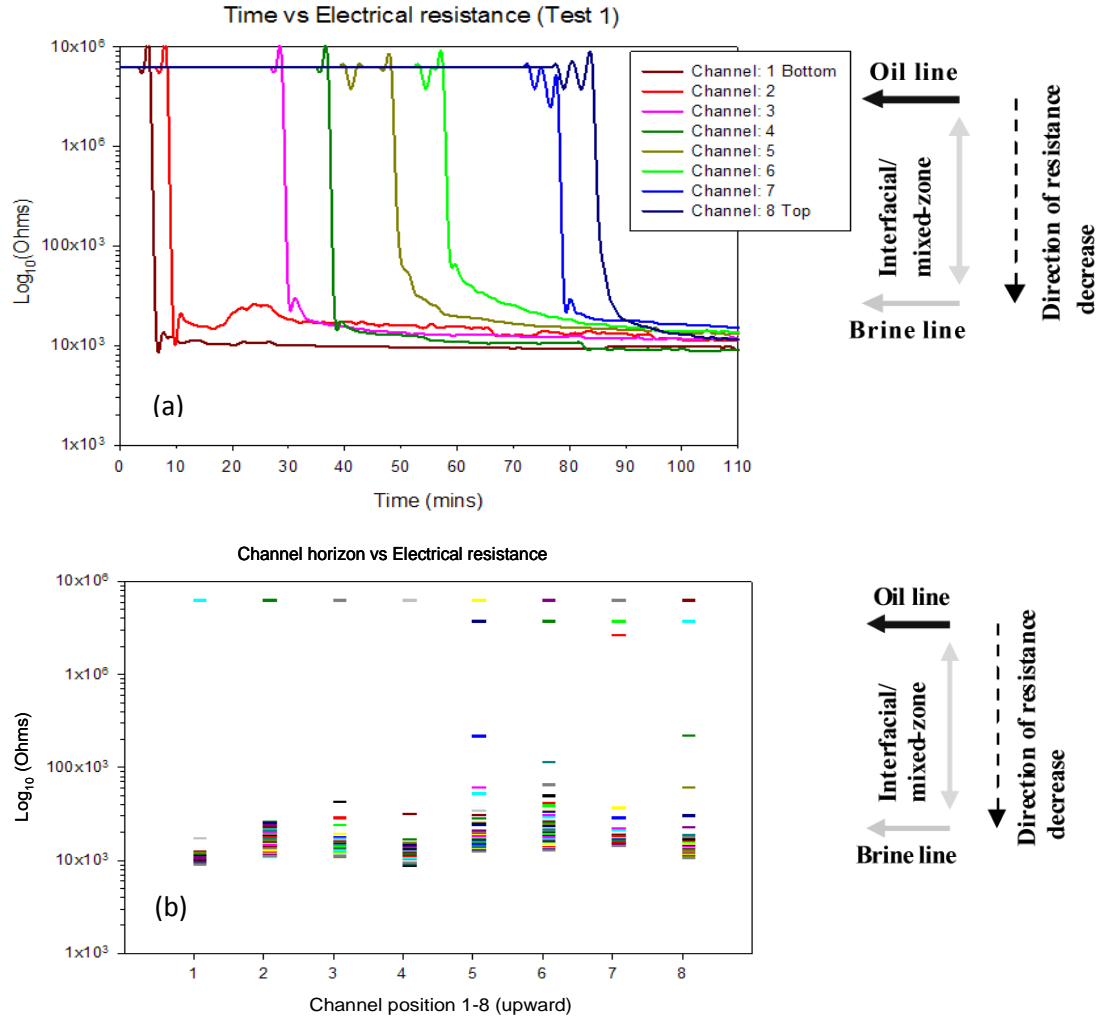
**Figure 8.13. (a) Electrical resistance variation with elapsed time in minutes, for immiscible displacement Test 1 (b) Time irrespective expression of resistance variation of same (Hassan et al., 2014 a).**

channel electrode position 4 and 5 one can clearly see that all of the panels-a of Figures 8.13 for Test 1, 8.14 for Test 3 and 8.15 for Test 2 the corresponding time of switching of the channels from a maximum to minimum value or magnitude does occur corresponding to consistent ultrasonograms in integration sense. In a physical sense it would indicate indirectly sensed change of state of the fluid fraction. It is thus cross-confirmed by a direct detection a localization of oil phase identified by oil line, a brine phase identified by brine line and also verify occurrence of an interfacial immiscible zone bounded within.
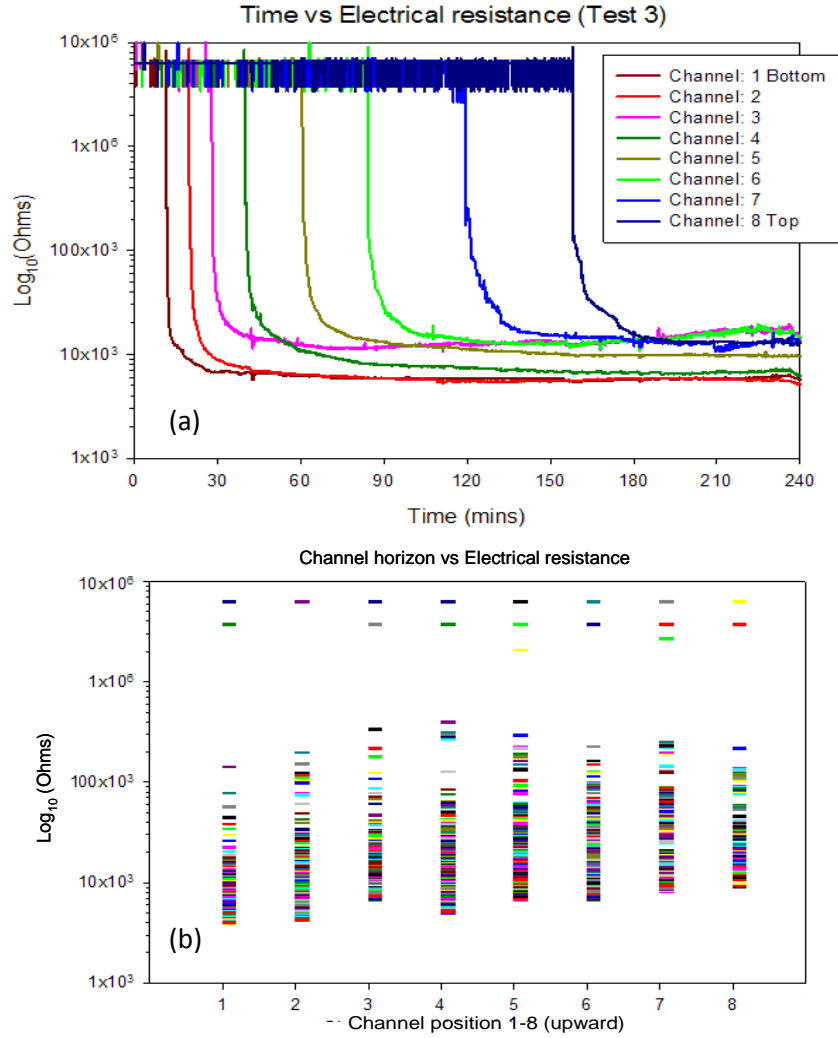
**Figure 8.14. (a) Electrical resistance variation with elapsed time in minutes, for immiscible displacement Test 3 (b) Time irrespective expression of resistance variation of same (Hassan et al., 2014 a).**

In terms of a definite unequal pattern of temporal separation between switching of successive channels, alongside a subtle but significant degree of variation in electrical resistance change from a maximum to a minimum value occurring differently for each channel, a flow rate dependent evolution or miscibility could be speculated. It could be further confirmed by examining the time-independent panels-b of Figures 8.13-8.14 showing clearly a pattern of conductivity frozen in time at each channel horizon precisely collectively unraveling, otherwise invisible, a

174

frontal view of the graphical results of panels-a in all said figures. A comparative examination of panels-b of all figures clearly show a flow rate dependence of the immiscible displacement process directed upwards within the flow cell. Panels-b of Figure 8.13 and 8.14 clearly inform about a more diffused and well defined evolution of the mixed phase in terms of conductivity spread almost defining a physical zone of brine flow. In this regard, still, the situation in Figure panel 8.13 b is different than that of 8.14 b. The zone of interest, since, in the former situation appears to assume a less conductive spread in physical sense than that of the latter as if there was relatively significant if not substantial resistive type or oil flow too. This also suggests occurrence of some degree of pluming. However for the latter situation it appears that the existence of flow is substantially if not totally in conductive regime suggesting an efficient displacement of oil with brine. Interestingly the speculated inferences also corroborate to the analyses development and subsequent findings of ultrasonograms examination. Especially when the case discussed above is compared to the situation of panel-b of Figure 8.15 where the conductive spread or electrolytic concentration marker of spatial existence of brine flow is pretty narrow for all channels however counter intuitively the flow rate is significantly high in proportionate sense, as 0.64 ml/s against 0.044 ml/s and 0.11 ml/s for Test 2, Test 1and Test 3 respectively.

One interesting aspect to recall before extending the discussion further is that the ultrasonic measurements have all been single point measurements imaging a dynamic process while the electrical resistance measurements were all made along the full length of the so called target of interest or the core analogue. Hence the speculated spatio-temporal extents of features of primary interest identified in ultrasonograms are clearly resolved by the electrical resistivity data adding confidence to inferring. In this regard the speculation or inferring of a liquefaction type situation could be examined where such anomalies as low Vp/Vs and Poisson's ratio were identified. In addition, with recollection of the Vp/Vs and Poisson's explained previously, and keeping in view one of the situations explained by
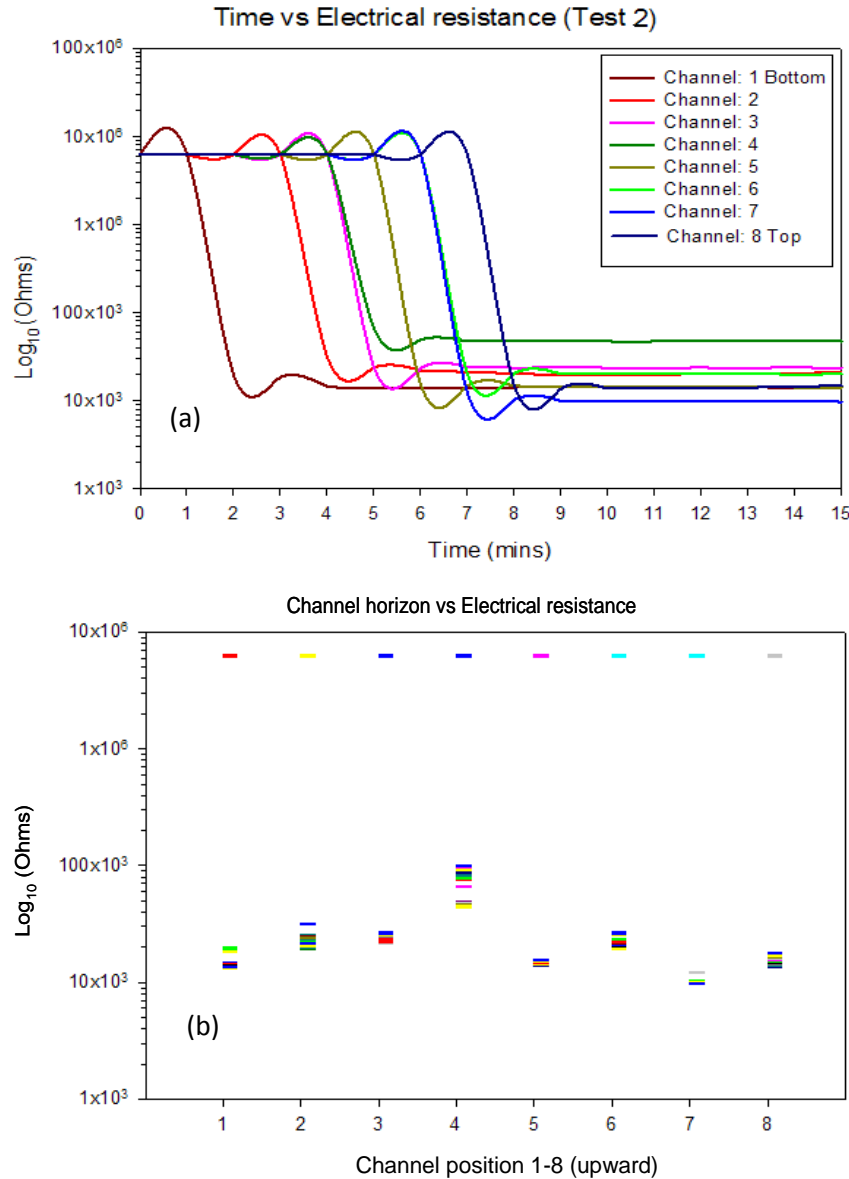
**Figure 8.15.(a) Electrical resistance variation with elapsed time in minutes, for immiscible displacement Test 2 (b) Time irrespective expression of resistance variation of same (Hassan et al.,2014a).**

Chen and Wada (1986) in their laser assisted photographic analyses previous argumentation is supported. This is to say that with a saturant state altered such that water (or brine) and oil coexist, such a consistency may occur to have physico-chemical effect of causing a rheological behavior change. Such a change in rheological behavior can lead to an alteration of strength properties of unconsolidated sediments. Works of Oka et al. (2009) could be further cited where with help of many other references there in , they have propositioned a liquefaction type analyses based

176

on concepts of Biot theory. Special mention, out of their numerical investigations, is made of situations proximal to saturated sandy elasto-plastic type sediments where Poisson's ratio is very low or does appear negative. For negative Poisson's ratio situations in their modeling study instability occurs in terms of handling pore pressure effects which does not occur when the same is positive, under cyclical load. The reason for such instability translates to possible occurrence of a liquefaction type situation.

Overall, it could be assessed with the help of the electrical resistance data that the assumption or an impression of existence of an interface zone evolving further into a mixed zone when formed does prevail. The occurrence of liquefaction type effects, where a complex of local viscous effects and global inertial flow effects with an added affective decrease of confinement associated intergranular direct stress is reduced, may occur. An integration of data and analyses thus allows not only to confirm the fundamental problem at hand but also issues that would not be easily clarified from one type of data.

## 8.3 Summary

Similar as for the first study, summary of anticipated observations, following conceptualized models, in terms of an adequately insightful integrated interpretation of a controlled immiscible displacement is provided, for since:

In both P- and S-wave time domain waveforms oil phase, mixed phase and brine phase while mobile during the displacement process were distinctly identified, where time domain dim spot appeared a significant finding. Velocity and integrated amplitude analyses of P- and S-wave data confirmed time domain amplitude observation, and spectral analyses of same further provided significant information about spectral sensitivities, low frequency shift of viscosity against high frequency shift of density. Background intergranular friction and flow rate control of attenuation was evident, with higher S-waves sensitivity. Sensible electrical resistance variability confirmed P- and S-wave observations as direct detection above background matrix while corroborating other Vp/Vs and Poisson's ratio based analyses.

# Chapter 9: Conclusions

## 9.1 Summary

The conclusions assume a twofold notion. The immediate or direct one, related to application of an ultrasonic NDE to evaluate and characterize or monitor materials and processes as immiscible displacement experiments explained. The indirectly related salient ones while drawing relevant conceptual correspondence to field scale applications.   This pertains to all presented results of both of the studies. Unambiguous and vivid conclusions are summarized below, given both the applied or subject method of investigation and addressed object.

In the first study involving S-waves evaluation of periodic fractured sediment or medium following conclusions could be arrived at explicitly

- S-wave (ultrasonic) velocity and amplitudes with polarity sensitivity to strength properties and degree of heterogeneity and direction (or azimuth) is observably significant.

- S-wave characteristic preferential splitting i.e., S1 and S2,  through fractured geological media is significantly visibly stable and thus quantifiable.

- Correlation of S-wave anisotropy and permeability anisotropy, given above, is quite plausible.

- Acquisition azimuth independent stop band "notch type" artifacts with a definite and peculiar spectral periodicity pattern confirm sensitivity to crack/ fracture existence and spacing.

- Spectral dependence upon, fracture density and compliance is inferable in addition to other diagnostics indicated above.

P- and S-wave propagation while characterizing granular medium sediment involving immiscible displacement tests given elastic deformational characteristics, in case of the second study unraveled following findings as conclusive

- When in dry state the stimulated granular material behavior for P-waves appeared that of an energizing in nature, while that of S-wave clearly appeared comparable to a relaxation and decaying nature with possibility of introducing (power law type) material reorganization.

- Both P- and S-wave velocity and amplitude variation information unambiguously isolated and defined existence of the interfacial monolayer (interfacial zone) and its evolution as a mixed zone or mixed phase marked by plumes or fingers of invading phase along with pure phases as oil and brine i.e., three discrete phases, repeatedly observable.

- Observation of low amplitude artifact i.e., dim spot, repeatedly, in case of both P- and S-waves identifying the interfacial zone was a significant finding, independent of flow rate.

- Spectral attenuation of both P- and S-waves showed density and viscosity dependence, where amplitude decay appeared fluid density dependent predominantly, while frequency shift as viscosity sensitive, with a difference of degree of sensitivity. Subtle control of background packing effect and flow rate upon spectral variability was readily deducible among various tests.

- Vp/Vs and Poisson's ratios based strength behavior evaluation further manifested that aseismically or seismically stimulated saturated

unconsolidated sediments may behave as liquefied material with an anisotropic character marked by negative Poisson's ratio.

- Electrical resistance measurements alone offered similar confirmatory observation regarding immiscible displacement characterization apparently to that of P- and S-wave.

- When examined integrated with P-and S-wave data however provided deeper insights such as a more understandable coincident physical sense of degree of continuous spatiotemporal distribution of brine (radical concentration) throughout the sediment analogue assisted with data at several horizons.

- The mutual corroboration of ultrasonic (indirect and surrounding dependent) and electrical resistivity results (direct and surrounding independent) in evaluating several features of interest add to the overall quality of the inferring and indirectly quality and reliability of the data. This also clearly signifies the importance of understanding interdependence of data integration and acquisition or instrumentation and/or array design upon attained resolution.

The findings signify remarkable attributes which provide substantial conceptual relevance to solving variety of engineering and environmental problems by delineating near subsurface, from various public and industrial perspectives. A few to name are stress and fracture direction delineation in unconventional developments of energy sector, coastal fractured aquifer hydrogeological and geotechnical analyses and bedrock strength response modeling against seismic and aseismic cyclical loading from hazard prevention stand point. A dynamic characterization of immiscible displacement, by imaging or monitoring , when compared to usual static bench top experiments, was remarkable within its own right, given, especially, achievement of integrated data acquisition and imaging i.e., P-wave, S-wave and electrical resistance, with significant control of parameters of interest.

## 9.2 Remarks for Future Directions

In field, combined sensitivity of P- and S-waves to fluid density and also viscosity, especially that of S-waves could help identify and create inventory of particular hazardous chemicals or toxin defining characteristic parameters (out comes) to explain or characterize predict unknown subsurface fluid flow conditions. It could also help standardize equipment and methods

In laboratory NDE elements of granular material under ultrasonic P- and S-wave stimulation be more closely investigated to understand the nature of possibilities (of directions) of intergranular tractions given surface properties. Such tendencies as translational, rotational and their combinations to better evaluate relation between proverbial localized stick-slip behavior and change translated to global strength properties with thermodynamic implications. This could imply broad spectrum of geotechnical investigations. Combined P- and S-wave capabilities could be used to devise methods as stimulation based traction so as to energize and organize entities of interest at micro to nano scales. This could find applications several medical purposes. Same concepts could also be translated to development of nanostructures or components.

The direct detection capabilities of electrical and associated methods could be reinvented both for depth and shallow surveys with improved, efficient and flexible instrumentation. In laboratory different multiple orientations multiple frequency ac could be used to design experiments in geotechnical and geo-environmental realms to test or improve existing algorithms and result generators.

# BIBLIOGRAPHY

Angel, R. J., Jackson, J. M., Reichmann, H.J. & Speziale, S. (2009). Elasticity measurements on minerals: a review. *European Journal of Mineralogy, 1-26.* DOI: 10.1127/0935-1221/2009/0021-1925.

Apparao, A., Roy, A. & Mallick, K. (1969). Resistivity model experiments, *Geoexploration*, *7* ,45-54.

Auken, E., Pellerin, L., Christensen, N. B. & Sorensen, K. (2006). A survey of current trend in near-surface electrical and electromagnetic methods. *Geophysics, 71* (5), 249-260.

Ayan, C., Collin, N., Cowan, G., Emmanuell, E., Wannel, M., Goode, P., et al. (1994). Measuring permeability anisotropy the latest approach. *Oil field review, 6*, 24-35.

Bandis, S. C. (1990). Mechanical properties of rock joints. In N. Barton, & O. Stephansson, *Rock Joints* (pp. 125-140). Rotterdam: Proceeding of the International Symposium on Rock Joints, A.A. Balkema.

Bathurst, R. J. & Rothenburg, L. (1988). Note on a random isotropic granular material with a negative Poisson's ratio. *International Journal of Engineering Science, 26* (4), 373-383.

Becker, M. W., Georgian, T., Ambrose, H., Siniscalchi, J. & Fredrick, K. (2004). Estimating flux and flow of ground water discharge using water temperature and velocity. *Journal of Hydrology, 296*, 221-223.

Berryman, J. G. (1980). Confirmation of Biot's theory. *Applied Physics Letters, 37*, 382-384.

Berryman, J. G. (1985). Scattering by a spherical inhomogeneity in a fluid saturated porous medium. *Journal of Mathematical Physics, 26*, 1408-1419.

Berryman, J. G. (1988). Seismic wave attenuation in fluid-saturated porous media. *Pure and Applied Geophysics, 128*, 423-432.

Berryman, J. G. (2009). Fluid effects on seismic waves in hard rocks with fractures and soft granular media. *Proceedings of the Fourth Biot Conference on Poromechanics* (pp. 598-603). New York: Destech Publications.

Biot, M. A. (1961). Mechanics of deformation and acoustic propagation in porous media. *Journal of Applied Physics, 33* (4), 1482-1498.

Biot, M. A. (1941). The theory of three dimensional consolidation. *Journal of Applied Physics, 12* (2), 155-164.

Biot, M. A. & Willis, D. G. (1957). The elastic coefficients of theory of consolidation. *Journal of applied mechanics* , 594-601.

Blau, L. W. (1933). *Patent No. 911137.* United States, Houston, Texas.

Bolster, D., Neuwiler, I., Dentz, M. & Carrera, J. (2011). The impact of buoyancy on the front spreading in heterogeneous porous media in two-phase immiscible flow. *Water Resources Research, 46*, 1-17.

Bourbie, T., Coussy, O., & Zinszner, B. (1987). *Acoustics of porous media.* Paris: Gulf publishing company.

Brenner, H. (2011). Beyond the no-slip boundary condition. *Physical Review E* , 046309,1-8.

Brill, D., Gaunurd, G. & Uberall, H. (1980). Resonance theory of elastic shear-waves scattering from spherical fluid obstacles in solids. *Journal of the Acoustical Society of America, 67*, 414-424.

Buckingham, M. J. (2000). Wave propagation, stress relaxation, and grain-to-grain shearing in saturated, unconsolidated marine sediments. *Journal of the Acoustical Society of America, 108*, 2796–2815.

Buckingham, M. J. (2004). Wave and material properties of marine sediments: Theoretical relationships for geoacoustical inversions. *High frequency ocean acoustic conference*, (p. Invited paper). La Jolla.

Buckingham, M. J. (2007). On pore-fluid viscosity and the wave properties of saturated granular materials including marine sediments. *Journal of the Acoustical Society of America, 122*, 1486-1501.

Butt, S. D. (2001). Experimental measurement of P-wave attenuation due to fractures over the 100 to 300 kHz bandwidth. *Pure and Applied Geophysics*, *158* (9-10), 1783-1796.

Carino, N. J. (2004). Stress Wave Propagation Methods. In V. M. Malhotra, & N. J.

Carino, *Handbook on nondestructive testing of concrete* (pp. 14,1-28). West Conshohocken, PA: CRC Press LLC.

Chen, J. D. & Wada, N. (1986). A new technique for visualizing the distribution of oil, water and quartz grains in a transparent, three-dimensional, porous medium. *SPE Formation Evaluation, April*, 205-208.

Cherry, J. T. & Waters, J. H. (1968). Shear-wave recording using continuous signal methods. Part 1- Early development. *Geophysics, 33* (2), 229-239.

Chotiros, N. P. (1995). Biot model of sound propagation in water-saturated sand. *Journal of the Acoustical Society of America, 97*, 199-214.

Chotiros, N. P. (2002). An inversion of Biot parameters in water saturated sand. *Journal of the Acoustical Society of America, 112* (5-1), 1853-1868.

Clennell, M. B. (1997). Tortuosity: a guide through the maze. *Geological Society, London , Special Publications, 122*, 299-344.

Corapcioglu, Y. M. & Tuncay, K. (1996). Propagation of waves in porous media. In *Advances in porous media* (Vol. 3, pp. 361-440). Philadelphia: Elsevier B.V.

Costley, R. D. & Bedford, A. (1988). An experimental study of acoustic waves in saturated glass beads. *Journal of the Acoustical Society of America, 83* (6), 2165-2174.

Crampin, S. (1981). A review of wave motion in anisotropic and cracked and elastic media. *Wave motion, 3*, 343-391.

Crampin, S. (1985a). Evaluation of anisotropy by shear-wave splitting. *Geophysics, 50* (1), 142-152.

Crampin, S. (1985b). Evidence of aligned cracks in the Earth's crust. *First Break, 3* (3), 12-15.

Crampin, S. (1978). Polarization as a possible dilatancy diagnostic. *Geophysical Journal of Royal Astronomical Society, 53* (3), 476-496.

Crampin, S. (1989). Suggestions for a consistent terminology for seismic anisotropy. *Geophysical prospecting, 37* (7), 753-770.

Crampin, S. & Booth, D. C. (1985). Shear-wave polarizations near the north Anatolian Fault-II. Interpertation in terms of crack induced anisotropy. *Geophysical Journal of Royal Astronomical Society, 83*, 75-92.

Crawford, J. M., Doty, W. E. & Lee, M. R. (1960). Continuous signal seismograph. *Geophysics, 25* (1), 95-105.

Curtis, M. R. (1967). Flow analysis in producing wells. *SPE of AIME* , 1-12.

Daft, L. & William, A. (1906). *Patent No. 817,736.* England/London.

Davies, J. T. & Rideal, E. K. (1963). *Interfacial Phenomenon.* New York: Academic Press Inc.

Digby, P. J. (1981). The effective elastic moduli of porous granular rocks. *Journal of Applied Mechanics* , 803-808.

Dobrin, M. B. & Dunlap, H. F. (1957). Geophysical research and progress in exploration. *Geophysics, 22* (2), 412-433.

Dohr, G. & Janle, H. (1980). Improvements in the observation of shear waves. *Geophysical Prospecting, 28* (2), 208-220.

Duffy, J. & Mindlin, R. D. (1957). Stress-strain relations and vibrations of a granular medium. *Journal of Applied Mechanics, 79*, 585-593.

Einspruch, N. G., Witterholt, E. J. & Truell, R. (1960). Scattering of a plane transverse wave by a spherical obstacle in an elastic medium. *Journal of Applied Physics , 31*, 806–818.

England, W. A., Mackenzie, A. S., Man, D. M. & Quigley, T. M. (1987). The movement and entrapment of petroleum fluids in subsurface. *Journal of Geological Society of London, 144*, 327-347.

Erickson, E. L., Miller, D. E. & Waters, K. H. (1968). Shear-wave recording using continuous signal methods. Part 2- Later experimentation. *Geophysics, 33* (2), 244-254.

Evison, F. F. (1952). The in adequacy of standard seismic techniques for shallow surveying. *SEG Digital Library* , 867-875.

Fedorov, A. F. (1968). *Theory of elastic waves in crystals.* New York: Plenum Press.

Flores, C. P., Hoditch, H. A. & Ayers, W. B. (2011). Economics and technology drive developments of unconventional oil and gas reservoirs : Lessons learned in united states. 1-15.

Flores, M. R. (2014). *Coal and coalbed gas.* Sandiego: Elsevier Inc.

Frempong, P., Donald, A. & Butt, S. D. (2007). The effect of pore pressure depletion and injection cycles on ultrasonic velocity and quality factor in a quartz sandstone. *Geophysics, 72* (2), E43-E51.

Gassman, F. (1951a). Elastic wave through a packing of spheres. *Geophysics, 16* (4), 673-685.

Gassman, F. (1951b). Uber die Elastizitat Poroser Medien: Vier. der. *Natr. Gesellschaft in Zurich, 96*, 1-23.

Gaunaurd, G. C. & Uberall, H. M. (1979). Deciphering the scattering code contained in the resonance echoes from fluid-filled cavities in solids. *Science* , 61-64.

Gish, O. H. & Rooney, W. J. (1925). Measurement of resistivity of large volume of undisturbed earth. *Journal of geophysical research, 30* (4), 161-188.

Goldenberg, C. & Goldhirsch, I. (2005). Friction enhances elasticity in granular solids. *Nature, 435*, 188-191.

Grant, F. S. & West, G. F. (1965). *Interpretation theory in applied geophysics.* New York: McGraw Hill Book Co.

Greaves, N. G. (2013). Poisson's ratio over two centuries: Challenging hypotheses. *Notes and Records of the Royal Society.67*, pp. 37-58. The Author(s) Published by the Royal Society.

Greenwood, J. A. & Williamson, B. J. (1966). Contact of nominally flat surfaces. *Proceedings of the Royal Society .295*, pp. 300-319. London: Proceedings Royal Society A Mathematical Engineering and Physical Sciences.

Griffith, A. A. (1921). The phenomena of rupture and flow in solids. *Philosophical Transactions of the Royal Society of London, 221* (Series A), 163-198.

Griffiths, D. H. & King, R. F. (1980). Theory of electrical resistivity surveying. In D. H. Griffiths, & R. F. King, *Applied Geophysics for Geologists and Engineers.* Oxford: Pregmon Press Ltd.

Gueven, I., Luding, S. & Holger, S. (2013). *AIP Conference Proceedings.1542*, pp. 581-584. Sydney: AIP.

Gurevich, B., Sadovnichaja, A. P., Lopatnikov, S. L. & Shapiro, S. A. (1993).

Seismic wave scattering by an inclusion in a fluid-saturated porous medium. *SEG Annual Meeting*, (pp. 1018-1021). Washington, DC.

Hamilton, E. L. (1971). Prediction of In-Situ acoustic and elastic properties of marine sediments. *Geophysics* , 266-284.

Hamilton, E. L. & Bachman, R. T. (1982). Sound velocity and related properties in marine sediments. *Journal of Acoustical Society of America, 72*, 1891-1904.

Hasbrouck, W. P. & Padget, N. (1982). Use of shear-waves in evaluation of strippable coal resources. *Proceedings 5th ROMOCO symposium .118*, pp. 203-210.

Utah Geological and Mineral Survey Bulletin.

Hashin, Z. & Shtrikman, S. (1963). A variational approach to the elastic behavior of multipahse materials. *Journal of the Mechanics and Physics of Solids, 11* (2).

Hassan, B., Belhaj, H., Butt, S. D. & Islam, R. (2006). Imaging dual-phase flow in porous media. *Petroleum Research Atlantic Canada, Abstract.* Halifax: PRAC.

Hassan, B., Butt, S. D. & Hurich, C. A. (2014 c). An assessment of S-wave potential for integrated geotechnical and geohydrological characterization of near surface. *Congresso SGI-SIMP.31*, p. 662. Milan: Societa Geologica Italiana.

Hassan, B., Butt, S. D. & Hurich, C. A. (2013). An experimental study of S-wave polarization by transmission through fractured porous media. *Symposium on the Application of Geophysics to Engineering and Environmental Problems.* Colorado: EEGS, SAGEEP.

Hassan, B., Butt, S. D. & Hurich, C. A. (2015 d). Ascertaining grain scale effects of seismic or aseismic stimulation upon strength of near surface geological materials. *21st European Meeting of Environmental and Engineering Geophysics*, (p. 26254). Turin.

Hassan, B., Butt, S. D. & Hurich, C. A. (2015 b). Control of saturant's state upon intergranular adhesion affecting seismic and aseismic near surface site strength response inferred by combined Vp/Vs and Poisson's ratio examination. *Congresso SIMP-SGI-So.Ge.I-AIV 2015.35 (2)*, p. 152. Florence: Societa Geologica Italiana.

Hassan, B., Butt, S. D. & Hurich, C. A. (2014 d). Evaluation of time lapse acoustic monitoring of immiscible fluid flows in near surface by attenuation examination method. *20th European meeting of Environmental and Engineering Geophysics* (p. 22321). Athens: European Association of Geoscientists and Engineers.

Hassan, B., Butt, S. D. & Hurich, C. A. (2015 a). Examination of S-wave peculiar resonance spectra for improved characterization of near-surface fluid releases for effective hazard response. *Symposium of the Application of Geophysics to Engineering and Environmental Problems* (pp. 219-222). Austin: EEGS, SAGEEP.

Hassan, B., Butt, S. D. & Hurich, C. A. (2014 b). Investigation of aseismic monitoring of near surface fracture systems by examining S-wave diffraction and interference spectra signature for geoenvironmental hazard prognosis in coastal areas. *Congresso SGI-SIMP, Abstracts.31-1*, p. 642. Roma: Societa Geologica Italiana.

Hassan, B., Butt, S. D. & Hurich, C. A. (2014 a). Results of a laboratory study highlighting the potential of integrated P-wave and Electrical methods application in near-surface. *Symposium on the Application of Geophysics to Engineering and*

*Environmental Problems* (pp. 422-433). Boston: EEGS, SAGEEP.

Hassan, B., Butt, S. D. & Hurich, C. A. (2015 c). Understanding scale and direction dependent strength susceptibility of fault systems to seismic and aseismic effects by examining lateral and dilational displacements characteristics using S-waves. *Congresso SIMP-SGI-So.Ge.I-AIV 2015.35-2*, p. 153. Societa Geologica Italiana.

Hassan, B., Butt, S. D., Hurich, C. A. & Bhatia, N. (2007). Development of an innovative apparatus to study flow through porous media. *IEEE Newfoundland Electrical and Computer Engineering Conference* (pp. 1-4). St. John's: IEEE NL Section.

Hegemeir, G. A. & Bache, T. C. (1973). A continuum theory of wave propagation in laminated composites, Case 2: Propagation normal to laminates. *Journal of Elasticity, 3* (2), 125-140.

Hegemeir, G. A. & Nayfeh, A. H. (1973). A continuum theory of wave propagation in laminated composites, Case 1: Propagation normal to laminates. *Journal of Applied Mechanics, 40* (2), 503-510.

Heinbuch, U. & Fischer, J. (1989). Liquid flow in pores: Slip, no-slip, or multilayer sticking. *Physical Review A, 40* (2), 1144-1146.

Helbig, K. & Mesdag, C. S. (1982). The potential of shear wave observations. *Geophysical prospecting, 30* (4), 413-431.

Helbig, K. & Thomsen, L. (2005). 75-plus years of anisotropy in exploration and reservoir seismics: A historical review of concepts and methods. *Geophysics, 70* (6), 9ND-23ND.

Hidalgo, R. C., Grosse, C. U., Kun, F., Reinhardt, H. W. & Herrman, H. J. (2002). Evolution of percolating force chains in compressed porous media. *Physical Review Letters, 89* (20), 205501,1-4.

Hill, R. (1963). Elastic properties of reinforced solids: Some theoretical principles. *Journal of the Mechanics and Physics of Solids, 11* (5), 357-372.

Hoekstra, P., Sellman, P. V. & Delaney, A. (1975). Ground and airborne resistivity surveys of permafrost near Fairbanks, Alaska. *Geophysics, 40*, 646-651.

Homsy, G. M. (1987). Viscous fingering in porous media. *Annual Reviews of Fluid Mechanics* , 271-311.

Horton, C. W. (1943). Secondary arrivals in a velocity survey. *Geophysics, 8* (3), 290-296.

Hu, M. Z. & Ting, T. C. (1983). Wave propagation parallel to layers in elastic or viscoelastic layered composites. *Journal of Structural Mechanics, 11* (1), 13-35.

Hubbart, M. K. (1932). Results of an earth-resistivity survey on various geological structures in Illinois. *AIME Tech. Pub., no.463*, 23.

Hummel, J. N. (1932). *AIMI Trans. Geophysical prospecting, 97*, 392-422.

Hunter, J. A. (1980). Mating the digital engineering seismograph with the small digital computer- some useful techniques. *50th SEG Annual International Meeting.* Houston, Texas: Society of Exploration Geophysicists.

Hunter, J. A., Burns, R. A., Good, R. L., Gagne, R. M. & MacAulay, H. M. (1982). Field experience with the "optimum window" hammer seismic reflection technique. *52nd SEG Annual Meeting, Expanded Abstracts* (pp. 466-468). Dallas, Texas: Society of Exploration Geophysicists.

Hunter, J. A., Burns, R. M. & Good, R. L. (1980). Optimum field techniques for bedrock reflection mapping with the multichannel engineering seismograph. *50th SEG Annual International Meeting, Expanded Abstracts.* Houston, Texas: Society of Exploration Geophysicists.

Hunter, J. A., Pullan, S. E., Burns, R. A., Gagne, R. M. & Good, R. L. (1984). Shallow seismic reflection mapping of the overburden-bedrock interface with the engineering seismograph-some simple techniques. *Geophysics, 49* (8), 1381-1385.

Huntington, H. B. (1958). *The elastic constants of crystals.* New York: Academic Press Inc.

Imai, T., Fumato, H. & Yakota, K. (1976). *P- and S-wave velocities in subsurface layers of ground in Japan.* Oyo: Oyo Technical Note, TN-14, Urawa research institute Japan.

Jacobsen, M., Johansen, T. A. & McCann, C. (2003). The acoustic signature of fluid flow in complex porous media. *Journal of applied geophysics, 54*, 219-246.

Jager, H. M., Nagel, S. R. & Behringer, R. P. (1996). Granular solids, liquids and gases. *Reviews of Modern Physics, 68* (4), 1260-1273.

Johnson, D. L. (1981). Elastodynamics of porous media. *Macroscopic Properties of Disordered Media Proceedings* (pp. 88-110). New York: Springer-Verlag.

Johnson, D. L. (1980). Equivalence between fourth sound in liquid He II and low temperature at the Biot consolidated porous media. *Applied physics letters, 37*, 1065-1067.

Johnston, D. H. (2013). *Practical Applications of Time- lapse Seismic Data.* Tulsa,Ok: Society of Exploration Geophysicists.

Johnston, D. H., Toksoz, M. N., & Timur, A. (1979). Attenuation of seismic waves in dry and saturated rocks: II. Mechanisms. *Geophysics* , 691-711.

Jolly, R. N. (1956). Investigation of shear waves. *Geophysics, 21* (4), 905-938.

Jones, J. P. (1962). Effect of uniform flow on elastic waves in a porous, elastic solid. *Journal of the Acoustical Society of America, 34* (9), 1173-1175.

Jones, J. P. (1969). Pulse propagation in poroelastic solid. *Journal of Applied Mechanics, 36* (4), 878-880.

Jones S. C.(1972), A rapid accurate unsteady-state Klinkenberg permeameter, *SPE* 3535, 383-397.

Jones, T. D. (1986). Pore fluids and frequency-dependent wave propagation in rocks. *51* , 1939-1951.

King, M. S., Zimmerman, R. W. & Corwin, R. F. (1988). Seismic and electrical properties of unconsolidated permafrost. *Geophysical Prospecting, 36*, 349-364.

Kingrey, W. D., Bowen, H. K. & Uhlman, D. R. (1975). *Introduction to ceramics.* Cambridge, Massachusetts: John Wiley and Sons.

Lankston, R. W. (1990). High resolution refraction data acquisition and interpertation. In S. H. Ward, *Geotechnical and environmental geophysics* (Vol. 1, pp. 45-74). Tulsa, Ok: Society of Exploration Geophysicists.

Leimbach, G. & Lowy, H. (1910). *Patent No. 237949-246836.* Germany.

Lekmine, G., Pessel, M. & Auradou, H. (2009). 2D Electrical resistivity tomography survey optimization of solute transport in porous media. *Archeo Sciences, 33*, 309-312.

Leonardon, E. G. (1932). Discussion of the paper of M. K. Hubbart-1932. *AIME Trans. Geophysical Prospecting* , 32.

Liu, Q. (2007). *Literature review: Materials with negative Poisson's ratio and special application to aerospace and defence.* Defence science and technology organization., Department of Defence. Australian Government.

Lorenz, P. B. (1961). Tortuosity in porous media. *Nature, 189*, 386-387.

Luding, S. (2005). ( Granular media) Information propagation. *Nature* , 159-160.

Lumley, D. E. (1994). 4-D seismic monitoring of reservoir fluid-flow processes. *Proceedings, Mathematical Methods in Geophysical Imaging.2301 (70)*, pp. 70-81. San Diego: SPIE.

Lumley, D. E. (2001). Time lapse seismic reservoir monitoring. *Geophysics, 66*, 50-53.

Lundberg, H.& Nathorst, H. (1919). *Teknisk Tidskrift, 49*, 42-46.

Malhotra, V. M. & Carino, M. J. (2004). *Handbook of nondestructive testing of concrete.* Boca Raton, Florida: CRC Press LLC.

Markov, M. G. (2007). Effect of Interfacial Slip on the Kinematic and Dynamic Parameters of Elastic Waves in a Fluid-Saturated Porous Medium. *Acoustical Physics, 53* (2), 213-216.

Mavko, G., Mukerji, T. & Dvorkin, J. (2009). *The rock physics handbook: Tools for seismic analysis in porous media.* New York: Cambridge University Press.

Mazotti, M., Pini, R. & Storti, G. (2009). Enhanced coalbed methane recovery. *The Journal of Supercritical Fluids, 47* (3), 619-627.

McBride, J. R. & Kraft, D. W. (1972). Scattering of transverse elastic wave by an elastic sphere in a solid medium. *Journal of Applied Physics, 43*, 4853-4859.

McMechan, G. A. (1982). Resonant scattering by fluid filled cavities. *Bulletin of the Seismological Society of America, 72* (4), 1143-1153.

Meurs, V. P. (1957). The uses of transparent three-dimensional models for studying the mechanism of flow processes of oil reservoirs. *SPE Journal, 10*, 295-301.

Miller, R. K. & Tran, H. T. (1979). Reflection, refraction and absorption of elastic waves at a frictional interface: SH Motion. *Journal of Applied Mechanics, 46* (3), 625-630.

Miller, R. K. & Tran, H. T. (1981). Reflection, refraction and absorption of elastic waves at a frictional interface: P and SV motion. *Journal of Applied Mechanics, 48* (1), 155-160.

Mindlin, R. D. (1949). Compliance of elastic bodies in contact. *Journal of Applied Mechanics, 16*, 259-268.

Mooney, H. M. (1980). *Handbook of engineering geophysics.* Minneapolis,

Minnesota: Bison Instruments Inc.

Mungan, N. (1966). Interfacial effects in immiscible liquid-liquid displacement in porous media. *Society of Petroleum Engineers Journal, 6* (3), 217--224.

Mungan, N. (1964). Role of wettability and interfacial tension in water flooding. *Society of Petroleum Engineers Journal (Sinclair Research Inc.), 4* (2), 115-123.

Nechaev, Y. V. & Martynov, Y. I. (1965). *Application of the electrical prospecting to the prediction of landslide phenomena in the Grushevsky quarry.* Moscow: Nedra Publ. House.

Newman, J. L., Waddell, C. & Sauder, H. L. (1956). A flow meter for measuring subsurface flow rates. 49-52.

Nichols, C. R. & Williston, S. H. (1932). *Patent No. 1,841,376.* Dallas, Texas.

Niedell, S. N. (1990). *Stratigraphic modelling and interpretation: Geophysical principles and techniques.* Tulsa, Ok: American Association of Petroleum Geologists.

Nolte, D. D., Nolte, L. P., Beach, J. & Zeigler, C. (2000). Transition from the displacement discontinuity limit to the resonant scattering regime for fracture interface waves. *International journal of rock mechanics and mining sciences, 37* (1), 219-230.

Nowick, A. S. & Berry, B. S. (1972). *Anelastic relaxation in crystalline solids.* New York: Academic Press Inc.

Ogilvy, A. A. & Bogoslovsky, V. A. (1979). The possibilities of geophysical methods applied for investigating the impact of man on the geological medium. *Geophysical prospecting, 27* (4), 775-789.

Oka, F., Heitor, A. P., Kita, N. & Kimoto, S. (2009). Effect of Poisson's ratio on the dynamic instability of water-saturated elasto-plastic soil. *Proceedings of the Fourth Biot Conference on Poromechanics* (pp. 1103-1107). New York: Destech Publications Inc.

Pakiser, L. C. & Warrick, R. E. (1956). A preliminary evaluation of the shallow reflection seismograph. *Geophysics* , 388-405.

Pakiser, L. C., Mabey, D. R. & Warrick, R. E. (1954). Mapping shallow horizons with shallow seismograph. *AAPG Bulletin, 38* (11), 2382-2394.

Palmer, D. (1981). An introduction to generalized reciprocal method. *Geophysics, 46* (11), 1508-1511.

Pickup, G. E., Ringrose, P. S., Jensen, J. L. & Sorbie, K. S. (1994). Permeability tensors for sedimentary structures. *Mathematical Geology, 26* (2), 227-250.

Plona, T. J. (1980). Observation of the second bulk compressional wave in porous medium at ultrasonic frequencies. *Applied Physics Letters, 36*, 259-261.

Plona, T. J. & Johnson, D. L. (1980). Experimental study of two bulk compressional modes in water saturated porous structures. *Ultrasonic Symposium* (pp. 868-872). IEEE.

Plona, T. J. & Johnson, L. D. (1983). Acoustic properties of porous systems: I. Phenomenological descriptions. *AIP Conference proceedings, Physics and Chemistry of Porous Media*, *107*. New York.

Radjai, F. & Roux, S. (1995). Friction-induced self-organization of a onedimensional array of particles. *Physical Review E* , 6177-6188.

Radjai, F., Evesque, P., Bideau, D. & Roux, S. (1995). Stcik-slip dynamics of one dimensional array of particles. *Physical Review E, 52* (5), 5555-5554.

Radjai, F., Jean, M., Moreau, J. J. & Roux, S. (1996). Force distribution in dense two dimensional granular systems. *Physical Review Letters, 77* (2), 274-277.

Rasolofosaon, P. J. & Zinszner, B. E. (2009). Poroelastic equations closely examined by ultrasonic experiments in rocks. *Proceedings of the Fourth Biot Conference on Poromechanics* (pp. 661-666). New York: Destech Publications Inc.

Reynolds, J. M. (1997). *An introduction to applied and environmental geophysics* (1997 ed.). West Sussex, England: John Wiley & Sons Ltd.

Rice, R. B., Allen, S. J., Gant, J. O., Hodgson, R. N., Larson, D. E., Lindsey, J. P., et al. (1981). Developments in exploration geophysics. 1975-1980. *Geophysics, 46* (8), 1088-1099.

Ricker, N. & Lynn, R. D. (1950). Composite reflections. Geophysics , 15 (1), 30-49. Rust, W. M. (1938). A historical review of electrical prospecting methods. (1-6, Ed.) *Geophysics, 3* (1).

Ryan, R. J. (1998). The Falls Brook Quarry near Three Mile Plains, in Classic Carboniferous sections of Minas and Cumberland Basin in Nova Scotia. *The Society of Organic Petrology Annual General Meeting Field Trip.* Nova Scotia Department of Natural Resources, Open file report ME 1998-5.

Salin, D. & Schon, W. (1981). Acoustics of water saturated packed glass spheres. *Journal de Physique Letters, 42* (22), L477-L480.

Schepers, R. (1975). A seismic reflection method for solving engineering problems. *Geophysics, 41*, 367-384.

Sears, F. W. (1958). *Optics.* Addison-Wesley Publishing Company Inc.

Shaw, H., Burkshaw, J. M. & Newing, S. T. (1931). *Applied geophysics : A brief history of the development of the apparatus and methods employed in the investigation of subterranean structural conditions and the location of mineral deposits.* London: Science Museum, Great Britain.

Sheriff, R. E. & Geldart, L. P. (1982). *Exploration Seismology.* New York: Cambridge University Press.

Shwartz, L. & Plona, T. J. (1984). Ultrasonic propagation in closed-pack disordered suspensions. *Journal of applied physics, 55* (11), 3971-3977.

Siegfried, R. W. (2011). R& D Challenges associated with environmentally sensitive development of unconventional gas. *SEG Annual Meeting, Abstracts*, (pp. 3698-3699).San Antonio.

Slawinski, M. A. (2010). *Waves and rays in elastic continua.* NJ: World Scientific Publishing Co.

Smith, T. M., Sondergeld, C. H. & Rai, C. S. (2003). Gassmann fluid substitutions: A tutorial. *Geophysics, 68* (2), 430-440.

Stefanesco, S., Schlumberger, C. & Schlumberger, M. (1930). Sur la distribution electrique potentiellle autour d'une prise de terre ponctuelle dans un terrain a couches horizontales, et homogenes et isotropes. *Journal de Physique et le Radium, 1* (4), 132-140.

Stoll, R. D. (1977). Acoustic waves in ocean sediments. *Geophysics, 42*, 715-725.

Stoll, R. D. (1989). *Sediment acoustics* (Vol. 26). New York: Springer-Verlag.

Stoll, R. D. & Bryan, G. M. (1970). Wave attenuation in saturated sediments. *Journal of Acoustical Society of America, 47* (5-2), 1440-1447.

Stollar, R. L. & Roux, P. (1975). Earth resistivity surveys a method for defining ground-water contamination. *Ground water, 13* (2), 145-150.

Stumpel, H., Kahler, S., Meissner, R. & Milkereit, B. (1984). The use of seismic shear waves and compressional waves for lithological problems of shallow sediments. *Geophysical prospecting, 32* (4), 662-675.

Sun, Z., Gerrard, C. & Stephansson, O. (1985). Rock joint compliance tests for compression and shear loads. *International Journal of Rock Mechanics Mining Sciences and Geomechanics, Abstracts, 22* (4), 197-213.

Tagg, G. F. (1930). The earth resistivity method of geophysical prospecting: some theoretical considerations. *Mining magazine, 43* (3), 150-158.

Tanikawa, W. & Shimamoto, T. (2006). Klinkenberg effect for gas permeability and its comparison to water permeability for porous sedimentary rocks. *Hydrology and Earth Systems Sciences Discussions, 3*, 1325-1338.

Tatham, R.H. (1982). Vp/Vs and lithology: *Geophysics* 47(3), 336-344.

Tatham, R. H. & McCormack, M. D. (1991). *Multicomponent seismology in petroleum exploration.* Tulsa, Ok, USA: Society of Exploration Geophysicists.

Thomsen, L. (2002). *Understanding seismic anisotropy in exploration and exploitation* (Vol. 5). Tulsa, Ok: Society of Exploration Geophysicists.

Ting, T. C. & Mukonoki, I. (1979). A theory of viscoelastic analogy for wave propagation normal to the layering of a layered medium. *Journal of Applied Mechanics, 46*, 329-338.

Toksoz, M. N., Johnston, D. H. & Timur, A. (1979). Attenuation of seismic waves in dry and saturated rocks: I. Laboratory measurements. *Geophysics, 44*, 681-690.

Travis, K. P., Todd, B. D. & Evans, D. J. (1997). Departure from Navier-Stokes hydrodynamics in confined liquids. *Physical Review E, 55* (4), 4288-4295.

Vinogradova, O. I. (1996). Hydrodynamic interaction of curved bodies allowing silppage on their surfaces. *Langmuir, 12*, 5963-5968.

Vinogradova, O. I. (1999). Slippage of water over hydrophobic surfaces. *International Journal of Mineral Processing, 56*, 31-60.

Walton, K. (1977). Elastic wave propagation in model sediments-I. *Geophysical Journal of Royal Astronomical Society, 48*, 461-473.

Walton, K. (1975). The effective elastic moduli of model sediments. *Geophysical Journal of Royal Astronomical Society, 43*, 293-306.

Wang, H. F. (2000). *Theory of linear poroelasticity with applications to geomechanics and hydrology.* Princeton, NJ: Princeton University Press.

Wang, Z. (2000). The Gassman equation revisited: comparing laboratory data with Gassman's predictions, Seismic and acoustic velocities in rocks, Recent developments. (pp. 1-23). SEG Reprint Series.

Wang, Z. (2001). Y2K tutorial, fundamentals of seismic rock physics. *Geophysics, 66* (2), 398-412.

Wasely, R. J. (1973). *Stress wave propagation in solids; an introduction.* New York: Dekker,M.

Wehner, S. C., Raines, M. A., Davis, T. L. & Benson, R. D. (2000). Dynamic reservoir characterization and central vaccum unit. *SPE Annual Technical Conference and Exhibition* (pp. 1-8). Dallas: Society of Petroleum Engineers.

Wenner, F. (1915). A method of measuring earth resistivity. *Bulletin of the Bureau of Standards, 12* (4), 469-478.

Widess, M. B. (1973). How thin is the thin bed. *Geophysics, 38* (6), 1176-1180.

Wilmanski, K. (2005). Tortuosity and objective related accelerations in the theory of porous materials. *Proceedings of The Royal Society. A.461*, pp. 1533-1561. Berlin: Weierstrass Institute for Applied Analyses and Stochastics .

Winterstein, D. F. (1990). Velocity anisotropy terminology for geophysicists. *Geophysics, 55* (8), 1070-1088.

Winterstein, D. F. & Stefani, J. P. (1987). Symmetries of anisotropic rocks and what they mean for seismic waves. *SEG Technical Program Expanded Abstracts* (p. 856). Society of Exploration Geophysicists.

Woessner, W. W. & Sullivan, K. E. (1984). Results of seepage meter and mini-piezo meter study. *Ground Water, 22*, 561-568.

Wyllie, M. J. & Gregory, A. R. (1955). Flow through unconsolidated porous aggregates: Effect of porosity and particle shape on Kozney-Carman constants. *Industrial and Engineering Chemistry, 47* (7), 1379-1388.

Yamakawa, N. (1962). Scattering and attenuation of elastic waves. *Geophysical Magazine, 31*, 63-97.